



UNIVERSITY OF
LIVERPOOL



Establishment and characterisation of USP29 as a
novel regulator of Hypoxia Inducible Factor α

Thesis submitted in accordance with the requirements of the
University of Liverpool

for the degree of Doctor in Philosophy by

Amelie Schober

December 2016

ABSTRACT

The hypoxia signalling pathway controls the adaptation of cells to decreased oxygen availability. When oxygen becomes limiting, the central transcription factor of the pathway, hypoxia-inducible factor (HIF), is activated and induces the expression of a set of genes, which cause a glycolytic switch, enhance cell survival and induce angiogenesis. While those are necessary physiological adaptive processes, they are also hallmarks of cancer and hypoxia signalling is often found activated in cancer. However, current knowledge about the regulation of the hypoxia signalling pathway is not able to satisfactorily explain the deregulation found in cancer.

Therefore, the aim of this work was to discover new regulatory mechanisms that could be responsible for sustained hypoxia signalling and therefore might represent future therapeutic targets. We focused on how post-translational modifications affected the properties of the central proteins of the pathway. Using standard biochemical approaches and fluorescence lifetime imaging, we found that the ubiquitin specific protease 29 (USP29) is a deubiquitinase for HIF-1 α . Moreover, USP29 is the first ubiquitin protease towards HIF-2 α . USP29 de-conjugates poly-ubiquitin from HIF- α and prevents its proteasomal degradation, leading to its stabilisation even in normoxic conditions. Importantly, this action of USP29, while dependent on its catalytic activity, was not dependent on the classical prolyl-hydroxylation and pVHL-mediated ubiquitination, and therefore we propose that USP29 is a non-canonical HIF activator. As hardly any reports about USP29 were available, we next aimed to characterise this maternally imprinted protein. We found that USP29 itself was subject to poly-ubiquitin-mediated destabilisation, but was able to remove the ubiquitination itself and therefore auto-stabilise in a catalytic activity-dependent way. Furthermore, we demonstrated that USP29 formed homodimers in living cells. Finally, we found that USP29 mRNA levels correlated with disease progression and severity in prostate cancer and suggest that USP29 might become an attractive target for therapeutic targeting of hypoxia signalling in the future.

TABLE OF CONTENTS

Abstract.....	i
Table of Contents.....	ii
Abbreviations.....	vi
Chapter 1: Introduction.....	1
1.1 Hypoxia signalling.....	1
1.1.1 Oxygen.....	1
1.1.2 Discovery of the hypoxia signalling pathway.....	1
1.1.3 Hypoxia inducible factor HIF.....	2
1.1.4 Prolyl-hydroxylase domain containing proteins (PHDs).....	3
1.1.5 Hypoxia signalling and cancer.....	4
1.2 PTMs and deubiquitinases.....	6
1.2.1 PTMs in hypoxia signalling.....	6
1.2.2 Ubiquitination.....	7
1.2.3 Deubiquitination.....	9
1.2.4 USP29 (Ubiquitin-specific protease 29).....	9
1.2.4.1 Discovery of the <i>Usp29</i> gene.....	9
1.2.4.2 Imprinting and transcription of the Peg3 domain and the <i>Usp29</i> gene.....	10
1.2.4.3 USP29 biological functions.....	11
1.3 Hypoxia signalling and the ubiquitin proteasome system.....	11
1.3.1 DUBs in canonical hypoxia signalling.....	12
1.3.2 DUBs in non-canonical HIF signalling.....	12
1.3.3 Regulation of DUBs by hypoxia.....	14
1.3.4 Dysregulation of hypoxia-related DUBs in cancer (excerpt).....	15
1.3.5 DUBs as druggable targets for therapy.....	15
1.4 How to investigate signalling pathways.....	16
1.4.1 Fluorescence and fluorescence lifetime.....	17
1.4.2 Förster resonance energy transfer (FRET).....	18
1.5 Aims of the project.....	20
Chapter 2: Materials and Methods.....	21
2.1 Materials.....	21
2.2 Methods.....	21
2.2.1 Molecular Biology.....	21
2.2.1.1 Polymerase chain reaction (PCR).....	21
2.2.1.2 Mutagenesis.....	21
2.2.1.3 Restriction digestion.....	22

2.2.1.4 Gateway® Cloning.....	22
2.2.1.5 In-Fusion® HD Cloning	23
2.2.1.6 Plasmid propagation.....	23
2.2.2 Cell Culture and transfections	24
2.2.3 RNAi	24
2.2.4 RNA extraction and quantitative PCR (qPCR)	25
2.2.5 Immunofluorescence	27
2.2.6 MitoTracker staining	27
2.2.7 Western Blot.....	27
2.2.8 Antibodies	28
2.2.9 Ubiquitination assay with Ni-NTA purification.....	28
2.2.10 Ubiquitination assay with GFP-trap® pulldown	29
2.2.11 Co-immunoprecipitation using GFP-traps®	29
2.2.12 Size exclusion chromatography.....	30
2.2.13 Sequence alignment.....	31
2.2.14 Mass spectrometry (MS) analysis	31
2.2.15 Fluorescence Imaging.....	31
2.2.15.1 Acquisition of confocal fluorescence images.....	31
2.2.15.2 RICS measurements and data analysis.....	31
2.2.15.3 FRAP measurements.....	32
2.2.15.4 FLIM-FRET measurements	32
2.2.15.5 FLIM-FRET analysis	33
2.2.16 Statistical tests	33
Chapter 3: Generation and characterisation of tools for live cell imaging.....	36
3.1 Introduction.....	36
3.2 Effect of PHD3-SUMOylation on HIF-1 α binding	36
3.2.1 Generation of fluorescent PHD3 and HIF- α DM proteins	37
3.2.2 Validation of the differentially tagged PHD3 and HIF- α constructs in preliminary FRET experiments.....	39
3.2.3 Fluorescence tagging of the PHD3 SUMO mutants.....	41
3.2.4 Performance of the mRuby2 label.....	44
3.2.5 Measurement of diffusion coefficients and interaction	45
3.3 Exploration of PHD1 nuclear shuttling by FRAP.....	47
3.3.1 Fluorescence tagging of PHD1 WT and K118/120R mutant	47
3.3.2 FRAP experiments	48
3.4 Proof of principle – FLIM-FRET experiment	50
3.5 Fluorescence tagging of USP29.....	52
3.6 Discussion.....	54

3.6.1 Choice of the fluorescent tag.....	54
3.6.2 Measuring protein-protein interactions in live cells.....	54
Chapter 4: USP29 is a new regulator of HIF- α	56
4.1 Introduction	56
4.2 First experiments performed in Edurne Berra's lab.....	56
4.3 USP29 is a positive regulator of HIF-1 α	57
4.4 USP29 upregulates HIF-1 α in a non-canonical way.....	59
4.5 Universality of USP29's effect on HIF- α	62
4.6 USP29 stabilises HIF- α by protecting it from proteasomal degradation	62
4.7 USP29 interacts with and deubiquitinates HIF- α DM ^(PP/AA)	65
4.8 HIF-1 α is specifically targeted by USP29	69
4.9 USP29 targets the C-terminal part of HIF- α	69
4.10 MS analysis of HIF-1 α DM's PTMs	71
4.11 USP29 levels correlate with tumour progression and HIF target gene expression.....	73
4.12 USP29's effect on HIF-1 α in hypoxia	74
4.13 Further FLIM-FRET experiments: USP29 - HIF- α interaction.....	75
4.14 Searching for HIF-1 α 's non-canonical ubiquitin E3 ligase	76
4.15 Discussion.....	78
Chapter 5: Biochemical characterisation of USP29.....	80
5.1 Introduction	80
5.2 USP29 autoregulation.....	81
5.2.1 USP29 ^{C294S} is degraded by the proteasome	81
5.2.2 USP29 auto-deubiquitinates itself	82
5.2.3 Identification of USP29's ubiquitination target residues	83
5.2.4 USP29 forms dimers	85
5.2.5 Ube3a is not USP29's E3-ligase	88
5.3 USP29's protein interaction landscape	88
5.3.1 USP29's interactome.....	88
5.3.2 PCNA is interacting with USP29	91
5.3.3 Potential Ub E3 ligases for USP29.....	92
5.3.4 USP29 and mitochondria	95
5.4 Discussion.....	96
Chapter 6: Discussion	98
6.1 The (dis)advantages of fluorescence microscopy	98
6.2 UPS and non-canonical HIF signalling	99
6.3 Targeting hypoxia signalling via DUBs	100
6.4 The potential role of USP29 dimerisation	102

6.5 Expression of USP29	103
6.6 USP29 - an integrator of cell signals?.....	104
6.7 Outlook and perspective	106
Bibliography.....	161
Appendix 1: Review Article.....	I
Appendix 2: USP29 interactome.....	VIII
Appendix 3: Posters presented during the thesis.....	XXIV

ABBREVIATIONS

APS	ammonium persulfate
ATP	adenosine triphosphate
Ca9	carbonic anhydrase 9
CHX	cycloheximide
CQ	chloroquine
DM	double mutant
DMEM	Dulbecco's minimal essential medium
DMOG	dimethylxaloylglycine
DUB	deubiquitinating enzyme
EGFP	enhanced green fluorescent protein
EPO	erythropoietin
FBS	fetal bovine serum
FLIM	fluorescence lifetime measurement
FRET	Förster resonance energy transfer
GFP	green fluorescent protein
HA-tag	hemagglutinin-tag
HEK293	human embryonic kidney 293
HIF	hypoxia inducible factor
HRE	hypoxia response element
MEM	minimal essential medium
mRNA	messenger RNA
MS	mass spectrometry
NA	numerical aperture
PBS	phosphate buffered saline
PCNA	proliferating cell nuclear antigen
PCR	polymerase chain reaction
PHD	prolyl hydroxylase domain containing enzyme
PTM	post-translational modification
pVHL	von-Hippel-Lindau protein
qPCR	quantitative polymerase chain reaction

RNAi	RNA interference
ROI	region of interest
SDS	sodium dodecyl sulphate
shRNA	short hairpin RNA
siRNA	small interfering RNA
TEMED	tetramethylethylenediamine
Ub	ubiquitin
UBD	ubiquitin binding domain
UPS	ubiquitin proteasome system
USP	ubiquitin specific protease
WB	western blot
WT	wildtype

Chapter 1: Introduction

1.1 Hypoxia signalling

1.1.1 Oxygen

In the lungs oxygen is extracted from the atmospheric air and is bound by haemoglobin in the erythrocytes. As the erythrocytes travel through the circulatory system they deliver molecular oxygen to the cells. Cells rely on oxygen during the last step of the respiratory chain in the mitochondria for the aerobic production of ATP. If oxygen levels drop below a cell-dependent critical level, cells experience hypoxia and cannot sustain aerobic respiration. A switch to glycolysis, the less efficient, but oxygen-independent way of producing ATP is required to ensure cell survival. The sensing of cellular oxygen levels, the increase of oxygen and ATP availability, the switch between the modes of energy generation and ultimately the adaptation to the low oxygen environment, is controlled by the hypoxia signalling pathway.

1.1.2 Discovery of the hypoxia signalling pathway

A hypoxia inducible factor (HIF) was first described by Semenza et al. in 1992 as a nuclear factor that enhances transcription of the *erythropoietin (EPO)* gene in hypoxic conditions by binding to a 3' enhancer sequence element (Semenza and Wang, 1992) that had previously been identified (Semenza et al., 1991). Wang and Semenza further showed that in response to hypoxia, HIF exhibited DNA binding activity also in cells that do not transcribe the *EPO* gene, suggesting that HIF and the sequence it binds to, might be involved in a general hypoxic response (Wang and Semenza, 1993). Further experiments showed that HIF consisted of a HIF- α and HIF- β subunit and that both subunits contain a basic helix-loop-helix and a PAS domain (Wang et al., 1995; Wang and Semenza, 1995). While their mRNA levels were not regulated by hypoxia, HIF- α protein could be shown to be destabilised in normoxia (Huang et al., 1996; Salceda and Caro, 1997). Huang et al. showed that the destabilisation of HIF- α was mediated through the ubiquitin-proteasome pathway and that an oxygen dependent degradation (ODD) domain was controlling this process (Huang et al., 1998). Destabilisation depends on von-Hippel-Lindau protein (pVHL) (Maxwell et al., 1999), which mediates the oxygen-dependent ubiquitination of HIF- α (Ohh et al., 2000). Binding of pVHL to HIF-1 α 's ODD domain depends on the post-translational hydroxylation of two conserved proline residues (Pro-402 and Pro-564 in the case of human HIF-1 α) within the ODD (Ivan et al., 2001; Jaakkola et al., 2001) (Figure 1.1). A so far unknown Fe²⁺-, 2-oxoglutarate- and oxygen-dependent prolyl-4-hydroxylase (called HIF-PH) was suggested to be responsible for this modification (Jaakkola et al., 2001). Shortly after, three human HIF-PHs designated PHD1, PHD2 and PHD3 were identified by Bruick et al. and Epstein et al. (Bruick and McKnight, 2001; Epstein et al., 2001).

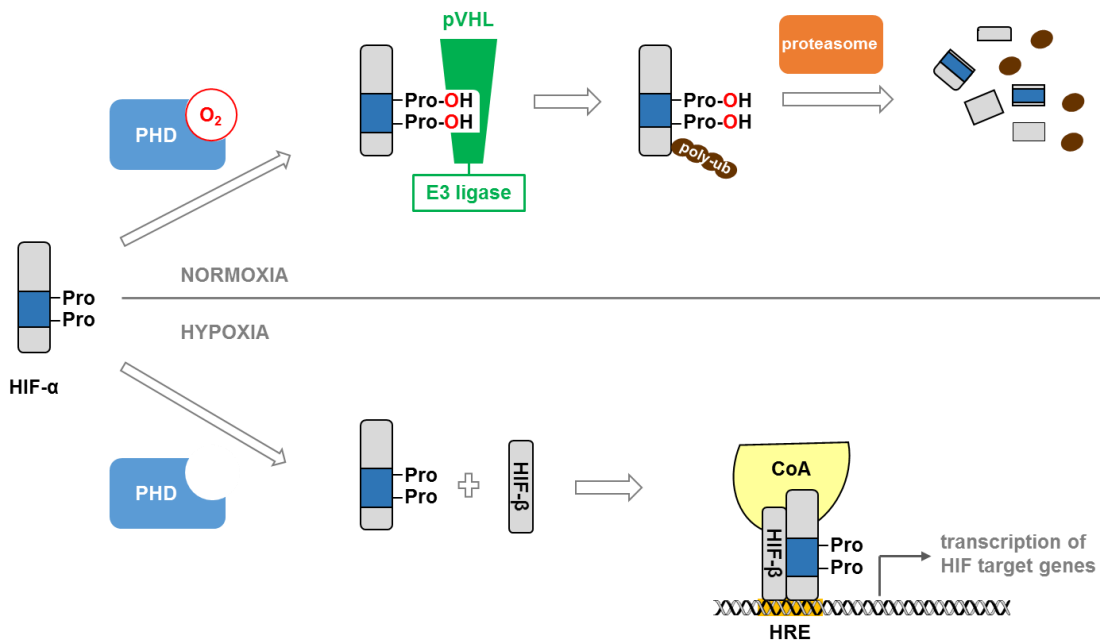


Figure 1.1: The canonical hypoxia signalling pathway. In normoxia PHD proteins use molecular oxygen to hydroxylate HIF- α on two proline residues within the oxygen dependent degradation domain (blue). Hydroxylated HIF- α is recognised by the ubiquitin E3 ligase pVHL (von-Hippel Lindau protein), poly-ubiquitinated and degraded by the proteasome. When oxygen becomes limiting (hypoxia), HIF- α evades PHD/pVHL-mediated degradation, dimerises with HIF-1 β and binds to hypoxia responsive elements (HRE) in the regulatory sequences of genes. HIF recruits co-activators (CoA) to transactivate the expression of its target genes.

1.1.3 Hypoxia inducible factor HIF

The hypoxia inducible factor consists of an α -subunit that is destabilised in normoxia and the β -subunit (HIF-1 β or ARNT) (Wang et al., 1995; Wang and Semenza, 1995) that was assumed to not underlie oxygen-dependent regulation but has recently been shown to be somewhat regulated by hypoxia (Wolff et al., 2013). HIF- α and HIF-1 β heterodimerise via their basic helix-loop-helix (bHLH)/PAS domains (Figure 1.2) and the dimer binds to HRE enhancer motifs on the DNA (Jiang et al., 1996; Wang and Semenza, 1993). HIF then recruits the general co-activators CBP/p300 via the transactivation domain (TAD) (Arany et al., 1996), leading to the expression of a wide set of HRE-controlled genes. Apart from the erythropoietin gene, these are genes that enhance the glycolytic potential of the cell by increasing the expression of glucose transporters and of glycolytic enzymes, such as GLUT1 and phosphoglycerate kinase 1, respectively (Iyer et al., 1998). Among the HIF target genes are also vascular endothelial growth factor (VEGF), which induces angiogenesis (Iyer et al., 1998) and the anti-apoptotic protein BCL-xL (Chen et al., 2009). The hydroxylation of an asparagine residue in HIF- α 's C-terminal transactivation domain (CTAD) by Factor Inhibiting HIF (FIH) negatively regulates the gene expression through inhibition of the binding of the co-activators, representing an additional layer of regulation (Lando et al., 2002; Mahon et al., 2001).

Three HIF- α subunits (HIF-1 α , HIF-2 α , HIF-3 α) have been described (Ema et al., 1997; Gu et al., 1998; Semenza and Wang, 1992) of which HIF-1 α and HIF-2 α are the major activators of hypoxia induced gene transcription (Figure 1.2).

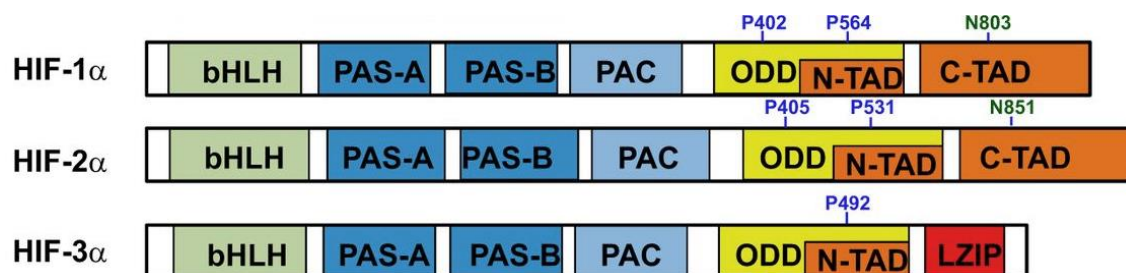


Figure 1.2: Domain structures of the α -subunit of the hypoxia inducible factors 1-3. All three HIF- α isoforms contain an N-terminal basic helix-loop-helix (bHLH) domain and a PAS domain for dimerisation with HIF- β , and an oxygen dependent degradation domain (ODDD) with one or two proline residues that are subjected to hydroxylation by PHDs. While HIF-3 α only contains one transactivation domain (TAD) followed by a leucine zipper domain, HIF-1 α and HIF-2 α contain an N-terminal (NTAD) and a C-terminal (CTAD) transactivation domain for recruitment of transcriptional coactivators. The CTAD contains an asparagine residue that can be subjected to FIH-mediated hydroxylation, leading to impaired recruitment of the transactivators CBP/p300. From (Duan, 2016)

1.1.4 Prolyl-hydroxylase domain containing proteins (PHDs)

Prolyl-hydroxylase domain containing proteins (PHDs) act as intracellular molecular oxygen sensors. In the presence of sufficient molecular oxygen and the cofactors Fe^{2+} and α -ketoglutarate, PHDs hydroxylate two proline residues within the oxygen dependent degradation domain (ODDD) of the α -subunit of HIF, leading to its pVHL-dependent subsequent degradation. The PHD family consists of four PHDs, called PHD1, PHD2, PHD3 and PHD4 (Bruick and McKnight, 2001; Epstein et al., 2001; Koivunen et al., 2007; Oehme et al., 2002). While the latter is bound to the membrane of the endoplasmic reticulum and its functions are only poorly understood, PHD1-3 have been characterised much more extensively (Table 1.1). They all share a similar domain structure but show differences in tissue expression pattern (Lieb et al., 2002), localisation within the cell (Metzen et al., 2003), protein stability and HIF- α target specificity (Appelhoff et al., 2004; Berra et al., 2003; Huang et al., 2002). PHD2 and PHD3 expression is upregulated during hypoxia, representing a negative feedback-loop allowing for rapid HIF- α destabilisation upon reoxygenation (Berra et al., 2003; Marxsen et al., 2004; Minamishima et al., 2009; Pescador et al., 2005). PHD2 has been described to be the main PHD controlling HIF-1 α stability and levels in normoxia (Berra et al., 2003).

Table 1.1: Comparison of the members of the prolyl hydroxylase family

	<i>PHD1</i>	<i>PHD2</i>	<i>PHD3</i>	<i>reference</i>
<i>alternative names</i>	HPH3	HPH2	HPH1	(Bruick and McKnight, 2001)
	EGLN2	EGLN1	EGLN3	(Epstein et al., 2001)
			SM-20	(Wax et al., 1994)
<i>localisation</i>	nucleus	cytoplasm	nucleus, cytoplasm	(Metzen et al., 2003)
<i>predominant form in</i>	testis	-	heart, liver	(Lieb et al., 2002)
<i>inducible by hypoxia</i>	no	+	++	(Aprelikova et al., 2004; Berra et al., 2003; Marxsen et al., 2004; Minamishima et al., 2009; Pescador et al., 2005)

1.1.5 Hypoxia signalling and cancer

Hypoxia signalling is an important physiological process to allow the survival of cells during oxygen deprivation, as it might occur during embryonic development, wound healing and at high altitudes (Semenza, 2012a). However, the adaptive processes that are initiated through the hypoxia signalling have transforming potential (Semenza, 2012b). For instance, the resistance to cell death, angiogenesis and the glycolytic switch are all hallmarks of cancer (Figure 1.3). Accordingly, HIF-1 α and HIF-2 α have been shown to be overexpressed in many human cancers (Talks et al., 2000) and can serve as negative prognostic marker in different cancers (Rankin and Giaccia, 2008). HIF- α overexpression does however not always correlate with the present oxygen levels (Mayer et al., 2008). In this context, Otto Warburg found already almost 100 years ago that cancer cells were highly glycolytic even in the presence of oxygen (Warburg et al., 1927) and hypothesised that the metabolic reprogramming was sufficient to cause cellular transformation (Warburg, 1956).

In the case of clear cell renal cell carcinoma (ccRCC) the loss-of-function of the ubiquitin E3 ligase pVHL is responsible for stabilised HIF- α and sustained hypoxia signalling (Maxwell et al., 1999). However in most other cancer types, it remains unexplained how the HIF- α expression is inappropriately upregulated. The gain or loss of post-translational modifications (PTMs) of HIF- α and other proteins of the hypoxia signalling pathway have the potential to modulate the canonical signalling pathway and could cause the deregulation.

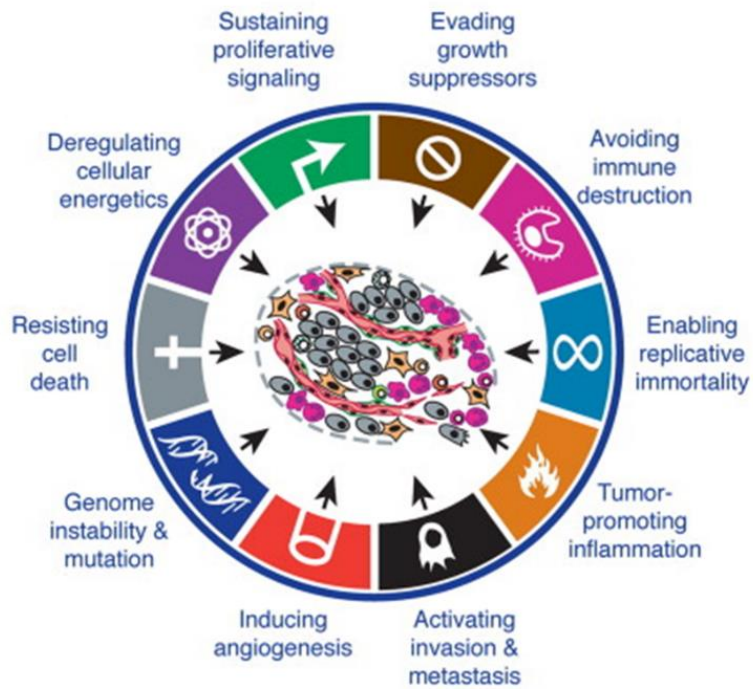


Figure 1.3: Hallmarks of cancer. Properties of cancer cells that are required for malign transformation and cancer progression. From (Hanahan and Weinberg, 2011).

1.2 PTMs and deubiquitinases

Post-translational modifications (PTMs) of proteins are the covalent and in most cases reversible attachment of a small functional group to a target protein. A PTM can alter the protein's enzymatic activity, localisation, stability, and/or interaction with other proteins. Therefore, these non-genetically encoded modifications that are mainly carried out by enzymes, add to the complexity of the proteome as they can ascribe different functionalities to the same gene product. Common PTMs include among others phosphorylation, acetylation and alkylation as well as the covalent linkage of fatty acids, saccharides or small proteins such as ubiquitin and SUMO (small ubiquitin related modifier) to the target protein (Ribet and Cossart).

1.2.1 PTMs in hypoxia signalling

Most proteins of the hypoxia signalling pathway are known to be subjected to post-translational modifications that modulate their function. Apart from being poly-ubiquitinated by the canonical regulator pVHL after PHD-mediated prolyl-hydroxylation, HIF-1 α and HIF-2 α are also ubiquitinated by other ubiquitin E3 ligases (see 1.3.1 and 1.3.2). Furthermore, the covalent attachment of SUMO to HIF-1 α and HIF-2 α has been reported to inhibit their transcriptional activity, the underlying mechanisms however are not fully understood (Bae et al., 2004; Berta et al., 2007; van Hagen et al., 2010). Interestingly, also HIF-1 β and CBP/p300 have been shown to be modified by SUMO and SUMOylation decreased the transactivation activity of the HIF complex (Huang et al., 2009; Tojo et al., 2002). SUMOylation also affects the upstream regulator of HIF - pVHL. pVHL SUMOylation by PIASy in hypoxia has been reported to increase its stability and to inhibit its ability to target HIF- α for degradation (Cai and Robertson, 2010; Cai et al., 2010). HIF- α is also subjected to phosphorylation by various different kinases in response to various stimuli and with different functional outcomes ranging from destabilisation to enhanced transcriptional activity (Dimova et al., 2009). For example, the phosphorylation of HIF-1 α by GSK-3 β targets HIF-1 α for pVHL-independent proteasomal degradation (Flugel et al., 2007). In contrast, phosphorylation by CDK1 stabilises HIF-1 α (Warfel et al., 2013). Protein kinase CK2-mediated phosphorylation of HIF-1 α does not affect HIF-1 α protein stability but impairs its binding to HIF-1 β and hence results in decreased HIF signalling (Kalousi et al., 2010). PKA has recently shown to activate HIF-1 signalling through direct phosphorylation by protecting HIF-1 α from proteasomal degradation and by stimulating its interaction with the co-activator CBP/p300 (Bullen et al., 2016).

Taken together, it becomes clear that apart from the oxygen-dependent canonical regulation of HIF signalling, there are many more mechanisms to regulate and fine-tune the pathway to adjust the response to the cell's needs.

1.2.2 Ubiquitination

Ubiquitin is a small protein that is ubiquitously expressed in all cell types. Two of the four ubiquitin coding genes *Ubb*, *Ubc*, *RpL40* and *RpS27*, encode poly-ubiquitin which is cleaved by enzymes with deubiquitinating activity into ubiquitin monomers (Redman and Rechsteiner, 1989). Monomeric ubiquitin gets covalently attached via its C-terminal glycine-glycine motif to the active site cysteine of an E1 ubiquitin-activating enzyme in an ATP-dependent manner. From the E1 enzyme it is transferred to a cysteine of an E2 ubiquitin-conjugating enzyme and ultimately with the help of a E3 ubiquitin-ligase the ubiquitin molecule is attached to a lysine residue of the target protein (see Figure 1.4A) (Pickart, 2001). The E3 ligase is determinant for the choice of the target protein as it establishes the specific contact between the target protein and the ubiquitin-loaded E2 enzyme. While RING-type E3 ligases bind E2 and target proteins via two different domains and hence mediate their direct interaction, HECT-type E3 ligases first accept the ubiquitin from the E2 enzyme and further transfer it onto the substrate protein. Ubiquitin contains seven internal lysine residues (K6, K11, K27, K29, K33, K48, K63) that can act as ubiquitin-acceptors themselves and therefore poly-ubiquitin chains can be built up. Moreover, poly-ubiquitin can be assembled by linking ubiquitin moieties to the N-terminus of the preceding molecule in a head-to-tail manner, creating linear poly-ubiquitin chains (Kirisako et al., 2006). While mono-ubiquitination is thought to be implicated in processes other than protein degradation, poly-ubiquitination was long understood to be the key signal for protein degradation by the proteasome. More closely examined, it is the type of poly-ubiquitin chain that determines the target protein's fate (see Figure 1.4B). While K48- and K11-linked poly-ubiquitination are thought to be the main signals for protein degradation (Chau et al., 1989; Matsumoto et al., 2010), K63 chains are known to be mainly implicated in lysosomal targeting as well as DNA damage and NF- κ B signalling (Clague et al., 2012; Deng et al., 2000; Spence et al., 1995). The latter is additionally regulated by linear ubiquitin chains (Haas et al., 2009). The role of the other types of chains and of mixed chains (Figure 1.4B bottom) is much less understood, yet in several specific protein contexts some specific functions have been ascribed to some types. Whether they represent the general behaviour of the given ubiquitin modification or whether there it depends on each individual target protein and its interactors remains to be investigated (Yau and Rape, 2016).

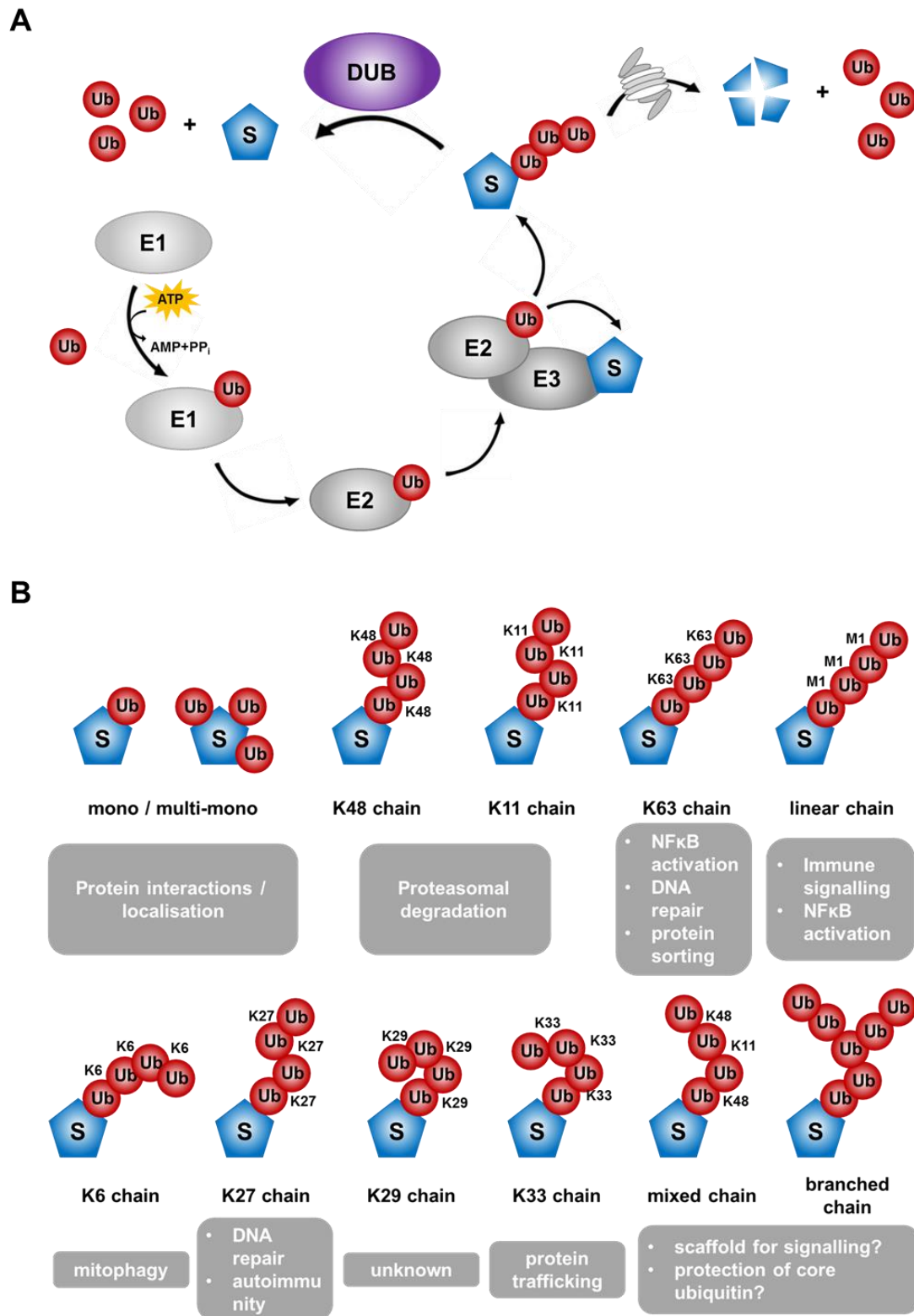


Figure 1.4: Protein ubiquitination. (A) Ubiquitin (Ub) is activated by the ATP-dependent covalent attachment to an E1 activating enzyme. Ubiquitin is then transferred to an E2 enzyme from where the ubiquitin is directly or indirectly transferred to a substrate protein (S) with the help of an E3 ligase. (Poly-) ubiquitinated substrate can either be degraded by the proteasome or the ubiquitination can be removed by a deubiquitinating enzyme (DUB). (B) Types of ubiquitin (U) conjugations to the substrate protein (S) and their functional implications (Yau and Rape, 2016).

1.2.3 Deubiquitination

Ubiquitination is a reversible process and mono- and poly-ubiquitin chains are removed from target proteins by a class of enzymes that exhibit ubiquitin-specific protease activity that allows for proteolytic cleavage of the isopeptide bonds between two ubiquitin moieties or between the target protein and the first ubiquitin molecule linked to it. The DeUBiquitinases (DUBs) are divided into families based on the sequence and fold of their catalytic site (Komander et al., 2009). The JAB1/MPN domain-associated metalloproteases (JAMMs) is the only family using a metalloprotease active site, and JAMMs are associated with the proteasome where they are responsible for the de-ubiquitination of target proteins prior to their degradation (Verma et al., 2002). All other families use a cysteine protease active site with a catalytic triad consisting of a cysteine, a histidine and an asparagine/aspartate residue. Among them, the biggest family are the ubiquitin specific proteases (USPs), currently having 56 members (Coyne and Wing, 2016). Further families are the ubiquitin COOH-terminal hydrolases (UCHs), the ovarian tumor proteases (OTUs), Machado–Joseph disease protein domain proteases (Josephins) and the most recent MINDYs (motif interacting with Ub-containing novel DUB family) (Abdul Rehman et al., 2016; Fraile et al., 2012; Komander et al., 2009). DUBs bind to their target proteins via ubiquitin binding domains such as ubiquitin-interacting motifs (UIM) and ubiquitin associated (UBA) domains. DUBs can trim poly-ubiquitin chains and remove them completely from the target protein by cleaving them one by one from the end (exo-cleavage) or by cleaving peptide bonds anywhere within the polyubiquitin chain (endo-cleavage). Furthermore, some DUBs display cleavage selectivity towards polyubiquitin chains of a certain linkage type (Komander et al., 2009).

1.2.4 USP29 (Ubiquitin-specific protease 29)

1.2.4.1 Discovery of the *Usp29* gene

The murine *Usp29* gene was discovered in 2000 by Kim et al. while looking for new genes lying in a conserved imprinted region around the *Peg3* gene (Kim et al., 2000). *Peg3* (paternally expressed gene 3) is maternally imprinted and encodes a zinc finger protein (Kuroiwa et al., 1996), which is expressed in murine brain tissue and has been shown to be required for appropriate maternal behaviour (Li et al., 1999). In 1999 the *Zim1* gene (imprinted zinc finger gene 1) was found adjacent to the murine *Peg3* gene. *Zim1* is a maternally imprinted gene and it also encodes a zinc finger protein (Kim et al., 1999). Subsequently, a third murine gene within the same region was identified and was named ubiquitin-specific processing protease 29 (*Usp29*) due to its homology with a putative yeast ubiquitin hydroxylase (Kim et al., 2000). The murine gene contains 5 exons, with the entire ORF being located in exon 5 and coding for a 869 amino acid long protein. The expression of the gene from the paternal allele was mainly detectable in adult brain, but also in testis. The human *PEG3* gene is located on chromosome 19q13.4 and is mainly expressed in the ovary and placenta (Kim et al., 1997). As in mice, the human homologue of *Usp29* was found adjacent to the human *PEG3* gene and USP29 mRNA was only detectable in adult testis, indicating a different expression pattern compared to mouse

(Kim et al., 2000). The human USP29 gene encodes a 922 amino acid long protein that shares 42.5% amino acid sequence identity with the murine homologue. However, mouse and human USP29 share the well conserved protease catalytic domain required for supposed DUB activity. This domain is split into two parts (Clague et al., 2013) with the catalytic cysteine C294 being located in the first part and the catalytic histidine 840 and asparagine 857 in the second part (Ye et al., 2009), indicating that the C-terminus needs to fold in to build up the functional catalytic site (Figure 1.5). USP29 further contains a pleckstrin homology (PH) domain as well as two ubiquitin interacting motifs (Clague et al., 2013). Interestingly bovine *USP29* RNA, even though having lost its protein coding capability due to missense mutations is still expressed in adult brain, possibly having some functions as a non-coding RNA (Kim et al., 2007).



Figure 1.5: USP29 domain structure. The N-terminal PH domain is displayed in blue. The catalytic domain (green) with its active site residues cysteine, histidine and asparagine is split into two parts with two ubiquitin interacting motifs (red) being located in between.

1.2.4.2 Imprinting and transcription of the *Peg3* domain and the *Usp29* gene

The *Peg3* domain contains seven genes, *Peg3*, *APeg3*, *Usp29*, *Zim1*, *Zim2*, *Zim3*, and *Zfp264* (Figure 1.6). These genes are controlled by five promoters of which three are differentially methylated on maternal and paternal alleles (DMR). *Peg3* and *Usp29* genes are subjected to the control of a common imprinting control region (ICR), a 5 kb long region located around the first exons of the *Peg3* and the *Usp29* genes. The DMRs are established either during oogenesis (bi-directional *Peg3/Usp29* promoter) or after fertilisation (Huang and Kim, 2009; Lucifero et al., 2004). The establishment of the methylation of the *Peg3/Usp29* DMR during oogenesis has been shown to be dependent on the transcription factor Ying Yang 1 (YY1) (Kim et al., 2009). The 7 genes are clustered on the two sides of the *Peg3* domain around a large 250 kb intergenic region, that while not containing any obvious ORF, contains 20 evolutionary conserved regions (ECRs) (Thiaville et al., 2013). One of these ECRs, ECR18 has been shown to interact with the bi-directional promoter of *Peg3/Usp29* and the *Zim2* promoter in testis and brain and to act as an enhancer. Additionally to its function in setting DNA methylation of the DMR, YY1 also seems to function as a direct transcription factor. Within the *Peg3* domain, YY1 binds to two conserved sequence elements, CSE1 and CSE2. Binding of YY1 to CSE1 seems to repress expression of both murine *Peg3* and *Usp29*. On the other hand, expression of *Peg3* but not *Usp29* is enhanced after binding of YY1 to CSE2 (Thiaville et al., 2013). Another group reported that the expression of USP29 was controlled by an enhancer element very similar to *c-myc*'s FUSE (Far Upstream *Cis* Element), which they therefore called uFUSE. FUSE binding protein 1 (FBP1) was shown to bind to the uFUSE and to activate expression of the *Usp29* gene upon its interaction with AIMP2 (p38/JTV1). Furthermore, they claim that AIMP2 translocates into the nucleus in response to oxidative stress and transactivates *Usp29* (Liu et al., 2011).

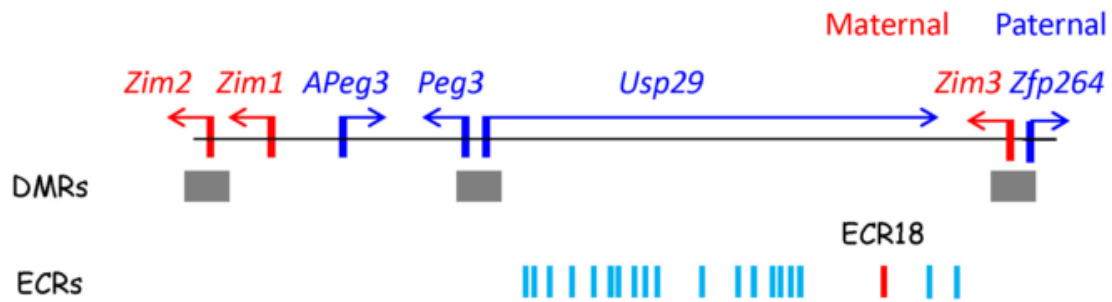


Figure 1.6: Organisation of the human Peg3 domain. The Peg3 domain contains 7 genes of which 3 are maternally (red) and 4 paternally (blue) expressed. Three differentially methylated regions (DMR) are responsible for the imprinting of the gene on either the paternal or the maternal allele. 20 evolutionarily conserved regions (ECR) spread over the central non-coding region of the Peg3 domain control its imprinting and transcription. (He and Kim, 2014)

1.2.4.3 USP29 biological functions

The first evidence of USP29's deubiquitinating activity and biological function was published in 2011 by Liu et al. They demonstrate that USP29 interacts with and stabilises the tumour suppressor p53 by de-ubiquitinating it in response to oxidative stress (Liu et al., 2011). USP29 was also shown to localise to double strand breaks in the DNA and to reverse the Rnf8-dependent "priming" mono-ubiquitination of local H2A histones. USP29 thereby prevents the recruitment and action of a second ubiquitin E3-ligase, RNF168, which is necessary for bulk histone ubiquitination, and hence focus formation and initiation of adequate DNA repair (Mosbech et al., 2013).

The checkpoint adapter protein claspin is the most recent protein that has been claimed to be regulated by USP29. Claspin is regulated by ubiquitin-dependent proteasomal degradation throughout the cell cycle and upon DNA damage and is required for checkpoint recovery. Martín et al. present data pointing to a role of USP29 in protecting claspin from destabilisation and show that USP29 is required for adequate S-phase progression (Martin et al., 2015).

1.3 Hypoxia signalling and the ubiquitin proteasome system

In the past decade it has been shown that apart from HIF- α many other members of the hypoxia signalling pathway are also regulated by the ubiquitin proteasome system (UPS). Furthermore, ubiquitin E3 ligases other than pVHL have been described to poly-ubiquitinate HIF- α . Deubiquitinases have been shown to also interfere with the hypoxia signalling pathway by reversing canonical and non-canonical ubiquitinations.

In the course of my PhD we published the Mini-Review article "*DUBs, new members in the hypoxia signalling club*" in *Frontiers in Oncology's* Research Topic "*Tumor hypoxia: Impact in tumorigenesis, diagnosis, prognosis and therapeutics*". The article summarises the current understanding, at that time, of how members of the hypoxia signalling pathway are regulated by ubiquitin ligases and deubiquitinases. Furthermore it highlights how DUBs are affected by hypoxia and where hypoxia-related DUBs have been implicated in diseases.

I drafted, wrote and revised the manuscript and answered to the reviewers in conjunction with Edurne Berra at CIC bioGUNE.

The following paragraphs 1.3.1-1.3.5 are excerpts from the article which is included in this thesis as Appendix 1.

1.3.1 DUBs in canonical hypoxia signalling

In the context of the canonical HIF signalling pathway, so far there are relatively few DUBs reported in the literature, and reports are mostly focused on the impact on HIF-1 α . USP20 (also called pVHL interacting deubiquitinating enzyme 2, VDU2) was the first DUB to be described to reverse pVHL-mediated HIF-1 α ubiquitination (Li et al., 2005). In turn, USP20 is a pVHL target (Li et al., 2002). MCPIP1 also deubiquitinates HIF-1 α to promote angiogenesis (Roy et al., 2013). In the context of ciliogenesis, USP8 has been found to bind to HIF-1 α 's PAS domain and to partially protect HIF-1 α from degradation (Troilo et al., 2014). More recently, UCHL1 has been shown to be a positive regulator of HIF-1 α protein stability acting on HIF-1 α 's ODDD (Goto et al., 2015).

Hicks et al. showed in a recent paper that Sprouty2 is a negative regulator of HIF- α , acting on the canonical hypoxia signalling pathway. Sprouty2 is associated with pVHL and destabilises HIF- α in hypoxia, presumably by mediating pVHL-dependent ubiquitination (Hicks and Patel, 2016). The same group had shown previously that Sprouty2 itself is regulated via PHD-dependent proline hydroxylation and subsequent pVHL-dependent ubiquitination and degradation (Anderson et al., 2011).

1.3.2 DUBs in non-canonical HIF signalling

Not surprisingly because of HIF's crucial role in cell fate, many more proteins have been described to be involved in the control of its stability. The heat-shock protein 90 (HSP90) that interacts with the PAS domain of HIF- α regulates its degradation in an O₂/PHD/pVHL-independent manner (Isaacs et al., 2002). HSP90 competes with RACK1 for binding to HIF- α and prevents the recruitment of the Elongin C/B Ub E3 ligase complex (Liu et al., 2007). A similar mechanism has been proposed for HIF- α activation by ErbB4 (Paatero et al., 2012). As for other HSP90 client proteins, Cullin5 also regulates HIF- α degradation independently of Elongin C/B function (Ehrlich et al., 2009). The tumor suppressors p53, TAp73 and pTEN promote the ubiquitin-mediated degradation of HIF-1 α via recruitment of the Ub E3 ligase Mdm2 (Amelio et al., 2015; Joshi et al., 2014; Ravi et al., 2000). Furthermore, Fbw7 ubiquitinates and induces HIF-1 α degradation following phosphorylation by GSK3 β (Cassavaugh et al., 2011; Flugel et al., 2012). Interestingly, this degradation can be antagonized by the ubiquitin-specific protease (**USP28**) (Flugel et al., 2012). Until now, this is the only non-canonical Ub E3-ligase-DUB pair identified for proteasomal degradation of HIF- α . HAF, the Hypoxia-Associated Factor, seems to play a dual role in the control of HIF- α stability and/or activity. While HAF acts as an Ub E3 ligase targeting HIF-1 α for degradation independently of oxygen availability, hypoxia-induced SUMOylated HAF promotes HIF-2 α transactivation

without affecting its stability (Koh et al., 2008; Koh et al., 2015). Furthermore, RNF4 controls the levels of SUMOylated HIF-2 α (van Hagen et al., 2010). **USP19** seems to be required for the hypoxic accumulation of HIF-1 α , though the effect is not dependent on its deubiquitinase activity (Altun et al., 2012). USP19 is further substrate of Siah-1 and Siah-2 Ub E3 ligases, which also control the stability of PHD1, PHD3 (Fukuba et al., 2007; Nakayama et al., 2004; Velasco et al., 2013). Thus, further studies are necessary to clarify the direct impact of USP19 in HIF-1 α ubiquitination.

The chaperone-dependent Ub ligase CHIP targets HIF-1 α but not HIF-2 α for degradation either by the proteasome or by the autophagic machinery, the second big protein degradation and recycling pathway that has been implicated in elimination of ubiquitinated HIF- α (Bento et al., 2010; Ferreira et al., 2013; Hubbi et al., 2013; Luo et al., 2010). In this regard, **Cezanne** (OTUD7B), a deubiquitinase targeting K11 Ub chains (Bremm et al., 2010), has been reported to protect HIF-1 α from lysosomal degradation. While this process is independent of HIF-1 α prolyl hydroxylation, it depends on the presence of pVHL (Bremm et al., 2014).

Calpain and the activation of the forkhead transcription factor FOXO4 destabilize HIF- α although the underlying molecular mechanisms are unknown (Tang and Lasky, 2003; Zhou et al., 2006). Further studies are also needed to characterize the role of Parkin in the regulation of HIF- α , based on its identification within the Parkin-dependent ubiquitinome by a proteomic approach (Sarraf et al., 2013). In contrast with all the previous reports, it is worth mentioning the role played by the Ub E3 ligase TRAF6. TRAF6 increases HIF-1 α , but not HIF-2 α , polyK-63 ubiquitination and protects the protein from proteasomal degradation (Sun et al., 2013).

The SUMO E3 ligase PIAS3 interacts with and stabilises HIF-1 α and HIF-1 α DM^(PP/AA) by protecting it from degradation (Nakagawa et al., 2015). However, while PIAS3 seems to SUMOylate HIF-1 α , the authors found that a catalytically inactive PIAS3 mutant was also able to increase HIF-1 dependent gene transcription, giving rise to the question of whether the SUMOylation of HIF-1 α was in fact responsible for the stabilising effect.

In addition to HIF- α stability, mRNA expression and activity of the transcriptional complex fine-tune HIF regulation. In this regard, USP52 is required for protection of HIF-1 α (but not HIF-2 α) mRNA from premature degradation and therefore allows the normal hypoxic induction of HIF-1 α (Bett et al., 2013). The case of USP52 is somewhat special as this protein although structurally related to the family of USPs, lacks the catalytic cysteine (Quesada et al., 2004). Besides protecting HIF-1 α protein from its degradation, Cezanne's catalytical activity is also required for maintaining basal levels of the E2F1 transcription factor. Moniz et al. demonstrated that E2F1 controls the expression of HIF-2 α mRNA and therefore, established an indirect role of the DUB Cezanne in HIF-2 α expression (Moniz et al., 2015).

Finally, a number of DUBs have been shown to regulate transcription factors and signaling pathways that cross-talk with HIFs likely contributing to the complexity and specificity of the cellular hypoxic response, even though they go beyond the scope of this review (Kim et al., 2015; Scortegagna et al., 2011; Zheng et al., 2014).

1.3.3 Regulation of DUBs by hypoxia

As for other enzymes, there are several possible layers of regulation of DUB activity. Next to the transcriptional regulation, the stability and translation of the mRNA can be regulated by mRNA-processing enzymes. The turnover and therefore, the availability of the mature protein can be set by a variety of post-translational modifications. PTMs can also interfere with the binding of the DUB to their target proteins or other interactors, as well as modulate reversibly and irreversibly the (auto) catalytical activity of the DUB. Hypoxia, being an extreme cellular stress condition, should be able to regulate deubiquitinating activity on all the possible different layers in order to adapt DUB functions to the cell's needs. However, the literature about the regulation of specific DUBs by hypoxia (1% O₂ if not specified differently) is still scarce and almost exclusively restricted to transcriptional regulation. For instance, the expression of USP13 is reduced upon treatment with as little as 6 h of 2% O₂ in melanoma cell lines (Scortegagna et al., 2011). The reduction of the mRNA translates also to the protein level and causes the loss of Siah2 stabilization. Similarly, in colon cancer cells hypoxia reduces USP46 mRNA and protein levels and therefore, diminishes USP46's stabilizing effect on the tumor suppressors PHLPP1 and PHLPP2, conferring to the colon cancer cells an increased paclitaxel resistance (Li et al., 2013; Wen et al., 2013). Guo et al. provide more detailed information about the hypoxia-mediated transcriptional regulation of the UCH CYLD. They suggest that the in glioblastoma cells seen decrease of CYLD mRNA and protein is due to the hypoxia-induced increase of the transcriptional repressors Snail and Hes1 (Guo et al., 2014b). In contrast, hypoxia has been shown to increase Cezanne via p38MAPK (Luong le et al., 2013).

An et al. claimed that CYLD is targeted for proteasomal degradation after interaction with the HPV E6 protein in hypoxia (An et al., 2008). This is to date the only report of a post-translational regulation of DUB activity by hypoxia. However, Lee et al. present evidence that the activity of many, if not most, DUBs depends on the redox state of the cell. They show that the catalytically active cysteine residue can be oxidized for instance by intracellular hydrogen peroxide, leading to the abolishment of the deubiquitinating activity. The inactivating oxidation can be reversed in the presence of reducing agents such as DTT or prevented by anti-oxidants (Lee et al., 2013). As hypoxia and mitochondrial ROS production are intrinsically linked it might not be too far-fetched to propose that hypoxia directly modulates DUB activity via ROS.

More recently, Scholz et al. have added a new DUB to the small collection of deubiquitinating enzymes that are regulated by hypoxia. OTUB1 is N-hydroxylated by FIH in an O₂-dependent manner. While the OTUB1-hydroxylation does not affect its stability or activity, it affects its interaction with other proteins and activates AMPK signalling and therefore metabolic changes (Scholz et al., 2016).

1.3.4 Dysregulation of hypoxia-related DUBs in cancer (excerpt)

Given the importance of Ub-mediated changes in protein function and homeostasis, it is not by chance that the entire process is highly regulated. Disruption of the ubiquitination cycle by mutations or altered expression of specific components within the cascade has been associated with several disorders. In particular, more than 30 DUBs have been associated with cancer directly or indirectly. Both, the loss of a specific DUB activity or its hyperactivity are non-desired events if the targets are tumor suppressors or oncogenes, respectively. Recurrent mutations of DUBs are rare in cancer with only few exceptions. Gene fusions with RUNX are reported for USP42 and USP16 in hematologic diseases such as chronic myelomonocytic leukemia and acute myeloid leukemia. However, dysregulated mRNA levels of DUBs are implicated in many malignancies. Here, we will focus only on a few examples of hypoxia-related DUBs, for a more extensive overview please refer to the very comprehensive review by (D'Arcy et al., 2015).

Germline mutations of the tumor-suppressor gene **CYLD** are prevalent in familial cylindromatosis, a genetic condition that leads to predisposition for developing multiple skin tumors (Bignell et al., 2000; Takahashi et al., 2000). In addition, CYLD deubiquitinating activity has been seen to be abolished in different cancers on the protein level by inactivating phosphorylations or destabilizing polyubiquitination (Massoumi, 2011). More recently, it has been reported that **USP8** is frequently mutated in adenomas causing Cushing's disease (Reincke et al., 2015).

USP28 is a DUB whose overexpression has been reported in breast and colon cancer, and glioblastoma (Popov et al., 2007; Wang et al., 2015b). A recent publication has proposed USP28 to be a potential predictive marker in bladder cancer, as they found correlation of USP28 with tumor histological grade, clinical stage, recurrence and survival (Guo et al., 2014a). Similar to USP28, **UCHL1** has also been proposed to be a useful biomarker, being overexpressed in gastric cancer (Gu et al., 2015) and in myeloma (Hussain et al., 2015), and epigenetically down-regulated in colorectal cancer (Abdelmaksoud-Dammak et al., 2015). As mentioned above, downregulation of **USP46** may serve as a biomarker of resistance to chemotherapy in colon cancer (Wen et al., 2013). Finally, despite being inconsistent to its role in the regulation of HIF-1 α and HIF-2 α , decreased **Cezanne** expression is associated with the progression and poor prognosis in hepatocellular carcinoma (Wang et al., 2015a).

1.3.5 DUBs as druggable targets for therapy

Modulators of individual UPS components are emerging as a novel class of anti-cancer drugs. The initial research focus had been directed towards targeting the proteasome, with activity described for many compounds with proteasome inhibitory activity including bortezomib. Because Ub E3 ligases provide substrate specificity, their direct targeting may avoid the deleterious side effects associated with the global inhibition of the proteasome, making them interesting candidates as drug targets. Nutlin-3 and JNJ-26854165 are classic examples directed

against the Ub E3 ligase MDM2 and are currently undergoing clinical evaluation as anticancer therapy.

Newly arising, DUBs may serve as equally or more useful targets. Indeed, DUBs are highly specialized and evolutionary linked to proteases, a typified pharmaceutical target class for drug discovery thanks to their well-characterized catalytical domain. Several partial and specific inhibitors against a small number of DUBs have been developed, have proved active in preclinical studies as reviewed recently by (D'Arcy and Linder, 2014) and provide feasibility for targeting these enzymes for anticancer purposes. Among them, HBX 41,108 is a partially-selective USP inhibitor because it inhibits USP5, USP7, USP8, UCHL3 in addition to caspase 3 (Colombo et al., 2010). This is to our knowledge the only DUB inhibitor so far described as targeting one of the DUBs linked to the HIF signaling pathway. Interestingly, inhibition of USP8 suppresses growth of gefitinib-resistant non-small cell lung cancer cells, though no link to the potential impact on HIF-1 α is reported (Jeong, 2015). It is tempting to speculate about new drugs directed against hypoxia-related DUBs that succeed to fight intratumoral hypoxia-signaling in the coming years.

1.4 How to investigate signalling pathways

The discovery of how signalling pathways work, that is how a stimulus is sensed by a receptor, how the message is transduced to an effector molecule and how the effector molecule executes its function, is key to understanding how alterations of a particular pathway can cause diseases and how to potentially treat them. Hence, various different techniques are used to identify the proteins involved, and unravel the mechanisms of the individual steps of the signal transduction.

Classical biochemical approaches are the standard and often the starting-point of the investigations. Western Blotting, immunoprecipitation, qPCR and reporter gene assays allow us to measure how protein levels and their modifications are affected by different stimuli, whether proteins are associated with each other in the cell, whether gene transcription is altered and to what extent the signal is transduced, respectively. Those assays give us very valuable data, however the collected data represents averaged results as they come from a bulk of cells, which might display significant heterogeneity in the individual response to the stimulus.

New single-cell techniques are already available and are being further developed in order to address this problem. The transcriptome of a single cell can now be examined by RNA sequencing (Wu et al., 2014) and while technically more challenging, the development of single cell proteomics methods are also on the rise (Lombard-Banek et al., 2016).

Bioinformatics have also become an important part of the analysis of signalling pathways. They are not only needed for the analysis of *omics* data for example, but can also simulate and predict signalling processes based on acquired data or on publicly available data sets or a combination of both.

Fluorescence-based single cell techniques require the labelling of the object of interest with a fluorescent label. For example, Fluorescence-Activated Cell Sorting (FACS) allows for

separation of living single cells depending on the presence of a fluorescence-labelled marker. Fluorescence imaging methods allow us to follow labelled proteins (or other structures) in single living cells over time and to study their spatial and temporal dynamics non-invasively in a way that no other technique is able to. Furthermore, the measurement of fluorescence is practically harmless to cells and can be easily quantified by intensity measurements. Apart from localising fluorescence-labelled proteins and determining their abundance, fluorescence imaging techniques allow us to measure their diffusion dynamics and their interaction.

1.4.1 Fluorescence and fluorescence lifetime

Fluorescence is the property of a molecule to absorb light of a certain wavelength and to emit a photon of a longer wavelength (Stokes, 1852). Both, the optimal absorption and emission wavelength, are determined by the atomic configuration of the fluorophore. If the incident photon carries the appropriate energy ΔE ($\Delta E = h \nu$, with ν being the frequency of the incoming wave), it can cause an electron to move from its energetic ground state S_0 to its first excited state S_1 (Figure 1.7A). From the excited state, the electron has several possibilities to relax back to the ground state, with the rates k of each possibility being intrinsically linked to the fluorophore's electronic configuration. Either the electron relaxes back by emitting a photon (fluorescence) (Figure 1.7A) or it changes into a "dark" excited triplet state via intersystem crossing (ISC) from where it can later relax back to the ground level emitting a phosphorescent photon. The rates of the different relaxation processes determine for how long a molecule stays in its electronically excited state. This time - the fluorescence lifetime - is characteristic of a given fluorophore and is independent of excitation wavelength, excitation rate and fluorophore concentration. Importantly, the fluorescence lifetime can be quantitatively measured experimentally. Two different methods, time domain and frequency domain measurements that require different instrumentation and analyses, are available to measure fluorescence lifetimes.

In the time-domain method (Figure 1.7B), a pulsed laser with optimally infinitely short laser pulses is used to excite the fluorophore. Excited fluorophores emit photons whose arrival times (typically in the range of a few nanoseconds) are recorded by time-correlated single photon counting (TCSPC) and plotted in a histogram. The fluorescence lifetime τ is then extracted by fitting the decay curve to a mono- (or multi) exponential decay function $I(t) = I_0 e^{-t/\tau}$, with $I(t)$ being the number of photons with the same arrival time t , and I_0 being an exponential prefactor.

The frequency-domain method relies on a continuous but intensity-modulated excitation source (Figure 1.7C). The fluorescence emission is equally modulated, but phase-shifted because of the delay between fluorophore excitation and photon emission - the fluorescence lifetime. The fluorescence lifetime of a given fluorophore can be altered by environmental conditions such as pH or viscosity of the medium, as well as by the presence of fluorescent and non-fluorescent quenchers (Lakowicz, 2006).

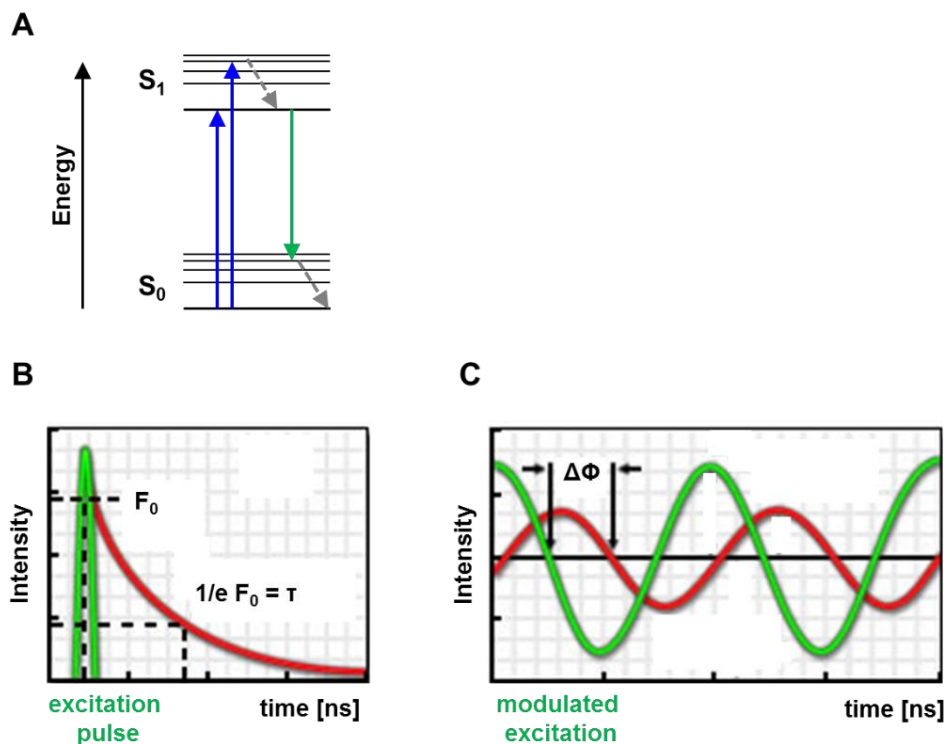


Figure 1.7: Fluorescence and fluorescence lifetime measurements. (A) Jablonski diagram: Absorption of light of a suitable wavelength (and energy) lifts the absorbing molecule into an electronically excited state (blue). The molecule relaxes back to the ground state by emitting a photon (fluorescence) (green). Grey arrows indicate non-radiative vibrational relaxation. (B): Time-domain method to measure fluorescence lifetime. After a short excitation pulse (green), emitted fluorescent photons (red) are recorded and fluorescence lifetime τ is extracted from the decay curve. C: Frequency-domain method to measure fluorescence lifetime. Excitation intensity (green) and accordingly the fluorescence emission (red) are modulated. The phase shift $\Delta\Phi$ between the two curves allows for extraction of the fluorescence lifetime τ . B and C adapted from <http://www.olympusmicro.com/primer/techniques/fluorescence/fret/fretintro.html>.

1.4.2 Förster resonance energy transfer (FRET)

In 1948, Theodor Förster explained the decrease of fluorescence in a concentrated fluorophore solution by the non-radiative energy migration from an excited fluorophore to another identical fluorophore in close proximity, which subsequently emits a fluorescent photon (Förster, 1948). The efficiency of the energy transfer is strictly dependent on the distance between donor and acceptor molecule as it decreases with the factor r_0^{-6} , with r_0 being the Förster radius that is specific to the donor-acceptor pair. This energy transfer is possible not only between identical fluorophores (homo-FRET), but also between two different fluorophores with distinct spectral properties (hetero-FRET or just FRET) (Figure 1.8A). The electronically excited molecule couples via dipole and spin moments with the acceptor molecule and transfers its energy non-radiatively, thereby relaxing back to the electronic ground state. For the energy transfer to be possible, the emission spectrum of the donor fluorophore must have significant overlap with the absorption spectrum of the acceptor. In case that sufficient overlap exists and both fluorophores are in close spatial vicinity (around r_0), FRET can occur and excitation of the donor results in fluorescence emission of the acceptor (Figure 1.8B). Therefore, FRET measurements can

provide information about optically not resolvable distances between a given donor-acceptor (or: FRET-) pair in the low nm range. In molecular biology, two proteins within these distances are typically directly interacting with each other, hence biologists have come up with different techniques to measure FRET between two fluorescence-labelled proteins in cells.

Classically, FRET efficiencies were calculated based on the fluorescence intensities of donor and acceptor fluorescence after excitation of the donor molecule: FRET efficiency $E = \frac{I_{\text{Acceptor}}}{I_{\text{Donor}}}$. Fluorescence intensities measured by this method were highly dependent on concentrations of both, donor and acceptor molecules. Additionally, the necessary overlap of donor absorption and acceptor emission spectra can cause direct excitation of the acceptor fluorophore by the donor excitation. This phenomenon, called spectral bleed-through, leads to the overestimation of the effective FRET efficiency. Therefore, in recent years the measurement of the fluorescence lifetime of the donor fluorophore has proved to allow more accurate determination of the FRET rate. Additionally, the choice of the FRET acceptor is less restricted as even a “dark” molecule, a quencher, can be used if it has the appropriate spectral properties in order to accept the energy transfer from the donor molecule.

Apart from determining intermolecular distances and hence binding, FRET measurements are also used for sensing intracellular molecules, such as calcium and ATP for example. FRET-based biosensors consist of the donor and the acceptor fluorophore, which are separated by a domain that can bind the molecule to be sensed (Hochreiter et al., 2015). Upon binding of the target molecule, this domain undergoes conformational rearrangements, which result in a change of distance between donor and acceptor and therefore in a change of donor fluorescence lifetime.

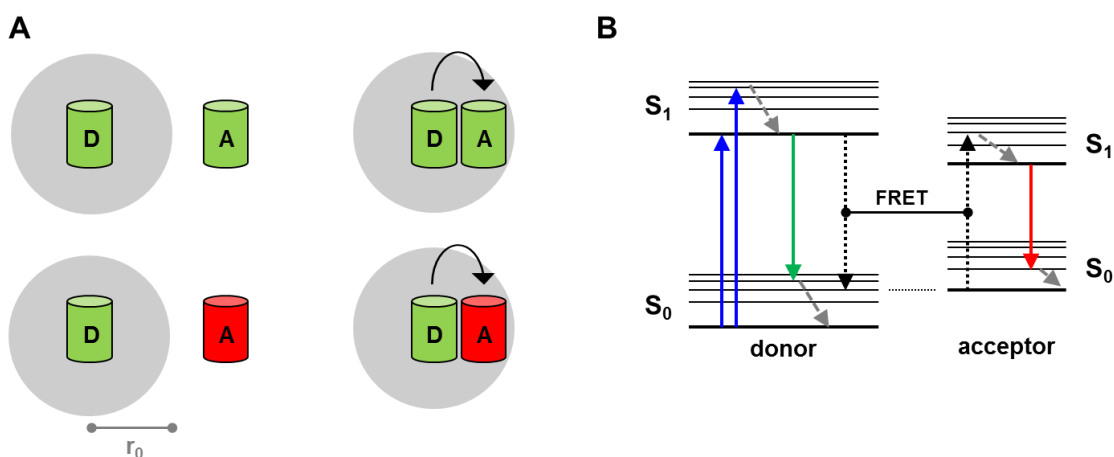


Figure 1.8: Förster Resonance Energy Transfer (FRET). (A) FRET can occur only when donor (D) and acceptor (A) fluorophore are within the distance of the Förster radius r_0 (grey). Homo-FRET occurs between two identical (top) and hetero-FRET between two different molecules with appropriate spectral overlap (bottom). (B) Jablonski diagram of FRET. After absorption of a photon (blue), instead of emitting a fluorescent photon (green), the excitation can be transferred non-radiatively via FRET (black) to an appropriate nearby acceptor molecule which consequently emits a fluorescent photon (red).

1.5 Aims of the project

In many diseases, including cancer, the hypoxia signalling pathway has been found deregulated and signalling switched on permanently (Rankin and Giaccia, 2008; Semenza, 2012b). While in the specific case of renal cell carcinoma the loss of pVHL is responsible for the sustained HIF signalling, in most cases the underlying molecular mechanisms remain poorly understood (Mayer et al., 2008). However, as many of the members of the pathway are known to be regulated by PTMs, it is tempting to speculate that alterations in the PTM profiles may cause the excessive signalling, either by up-or down-regulating the physiological modifications or by adding new modifications.

Hence, we hypothesised that cellular transformation might cause alterations of the PTMs of proteins of the hypoxia signalling pathway that result in abnormal signalling behaviour. The identification and characterisation of such aberrant modifications and the responsible regulators could help find new therapeutic approaches to modulate nonphysiological signalling.

The project plan was to first identify novel regulators of hypoxia signalling and to characterise the effect of the potential regulators on their respective target proteins on a molecular level. Next, we wanted to generate mutants that were either resistant to or would mimic the regulation. Further, the properties and down-stream effects of those mutants were to be characterised. A combination of biochemical assays in Edurne Berra's lab at CIC bioGUNE (Spain) and advanced fluorescence microscopy techniques in Violaine Sée's lab at the Centre for Cell Imaging (UoL) was used for this purpose.

First of all, we needed to generate fluorescent versions of the proteins of interest and validate them for live cell imaging purposes and advanced imaging techniques for later use were to be set up (described in chapter 3). An siRNA-based screen that had been performed in Edurne Berra's lab prior to my start had highlighted the deubiquitinase USP29 as a potential HIF regulator. We initially tested this hypothesis and established the role of USP29 as a novel non-canonical activator of HIF- α and characterised the molecular basis of the regulation (chapter 4, including a submitted manuscript). We then further characterised the USP29 protein itself, by investigating its own post-translational regulations and its interactome (Chapter 5, including a manuscript in preparation).

Chapter 2: Materials and Methods

2.1 Materials

All tissue culture media were purchased from Gibco. Chemicals were purchased from Sigma-Aldrich unless stated otherwise. Custom oligo primers were purchased from Invitrogen and Sigma-Aldrich, siRNAs were bought from Sigma-Aldrich.

2.2 Methods

2.2.1 Molecular Biology

2.2.1.1 Polymerase chain reaction (PCR)

Polymerase chain reaction is used to exponentially amplify double-stranded DNA from a single- or double stranded DNA template. The introduction of point mutations, restriction enzyme sites and flanking sequences is possible by adequate modification of the primers used for the amplification. Primers anneal to complimentary target DNA and allow the DNA polymerase for elongation thereby copying the target sequence.

DNA was amplified via PCR using KOD Hot Start DNA Polymerase (EMD Millipore). After an initial denaturation step for 5 minutes at 95°C, 30 cycles using the following scheme were performed: 1. denaturation: 95°C for 20 seconds, 2. annealing: primer-dependent temperature T_m for 15 seconds, 3. Elongation: 70°C for 30-90 seconds (depending on length of the DNA).

2.2.1.2 Mutagenesis

Stratagene's QuikChange® II XL Site-Directed Mutagenesis Kit (Agilent Technologies) was used to introduce single or multiple point mutations. The mutations were introduced by amplification of 100 ng of template DNA with 0.25 μ M forward and reverse primers (Table 2.1), in the presence of 1x reaction buffer, 6% (v/v) Quick solution®, 0.1 mM dNTPs with 1.25 units PfuUltra HF DNA Polymerase. After cycling (1 min 95°C, 18x (50 seconds 95°C, 50 seconds 60°C, 7 minutes 68°C), 7 min 68°C) template DNA was digested with 5 units of DpnI for 1h at 37°C and subsequently one sixth of the reaction was transformed into competent XL10-Gold (Agilent Technologies) cells.

Table 2.1: Primers used for site-directed mutagenesis

mutation	Primer sequence (5')
USP29 C294S	F: cccaatttgggaaacaccagttacatgaatgcagttttac R: gtaaaactgcattcatgtaactggtgtttcccaaattgggg
USP29 siResistant	F: gaaagcaggaatatgctcaagagattgacaaaacttcattttacgc R: gcgtaaaatgaagttttgtcaatctctttgagcatattcctgctttc
USP29 K127R	F: gaaagcaggaatatgctgagggaaattgacaaaacttc R: gaagttttgtcaatttcctcagcatattcctgctttc
USP29 K599R	F: cgttgaaccagacaggaatgccgacctac R: gtagtcggcattcctgtctggttcaacg
USP29 K668R	F: gtatgaagatggagggaggctgatcagcagc R: gctgctgatcagcctccctccatctcatac
HIF-1 α K752/755/758R	F: catcactttcttgagacgtgtaagaggatgtagatctagtgaacag R: ctgtcactagatctacatcctcttacacgtctccaagaaagtgatg

2.2.1.3 Restriction digestion

Restriction enzymes can be isolated from bacteria and cut DNA at specific 4-8 bp long palindromic sequences, creating either blunt ends or ends with overhangs. DNA was incubated with the restriction enzyme(s) of choice (1 μ l / 1 μ g of DNA) in appropriate buffer for at least 1 hour at 37°C and DNA fragments were separated by size on 1% agarose gels containing SYBR® Safe DNA Gel Stain that allows for visualisation of the bands under UV exposure.

2.2.1.4 Gateway® Cloning

At the beginning we used the two-step Gateway® system (Invitrogen™) to readily generate fluorescent fusion proteins with the fluorescent protein being fused either to the N- or the C-terminus of the protein to be tagged. As the first step, the coding sequence of the protein was amplified by PCR including specific attB flanking sequences. The λ -phage derived enzyme BP-Clonase™ II then inserted the PCR product into the entry vector pG-DONR/Zeo through a recombination process via the attB sites in the PCR product and the attP sites in the entry vector. The entry clone was transformed and the purified plasmid DNA served as the donor for the second recombination reaction. LR Clonase™ II catalysed the recombination between the newly generated attL sites of the entry clone and the attR sites of any destination vector that contained the coding sequence of a fluorescent protein 5' or 3' of the attR sites. Thus, an

expression vector containing the coding sequence for a chimeric fluorescent protein was generated. All unwanted by-products of the BP and the LR reaction were dismissed during the transformation procedure as they contained the *ccdB* gene that is toxic for the used *E. coli* strain (DH5 α). BP and LR reactions were performed following the supplier's protocol. For BP and LR reactions 150 ng of entry vector or destination vector and equimolar amounts of PCR product or entry clone, respectively were used and the reaction was incubated at 25°C overnight. Proteinase K was then added and incubated at 37°C for 10 min prior to transformation of a total amount of 2-5 ng DNA into chemically competent DH5 α .

2.2.1.5 In-Fusion® HD Cloning

In-Fusion® HD Cloning (Clontech) was used to quickly transfer a fluorescent label into expression vectors or inserting ORFs behind or in front of a fluorescent label. As it is a one-step reaction and practically all vectors and inserts can be used, this method is quicker and more convenient than the Gateway® Cloning. The destination vector was linearised by single or double digestion or by PCR and the insert was amplified by PCR using specific primers creating overhangs that were complimentary to the vector backbone at the site of insertion. Next, linearised vector and PCR product were gel-purified with a gel purification kit (Macherey-Nagel) and the In-Fusion® reaction was set up with an insert:vector-ratio of 2:1. Of the 1:10-diluted In-Fusion reaction 2.5 μ l were transformed into 50 μ l competent Stellar™ cells.

2.2.1.6 Plasmid propagation

Amplification of circular plasmid DNA was carried out by transforming the DNA into chemically competent *E. coli* DH5 α (Invitrogen™), XL10-Gold (Agilent Technologies) or Stellar™ (Clontech) cells. Therefore the plasmid needed to contain a bacterial origin of replication and an antibiotic resistance for selection purposes. 2-5 ng of plasmid DNA were incubated with 50 μ l of competent bacteria for 30 min on ice. Bacteria were then heat-shocked in a 42°C waterbath for 45 seconds and after 2 minutes on ice, 450 μ l of SOC-medium was added. Bacteria were allowed to grow for 1 hour at 37°C in a shaker (225 rpm) before plating 50 and 300 μ l onto LB plates containing the selection antibiotic (50 μ g/ml kanamycin or 100 μ g/ml ampicillin). Plates were incubated overnight at 37°C and single colonies were picked and inoculated into 5 and 200 ml of antibiotic containing LB-medium for minicultures and maxicultures respectively and allowed to grow for 16 hours. The GeneJET Plasmid Miniprep Kit (Thermo Fisher Scientific) and the PureLink® HiPure Plasmid Maxiprep Kit (Invitrogen™) or the QIAGEN Plasmid Maxi Kit were used for plasmid purification from mini- and maxicultures, respectively.

All sequences were verified by sequencing with appropriate primers either by STABvida or by GATC Biotech.

2.2.2 Cell Culture and transfections

HEK293T cells were cultured in DMEM + GlutaMAX™ supplemented with 5 % FBS at 37°C and 5 % CO₂. Sub-confluent plates were trypsinised and cells for experiments were plated at a density of 27 000 cells/cm².

HeLa and PC3 cells were cultured in DMEM + GlutaMAX™ supplemented with 10 % FBS and SK-N-AS cells with additionally 1 % non-essential amino acids. A2780 and LNCaP were cultured in RPMI + GlutaMAX™ supplemented with 10 % FBS and MDA-MB-231 and SH-SY5Y cells were cultured in DMEM:F12(1:1) + GlutaMax supplemented with 10% FBS. For experiments all cell lines were trypsinised and plated at 30 000 cells/cm².

The next day, cells were transfected using Lipofectamine® 2000 (Thermo-Fisher Scientific) at a Lipofectamine:DNA ratio of 2:1 using Opti-MEM medium. With the exception of the HEK293T cells, the medium was changed 6 hours after transfection. Lysis was done 24 hours post-transfection and cells lysates were further processed for Western Blot or pull-downs.

For cell imaging experiments, HeLa cells were plated at 10 000 cells/cm² and transfected the following day using FuGENE® 6 (Promega) at a ratio FuGENE:DNA of 2:1. Cells were imaged 24h post-transfection.

2.2.3 RNAi

In order to silence the expression of endogenous or overexpressed proteins, cells were silenced with 20 nM siRNAs (Table 2.2). The first transfection of the siRNAs with Lipofectamine® 2000 (3 µl Lipofectamine® 2000 per 3.5 cm dish) was made in suspension at the moment of plating, 24 h later the cells were transfected again with the siRNAs (and eventually with the corresponding DNA) after a medium change. Cells were analysed 48h after the first transfection.

Table 2.2: sequences of siRNA

siRNA	siRNA sequence
siControl	5'- CCUACAUCCCGAUCGAUGAUGdTdT
siDDB1	5'- UAACAUGAGAACUCUUGUCdTdT (Li et al., 2006)
siFbw7	5'- CGGGTGAATTTATTCGAAAdTdT (Zhao et al., 2010)
siHIF1 α	5'- AAAGGACAAGUCACCACAGGAdTdT
siHUWE1	5'- GAGUUUGGAGUUUGUGAAGdTdT (Hall et al., 2007)
siMDM2	5'- GACAAAGAAGAGAGUGUGGdTdT (Wu and Leng, 2015)
siPARK2	5'- AGUGCCGUAUUUGAAGCCUCAdT (Gong et al., 2014)
siPHD2	5'- CUUCAGAUUCGGUCGGUAAAGdTdT
siVHL	5'- GGAGCGCAUUGCACAUCAACGdTdT
siRLIM	5'- GUGAGAACCUAUGUCAGUAdT (Her and Chung, 2009)
siSKP1	5'- GCAAACUACUUAGACAUCAdTdT (Chan et al., 2012)
siSTUB1/CHIP	5'- UUCGCGAUUCGAAGAGCGCUGdTdT (Maruyama et al., 2010)
siTRAF6	5'- CUGUGCUGCAUCAAUGGCAdTdT (Zhong and Kyriakis, 2004)
siTRIM28	5'-GAUGAUCCCUACUCAAGUGdTdT (Sripathy et al., 2006)
siUSP29 #1	5'- GGAAUAUGCUGAAGGAAAUdTdT (Martin et al., 2015)
siUSP29 #2	5'- GGUCACUUUCAAAUCUGGAdTdT

2.2.4 RNA extraction and quantitative PCR (qPCR)

RNA was extracted from cells using Qiagen's RNeasy Mini Kit as described in the manufacturer's protocol. 1 μ g RNA was used as template for reverse transcription with qScript™ cDNA SuperMix (Quanta Biosciences). 1/100th of the reaction was subsequently used for qPCR using specific primer sets and 0.1 μ l TaqMan® probe (Roche) per sample (Table 2.3).

Table 2.3: Primer and TaqMan® probes used for quantitative qPCR

Gene	Primers	TaqMan® probe
PARK2	F: AAAACCACCAAGCCCTGTC R: TGCGGACACTTCATGTGC	#75
TRAF6	F: TCCTCTACCAGCGCCTTG R: TGGGTCCCTTCAGAAGTTCAT	#79
MDM2	F: GACTCCAAGCGCGAAAAC R:GGTGGTTACAGCACCATCAGT	#68
STUB1/CHIP	F: AGGCCAAGCACGACAAGTA R: AAAGCTGATCTTGCCACACA	#35
DDB1	F: CCCCTCAATTCAGATGGCTA R: GGTGAGGGTGCTATTGTTGG	#64
Skp1	F: CTGAGGAGATTCGCAAGACC R: ACCACTGGTTCTCTTTGCGTA	#69
TRIM28	F: TGGTCAATGATGCCCAGA R: CTTGGTCATGGTCCAGTGC	#1
HUWE1	F: TGAATGCTCTGGCTGCATAC R: AACCCCAGGTTTAGGATCAGA	#6
RLIM	F: CCGCAAAACTCAGATGAAAAT R: CCAGTTTGTCTGACAGAGTTAAGC	#63
Fbw7	F: CCTCCAGGAATGGCTAAAAA R: AATGAGTTCATCTAAAGCAAGCAA	#78
HIF-1 α	F: TCAAGCAGTAGGAATTGGA R: CGATCATGCAGCTACTACATCAC	#66
USP29	F: GGATCTCAAGGAATGGCTGA R: TTCATCTATGATGCTCTCCTCAAT	#28
Rplp0	F: TCTACAACCCTGAAGTGCTTGAT R: CAATCTGCAGACAGACACTGG	#6

2.2.5 Immunofluorescence

HeLa cells were seeded on glass coverslips and when necessary transfected 24h prior to fixation. Then, cells were washed with PBS and fixed with 4% paraformaldehyde for 10 min at room temperature. After three washes with PBS, cells were incubated for 20 min at room temperature with 50 mM NH₄Cl to reduce autofluorescence. Next, cells were incubated with blocking buffer (1% BSA, 0.1% Triton X-100, 0.4% Tween 20 in PBS) for 20 min in order to reduce unspecific binding of the antibody. Subsequently, the coverslips were incubated with the primary antibody diluted in blocking buffer overnight at 4°C. The next day, coverslips were washed three times with PBS and incubated with the secondary antibody diluted in blocking buffer. After thorough washing the coverslips were mounted on glass slides using Fluorescence Mounting Medium (Dako).

2.2.6 MitoTracker staining

HeLa cells were seeded on glass coverslips and transfected with a plasmid of interest if desired. 24 h post-transfection cells were incubated for 30 min with 100 nM MitoTracker® Red CM-H₂XRos (Thermo-Fisher Scientific) in growth medium, washed with PBS and fixed with 4% paraformaldehyde for 15 min at room temperature. Coverslips were mounted using Fluorescence Mounting Medium (Dako) and images were taken with a fluorescence LSM (Zeiss 780) with a 100x oil immersion objective.

2.2.7 Western Blot

Cells were lysed in 1.5x Laemmli (50 mM Tris-HCl pH 6.8, 1.25% SDS, 15% glycerol), lysates were frozen, boiled at 95°C for 15 min and sonicated. Protein quantification was performed with the DC™ Protein Assay (BioRad). Between 10 and 40 µg of protein were loaded on a self-cast SDS polyacrylamide (Bio-Rad) gel (7.5 %, 10 % or 12 %) or a 4-15 % gradient gel (Bio-Rad) and migrated at 160 V for 90 min. Then, proteins were transferred in a tank blot system onto a PVDF-membrane (EMD Millipore) with 100 V for 1h at 4°C. Membranes were stained with amidoblack, air-dried, rehydrated by washing with ethanol, 2 washes with TNT (50 mM Tris-HCl pH 7.4, 150 mM NaCl, 0.1 % Triton X-100) and 1 wash with TN (50 mM Tris-HCl pH 7.4, 150 mM NaCl). The membrane was then blocked for 1 hour with 5 % milk in TN and incubated with the primary antibody (diluted in 5 % milk in TN) at 4°C overnight. After 3 washes with TNT, 1 wash with TN and a short blocking step (5 % milk in TN), membranes were incubated with the HRP-conjugated secondary antibody for 1 h. After further washing steps, home-made ECL (solution A: 100 mM Tris-HCl pH 8.5, 0.4 mM coumaric acid, 2.5 mM luminol; solution B: 100 mM Tris-HCl, 2% H₂O₂; solution A:solution B = 1:1) was incubated on the membranes for 1 min and signal was detected with Amersham Hyperfilm ECL (GE Healthcare Life Sciences).

2.2.8 Antibodies

Table 2.3: Primary and secondary antibodies and the used dilutions

Antibody	Reference	Dilution	2 ^{ndary} antibody
β -actin	Sigma A5441	1 : 50 000	mouse 1 : 20000
CAIX	clone MN75, Bayer	1 : 1 000	mouse 1 : 5000
FLAG M2-HRP	Sigma A8592	1 : 1 000	-
GFP	Roche 11 814 460 001	1 : 1 000	mouse 1 : 5000
HA	Covance 16B12	1 : 10 000	mouse 1 : 10000
HIF-1 α 2087	Home-made (Richard et al., 1999)	1 : 5 000	rabbit 1 : 5000
HIF-1 α P564OH	Cell Signaling ab8980	1 : 1 000	rabbit 1 : 5000
His	Novagen 70796-3	1 : 1 000	mouse 1 : 10000
LC-3	Cell Signaling 2775s	1 : 1 000	rabbit 1 : 5000
Myc	Cell Signaling 9B11	1 : 1 000	mouse 1 : 5000
PCNA	Chromotek 16D10	1 : 2 000	rat 1 : 5000
PHD2	Home-made (Berra et al., 2003)	1 : 1 000	rabbit 1 : 5000
Ubiquitin (P4D1)	Santa Cruz (P4D1)	1 : 1 000	mouse 1 : 5000
USP29	Abcam ab57545	1 : 5 000	mouse 1 : 5000
2 ^{ndary} antibodies	Reference		
anti-mouse-HRP	Promega W4021		
anti-rabbit-HRP	Promega W4011		
anti-Rat-HRP	Jackson ImmunoResearch		

2.2.9 Ubiquitination assay with Ni-NTA purification

Cells transfected with (His)₆-Ubiquitin and myc-HIF-1 α DM were treated with 10 μ M MG132 for 4 h prior to lysis to accumulate ubiquitinated proteins. Cells in 10 cm dishes were lysed with 5 ml lysis buffer (6 M guanidinium-HCl, 0.1 M Na₂HPO₄/NaH₂PO₄, 0.01 M Tris-HCl pH 8), sonicated to decrease viscosity and centrifuged for 15 min at 3500 rpm. Supernatant was incubated in the presence of 10 mM β -Mercaptoethanol with blocked Nickel-NTA agarose beads for 2-3 h (blocking of the beads with 0.05 % BSA in PBS overnight followed by washes with PBS). Beads were washed with lysis buffer, 3x washing buffer 1 (8 M urea, 0.1 M Na₂HPO₄/NaH₂PO₄, 0.01 M Tris-HCl pH 8, 10 mM β -Mercaptoethanol, 5 mM Imidazol), 3x washing buffer 2 (8 M urea, 0.1 M Na₂HPO₄/NaH₂PO₄, 0.01 M Tris-HCl pH 6.3, 10 mM β -Mercaptoethanol, 5 mM Imidazol) and incubated with disruption buffer (150 mM Tris pH 6.8,

6% SDS, 30% glycerol, 10% β -Mercaptoethanol, 0.2% bromphenolblue) for 1 h at 37°C. Beads were boiled for 5 min and eluted proteins were subjected to SDS-PAGE for subsequent probing with anti-myc and anti-(His)₆ antibody.

2.2.10 Ubiquitination assay with GFP-trap® pulldown

The assay has been published previously (Lee et al., 2014). Here, HEK293T cells co-transfected with FLAG-Ubiquitin and GFP-USP29 or myc-Clover-HIF-1 α DM were treated 24h post-transfection with 10 μ M MG132 for 2-4h prior to lysis to accumulate ubiquitinated proteins. Lysis was performed on ice from 3.5 cm dishes with 300 μ l lysis buffer (50 mM Tris-HCl pH 7.5, 150 mM NaCl, 1 mM EDTA, 0.5% Triton X-100, 40 mM β -Glycerolphosphate, 1 μ g/ml Leupeptin, 1 μ g/ml Aprotinin, 1 μ g/ml Pepstatin A, 7 mg/ml N-ethylmaleimide (NEM)). Lysates were centrifuged for 15 min at 13000 g at 4°C and the supernatant was diluted with dilution buffer (50 mM Tris-HCl pH 7.5, 150 mM NaCl, 1 mM EDTA, 40 mM β -Glycerolphosphate, 1 μ g/ml Leupeptin, 1 μ g/ml Aprotinin, 1 μ g/ml Pepstatin A, 7 mg/ml N-ethylmaleimide (NEM)) to reduce detergent concentration to 0.2%. The diluted lysate was incubated for 2.5h at RT with 15 μ l pre-washed GFP-traps® (Chromotek). Then, beads were washed with 500 μ l dilution buffer and subjected to 3 stringent washes in denaturing conditions with 8 M urea in 1% SDS in PBS, followed by one wash in 1% SDS in PBS. GFP-fusion proteins were then eluted from the beads by boiling 10 min in elution buffer (250 mM Tris-HCl pH 7.5, 40% glycerol, 4% SDS, 0.2% bromophenol blue, 5% β -mercaptoethanol). The eluate was migrated two times on pre-cast 4-15% Tris-glycine gradient gels and membranes were probed with anti-GFP and anti-FLAG M2-HRP antibody.

2.2.11 Co-immunoprecipitation using GFP-traps®

HEK293T cells were transfected with the GFP-tagged protein of interest and 24h post-transfection cells were lysed on ice with lysis buffer (50 mM Tris-HCl (pH 8), 120 mM NaCl, 1 mM EDTA, 1 % IGEPAL CA-630, 40 mM β -Glycerolphosphate, 1 μ g/ml Leupeptin, 1 μ g/ml Aprotinin, 1 μ g/ml Pepstatin A). Lysates were centrifuged for 15 min at 13000 g at 4°C and the supernatant was diluted with Co-IP buffer (50 mM Tris-HCl (pH 8), 120 mM NaCl, 1 mM EDTA, 40 mM β -Glycerolphosphate, 1 μ g/ml Leupeptin, 1 μ g/ml Aprotinin, 1 μ g/ml Pepstatin A) to reduce detergent concentration to 0.2%. The diluted lysate was incubated for 1h at 4°C with 15 μ l pre-washed bab-20 (Chromotek) beads for pre-clearing. The lysate was then incubated with 15 μ l pre-washed GFP-traps® overnight at 4°C. The beads were subjected to 3 washes with dilution buffer and 1 washing with PBS, before the bound protein was eluted from the beads by boiling them for 10 min in elution buffer (250 mM Tris-HCl pH 7.5, 40% glycerol, 4% SDS, 0.2% bromophenol blue, 5% β -mercaptoethanol). The eluate was analysed by Western Blot.

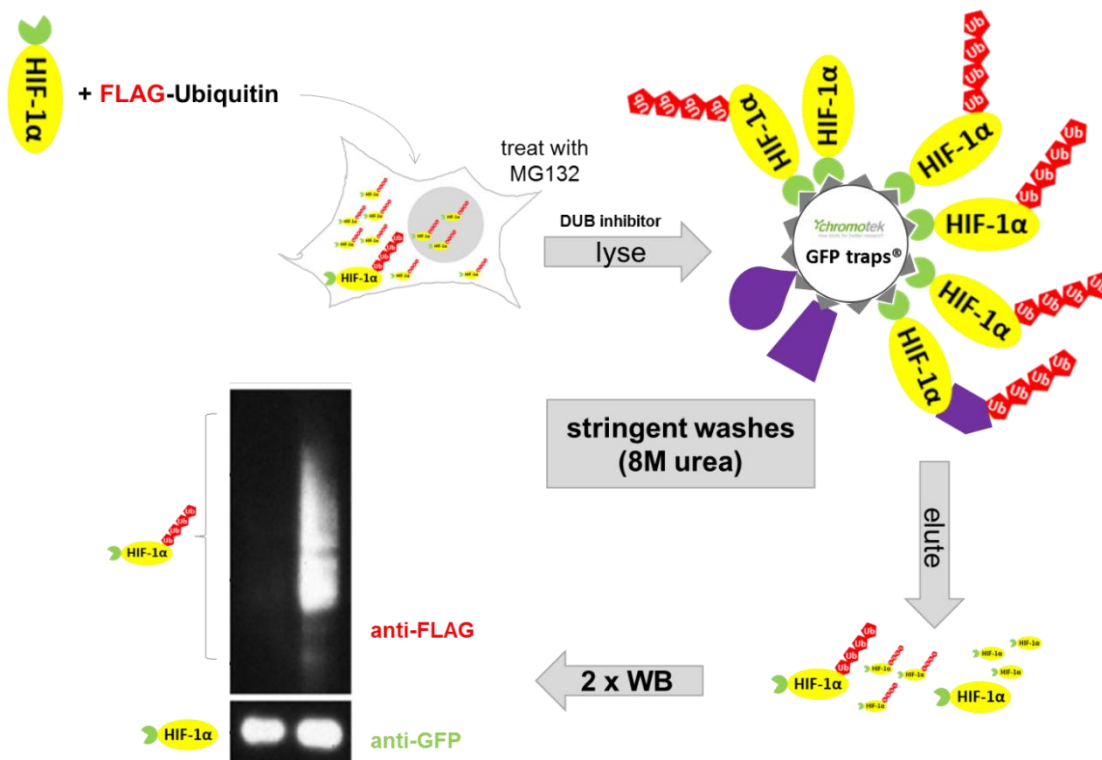


Figure 2.1: Scheme of GFP-trap® ubiquitination assay. HEK293T cells were transfected with FLAG-ubiquitin and a green-fluorescent protein-fused protein of interest (here HIF-1 α). Cells were treated with MG132 and lysed in the presence of a DUB inhibitor. The lysate was incubated with GFP-traps®. The traps were then subjected to stringent washes in order to discard proteins that bind unspecifically to the beads or are associated with the GFP-fused protein (purple). Next, the captured protein was eluted from the beads and migrated twice for detection of ubiquitinated- and non-modified protein of interest by WB with an anti-FLAG or anti-GFP antibody, respectively.

2.2.12 Size exclusion chromatography

Cells overexpressing HA-USP29 were lysed on ice with lysis buffer (50 mM Tris-HCl (pH 8), 120 mM NaCl, 1 mM EDTA, 1 % (v/v) IGEPAL CA-630, 40 mM β -Glycerolphosphate, 1 μ g/ml Leupeptin, 1 μ g/ml Aprotinin, 1 μ g/ml Pepstatin A). The lysate was centrifuged for 15 min at 13000 g at 4°C for preclearing and the pellet was discarded. The sample was then loaded onto a previously equilibrated Superdex™ 200 10/300 GL (GE Healthcare Europe GmbH) with flow buffer (50 mM Tris-HCl (pH 8), 120 mM NaCl, 1 mM EDTA) and proteins were separated via size exclusion chromatography with the biggest proteins and aggregates of such eluting first and small proteins eluting later. The eluates were collected in 24 fractions of 0.5 ml and 5% of the fractions of interest were run on SDS-PAGE and/or a in a native gel for subsequent detection of HA-USP29 by immunoblotting. A BSA solution was run on the column before and after the sample and allowed for estimation of the molecular weight in the fractions as BSA eluted in two fractions, representing dimeric and monomeric BSA.

2.2.13 Sequence alignment

Sequence alignments were performed using the website expasy.org

2.2.14 Mass spectrometry (MS) analysis

For MS analysis sample was prepared as described in 2.2.11 but scaling up to three 10cm-dishes per condition (approximately 12 mg protein) and analysed in CIC bioGUNE's Proteomics Facility. Samples were processed following both a gel-based and a gel-free strategy. On the one hand, the sample was separated by SDS-PAGE and specific bands were cut out and digested individually with trypsin. In addition to the gel-based strategy, the whole crude sample was submitted to in-solution tryptic digestion. Triplicates of each experiment were carried out. Peptides were loaded onto a nanoAcquity UPLC (Waters) coupled to an LTQ Orbitrap XL ETD (Thermo Fisher Scientific) and identified using Mascot search engine (www.matrixscience.com, Matrix Science, London, UK) with Proteome Discoverer v.1.2. software (Thermo Electron, Bremen, Germany). Proteins with a spectral-count ratio of at least 3 (including exclusive binding partners) when compared to a GFP-only control sample in at least 2 out of 3 replicates were considered to be specifically binding to the bait. STRING 10 (Search Tool for the Retrieval of Interacting Genes/Proteins) software (<http://string-db.org/>) was used to display proteins that were detected in all three replicates as functional clusters.

2.2.15 Fluorescence Imaging

2.2.15.1 Acquisition of confocal fluorescence images

Confocal fluorescence images were acquired in the Centre for Cell Imaging on the Zeiss LSM 510, 710 and 780 with the available argon and diode lasers and inbuilt detectors (Table 2.4). For optical sectioning a pinhole of one airy unit (1 AU) was chosen. The laser power was kept as low as possible to avoid photobleaching and saturation of the signal.

Table 2.4: Settings for the acquisition of fluorescence images

Fluorophore	Excitation wavelength	Emission filter
ECFP	458 nm (argon laser)	500 – 580 nm
GFP, Clover, Alexa Fluor 488	488 nm (argon laser)	500 – 540 nm
EYFP	514 nm (argon laser)	500 – 580 nm
dsRedXP, mRuby2, mCherry	561 nm (DPSS laser)	588 - 650 nm

2.2.15.2 RICS measurements and data analysis

For Raster Image Correlation Spectroscopy (RICS), HeLa cells were transfected with the expression vector of interest at least 24 hours before measurements and medium was replaced

by phenol-red free medium. RICS measurements were performed on a ZEISS LSM 710 at 37°C and 5% CO₂ with a 63x water immersion objective. Red-labelled proteins were excited with a DPSS 561-10 laser and green fluorescent proteins with the 488nm-line of an Argon laser at 0.5 – 2% excitation power. A frame of 256x256 pixels with a pixel size of 0.04 μm was recorded by scanning the sample monodirectionally with a pixel dwell time of 6.3 μs. A time series of 70 images was acquired. For RICS analysis SimFCS Software was used. A moving average of 10 frames was subtracted and the auto-correlation function was fitted on the basis of all 70 frames.

2.2.15.3 FRAP measurements

Series of images were acquired of cells transfected with a red fluorescent labelled protein prior to photobleaching with the Zeiss LSM780. Then, the fluorescence in a defined region of interest (ROI) was irreversibly destroyed by subjecting the ROI to 30 iterations of bleaching with the 561 laser line at 100% output power. Subsequently, a series of images was taken to record the red fluorescence recovery after photobleaching (FRAP) in the ROI caused by the dynamic relocation of non-bleached protein from places outside of the ROI.

2.2.15.4 FLIM-FRET measurements

Fluorescence Lifetime Imaging (FLIM) was used to measure Förster Resonance Energy Transfer (FRET). First, regular fluorescence images were taken with the Zeiss LSM780. For excitation of green fluorophores the 488nm line of the Argon laser and for red fluorophores the 561nm diode laser was used. Next, a fluorescence lifetime image of the GFP or Clover donor fluorophore in absence of any possible FRET acceptor fluorophore was acquired with the PicoQuant FLIM upgrade kit (Figure 2.2A top). After that, FLIM images of the donor fluorophore in the presence of the red-fluorescent acceptor fluorophore were acquired (Figure 2.2B top). FLIM image acquisition was carried out by scanning the sample with the LSM780 (Zeiss) scan head unidirectionally and without averaging, recording frames of 256 x 255 pixel with a pixel dwell time of 25.21 μs. Excitation of the green-fluorescent donor fluorophore was controlled by the PDL 828 "Sepia II" unit (PicoQuant) operating a 485 nm pulsed diode laser (PicoQuant) with a repetition rate of 40 MHz. The fluorescence emission was collected by the C-Apochromat 40x/1.2 W Corr M27 (Zeiss) and diverted through a 520/535 nm bandpass filter onto a Hybrid Detector PMA 40 (PicoQuant). The laser power was adjusted to obtain maximal count rate of 2000 kcounts per second (corresponding to 5% of the repetition rate) and a total of 10⁵ peak photons were collected over a time of about 3-5 min. The exact time between the excitation pulse and the arrival of a photon on the detector was recorded by the TimeHarp260 (PicoQuant) time-correlated single photon counting (TCSPC) device. In the SymPhoTime 64 Software (PicoQuant) each detected photon was plotted according to its arrival time, thereby building up a fluorescence decay curve (Figure 2.2 A and B, bottom). Together with every dataset an instrument response function (IRF) was recorded for analysis purposes (Figure 2.2C). To that end, the fluorescence lifetime of erythrosine B was quenched with a saturated potassium iodide solution to as little as 24 ps and the lifetime was measured with the same settings as the dataset (Szabelski et al., 2009). With 24 ps the quenched lifetime is shorter than the length of

the excitation pulse and therefore the measured decay represents internal properties of the instrumentation, such as the rise and length of the excitation pulse and the reaction times of the detector and the counting device. SymPhoTime 64 software (PicoQuant) controlled all PicoQuant hardware devices. At least 5 cells of each condition were measured, and experiments were repeated at least 2 times.

2.2.15.5 FLIM-FRET analysis

The SymPhoTime 64 software package (PicoQuant) was used for analysis of the FLIM data. A pseudo-coloured FastFLIM image was depicted based on the average arrival time of all photons per pixel, with red pixels representing long average lifetimes and blue pixels representing short average lifetime (Figure 2.3A). For lifetime fitting each FLIM was analysed individually. Only photons within regions of interest (ROI) were included (e.g. the nucleus) (Figure 2.3A). The decay curve was reconvoluted with the corresponding IRF to correct for instrumental resolution and fitted to a decay function (Figure 2.3B). The simplest decay is a mono-exponential decay, however as can be seen in Figure 2.3C, fluorophores do not always decay mono-exponentially, resulting in a bad fit which is represented by an oscillating residuals curve. A bi-exponential fit results in a better fit with the residuals around noise level (Figure 2.3D). The fitting equation is $I(t) = A_1 \times e^{\frac{-t}{\tau_1}} + A_2 \times e^{\frac{-t}{\tau_2}}$, with τ_1 and τ_2 being two components of the lifetime decay. The intensity based average lifetime $\tau_{Av Int}$ was extracted (Figure 2.3E) and average lifetimes for each experimental condition were calculated. When FRET occurred, there was a significant decrease of average $\tau_{Av Int}$ values in cells that contained both donor and acceptor fluorophores as compared to cells that contained donor fluorophores only.

2.2.16 Statistical tests

All experiments were performed at least three times. Origin Pro 2015 was used to calculate averages and standard deviations and to do hypothesis testing. Two different conditions were subjected to Student's T-Test and only results where their means had a 95% probability of being different were considered statistically significant ($p < 0.05$).

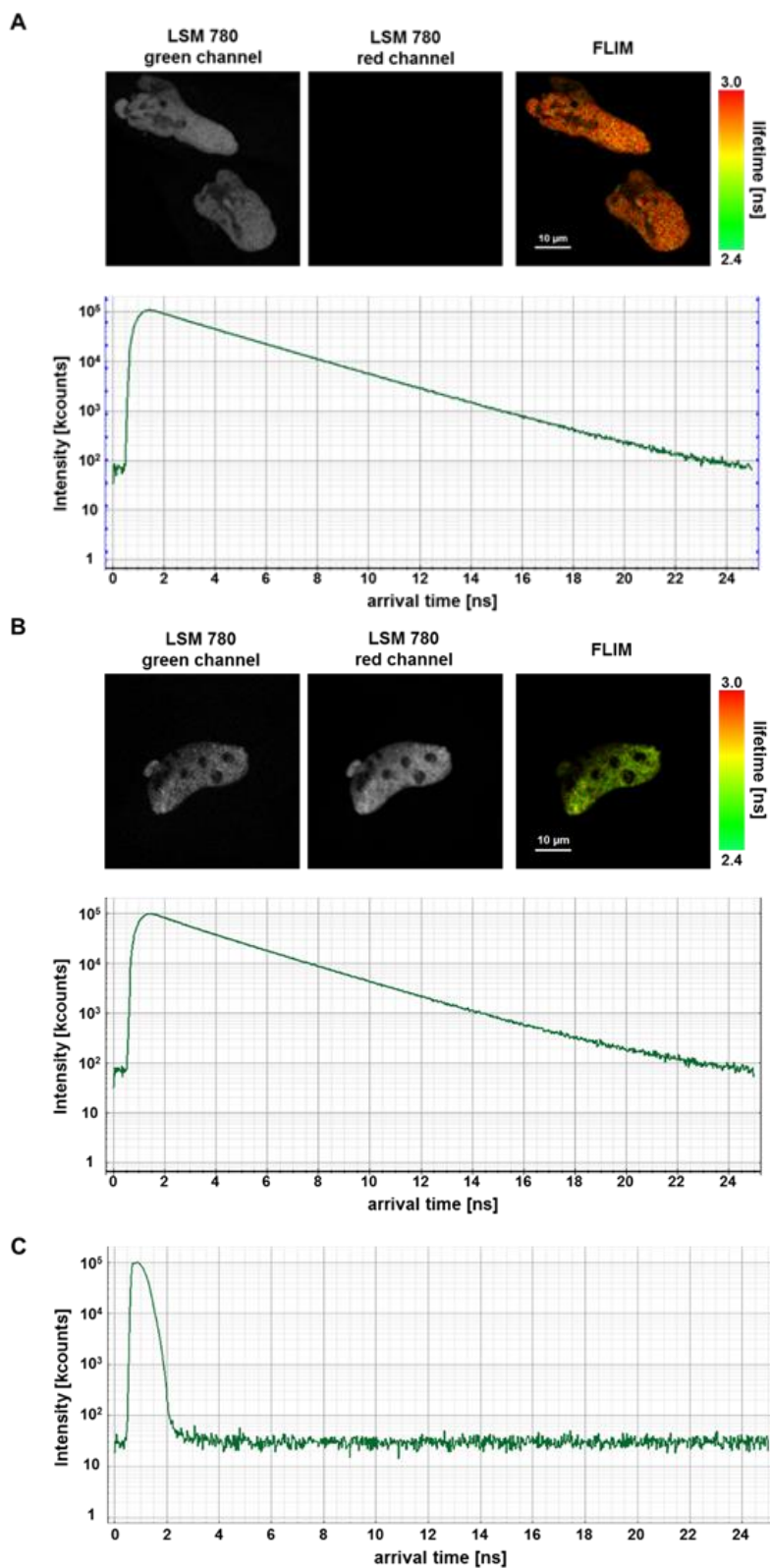


Figure 2.2: FLIM-FRET measurements. (A) Fluorescence and fluorescence lifetime images (FLIM) of a GFP-fused protein (top) and the corresponding time-correlated single photon counting (TCSPC) curve, representing a histogram of the arrival times of all collected photons (bottom). (B) same as A, but the GFP-fused protein interacts with the red-fluorescence-tagged protein. (C) The TCSPC curve of erythrosine B (in KI) represents the instruments response function (IRF).

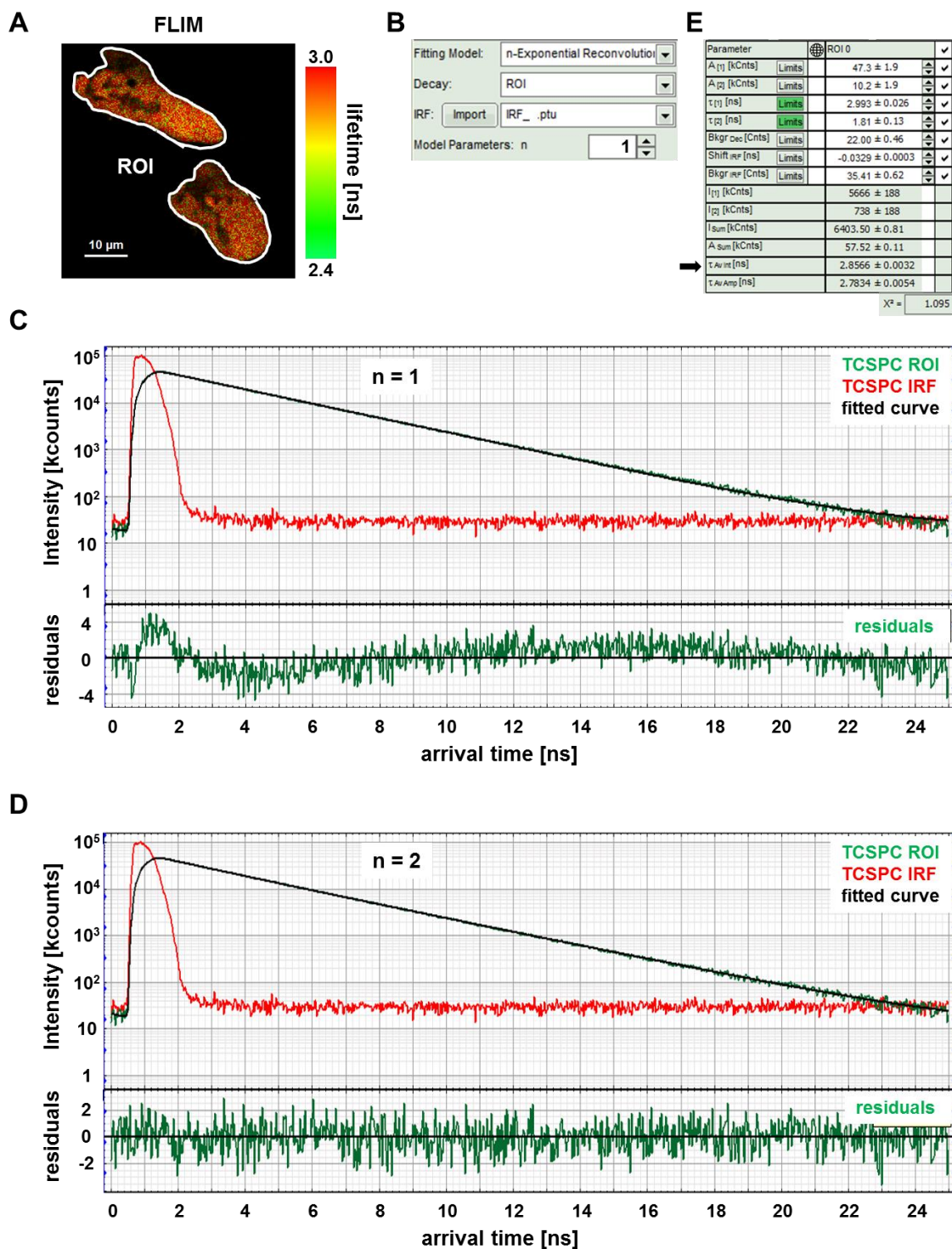


Figure 2.3: FLIM analysis. An ROI (white contour line) is defined in the fluorescence lifetime image (FLIM) (A). The setup of the fitting parameters in the SymPhoTime 64 software is shown in B. The TCSPC curve of the ROI (green) is reconvoluted with the measured IRF (red) and fitted to a mono- (C) or bi-exponential (D) decay curve. The fitted curve is shown in black and the quality of the fitting is displayed below the TCSPC curves in the residuals diagram in green. The average intensity-based lifetime $\tau_{Av Int}$ (arrow) is extracted from the fitting results window (arrow) (E).

Chapter 3: Generation and characterisation of tools for live cell imaging

3.1 Introduction

The thesis' objective was to find and characterise new regulators of hypoxia signalling. We planned to use, amongst others, fluorescence imaging techniques to explore the properties of such regulators and the molecular basis of the regulation at single cell level in living cells. To this aim, key proteins needed to be available as a fusion with a fluorescent tag. Fluorescent tags can be small organic dyes or fluorescent proteins. While organic dyes need to be taken up by the cell and then react specifically with the target protein, fluorescent proteins can be synthesized by the cell itself. Fluorescent proteins naturally occur in marine species such as jellyfish and corals and are nowadays available in all different colours. Tagging of a fluorescent protein with a protein of interest can be achieved by fusing the DNA sequences of the open reading frames (ORF) of both proteins. This construct can then be transfected into and expressed by the cells. Because fluorescent proteins are considerably bigger than organic dyes (up to 35 kDa compared to up to 1 kDa), they are more prone to interfere with the protein's functions and properties and therefore careful choice of the fluorescent protein and characterisation of the fusion protein are required.

As a starting point, work from Edurne Berra's lab was used. They had shown that PHD1 and PHD3 are SUMOylated and while SUMOylation increased the cytoplasmic population of PHD1, in the case of PHD3 it caused a decreased HIF1-dependent target gene expression. We wanted to investigate whether PHD1-SUMOylation was required for nuclear import and whether PHD3-SUMOylation altered its ability to directly bind to HIF-1 α .

This chapter summarises the efforts made to create fluorescent versions of the required proteins and to characterise and validate them. They were then used in several advanced imaging techniques, which were chosen and set-up to answer the different biological questions (3.2, 3.3). Chapter 3.4 is dedicated to the testing of the newly installed fluorescence-based FRET system, used to measure protein-protein interactions.

Furthermore, a fluorescent version of USP29, the central protein of chapters 4 and 5, was generated and validated (3.5).

3.2 Effect of PHD3-SUMOylation on HIF-1 α binding

Work by Edurne Berra's PhD student Analía Nuñez-O'Mara had shown that PHD3 was post-translationally conjugated to the small ubiquitin-like modifier (SUMO) protein, both in a cell-free *in vitro* SUMOylation system and *in cellulo*. They had found that the SUMOylation of PHD3 inhibited the transcriptional activity of HIF-1 in a prolyl hydroxylation- and degradation-independent way. However, they had been unsuccessful at clarifying whether PHD3-

SUMOylation impacted directly on its interaction with HIF-1 α . Based on this, we set out to measure this interaction depending on PHD3's SUMOylation status by Förster resonance energy transfer (FRET). Therefore, appropriate fluorescent fusion proteins of the interacting proteins were required. At the time we only had intensity-based FRET techniques at hand, which required a cyan FRET-donor and a yellow FRET acceptor, were available. For future more modern and robust FLIM-based FRET experiments a green FRET-donor and a red FRET acceptor were also necessary. Therefore, I generated in parallel both pairs for initial tests, choosing fluorescent proteins that were available in the lab.

3.2.1 Generation of fluorescent PHD3 and HIF- α DM proteins

PHD3 has been reported to localise to the cytoplasm as well as in the nucleus (Metzen et al., 2003). Moreover, two different groups have reported that PHD3 “homo-multimerises” or “aggregates” and that these complexes have biological importance as they confine PHD3 catalytic activity (Nakayama et al., 2007; Rantanen et al., 2008; Rantanen et al., 2013).

In order to see whether the orientation of the fluorescent label affected PHD3's localisation or altered its aggregation properties, dsRedXP and ECFP were N-terminally as well as C-terminally fused to PHD3 using the Gateway® system (Figure 3.1A). dsRedXP- and ECFP-fused PHD3 localised to the cytoplasm as well as to the nucleus, regardless on whether the fluorescent protein was fused to PHD3's N- or C-terminus. Small aggregates could also be found in most cells.

The Gateway® system was also used to generate N-terminal green (Clover) and C-terminal yellow (EYFP) fluorescent HIF- α DM fusion proteins. In these HIF- α double mutant (DM) proteins the two proline residues within the oxygen dependent degradation domain have been replaced by alanines (P402A and P564A), making the proteins resistant to PHD-dependent hydroxylation and subsequent degradation (Berra et al., 2003). As expected, HIF-1 α DM and HIF-2 α DM displayed nuclear localisation (Figure 3.1B), but while HIF-1 α DM was distributed homogeneously throughout the nucleus, HIF-2 α DM formed very defined speckles, as has been recently described (Taylor et al., 2016).

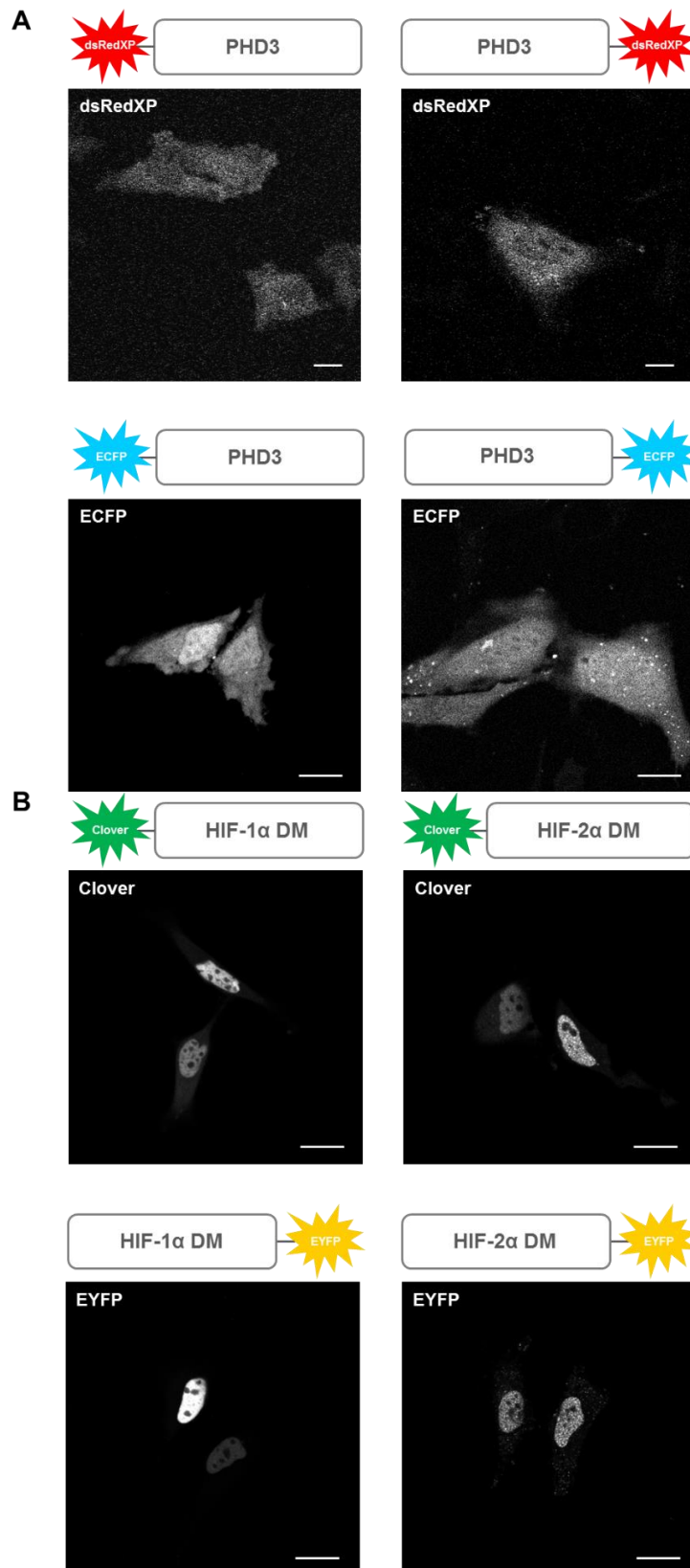


Figure 3.1: Generation of fluorescent PHD3 and HIF- α proteins. All plasmids were generated using Gateway® or In-Fusion® cloning, transfected into HeLa cells and imaged 24 h post-transfection. (A) N- and C-terminal fusions of dsRedXP and ECFP to PHD3. (B) N-terminal and C-terminal fusions of Clover and EYFP, respectively, to HIF-1 α DM and HIF-2 α DM. The scale bar is 20 μ m.

3.2.2 Validation of the differentially tagged PHD3 and HIF- α constructs in preliminary FRET experiments

The distance between FRET-donor and FRET-acceptor and their orientation to each other determines whether and with which efficiency FRET can occur. As the orientation of PHD3 and HIF- α in the binding complex is not known, we performed preliminary intensity based FRET acceptor photobleaching experiments to determine if N- or C-terminal PHD3 fusions were more suitable FRET donors for the EYFP-fused HIF α DM.

For that purpose the fluorescence emission of the donor fluorophore was recorded in the presence of the acceptor. Next, the acceptor fluorophore was irreversibly destroyed by intensive excitation with high laser power and was hence unable to serve as a FRET acceptor. Therefore, after acceptor photobleaching the donor emission increased. This rise of donor fluorescence could be detected for instance by performing λ -scans, which record the emission spectrum over a range of wavelengths.

Here, we used this method to investigate whether ECFP-PHD3 or PHD3-ECFP were more suitable to act as a FRET donor for HIF-1/2 α DM-EYFP. HeLa cells were co-transfected with ECFP-PHD3 or PHD3-ECFP and HIF-1 α DM-EYFP or HIF-2 α DM-EYFP. Figure 3.2 shows representative λ -scans of individual representative cells of each condition. The peak at 510 nm represents the ECFP (donor) emission and the peak at 540 nm represents the acceptor emission. The spectrum before bleaching is displayed in red and the post-bleach spectrum in black. Successful photobleaching of the acceptor can be seen as the intensity decrease in the acceptor emission peak. As a sign of FRET, the donor emission peak rose slightly after photobleaching. This was true in all tested combinations, indicating that ECFP-PHD3 and PHD3-ECFP were both able to serve as FRET-donors, when using HIF-1/2 α DM-EYFP as the FRET acceptor.

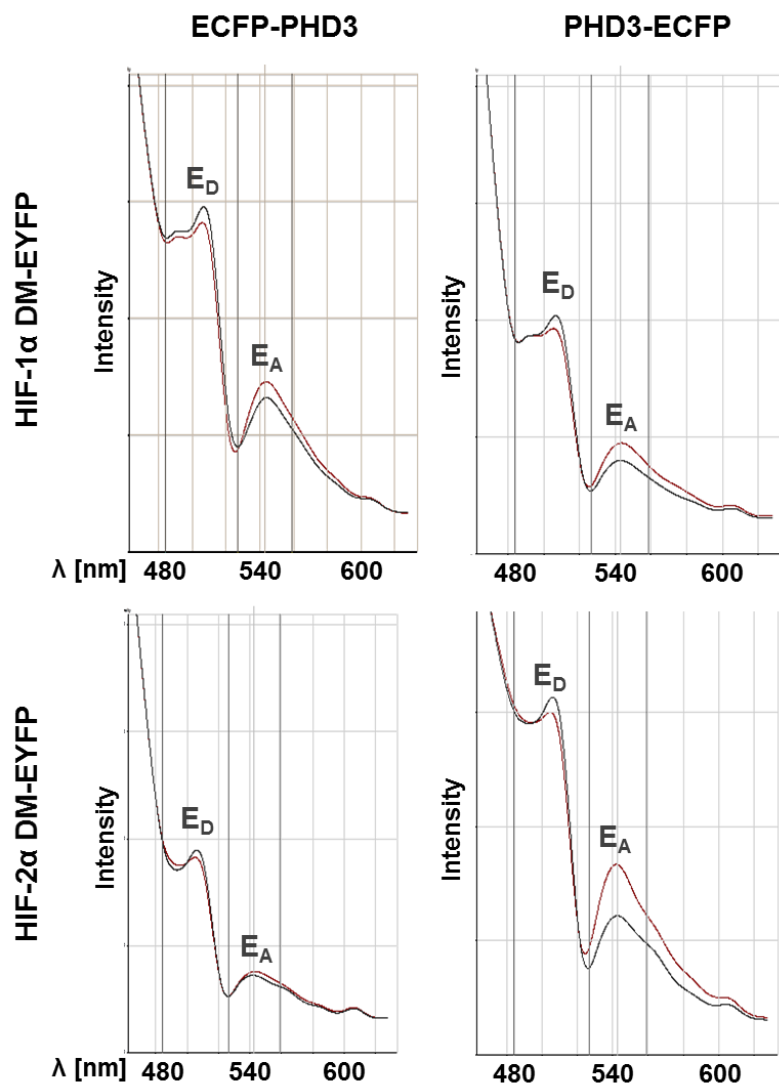


Figure 3.2: FRET acceptor photobleaching measurements. HeLa cells were co-transfected with ECFP-tagged PHD3 and EYFP-tagged HIF- α and FRET experiments were performed 24 hours post-transfection. A λ -scan of the ECFP emission (red) was recorded before photobleaching the EYFP fluorescence by subjecting a defined region to 30 iterations of bleaching at 514 nm with 100% laser power. Then a λ -scan of the ECFP emission was recorded again (black). The donor emission (E_D) peaks around 510 nm and the acceptor emission (E_A) peaks around 540 nm.

Taking the localisation and FRET results together, we did not find any major differences in PHD3 localisation when fused C- or N-terminally to dsRedXP or ECFP, and with both orientations it was possible to measure some FRET between ECFP-tagged PHD3 and HIF-1/2 α DM-EYFP. Therefore, we were ready to start to investigate how PHD3 SUMOylation affected its interaction with HIF-1/2 α DM.

3.2.3 Fluorescence tagging of the PHD3 SUMO mutants

In order to understand how the SUMOylation of PHD3 affected HIF signalling, Edurne Berra's lab had generated a panel of PHD3 SUMO-mutants. The mutation of three lysine residues within PHD3 abolished its capability to be SUMOylated, and therefore this SUMOylation dead mutant was called PHD3 Δ SUMO. In order to mimic the SUMOylated version, either SUMO1 or SUMO3 were fused to PHD3's C-terminus, generating chimeric PHD3-SUMO1 and PHD3-SUMO3 proteins. Thus, we decided to fuse the red fluorescent protein to PHD3's N-terminus, hoping to allow the C-terminally fused SUMO moiety to behave as naturally as possible. In the anticipation of the FLIM system to be installed, we generated dsRedXP-PHD3 Δ SUMO, dsRedXP-PHD3-SUMO1, and dsRedXP-PHD3-SUMO2/3 using the Gateway® system (Figure 3.3). Strikingly, we found that all mutants seemed to be excluded from the nucleus as opposed to a more homogenous distribution throughout the cell that we had found previously.

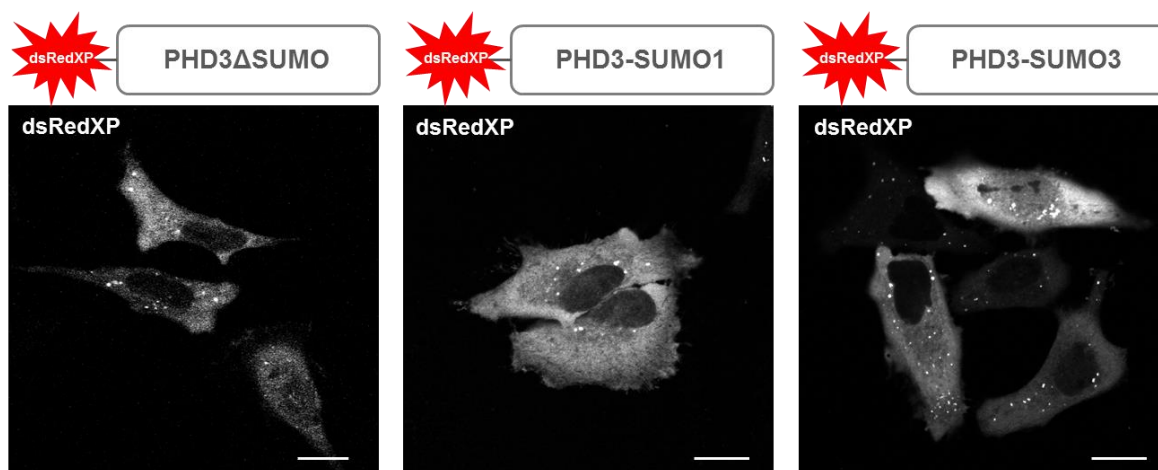


Figure 3.3: Expression vectors encoding PHD3 SUMO mutants N-terminally fused to dsRedXP. Plasmids were generated using Gateway® cloning and transfected into HeLa cells 24 hours prior to imaging. The scale bar is 20 μ m.

Therefore, we wanted to scrutinise the localisation of all the constructs, including the dsRedXP- and ECFP-tagged PHD3 wildtype and SUMO mutants. In order to compare them with the non-fluorescent parental HA-tagged construct, we fixed all samples and stained with an anti-PHD3 antibody. Interestingly, we found that the HA-tagged constructs showed stronger nuclear localisation than the correspondent dsRedXP-tagged versions (**Figure 3.4A**). Fluorescence intensities in unsaturated cells were measured in equally shaped and sized regions of interest (ROIs) in representative areas of nucleus and cytoplasm using ImageJ and the fluorescence intensity ratios nucleus:cytoplasm are shown in **Figure 3.4 B**. dsRedXP-tagged PHD3 proteins clearly displayed a statistically significant reduction of nuclear localisation as compared to the ECFP- and HA-tagged PHD3 fusion proteins.

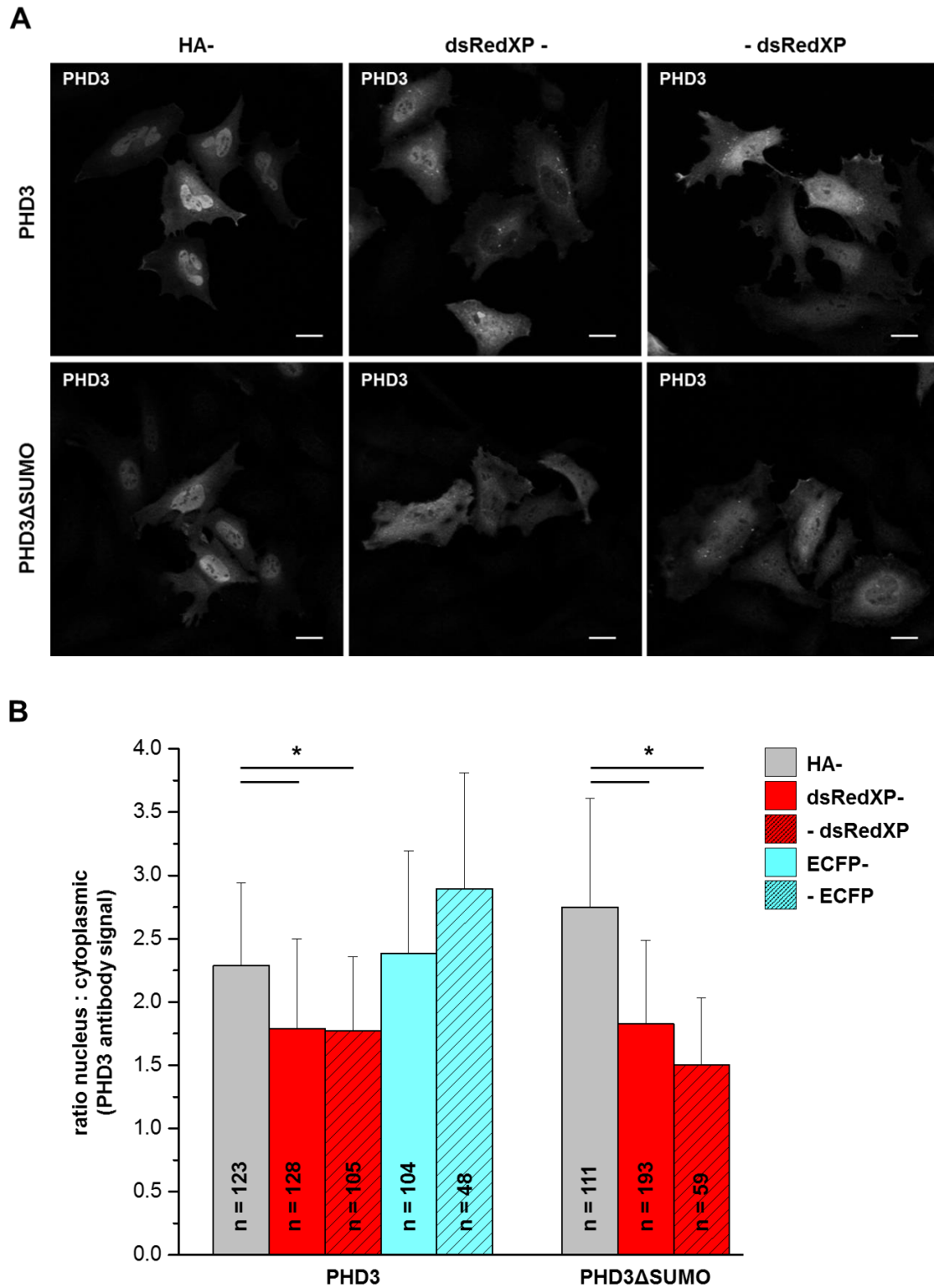


Figure 3.4: Localisation of HA- and dsRedXP-tagged PHD3 WT and PHD3ΔSUMO. HeLa cells were transfected 36 hours before PFA fixation, stained with PHD3 antibody and Alexa Fluor 488 secondary antibody. (A) Pictures were taken with a 40x oil objective. The scale bars are 20 μm. (B) Fluorescence intensities of Alexa Fluor 488 were measured in ROIs in nucleus and cytoplasm using ImageJ. (*) indicates that there was a statistically significant difference in the two-sided Student's T-Test.

Having found that the dsRedXP-label induced a change in protein localisation, the question emerged to what extent the occurrence of aggregates was influenced by the label. To assess that, the fixed and PHD3 antibody stained cells were classified into groups according to the amount of visible aggregates (Figure 3.5). While less than 35% of cells expressing HA-tagged wildtype PHD3 exhibited visible aggregation, more than 70% and 45% of cells expressing N- or C-terminally dsRedXP-tagged PHD3 showed aggregates. The percentage of cells that contained aggregates was also increased from less than 35% in the HA-tagged PHD3 Δ SUMO mutant to more than 75% and 60% for the N- and C-terminally dsRedXP-tagged PHD3 Δ SUMO, respectively, suggesting that labelling with dsRedXP did indeed boost PHD3 aggregation.

Hence, we concluded that as dsRedXP itself forms a tetramer (Baird et al., 2000) it might reinforce PHD3's intrinsic property to aggregate (Nakayama et al., 2007; Rantanen et al., 2008; Rantanen et al., 2013), resulting in an artifactual aggregation. This aggregation might be directly responsible for the reduction in the nuclear accumulation through PHD3 sequestration in the cytoplasm and exclusion of PHD3 aggregates from the nucleus.

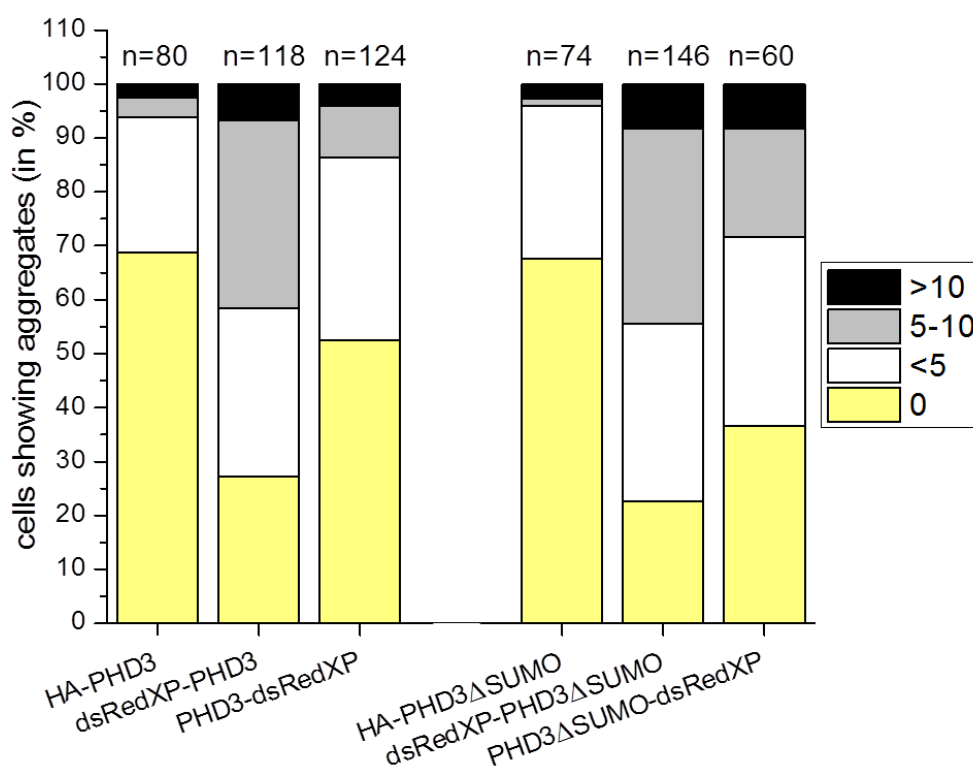


Figure 3.5: Influence of the fluorescent label on PHD3 aggregation. HeLa cells were transfected with the HA- and dsRedXP-tagged proteins, fixed, immunostained with anti-PHD3 antibody and pictures were taken (see Figure 3.4A). Cells were classified into groups according to the amount of visible aggregates.

dsRedXP was therefore not a suitable label for tagging PHD3 and an alternative fluorescent protein needed to be found in order to be able to perform the planned FLIM-based FRET experiments. To solve the problem of label-mediated aberrant localisation and aggregation, we decided to test the new fluorescent protein mRuby2 for tagging of PHD3 and to test its performance. mRuby2 is a monomeric red fluorescent protein that has improved brightness and

photostability compared to its parent mRuby and has been engineered and described by Lam et al. as an efficient FRET acceptor for the green fluorescent protein Clover (Lam et al., 2012).

3.2.4 Performance of the mRuby2 label

The coding sequence of mRuby2 was N-terminally inserted into the expression vectors encoding PHD3 WT and PHD3 Δ SUMO using In-Fusion® HD Cloning. Localisation and aggregation properties of the mRuby2-labelled PHD3 proteins were assessed after transfection into HeLa cells and anti-PHD3 antibody staining as previously. mRuby2-tagged PHD3 WT and PHD3 Δ SUMO displayed similarly strong nuclear localisation as the HA-tagged proteins (Figure 3.6A and B) and mRuby2 did not significantly alter PHD3-aggregate formation (Figure 3.6C).

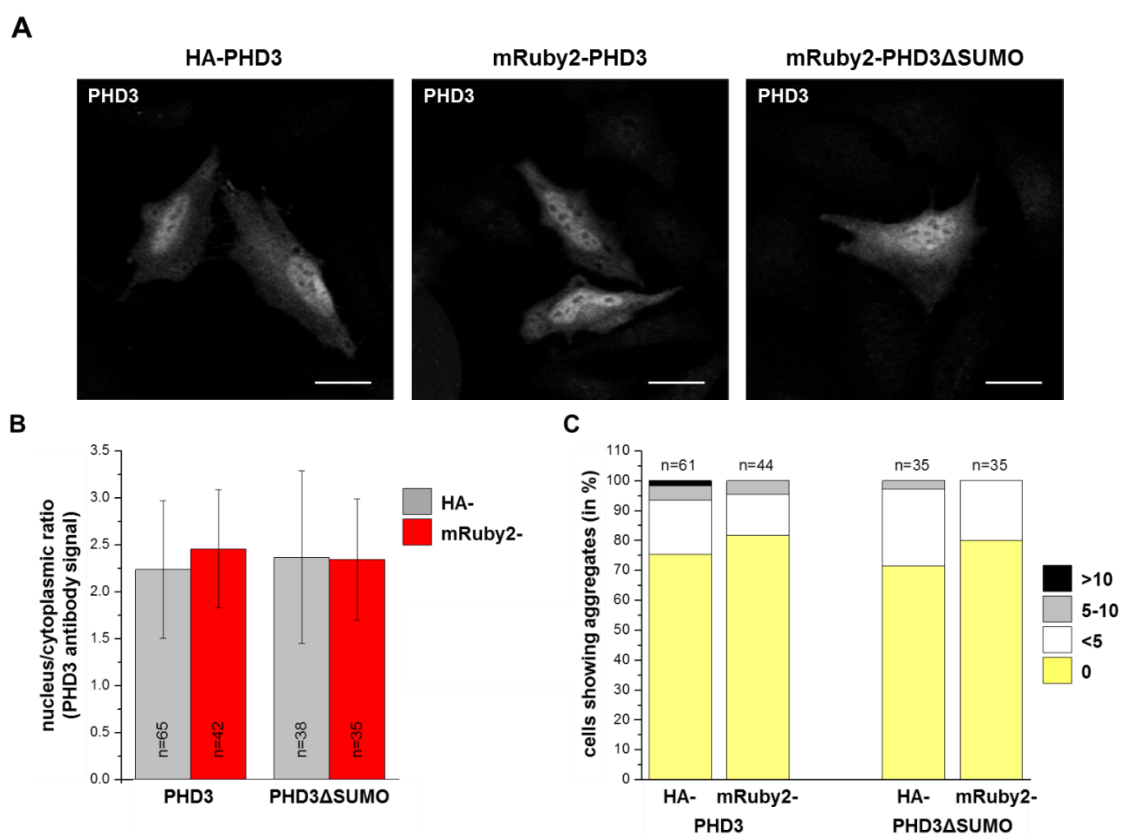


Figure 3.6: Performance of mRuby2 as a fluorescent label for PHD3. Localisation and aggregation of mRuby2-labelled PHD3 WT and PHD3 Δ SUMO were evaluated after transfection of the expression vectors into HeLa cells, fixation and permeabilisation of the cells and staining with PHD3 antibody. Immunofluorescence images (A) were used to assess localisation (B) and aggregation (C) of the tagged PHD3 proteins. The scale bar is 20 μ m.

Taking these data together, mRuby2 seemed to be a suitable label for PHD3 and mRuby2-PHD3 WT and mRuby2-PHD3 Δ SUMO could be used for further experiments. As the FLIM system was not available yet at that point, we initially sought to test whether the measurement of the diffusion coefficients of the proteins could give us information about their interaction. This is for example possible with fluorescence cross-correlation spectroscopy (FCCS), but we

used a less known method called Raster Image Correlation Spectroscopy (RICS) that had just been implemented on one of the CCI's systems by the Master's student Julien Dumont.

3.2.5 Measurement of diffusion coefficients and interaction

Raster Image Correlation Spectroscopy (RICS) is a technique to measure diffusion coefficients of fluorescent molecules in solution or in cells. It makes use of the information inherent to an image or a series of images that have been taken with a laser scanning microscope. As the microscope scans a sample, the laser beam dwells for a specific time on a pixel of a defined size, detecting a signal if a fluorophore is present in the scanned pixel before moving on to the next pixel (Figure 3.7). Mobile molecules within the sample can therefore be detected in consecutive pixels creating a trace of their motion on the image. Software can be used to calculate an autocorrelation function based on the temporal and spatial information inherent to the image or the series of images, from which a diffusion coefficient can be extracted. Diffusion coefficients as a measure of the mobility of proteins within a cell can indicate whether proteins diffuse freely or whether they do interact with other cellular components. Two interacting proteins will essentially have the same diffusion coefficient, however the same diffusion coefficient is not sufficient to state interaction of two proteins. RICS had been recently used to measure the binding of the transcription factor p53 to DNA or interacting proteins upon DNA damage (Hong et al., 2010), as well as to measure the movement of DNA lipoplexes through the cytoplasm (Mieruszynski et al., 2015).

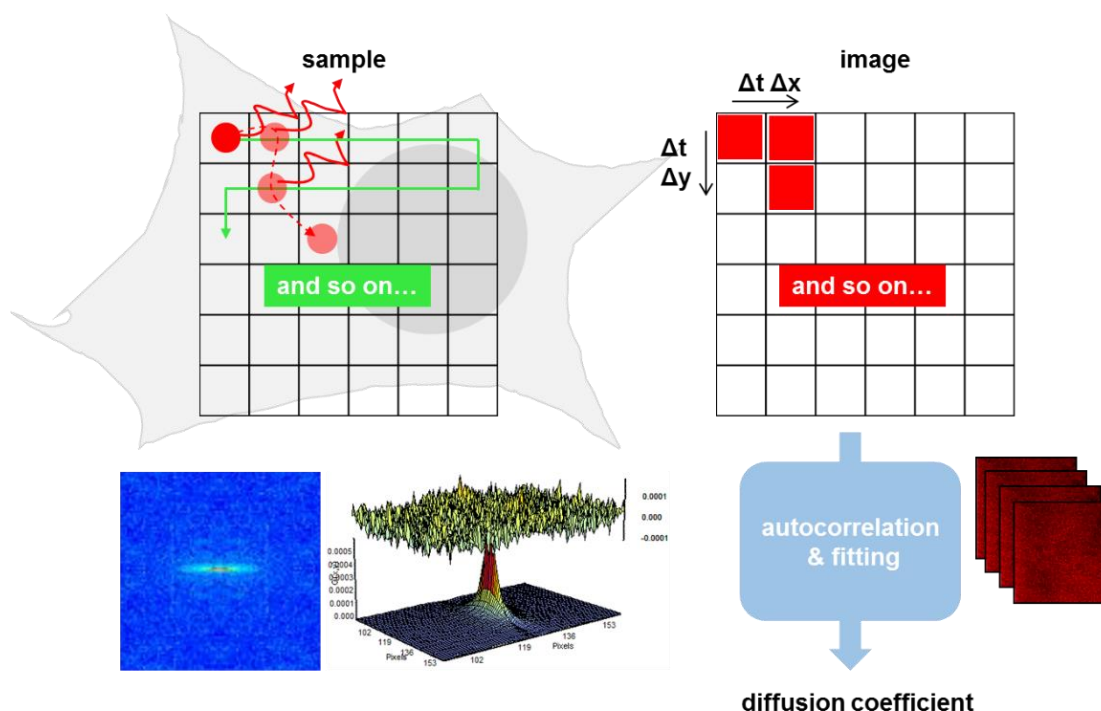


Figure 3.7: Raster Image Correlation Spectroscopy (RICS). The laser beam (green) scans the sample (left) pixel by pixel and a signal is recorded in the image (right) if a fluorophore (red circle) is present in the pixel. As the fluorophore moves (red dotted line) throughout the sample, it can be detected in consecutive pixels. Several images are used for the calculation of the autocorrelation function and subsequent fitting (bottom right) to extract the diffusion coefficient.

As a reference of our system, the diffusion coefficient of EGFP in HeLa cells was measured (Figure 3.8A). The values of $21 \mu\text{m}^2/\text{s}$ in the nucleus and $13 \mu\text{m}^2/\text{s}$ in the cytoplasm are in the same range as diffusion coefficients reported in the literature (Figure 3.8C).

We next measured the diffusion coefficient of HIF-1 α DM-Clover in the nucleus and found it to be with $5 \mu\text{m}^2/\text{s}$ considerably lower than EGFP's, indicating that in contrast to EGFP, HIF-1 α DM-Clover was not diffusing as freely as EGFP (Figure 3.8D). This is in accordance with the fact that as a dimeric transcription factor HIF-1 α binds to other proteins (HIF-1 β and its coactivator CBP/p300) and to DNA. Interestingly, the nuclear diffusion coefficients of the mRuby2-fused PHD3 proteins were with 5-6 $\mu\text{m}^2/\text{s}$ very similar to HIF-1 α DM-Clover's (Figure 3.8E). This might already indicate that PHD3 and HIF-1 α DM might be part of the same multiprotein complex. On the basis of this assumption, it would be impossible to measure increased or decreased interaction of PHD3 Δ SUMO with HIF-1 α DM based on their diffusion coefficients. Accordingly, Figure 3.8D shows that we measured no change in the diffusion coefficient of HIF-1 α DM-Clover in the presence of neither mRuby2-PHD3 WT nor mRuby2-PHD3 Δ SUMO. Reciprocally, when measuring the diffusion coefficient of mRuby2-PHD3 WT or mRuby2-PHD3 Δ SUMO alone or in the presence of HIF-1 α DM-Clover, no differences were detectable (Figure 3.8E).

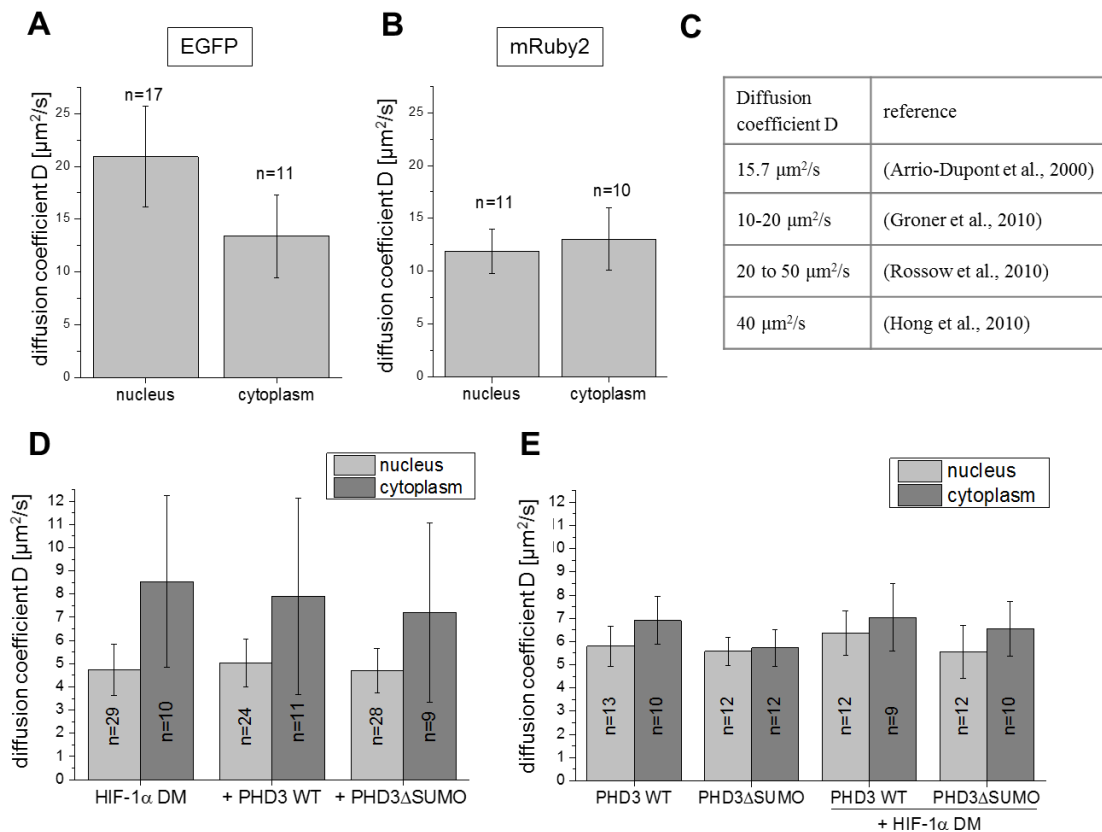


Figure 3.8: RICS measurements in HeLa cells. Diffusion coefficients of EGFP (A) and mRuby2 (B) were measured in nucleus and cytoplasm. (C) Reference values for EGFP diffusion from the literature. (D) Diffusion coefficient of HIF-1 α DM-Clover alone and in the presence of mRuby2-PHD3 WT and mRuby2-PHD3 Δ SUMO. (E) Diffusion coefficient of mRuby2-PHD3 WT and mRuby2-PHD3 Δ SUMO alone and in the presence of HIF-1 α DM-Clover.

Taken together, RICS measurements could not provide answers to the question whether the SUMOylation of PHD3 had a direct impact on binding of PHD3 to HIF-1 α DM. Therefore, techniques that are able to measure the binding of two proteins to each other more directly, are indispensable. The method of choice was FLIM-based FRET, however I was unable to obtain conclusive results either, possibly due to the low fluorescence signal of the FRET acceptor. Hence, the data about the effect of PHD3 SUMOylation on HIF-1 transactivation were published without the additional information of how their binding to each other was affected (Nunez-O'Mara et al., 2015).

3.3 Exploration of PHD1 nuclear shuttling by FRAP

Work by Almudena Gerpe-Pita in Edurne Berra's lab showed that not only PHD3, but also PHD1 is SUMOylated. She had identified that PHD1's lysine residues K118 and K120 were subjected to SUMOylation. The mutation of both residues to arginines (K118/120R), did not only reduce PHD1 SUMOylation, but increased also the cytoplasmic fraction of PHD1. Interestingly, K118 and K120 are located within PHD1's nuclear localisation signal (NLS). Upon inhibition of nuclear export with Leptomycin B however, the increased cytoplasmic localisation was reversed. This suggested that PHD1-SUMOylation might be required for retention of PHD1 in the nucleus (Gerpe-Pita et al., *in preparation*). In order to test this hypothesis, I performed fluorescence recovery after photobleaching (FRAP) experiments.

3.3.1 Fluorescence tagging of PHD1 WT and K118/120R mutant

As the mRuby2 fluorescent label had proved to be a suitable N-terminal tag for the PHD3 protein, the mRuby2 coding sequence was fused to PHD1's and PHD1 K118/120R's N-termini by In-Fusion cloning. Reassuringly, the mRuby2-fusion proteins displayed the same localisation as the respective HA-tagged constructs, with PHD1 being exclusively localised to the nucleus and PHD1 K118/120R also populating the cytoplasm (Figure 3.9).

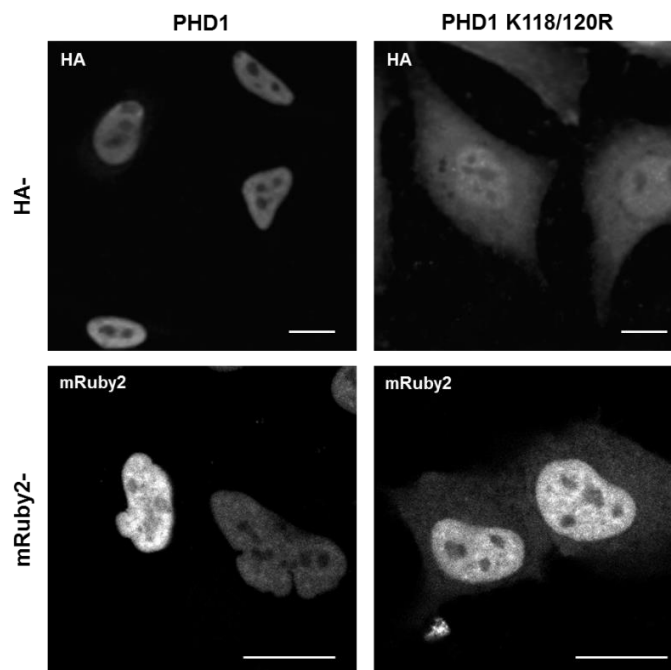


Figure 3.9: HA- and mRuby2-PHD1 constructs. HeLa cells were transfected with HA- (top) and mRuby2- (bottom) tagged PHD1 and PHD1 K118/120R and imaged 24h post-transfection. HA- images were taken by Almudena Gerpe-Pita. The scale bar is 20 μ m.

3.3.2 FRAP experiments

Qualitative Fluorescence Recovery After Photobleaching (FRAP) experiments were performed in order to understand the dynamics of nuclear import of PHD1 and PHD1 K118/120R. For that purpose, HeLa cells were transfected with the newly generated constructs and consecutive images were acquired for approximately 30 min. Then the entire nuclear population of mRuby2-tagged PHD1 was irreversibly photobleached (Figure 3.10, dotted white line) and the fluorescence recovery in the nucleus was recorded over the following 30 min. Both, PHD1 WT and the K118/120R mutant recovered nuclear fluorescence over time (Figure 3.10). These results confirmed that the K118/120R mutation did not prevent the nuclear import of PHD1. In the case of mRuby2-PHD1 nuclear fluorescence recovery was very slow and incomplete as can be seen by a very gentle linear recovery curve (Figure 3.10 top). This is likely to be due to the small pool of cytoplasmic mRuby2-PHD1, which largely restricts the speed of nuclear recovery to the rate of *de novo* synthesis of the protein. In contrast, in the case of PHD1 K118/120R nuclear recovery was much faster and more pronounced, as seen by an initial steep linear curve that reaches a high plateau after about 10 min (Figure 3.10 bottom). This quick and strong nuclear fluorescence recovery can be explained by the mobilisation of the cytoplasmic fraction of mRuby2-PHD1 K118/120R to the nucleus. The FRAP data are therefore in line with Almudena's biochemical data and point towards an important role of PHD1-SUMOylation in the nuclear retention of PHD1 and will be included in the respective manuscript, which is currently been prepared. It has been suggested already more than a decade ago, that some proteins were SUMOylated within their NLS upon entering the nucleus (Seeler and Dejean, 2003). SUMOylation might be required for instance to allow the tethering of PHD1 to nuclear

structures or to prevent PHD1's interaction with its nuclear export receptor. In line with this, other reports show that SUMOylation is required for nuclear retention of other proteins, such as the transcriptional repressor DREAM and the ubiquitin E3 ligase TRAIP (Palczewska et al., 2011; Park et al., 2016).

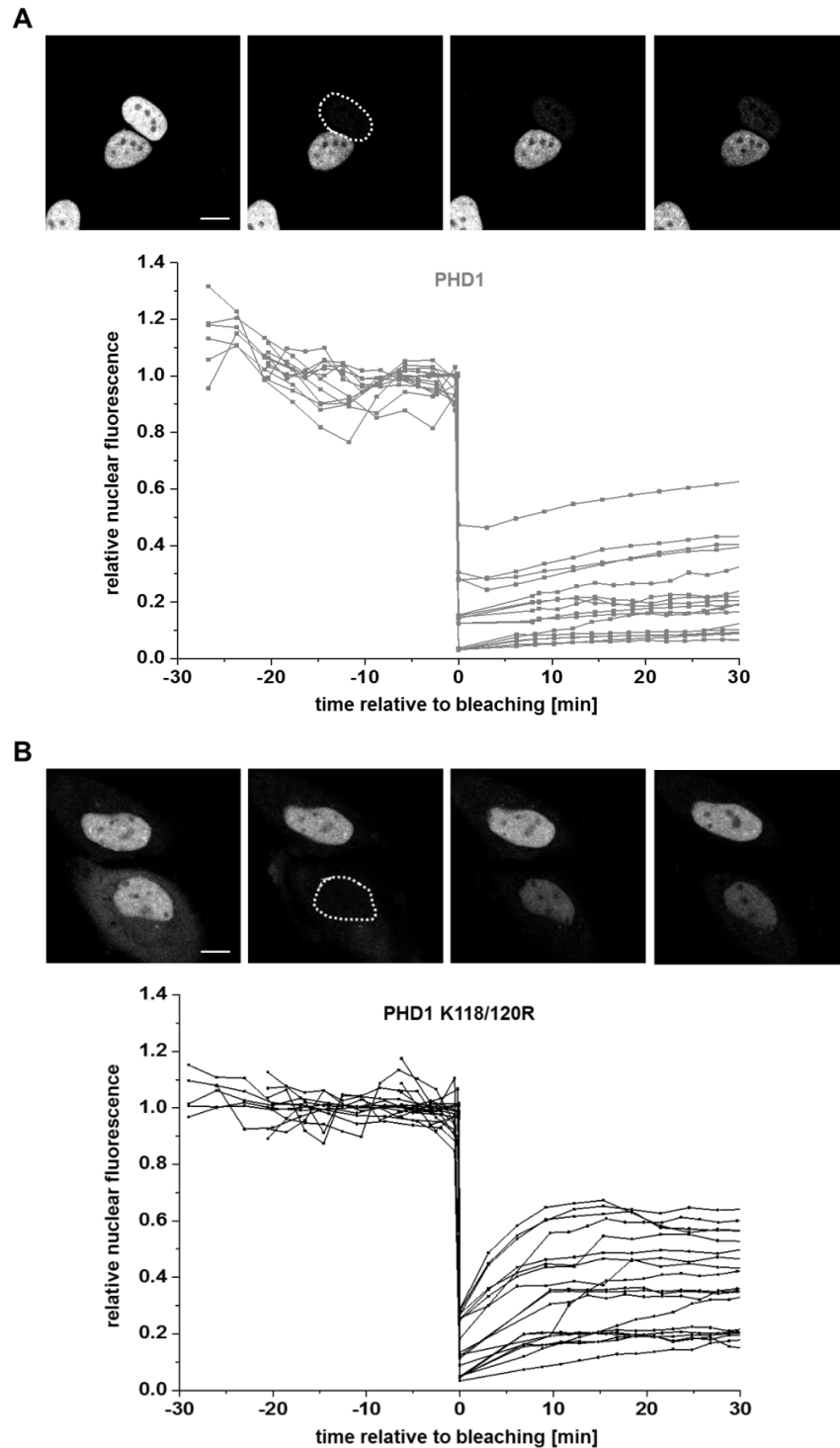


Figure 3.10: Nuclear fluorescence recovery after photobleaching (FRAP) for PHD1 and PHD1 K118/120R. HeLa cells were transfected with mRuby2-PHD1 (A) or mRuby2-PHD1 K118/120R (B) and 24 h post-transfection cells were imaged for 30 min. Subsequently, the entire nucleus was bleached ($t=0$) and the fluorescence recovery in the bleached region (dotted white lines) was recorded for 30 min. Scale bars are 10 μm .

3.4 Proof of principle – FLIM-FRET experiment

FLIM-based FRET measurements to measure protein-protein interactions are very sensitive and highly reproducible, but the proper setup of the instrumentation and the analysis pipeline are crucial for acquisition of reliable results. After the installation of the new FLIM system, we sought to measure the interaction of a relevant and well-defined pair of proteins to test the new system. The two subunits of HIF-1, HIF-1 α and HIF-1 β , form a tight dimer that binds to HRE sequences present within hypoxia-responsive genes and recruits coactivators to stimulate gene expression (Jiang et al., 1996).

Clover-HIF-1 α DM was used as FRET donor and dsRedXP-HIF-1 β was used as FRET acceptor. HeLa cells were transfected with Clover-HIF-1 α DM alone or co-transfected together with dsRedXP-HIF-1 β . First, conventional high-resolution fluorescence images were taken (Figure 3.11A, first two columns). Next, fluorescence lifetime images (FLIM) of Clover-HIF-1 α DM in both conditions were acquired (Figure 3.11A, last column). In the FLIM each pixel is pseudo-coloured according to the average arrival time of all photons within the pixel. Long average arrival times are displayed in red and short mean arrival times are displayed in blue. In the absence of a FRET acceptor, the fluorescence lifetime image of Clover-HIF-1 α DM showed long lifetimes in the red spectrum. However, when the FRET acceptor dsRedXP-HIF-1 β was present, Clover-HIF-1 α DM lifetime images was yellow and green, reflecting shorter lifetimes. This decrease in lifetime is due to FRET and therefore indicates that within the cell HIF-1 α DM and HIF-1 β are in very close proximity to each other, as expected. Importantly, when the dsRedXP was photobleached and therefore unable to accept the energy transfer from the donor, Clover-HIF-1 α DM's lifetime increased again (Figure 3.11B). This confirmed that the measured fluorescence lifetime reduction was indeed due to the close interaction with and FRET to dsRedXP-HIF-1 β .

For the quantification the fluorescence lifetimes, intensity-based average fluorescence lifetimes in the nucleus were extracted from the FLIM measurements as described in the Methods section. In the case of Clover-HIF-1 α DM alone we measured an average lifetime of 2.9 ± 0.024 ns from 17 cells from 3 independent experiments (Figure 3.11C). In the presence of dsRedXP-HIF-1 β the fluorescence lifetime of Clover-HIF-1 α DM is significantly decreased to 2.7 ± 0.069 ns, indicating FRET (17 cells from 3 independent experiments) and confirming their close spatial proximity.

Hence, we have a functioning FLIM-FRET system at hand that will allow us to measure the interaction of two proteins with each other.

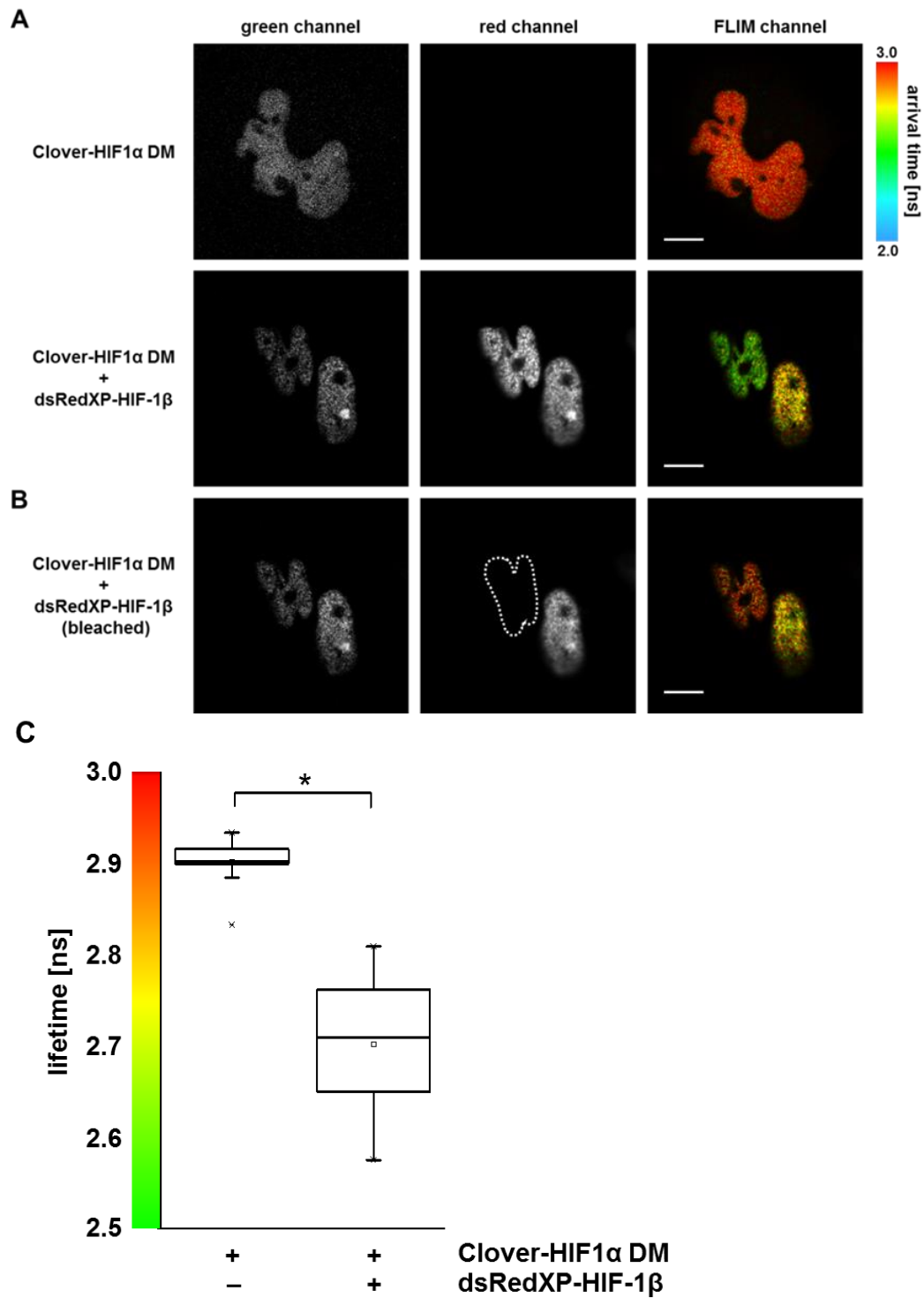


Figure 3.11: FLIM-FRET measurements of the HIF-1α/β pair. HeLa cells were transfected with Clover-HIF-1α DM alone or co-transfected with dsRedXP-HIF-1β. (A) Representative conventional fluorescence and pseudo-coloured fluorescence life time images (FLIM) of both conditions. The scale bars are 10 μm long. (B) The fluorescence of the acceptor was bleached by high intensity laser irradiation (dotted line) and a FLIM image was acquired after successful bleaching. (C) The nuclear average intensity-based lifetime was extracted from FLIM images of three independent experiments (total n=17 per condition) and displayed in a box plot. $p = 4.71 \cdot 10^{-10}$.

3.5 Fluorescence tagging of USP29

On the search for new regulators of hypoxia signalling, other preliminary work in Edurne Berra's lab had pointed towards a possible implication of the deubiquitinase USP29. The rest of this thesis is dedicated to the thorough investigation of USP29's role in HIF signalling (chapter 4) and to the characterisation of the USP29 protein itself (chapter 5). The experiments that are presented in those chapters, were to a large part performed with HA- as well as GFP-tagged USP29 constructs from (Liu et al., 2011). Both constructs displayed the same exclusively nuclear localisation as had been described previously (Urbe et al., 2012) (Figure 3.12).

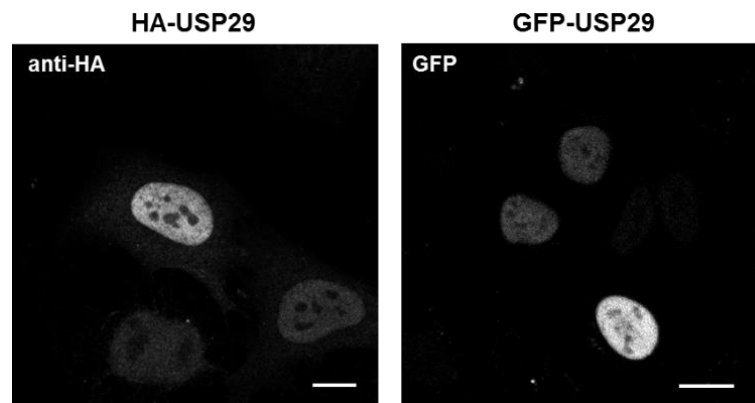


Figure 3.12: USP29 localises to the nucleus. HeLa cells were transfected with HA-USP29 or GFP-USP29 and after 24 h either fixed and stained with anti-HA antibody or imaged directly, respectively. The scale bar is 20 μm .

For FLIM- based FRET experiments, we needed a red fluorescent version of USP29. Therefore, the GFP coding sequence was replaced by the red fluorescent protein mRuby2 as it had proved to be a suitable label even for PHD1 and the aggregation prone PHD3 (3.2.4). Surprisingly, mRuby2-9aa-USP29 did not show any fluorescence when transfected into cells, even though in western blots we were able to detect a band corresponding to full-length and in-frame expressed mRuby2-9aa-USP29 with anti-USP29 antibody (Figure 3.13A). However, the antibody also detected a second band of a lower molecular weight, which could be the result of a post-translational cleavage of mRuby2-9aa-USP29. Additionally, the overexpressed mRuby2-9aa-USP29 was not able to induce the accumulation of its target HIF-1 α (see chapter 4.3). This suggested that the construct was not functional. To decrease potential interference of the mRuby2 with USP29 and vice versa, we extended the linker sequence from 9 to 15 and 21 aa. Indeed, these constructs displayed faint fluorescence, however the localisation was dispersed (Figure 3.13B). We hypothesised that for unknown reasons mRuby2 disturbed USP29 function and/or USP29 impeded appropriate mRuby2 fluorophore maturation. We replaced mRuby2 with mCherry, another monomeric red fluorescent protein, and the new construct mCherry-15aa-USP29 was localised exclusively in the nucleus, reproducing the localisation pattern we had seen for HA-USP29 and GFP-USP29 and displayed very bright fluorescence (Figure 3.13B). Importantly, mCherry-15aa-USP29 was able to accumulate HIF-1 α DM^(PP/AA), indicating that the mCherry-tag did not interfere with USP29's catalytic activity (Figure 3.13C). Therefore, this construct was chosen for use in experiments that are presented in the following two chapters.

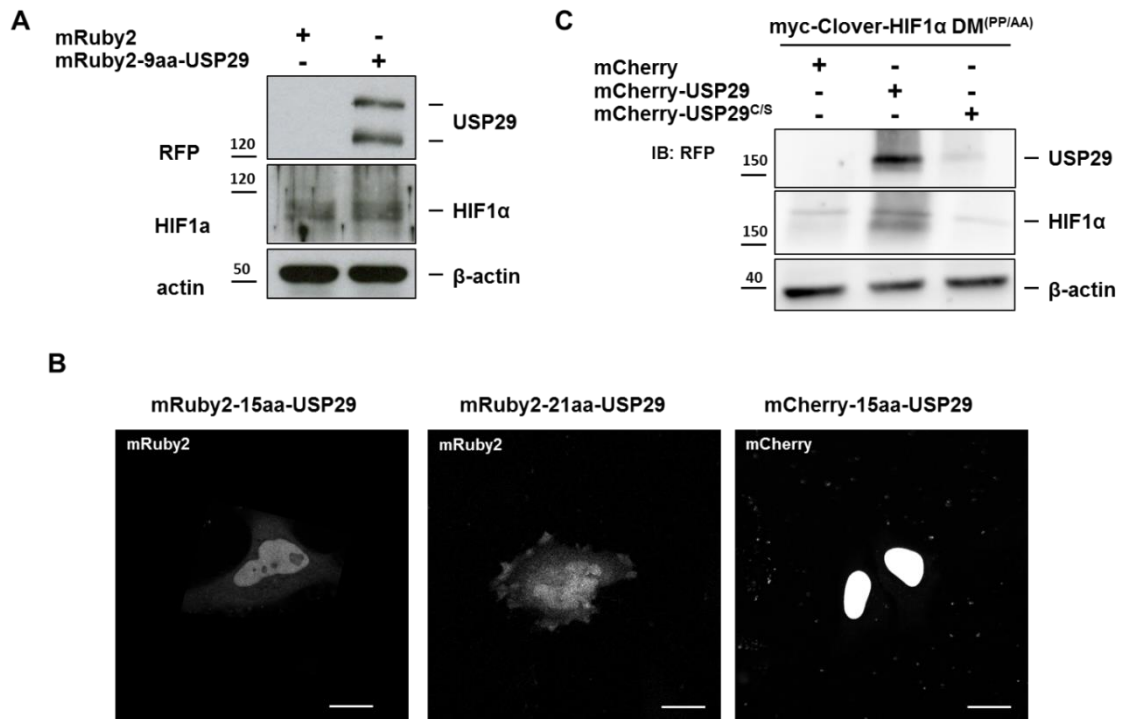


Figure 3.13: Generation of a red fluorescent USP29. (A) HEK293T cells were transfected with mRuby2-9aa-USP29 and the lysate was probed for USP29 and HIF-1α by WB. (B) mRuby2-15aa-USP29, mRuby2-21aa-USP29 or mCherry-15aa-USP29 were transfected into HeLa cells and pictures were taken 24h post-transfection with the same acquisition settings. Scale bars are 20 μm. (C) mCherry, mCherry-15aa-USP29 and mCherry-15aa-USP29^{C/S} were co-transfected together with myc-Clover-HIF-1α DM^(PP/AA) into HEK293T cells. Red fluorescent protein and HIF-1α were detected by immunoblotting.

3.6 Discussion

3.6.1 Choice of the fluorescent tag

Fluorescence imaging gives us insights into what happens inside living cells on a molecular level. It allows us to study how molecules move in real time and how they dynamically interact with one another. However, to be able to visualise and follow the molecules of interest they need to be labelled with a fluorescent dye. Modern monomeric fluorescent proteins that are used as tags for the protein of interest, fold independently and have short maturation times, are photostable and bright, and therefore allow for imaging with low laser power and hence reduce the amount of photodamage. However, with their size of approximately 35 kDa they can interfere with the correct folding and/or functioning of the tagged protein.

We found that the tetrameric fluorescent protein dsRedXP boosted the aggregation of PHD3 and resulted in an incorrect intracellular localisation. This is not an unprecedented case. Han et al. found that the fusion of a fluorescent protein such as GFP or mCherry to Caveolin-1 induced its mislocalisation and altered its oligomerisation status (Han et al., 2015). Similarly, Landgraf et al. found that tagging bacterial Clp protease with a panel of monomeric fluorescent proteins such as sfGFP, Venus and mCherry caused the protease to concentrate in a single focus (Landgraf et al., 2012). Immediately after cell division the focus was only present in one of the two daughter cells resulting in a substantial difference in protease activity between them. The introduction of a mutation into the GFP (GFPmut3) or the usage of Dendra2 or Dronpa could restore the correct homogenous localisation and distribution of Clp between the daughter cells. Furthermore, they showed that other bacterial proteins that had previously been described to form foci did not do so when fused to GFPmut3. Likewise, when we fused the monomeric protein mRuby2 to PHD3, the native localisation and aggregation pattern was reproduced. Moreover, mRuby2 also proved to be a suitable tag for PHD1.

However, when we fused mRuby2 to USP29, the chimeric protein displayed very faint fluorescence, seemed to be retained in the cytoplasm and to have lost its ability to stabilise its target protein HIF-1 α . While the fluorescence intensity was slightly improved when increasing the linker between mRuby2 and USP29 from 9 amino acids (aa) to 15 aa, a further increase to 21 aa did not further enhance the weak signal, and the localisation remained aberrant. The problem was solved by fusing USP29 to an alternative monomeric fluorescent tag, mCherry. The mCherry-USP29 displayed bright, nuclear fluorescence and was able to accumulate HIF-1 α , attesting its functionality.

Taken together, it becomes clear that there is not such a thing as a universal fluorescent protein tag that readily labels any given protein with the guarantee of not affecting its function.

3.6.2 Measuring protein-protein interactions in live cells

Most, if not all, signal transduction mechanisms depend on the interaction of two or more proteins with each other (Pawson and Nash, 2000). To understand the signalling dynamics, it is

therefore crucial to be able to reliably measure protein-protein interactions in living cells. Several live cell imaging methods are available for that purpose. Diffusion-based techniques such as RICS and FCS allow us to determine quantitatively the diffusion coefficient of one labelled protein at a time. The RICS approach has recently been used successfully to measure the recruitment of p53 to DNA upon DNA damage (Hong et al., 2010) and to measure the homo-dimerisation of the EGFR upon stimulation with EGFR (Kluba et al., 2015). In both cases this was possible because of a dramatic change of their diffusion coefficient following the respective stimulation. Generally however, while two (or more) proteins that are associated do have the same diffusion behaviour, same diffusion coefficients are not sufficient to state their interaction. In particular, if two proteins are part of a big multiprotein complex and/or tethered to high molecular structures such as the DNA, their diffusion behaviour will be identical independently of whether within the complex the two are directly bound to each other or not.

In order to more directly and quantitatively measure the interaction of two proteins with each other, the (FLIM-)FRET and FCCS technique can be used. The most direct proof of interaction is delivered by FRET experiments as FRET can only occur when donor and acceptor fluorophore are within a few nanometres' distance. FLIM-based FRET measurements are especially useful as the fluorescence lifetime is a very robust property, resulting in low cell-to-cell- and experiment-to-experiment variability (Becker, 2012). Apart from their distance, the orientation of donor and acceptor fluorophore are important for FRET to occur and depending on the proteins to be measured, FRET measurements might not be successful. In this case the diffusion-based FCCS method might help to find an answer to the questions. By being able to measure the diffusion coefficients of two differentially labelled proteins within the small focus volume, FCCS adds spatial information to the diffusion measurements (Bacia et al., 2006). Two interacting proteins therefore not only exhibit the same diffusion parameters, but also appear in the focal volume together.

Taken together, fluorescent live cell imaging is a powerful tool, but correct selection and validation of the fluorescent label and the adequate technique for each and every particular protein and research question is crucial for obtaining meaningful results. There is not *one* fluorescent protein tag, which can warrant that the tagged protein behaves as its endogenous counterpart. Instead, the careful assessment of localisation and activity of the fusion protein is required, preferably by comparing it with the properties of the endogenous protein, or if this is not possible by comparing it to the protein when fused to a small peptide-tag.

Chapter 4: USP29 is a new regulator of HIF- α

4.1 Introduction

The canonical hypoxia signalling pathway that senses low oxygen concentrations and triggers processes involved in cell survival and adaptation was discovered more than 20 years ago (Semenza and Wang, 1992). In the last 2 decades the understanding of the pathway has expanded and more and more proteins are now known to modulate HIF signalling. At the same time it became clear that the hypoxia signalling pathway was deregulated in many cancers. Sustained expression of HIF target genes confers resistance to induced cell death and makes cells highly glycolytic, as well as induces angiogenesis (Semenza, 2012b). However, despite the amount of information available nowadays, the mechanisms that cause the inappropriate HIF signalling remain not fully understood.

The hypoxia signalling pathway is heavily regulated by the ubiquitin proteasome system. In particular, the stability of the α -subunit of the central transcription factor HIF is regulated through ubiquitination. But also other important members of the pathway, such as PHD1 and PHD3 are subjected to ubiquitination and subsequent degradation (Fukuba et al., 2007; Nakayama et al., 2004; Velasco et al., 2013). Hence, enzymes that de-conjugate ubiquitin could have the potential to modify the hypoxic response significantly. Indeed, several of such deubiquitinases (DUBs) had already been shown to impact hypoxia signalling (see 1.3.1 and 1.3.2). Based on the fact that DUBs are potentially druggable enzymes, Edurne Berra's lab decided to perform a DUB screen in order to identify potential new regulators of the hypoxia signalling pathway. Such a new regulator could help to expand the understanding of how and why hypoxia signalling is deregulated in disease and might in the future serve as a biomarker or even a drug target.

This chapter presents the work done to establish USP29 as a novel non-canonical regulator of HIF- α . Using a combination of standard biochemical methods in Edurne Berra's lab, as well as advanced live cell imaging in Violaine Sée's lab, we found that USP29 activated hypoxia signalling by directly acting on HIF- α . Parts of this chapter are part of a manuscript, which is being tried to publish. My contribution to the work is stated in italics in each figure legend.

4.2 First experiments performed in Edurne Berra's lab

Encarni Perez-Andrés transfected a library of pools of shRNAs targeting more than 60 DUBs into HeLa cells together with an HRE-luciferase reporter gene (Figure 4.1A). The cells were exposed to either normoxia or hypoxia and HIF transcriptional activity was read out using the luciferase assay. The experiment was carried out three times in triplicates, and several DUBs were shown to have an effect on HIF activity. Among them, the ubiquitin-specific protease 29 (USP29) was one of the top hits. Validation experiments performed by Sara Pozo and Onintza Carlevaris confirmed that the knock-down of endogenous USP29 with the pool of shRNAs did

significantly and reproducibly decrease HRE-luciferase activity as well as the expression of HIF-target genes in normoxia and hypoxia. Furthermore, not only the pool, but also all three independent shRNAs targeting USP29 did reproduce the inhibitory effect on HIF-driven transcriptional activity (Figure 4.1B).

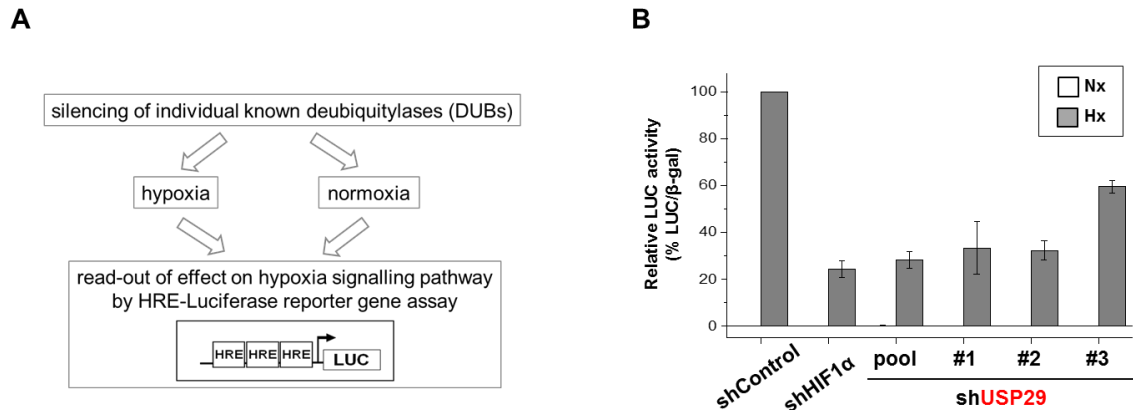


Figure 4.1: Identification and validation of USP29 as an activator of HIF signalling. (A) HeLa cells were silenced with pools of 3 individual shRNAs targeting DUBs and transfected with a HRE-luciferase reporter plasmid. Cells were exposed to normoxia and hypoxia and luciferase activity was determined. (B) HeLa cells were silenced for HIF-1 α and USP29 with three different shRNAs and transfected with HRE-luciferase. The luciferase activity was measured after incubation in normoxia or hypoxia (24h). *These Experiments were performed by members of Edurne Berra's lab.*

4.3 USP29 is a positive regulator of HIF-1 α

Apart from significantly reducing the hypoxia-driven HRE-luciferase expression (Figure 4.2A), the silencing of endogenous *USP29* with a pool of 3 independent shRNAs in HeLa cells also abrogated the hypoxic induction of the HIF target gene *CA9* (Figure 4.2B). The pool of shUSP29s efficiently silenced GFP-USP29 at mRNA and protein levels (Figure 4.3A). Interestingly, in cells silenced for endogenous *USP29* the accumulation of HIF-1 α protein in hypoxia was significantly decreased and the induction of *CAIX* and *PHD2* was impaired to a similar extent as when silencing *HIF1A* (Figure 4.2C). Anyhow, *HIF1A* mRNA was not affected by the silencing of *USP29* (Figure 4.3B). More importantly, similar to the pan-hydroxylase inhibitor DMOG, the ectopic expression of USP29 led to the accumulation of endogenous HIF-1 α , *CAIX* and *PHD2* even in normoxia (Figure 4.2D). Nonetheless, *HIF1A* mRNA expression was not affected by the USP29 overexpression (Figure 4.3C), pointing to USP29 as a novel upstream post-translational activator of HIF-1 α .

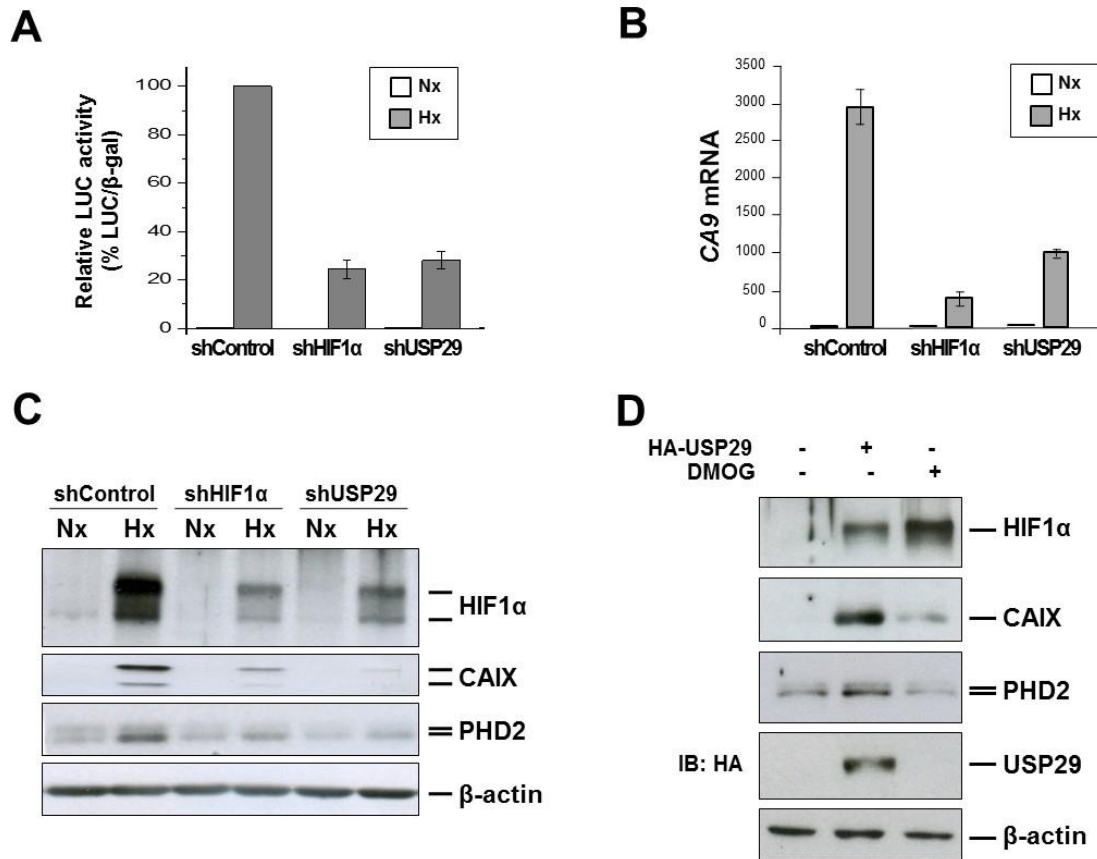


Figure 4.2: USP29 is a positive regulator of HIF-1 α . (A) HeLa cells were silenced with scrambled or shRNAs targeting HIF1A and USP29 and transfected with a reporter vector (pRE- Δ tk-Luc) containing three copies of the HRE from the erythropoietin gene and CMV- β -gal to normalize for transfection efficiency. Cells were incubated for 16 h in normoxia (21% O₂) or hypoxia (1% O₂) and luciferase and β -galactosidase activities were measured. (B) HeLa cells were treated as in A and total RNA was extracted, reverse-transcribed and expression of CA9 was determined by qPCR. (C) Whole cell extracts (WCE) from HeLa cells treated as in A were subjected to SDS-PAGE followed by immunoblotting with the indicated antibodies. (D) HEK293T cells were transfected with empty vector or HA-USP29 and left untreated or treated with DMOG for 4 hours prior to lysis. WCE were subjected to SDS-PAGE and immunoblotting was performed using the indicated antibodies. *All experiments were performed by the EB lab.*

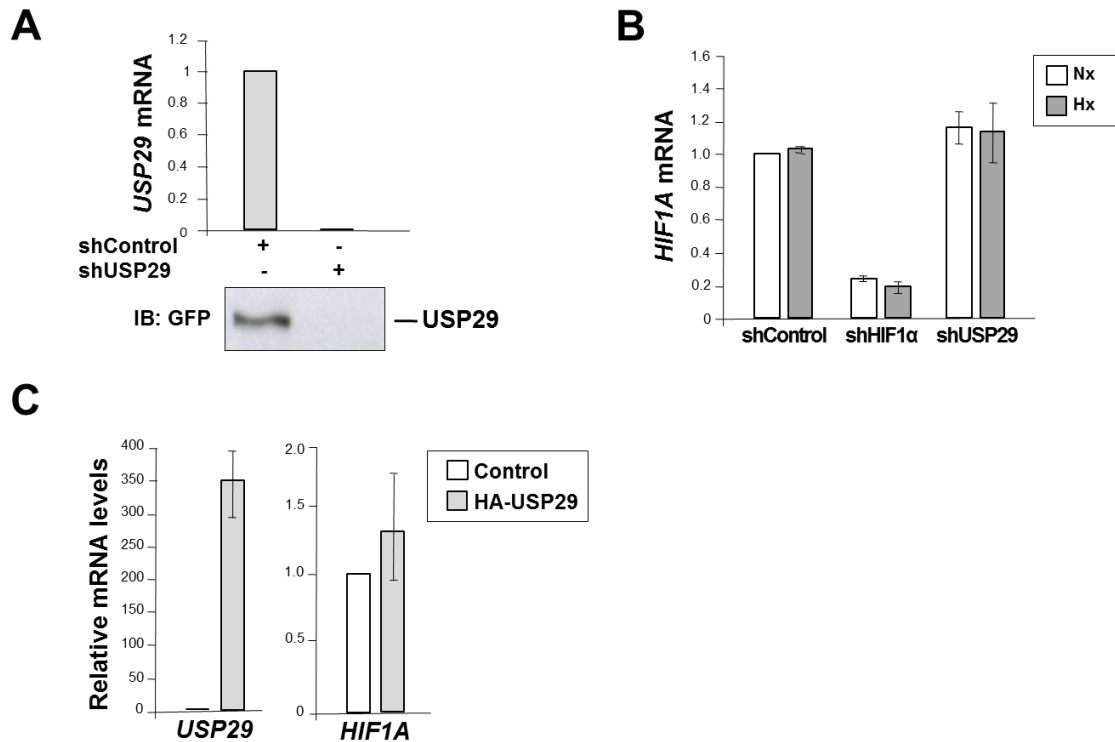


Figure 4.3: USP29 is a positive regulator of HIF-1 α (supplement). (A) HeLa cells were silenced with scrambled or shRNAs targeting USP29 and transfected with GFP-USP29. RNA and protein were extracted and subjected to qPCR and immunoblotting, respectively. (B) HeLa cells were silenced with scrambled shRNAs or shRNAs targeting HIF1A and USP29 and incubated for 16 h in normoxia (21% O₂) or hypoxia (1% O₂). Total RNA was extracted, reverse-transcribed and expression of HIF1A was determined by qPCR. (C) HEK293T cells were transfected with empty vector or HA-USP29, RNA was extracted and expression of USP29 as well as HIF1A was determined by qPCR. *All experiments were performed by the EB lab.*

4.4 USP29 upregulates HIF-1 α in a non-canonical way

Surprisingly, the HIF-1 α that accumulated in the presence of USP29 in normoxic conditions induced PHD2 and CAIX (Figure 4.2D), albeit being prolyl-hydroxylated (Figure 4.4A). Furthermore, the ectopic expression of USP29 also accumulated HIF-1 α DM^(PP/AA), a HIF-1 α mutant whose two oxygen-sensitive proline residues have been replaced by alanines (P402/564A), suggesting that USP29 regulates HIF-1 α in a non-canonical way (Figure 4.4B). Consistently, silencing of endogenous *USP29* with 2 different siRNA sequences decreased both, HIF-1 α WT and HIF-1 α DM^(PP/AA) protein levels (Figure 4.4C and Figure 4.5A). As expected, the silencing of the canonical negative regulators, *PHD2/EGLN1* and *pVHL*, only affected HIF-1 α WT but not HIF-1 α DM^(PP/AA) (Figure 4.4C). Similarly, the overexpression of the Ub E3-ligase pVHL did only affect HIF-1 α WT, but not the DM protein (Figure 4.5B). Taken together, these results indicate that USP29 acts on HIF-1 α through a non-canonical mechanism.

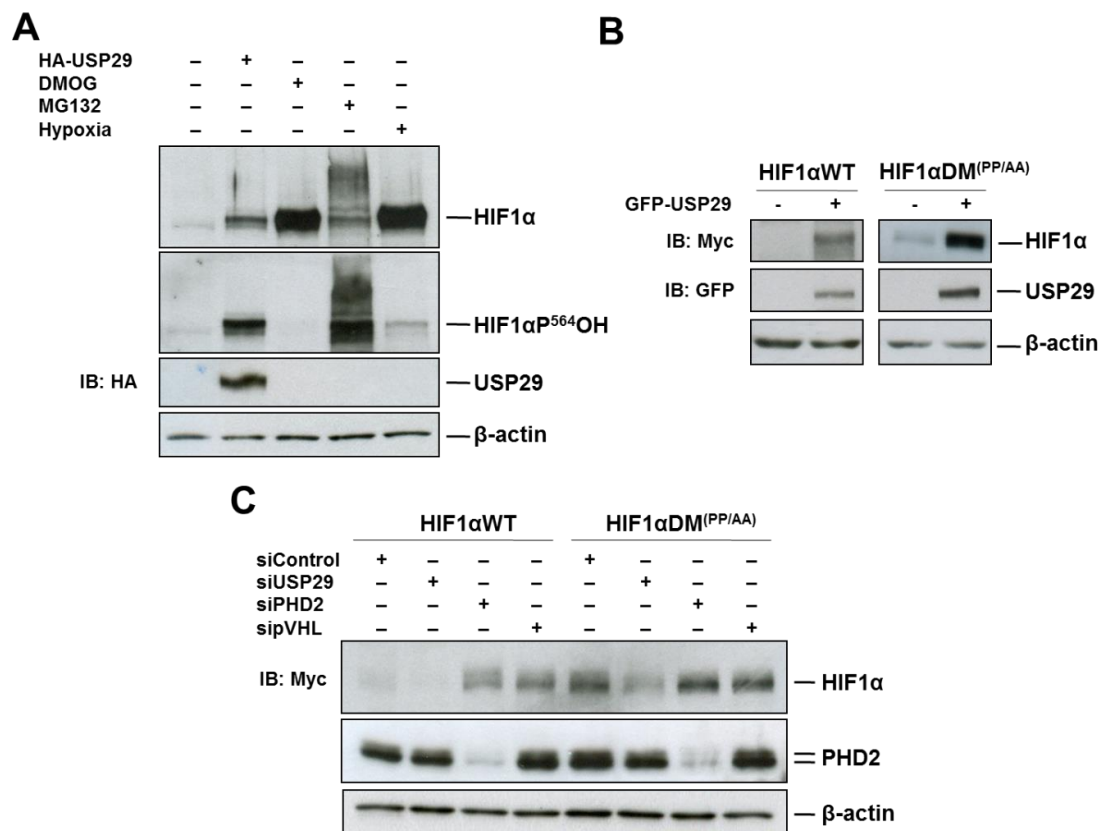


Figure 4.4: USP29 regulates HIF-1 α in a non-canonical way. (A) HEK293T cells were transfected with empty vector or HA-USP29 and treated with the hypoxia mimetic DMOG (1 mM), the proteasome inhibitor MG132 (10 μ M) or hypoxia (1% O₂) for 4 hours. WCE were prepared and analysed by immunoblotting with the indicated antibodies. (B) HEK293T cells were co-transfected with myc-HIF-1 α or myc-HIF-1 α DM^(PP/AA) and empty vector or GFP-USP29. Levels of myc- and GFP-tagged proteins in WCE were determined by immunoblotting in WCE. (C) HEK293T cells were silenced with control or siRNAs (20 nM) targeting endogenous *USP29*, *PHD2/EGLN1* or *pVHL* mRNA and transfected with myc-HIF-1 α or myc-HIF-1 α DM^(PP/AA). Total cell extracts were subjected to SDS-PAGE followed by immunoblotting with the indicated antibodies. *B* and *C* were performed *in vivo*.

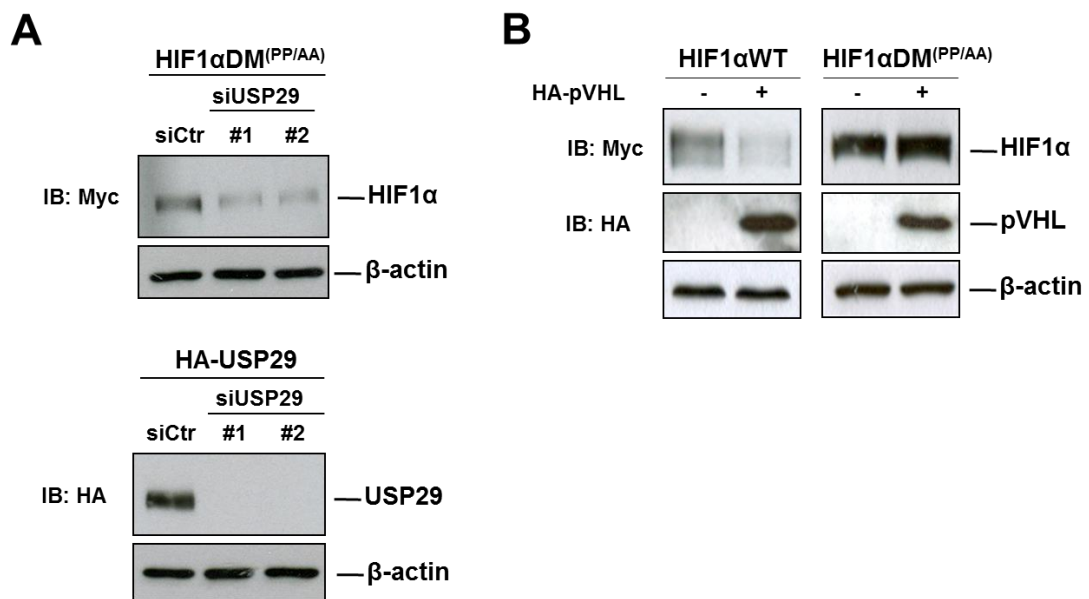


Figure 4.5: USP29 regulates HIF-1 α in a non-canonical way (supplement). (A) HEK293T cells were silenced with scrambled siRNA or two independent siRNA sequences (20nM) targeting USP29 and transfected with myc-HIF-1 α DM^(PP/AA) or HA-USP29. WCE were analysed by WB for the expression levels of myc-HIF-1 α DM^(PP/AA) or HA-USP29, respectively. (B) HEK293T cells were co-transfected with myc-HIF-1 α or myc-HIF-1 α DM^(PP/AA) and HA-pVHL. Total cell extracts were subjected SDS-PAGE followed by immunoblotting with the indicated antibodies. *All experiments were performed by me.*

4.5 Universality of USP29's effect on HIF- α

The effect of USP29 on HIF-1 α was observed in a variety of cell lines of different origins, including A2780 (ovarian cancer), PC3 and LnCaP (prostate cancer), SH-SY5Y and SK-N-AS (neuroblastoma) and MDA-MB-231 (breast cancer). In all tested cell lines the overexpression of USP29 led to an increase in HIF-1 α DM^(PP/AA) levels (Figure 4.6A), indicating that this regulation might be a wide phenomenon. Moreover, both, the wild type and the oxygen-insensitive DM^(PP/AA) forms of HIF-2 α /EPAS also accumulated upon overexpression of USP29 (Figure 4.6B).

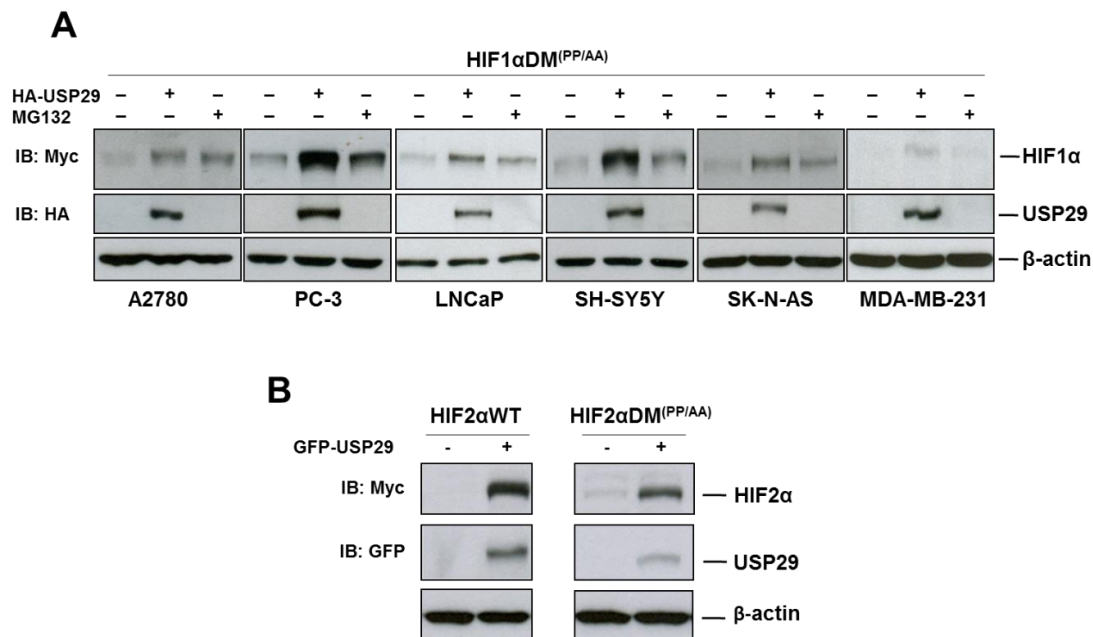


Figure 4.6: Wide impact of USP29 on HIF- α . (A) Cancer cell lines of different origins were co-transfected with myc-HIF-1 α DM^(PP/AA) and empty vector or HA-USP29 and left untreated or treated with the proteasome inhibitor MG132 (10 μ M) for 4 hours. WCE were subjected to SDS-PAGE followed by immunoblotting with the indicated antibodies. (B) HEK293T cells were co-transfected with myc-HIF-2 α or myc-HIF-2 α DM^(PP/AA) and empty vector or GFP-USP29 and total cell extracts were analysed by immunoblotting. *A was performed by me.*

4.6 USP29 stabilises HIF- α by protecting it from proteasomal degradation

In order to determine the molecular mechanism of HIF- α DM^(PP/AA) accumulation by USP29, we treated HEK293T cells with the proteasome inhibitor MG132 for 4 hours in the absence or presence of ectopic USP29 (Figure 4.7A). Both, the USP29 overexpression and the proteasome inhibition induced HIF-1 α DM^(PP/AA) accumulation, but the lack of additivity indicated that they both acted on the same pathway. Furthermore, as USP29 accumulated HIF-1 α DM^(PP/AA) more efficiently than MG132, we tested whether HIF-1 α DM^(PP/AA) was also degraded via the lysosomal pathway. Yet, the inhibition of this pathway by treatment with chloroquine failed to prevent HIF-1 α DM^(PP/AA) degradation (Figure 4.8A), confirming that it requires the proteasome activity and suggesting that the difference between MG132- and USP29-induced HIF-1 α DM^(PP/AA) accumulation was due to incomplete proteasome inhibition. Cycloheximide

experiments showed that USP29 increased HIF-1 α DM^(PP/AA)'s half-life from ≈ 1 to ≈ 3 hours (Figure 4.8B). More importantly, USP29 stabilised endogenous HIF-1 α upon reoxygenation (Figure 4.7B). Although USP29 did not avoid the initial HIF-1 α degradation within the first 10 minutes of reoxygenation, thereafter HIF-1 α levels remained stable during at least one hour in the presence of USP29, while the protein was not longer detectable 30 minutes after reoxygenation in the absence of USP29. To gain further insight into how USP29 stabilised HIF- α , we generated a catalytically inactive USP29 mutant by replacing its active site cysteine residue C294 with a serine (USP29^{C/S}). This mutation completely abrogated USP29's ability to accumulate HIF-1 α DM^(PP/AA) (Figure 4.7C), pointing towards a crucial role of USP29's ubiquitin specific peptidase activity in HIF- α DM^(PP/AA) stabilisation.

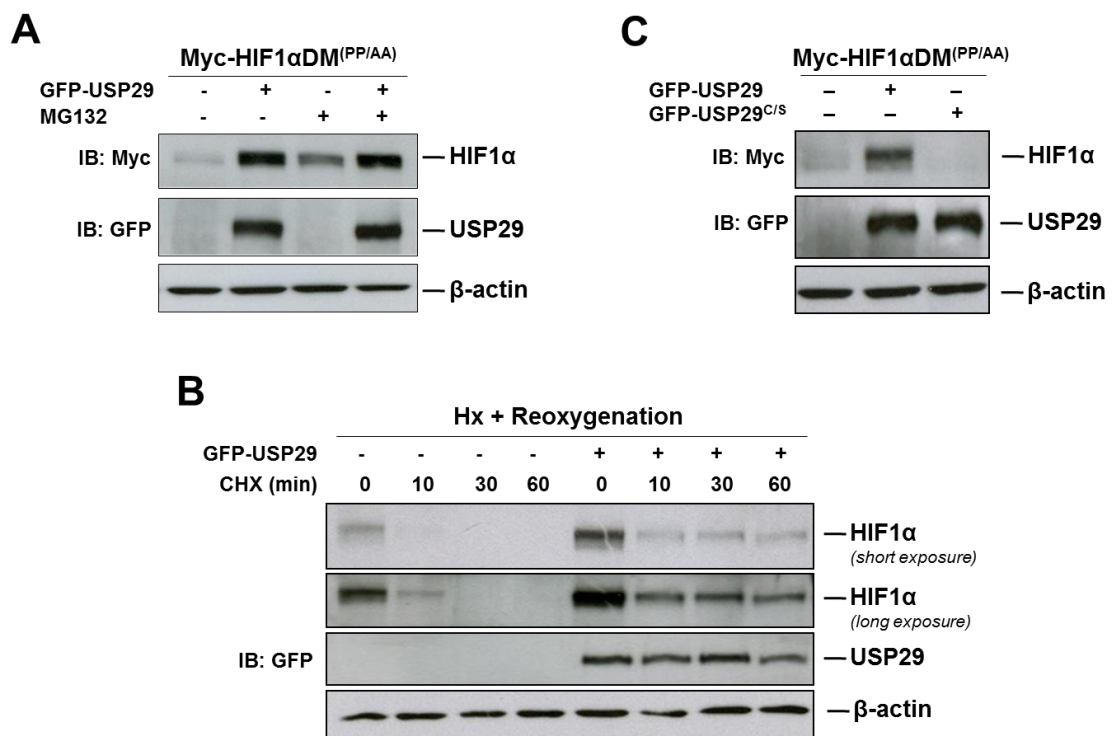


Figure 4.7: USP29 stabilises HIF-1 α by protecting it from proteasome-mediated degradation. (A) HEK293T cells were co-transfected with myc-HIF-1 α DM^(PP/AA) and empty vector or GFP-USP29 and left untreated or treated with the proteasome inhibitor MG132 (10 μ M) for 4 hours. Total cell extracts were subjected to SDS-PAGE followed by immunoblotting with the indicated antibodies. (B) HEK293T cells were transfected with empty vector or GFP-USP29 and incubated in hypoxia (1% O₂) for 4 hours. Then cells were treated with cycloheximide (20 μ g/ml) to inhibit protein synthesis, reoxygenated and cell extracts were prepared at the indicated time points. HIF-1 α protein levels were determined by Western Blotting. (C) HEK293T cells were co-transfected with myc-HIF-1 α DM^(PP/AA) and empty vector, GFP-USP29 or GFP-USP29^{C/S}. Cell extracts were subjected to immunoblotting with the indicated antibodies. *A and C were performed by me.*

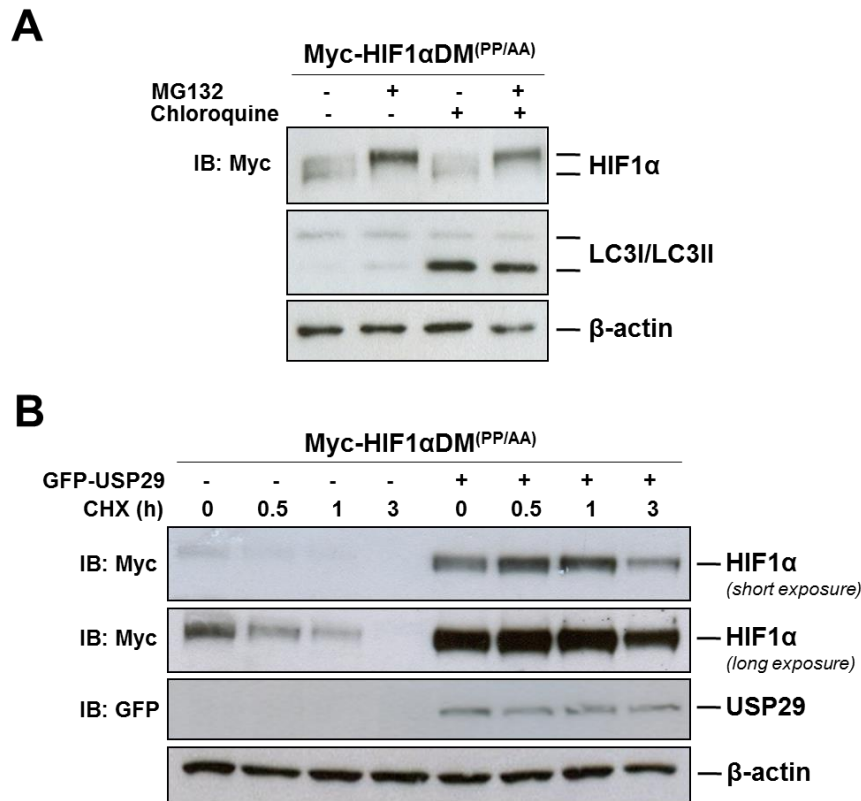


Figure 4.8: USP29 stabilises HIF-1 α by protecting from proteasome-mediated degradation (supplement). (A) HEK293T cells were transfected with myc-HIF-1 α DM^(PP/AA) and left untreated or treated with either the proteasome inhibitor MG132 (10 μ M), the autophagy inhibitor chloroquine (30 μ g/mL) or both inhibitors together for 6 hours. Protein levels were determined by immunoblotting of the whole cell extracts with the indicated antibodies. (B) HEK293T cells were co-transfected with myc-HIF-1 α DM^(PP/AA) and empty vector or GFP-USP29 and treated with cycloheximide (CHX) (20 μ g/ml) to inhibit protein synthesis. Cell extracts were collected at the indicated times after CHX addition and subjected to immunoblotting with the indicated antibodies. *A was performed by me.*

4.7 USP29 interacts with and deubiquitinates HIF- α DM^(PP/AA)

As the catalytical activity of USPs is responsible for removal of (poly)ubiquitin chains from their target proteins, we next tested whether USP29 was able to function as a deubiquitinase for HIF- α . To analyse the ubiquitination pattern of HIF-1 α DM^(PP/AA) we used Nickel-NTA-beads for specific purification of all the proteins conjugated to (His)₆-tagged ubiquitin *in cellulo*. However, the first experiments showed that myc-tagged HIF-1 α DM^(PP/AA) bound unspecifically to the Nickel-beads even in the absence of (His)₆-ubiquitin (Figure 4.9A). Therefore, this classical approach was not suitable for our purpose. At that time, an ubiquitination assay based on GFP-traps® had just been established and proved effective by Ugo Mayor's group (Lee et al., 2014). GFP-traps®'s single-chain camelid antibody has a very high affinity to various variants of green fluorescent proteins that permits very stringent washes without losing the targeted protein. We therefore inserted the Clover sequence into the myc-Clover-HIF-1 α DM^(PP/AA) construct and found that Clover did not interfere with HIF-1 α DM^(PP/AA) behaviour in response to different treatments. Myc-Clover-HIF-1 α DM^(PP/AA) accumulated upon treatment with MG132 and in the presence of USP29 but was not induced by DMOG or the catalytically inactive USP29^{C/S} (Figure 4.9B). According to these results, we successfully set-up the GFP-traps® based ubiquitination assay with myc-Clover-HIF-1 α DM^(PP/AA).

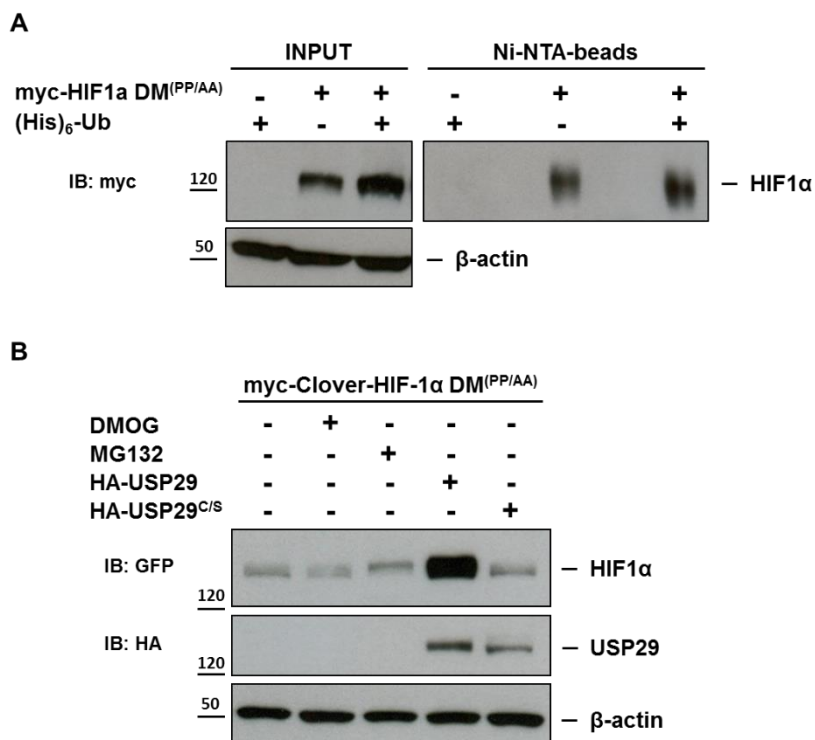


Figure 4.9: Setup of an HIF- α ubiquitination assay. (A) HEK293T cells were transfected with (His)₆-ubiquitin, myc-HIF-1 α DM^(PP/AA) or both together. Nickel-NTA-beads were used to pull down proteins that were conjugated to (His)₆-ubiquitin in denaturing conditions. (B) HEK293T cells were transfected with myc-Clover-HIF-1 α DM and treated with DMOG or MG132 or co-transfected with catalytically active or inactive HA-USP29. All experiments were performed by me.

First, we analysed the interaction between USP29 and HIF- α using fluorescence lifetime based FRET measurements. The fluorescence lifetime of the FRET donor, Clover-HIF-1 α DM^(PP/AA), was significantly decreased from 2.86 ± 0.02 ns to 2.7 ± 0.09 ns in the presence of the FRET acceptor mCherry-USP29 (Figure 4.10A). As FRET only occurs when both fluorophores are in very close proximity (around 6 nm), these data clearly show that USP29 is directly bound to HIF-1 α DM^(PP/AA). Similar results were obtained when we analysed the interaction between USP29 and HIF-2 α DM^(PP/AA) (Figure 4.11A). HIF-2 α DM^(PP/AA)-GFP's lifetime was significantly reduced from 2.39 ± 0.01 ns to 2.28 ± 0.06 ns in the presence of the FRET acceptor mCherry-USP29. Furthermore, when GFP-tagged HIF-1 α DM^(PP/AA) or GFP alone were immunoprecipitated from HEK293T cells, we found HA-USP29 to interact with GFP-tagged HIF-1 α DM^(PP/AA), but not with GFP alone (Figure 4.11B). Next, we cotransfected GFP-tagged HIF-1 α DM^(PP/AA) together with FLAG-ubiquitin either in the absence or the presence of HA-USP29 or HA-USP29^{C/S}. After the enrichment of the ubiquitinated proteome by MG132-treatment, GFP-HIF-1 α DM^(PP/AA) was pulled-down under highly denaturing conditions and anti-FLAG-antibody was used to detect ubiquitinated GFP-HIF-1 α DM^(PP/AA). We found that USP29 wild type, but not the catalytically inactive USP29^{C/S}, considerably decreased the basal ubiquitination of HIF-1 α DM^(PP/AA) and increased the non-modified population of HIF-1 α DM^(PP/AA) (Figure 4.10B). Accordingly, when silencing endogenous *USP29*, we observed increased poly-ubiquitination of HIF-1 α DM^(PP/AA) (Figure 4.10C), pointing towards a basal deubiquitinating activity of endogenous USP29. Expression of a siRNA-resistant USP29 restored the basal HIF-1 α DM^(PP/AA) ubiquitination pattern (Figure 4.10C right lane). Furthermore and in concordance with Figure 3B, USP29 also exerted deubiquitination activity towards HIF-2 α DM^(PP/AA) (Figure 4.11B). Taken together, our results indicate that endogenous and ectopic USP29 is an efficient deubiquitinase for HIF- α DM^(PP/AA) thereby increasing HIF- α stabilisation and subsequent HIF activation.

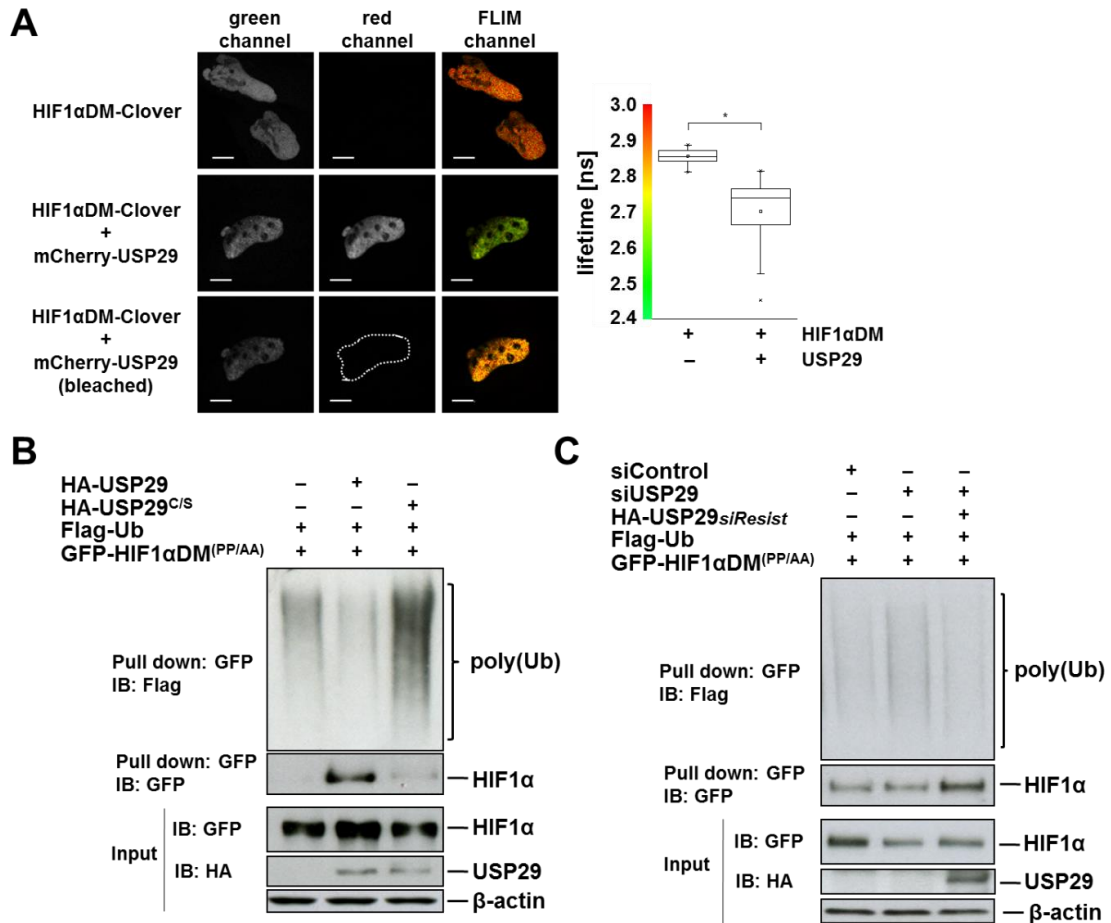


Figure 4.10: USP29 deubiquitinates HIF- α DM^(PP/AA). (A) HeLa cells were transfected with the FRET donor Clover- HIF-1 α DM^(PP/AA) alone or together with the FRET acceptor mCherry-USP29. Fluorescence images for donor (green) and acceptor (red) channel were acquired (left and central panel). The lifetime of the donor was measured and pseudo-colour coded fluorescence life time images (FLIM) were generated. From 3 independent experiments average lifetimes of the donor in the absence ($n = 34$) and the presence ($n = 25$) of the FRET acceptor were calculated. Scale bars are 10 μ m long, (*) $p = 1.32 \cdot 10^{-8}$. (B) HEK293T cells were co-transfected with GFP-HIF-1 α DM^(PP/AA), FLAG-ubiquitin and either HA-USP29 or HA-USP29^{C/S}. Cells were treated with the proteasome inhibitor MG132 (10 μ M) for 2 hours and lysed in the presence of the DUB inhibitor NEM. GFP-HIF-1 α DM^(PP/AA) was pulled down with GFP-traps® and subjected to stringent washes (8 M urea, 1% SDS). Ubiquitinated and non-ubiquitinated GFP-HIF-1 α DM^(PP/AA) protein in the eluate was analysed by immunoblotting with anti-FLAG and anti-GFP antibodies, respectively. (C) HEK293T cells were silenced with a control or a siRNA targeting *USP29* (20 nM) and co-transfected with GFP-HIF-1 α DM^(PP/AA), FLAG-ubiquitin and either empty vector or siRNA-resistant HA-USP29. Treatment of cells, pull-down with GFP-traps® and subsequent analysis of the ubiquitinated and non-ubiquitinated GFP-HIF-1 α DM^(PP/AA) protein in the eluate were performed as in (B). *All experiments were performed by me.*

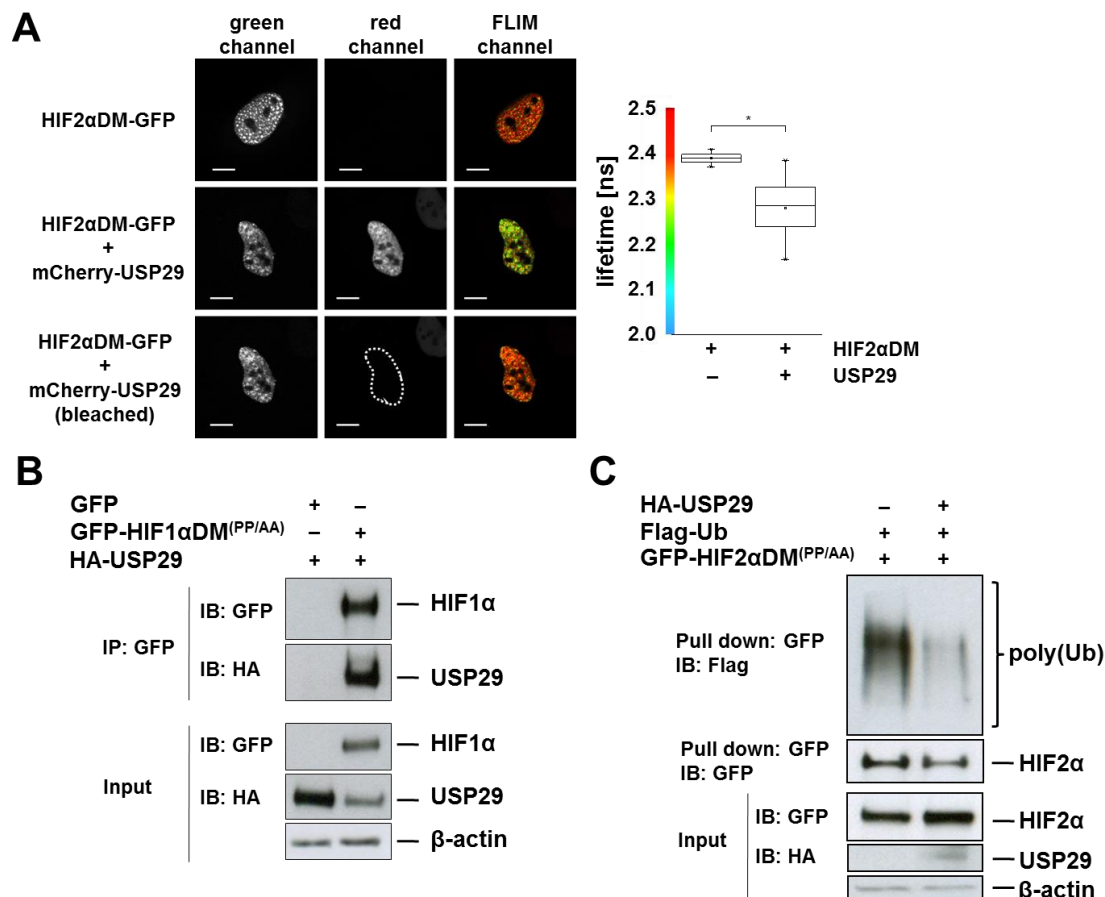


Figure 4.11: USP29 deubiquitinates HIF- α DM^(PP/AA) (supplement). (A) HeLa cells were transfected with the FRET donor HIF-2 α DM^(PP/AA)-GFP alone or together with the FRET acceptor mCherry-USP29. Fluorescence images for donor (green) and acceptor (red) channel were acquired (left and central panel). The lifetime of the donor was measured and pseudo-colour coded fluorescence life time images (FLIM) were generated. Average lifetimes of the donor in the absence (n = 25) and the presence (n = 29) of the FRET acceptor were calculated from 3 independent experiments. Scale bars are 10 μ m long, (*) p = 2.36*10⁻¹¹. (B) HEK293T cells were co-transfected with HA-USP29 and either GFP alone or GFP-HIF-1 α DM^(PP/AA). Cells were lysed in native conditions and GFP-tagged protein was immunoprecipitated with GFP-traps®. Immuno-complexes were analysed for the presence of HA-USP29 by immunoblotting. (C) HEK293T cells were co-transfected with GFP-HIF-2 α DM^(PP/AA), FLAG-ubiquitin and either HA-USP29 or empty vector. Cells were treated with the proteasome inhibitor MG132 (10 μ M) for 2 hours and lysed in the presence of the DUB inhibitor NEM. GFP-HIF-2 α DM^(PP/AA) was pulled down with GFP-traps® and subjected to stringent washes (8 M urea, 1% SDS). Ubiquitinated and non-ubiquitinated GFP-HIF-2 α DM^(PP/AA) protein in the eluate was analysed by immunoblotting with anti-FLAG and anti-GFP antibodies, respectively. *A and B were performed by me.*

4.8 HIF-1 α is specifically targeted by USP29

We have shown that overexpressed USP29 efficiently deubiquitinated and hence accumulated HIF-1 α and HIF-1 α DM^(PP/AA) in normoxic cells. To exclude that the deubiquitination was an unspecific event as a result of the overexpression of USP29, we tested whether the overexpression of another nuclear deubiquitinase would also accumulate HIF-1 α . While GFP-USP29 efficiently accumulated both, HIF-1 α and HIF-1 α DM^(PP/AA), the presence of overexpressed deubiquitinase activity in form of another nuclear DUB - USP11 - was not sufficient to do the same (Figure 4.12). Together with the siUSP29 data, this indicated that USP29 was indeed targeting HIF-1 α specifically.

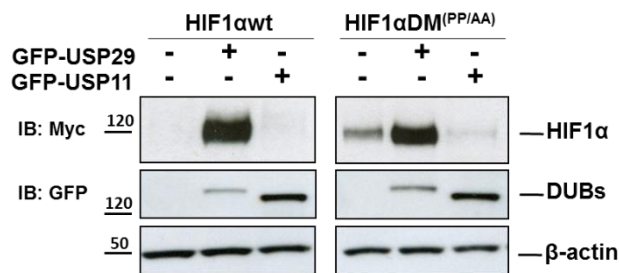


Figure 4.12: USP29 but not another nuclear DUB accumulates HIF-1 α . HEK293T cells were co-transfected with myc-HIF-1 α or myc-HIF-1 α DM^(PP/AA) and GFP-USP29 or GFP-USP11. Whole cell lysates were subjected to SDS-PAGE followed by immunoblotting with the indicated antibodies. The experiment was performed by EB's technician. *Experiment was performed by me.*

4.9 USP29 targets the C-terminal part of HIF- α

To identify the potential lysine residues targeted by USP29's deubiquitinating activity, we tested several truncated forms of HIF-1 α DM^(PP/AA) for their susceptibility to USP29. The N-terminal part, HIF1 α DM¹⁻⁶⁵⁷, was not affected by the presence of USP29 (and MG132, data not shown), while the C-terminal end (HIF-1 α ⁶³⁰⁻⁸²⁶) accumulated in the presence of USP29 similarly to the full-length protein (Figure 4.13A). The USP29^{C/S} mutant that lacked catalytical activity was not able to accumulate HIF-1 α ⁶³⁰⁻⁸²⁶ (Figure 4.14A). Correspondingly, USP29 acted also on the C-terminus of HIF-2 α (Figure 4.14B). We used truncations of the C-terminus to further confine the USP29 target site within HIF-1 α . HIF-1 α ⁶³⁰⁻⁷¹³ and HIF-1 α ⁶³⁰⁻⁷⁵⁰ were resistant to USP29-mediated accumulation (Figure 4.14C) and pointed out the importance of the very C-terminal tail of HIF-1 α for this regulation. This tail contains two evolutionary conserved lysines (K752 and K755), which are also shared by HIF-2 α and a neighbouring lysine (K758) (Figure 4.14D). Mutation of all three lysines to arginines (HIF-1 α DM^{KKK/RRR}) conferred to this mutated protein a higher stability in cycloheximide experiments (Figure 4.13B). Importantly, the basal ubiquitination of HIF-1 α DM^{KKK/RRR} was significantly reduced as compared to HIF-1 α DM (Figure 4.13C).

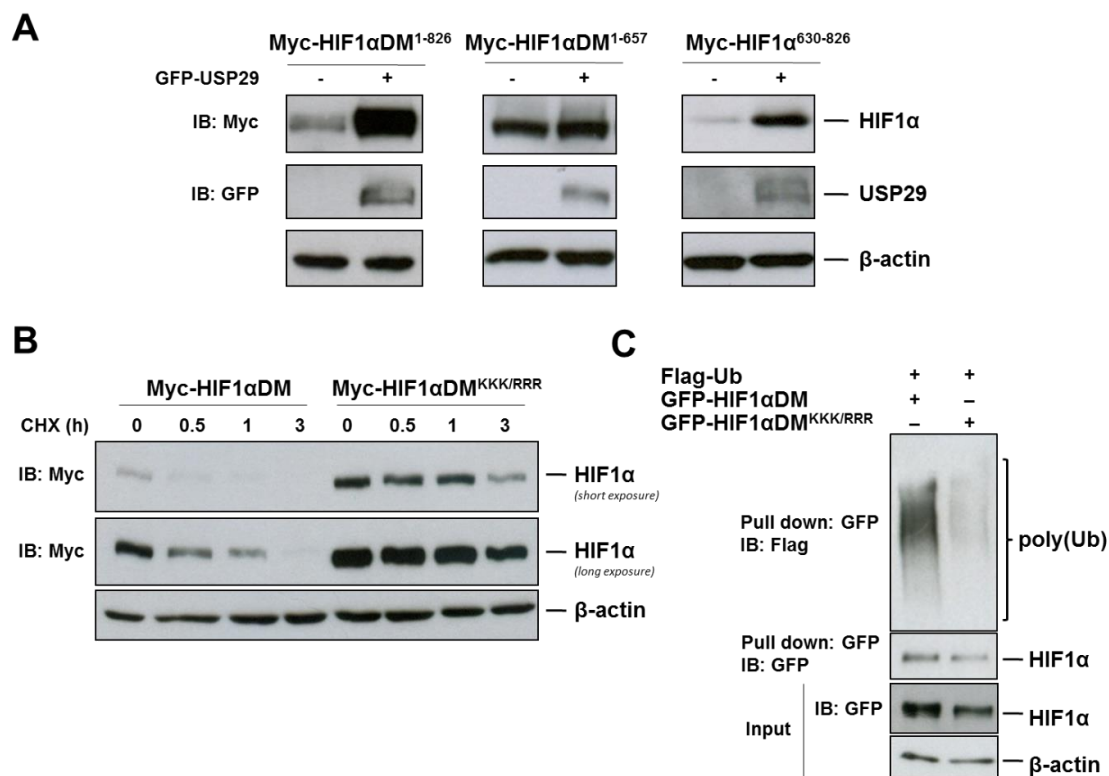


Figure 4.13: USP29 targets the C-terminal part of HIF- α . (A) HEK293T cells were co-transfected with myc-HIF-1 α DM¹⁻⁸²⁶, myc-HIF-1 α DM¹⁻⁶⁵⁷ or myc-HIF-1 α DM⁶³⁰⁻⁸²⁶ and either empty vector or GFP-USP29. Whole cell extracts were subjected to SDS-PAGE followed by immunoblotting with the indicated antibodies. (B) HEK293T cells were transfected with myc-HIF-1 α DM or myc-HIF-1 α DM^{KKK/RRR} and cells were treated with cycloheximide (CHX) (20 μ g/ml) to inhibit protein synthesis. Cell extracts were collected at the indicated times after CHX treatment and protein levels of the myc-tagged HIF-1 α DM^(PP/AA) proteins were analysed by western blot. (C) HEK293T cells were co-transfected with GFP-HIF-1 α DM or myc-HIF-1 α DM^{KKK/RRR} and FLAG-ubiquitin. Cells were treated with the proteasome inhibitor MG132 (10 μ M) for 2 hours and lysed in the presence of the DUB inhibitor NEM. GFP-tagged protein was pulled down with GFP-traps® and subjected to stringent washes (8 M urea, 1% SDS). Ubiquitinated and non-ubiquitinated GFP-HIF-1 α protein in the eluate was analysed by immunoblotting with anti-FLAG and anti-GFP antibodies, respectively. *B and C were performed by me.*

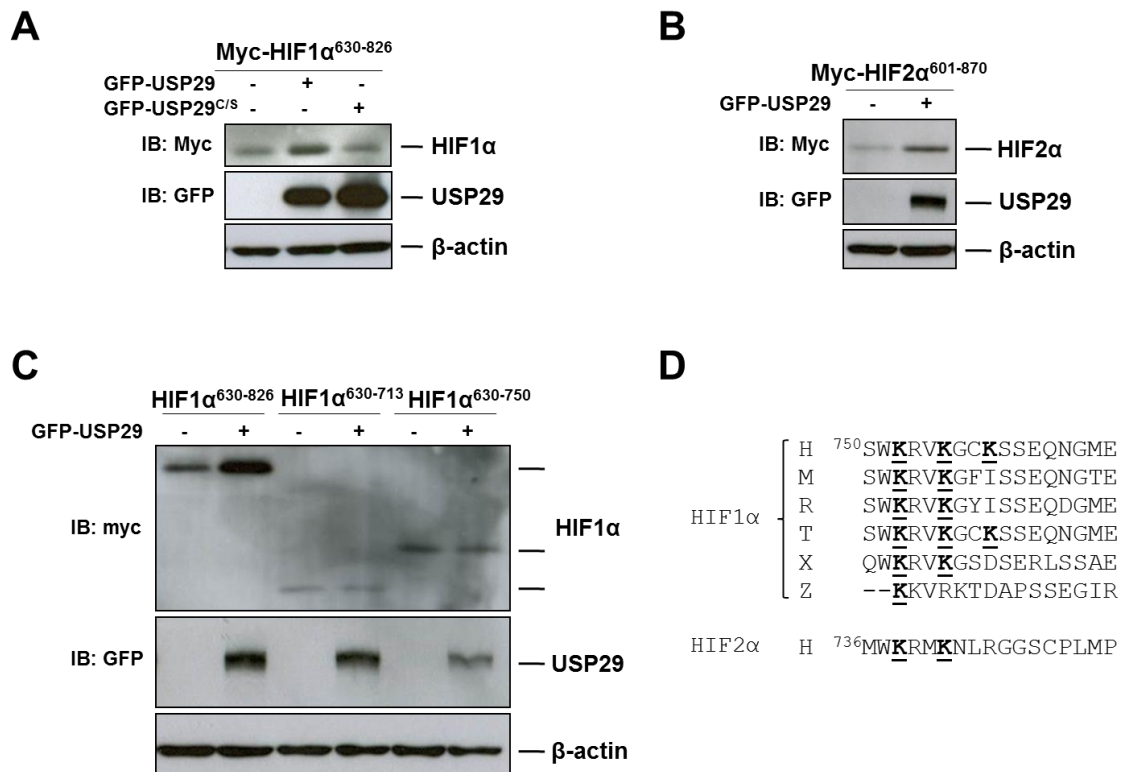


Figure 4.14: USP29 targets the C-terminal part of HIF- α (supplement). (A) HEK293T cells were co-transfected with myc-HIF-1 α DM⁶³⁰⁻⁸²⁶ and either empty vector, GFP-USP29 or GFP-USP29^{C/S}. Whole cell extracts were prepared and submitted to immunoblotting with the indicated antibodies. (B, C) HEK293T cells were co-transfected with (B) myc-HIF-2 α DM⁶⁰¹⁻⁸⁷⁰ or (C) myc-HIF-1 α DM⁶³⁰⁻⁸²⁶, myc-HIF-1 α DM⁶³⁰⁻⁷¹³ or myc-HIF-1 α DM⁶³⁰⁻⁷⁵⁰ and either empty vector or GFP-USP29. Whole cell extracts were prepared and submitted to immunoblotting with the indicated antibodies. (D) Alignment of the lysine-containing C-terminal sequence of HIF-1 α and HIF-2 α from human (H), mouse (M), rat (R), cow (T), xenopus (X) and zebrafish (Z). *A and D were performed by me.*

4.10 MS analysis of HIF-1 α DM's PTMs

We had located USP29's target site within HIF-1 α to three lysine residues at the very C-terminus of the protein. Upon mutation of K752, K755 and K758 to arginines basal poly-ubiquitination of HIF-1 α DM^{KKK/RRR} was clearly reduced as compared to HIF-1 α DM (Figure 4.13C). We sought to confirm this data by mass spectrometry. To that end, Clover-HIF-1 α DM^(PP/AA) and FLAG-ubiquitin were co-transfected into HEK293T cells and these cells were treated with MG132 to accumulate ubiquitinated populations, lysed and incubated with GFP-traps®. Stringent washes removed proteins that interacted non-covalently with Clover-HIF-1 α DM or the beads and subsequently Clover-HIF-1 α DM^(PP/AA) was eluted from the beads. On a SDS gel the eluate showed two major bands, which supposedly corresponded to Clover-HIF-1 α DM^(PP/AA) (Figure 4.15A, upper band) and to Clover (lower band). The upper band was cut out generously in order to include the high molecular weight poly-ubiquitinated populations of Clover-HIF-1 α DM^(PP/AA), and subsequently digested with trypsin. Fragments were loaded onto

the mass spectrometer and unique peptides were mapped to the HIF-1 α sequence (Figure 4.15B, red). Only a coverage of 36% of the sequence was obtained. As trypsin cuts C-terminally of lysine and arginine residues if they are not followed by a proline, K752 (underlined) is the last residue of a 32 amino acid long fragment while K755 and K758 (underlined) are part of di- and tripeptides, respectively, after complete trypsin digestion (Figure 4.15C). While the former is too long to be resolved by MS, the latter two are too short, even if they were ubiquitinated which would add a di-glycine to the lysine residue. This might explain why none of the three lysine residues was detected by the analysis. However, K48-linked poly-ubiquitin was present in the analysed sample. This is evidence for Clover-HIF-1 α DM^(PP/AA) being indeed poly-ubiquitinated with the classical signal for proteasomal degradation.

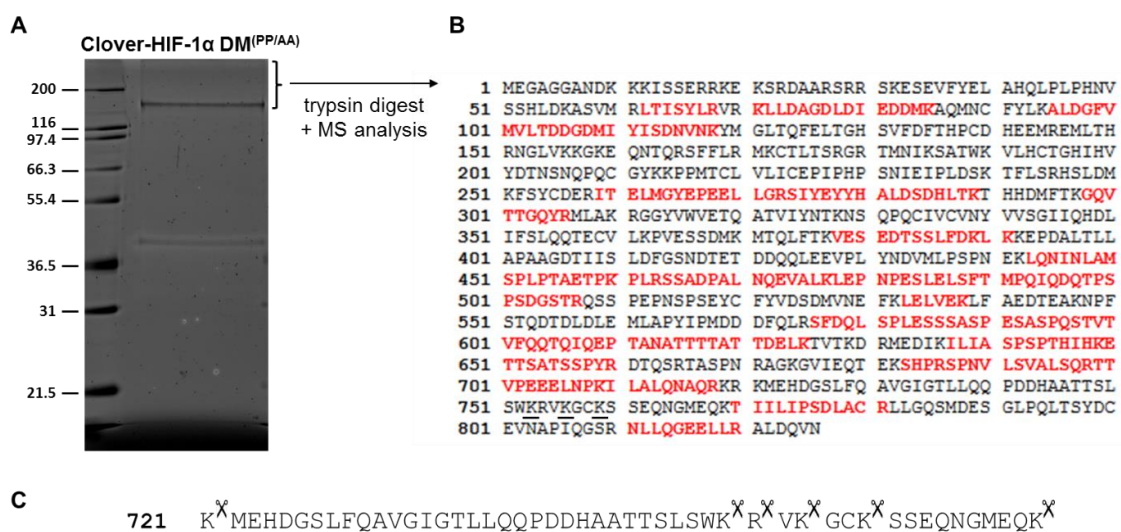


Figure 4.15: MassSpec analysis of HIF-1 α DM^(PP/AA). (A) Clover-HIF-1 α DM^(PP/AA) was pulled down from HEK293T cells in denaturing conditions after MG132 treatment, run on a SDS gel and stained with SYPRO®. The band corresponding to Clover-HIF-1 α DM^(PP/AA) was digested with trypsin and analysed on the mass spectrometer. (B) Unique identified peptides (red) were mapped to the HIF-1 α sequence. (C) Sequence context of the lysine residues of interest (K752, K755, K758, underlined). Scissors indicate tryptic cleavage sites. *Samples were prepared by me and processed by the proteomics platform at CIC bioGUNE:*

4.11 USP29 levels correlate with tumour progression and HIF target gene expression

The fact that USP29 stabilises HIF- α and is able to maintain hypoxia signalling switched on in normoxic conditions, led us to inquire its potential function in tumour progression. We therefore assessed whether USP29 expression was altered in certain tumours. Data mining analysis of publicly available databases revealed that *USP29* expression was significantly correlated with prostate cancer progression (Figure 4.16A). The expression levels of *USP29* mRNA increased from normal tissue over primary tumour to metastasis. Interestingly, *USP29* expression exhibited a significant association with the Gleason Score (GS), used in the clinics to stratify prostate cancer patients and predict their prognosis, as reflected by higher GS associated with higher *USP29* expression levels (Figure 4.16B). Furthermore, in the prostate cancer samples the expression of *USP29* also showed a significant positive correlation with the expression levels of the HIF target gene *CA9* (Figure 4.16C).

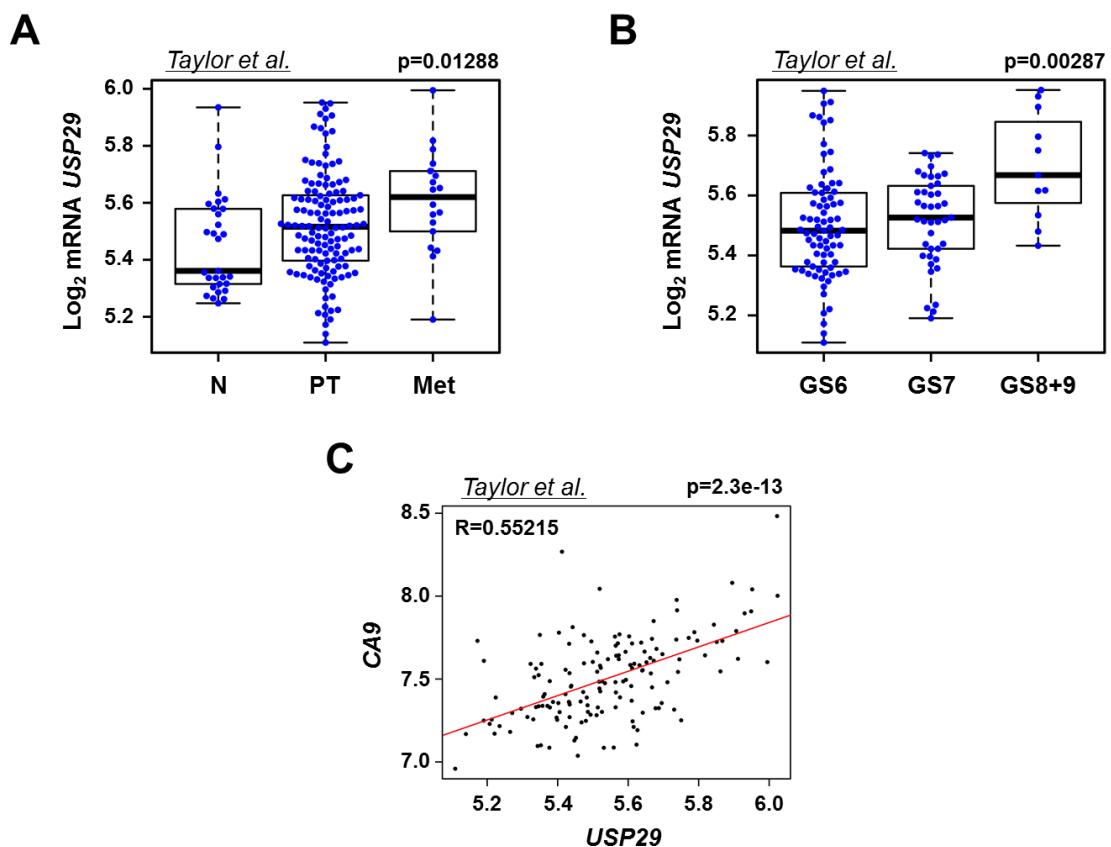


Figure 4.16: USP29 expression in prostate cancer. (A, B) Gene expression analysis of USP29 in a dataset of prostate cancer samples (Taylor et al, 2010). USP29 mRNA levels in prostate samples were compared on the basis of their tissue origin (A) or the Gleason score (GS) of the patient (B) (normal tissue (N): $n = 29$, primary tumours (PT): $n = 131$; metastatic tumours (Met): $n = 19$). (C) Correlation analysis between USP29 and CA9 mRNA levels in the aforementioned dataset of primary prostate cancer samples (Taylor, $n = 131$). Analysis was performed by Ana M Aransay at CIC bioGUNE.

4.12 USP29's effect on HIF-1 α in hypoxia

USP29 removes non-canonical poly-ubiquitin chains from HIF-1 α . In contrast to the canonical poly-ubiquitination by pVHL, HIF-1 α could be modified by those chains in hypoxia as well. Yet, we found that in 1% O₂, USP29 overexpression was not able to further enhance HIF-1 α accumulation (Figure 4.17A). In 5% O₂, however, USP29 was able to further accumulate HIF-1 α (Figure 4.17B). This indicated that in mild hypoxia HIF-1 α might be still poly-ubiquitinated by pVHL as well as by the other ubiquitin E3 ligase whose action is counteracted by USP29.

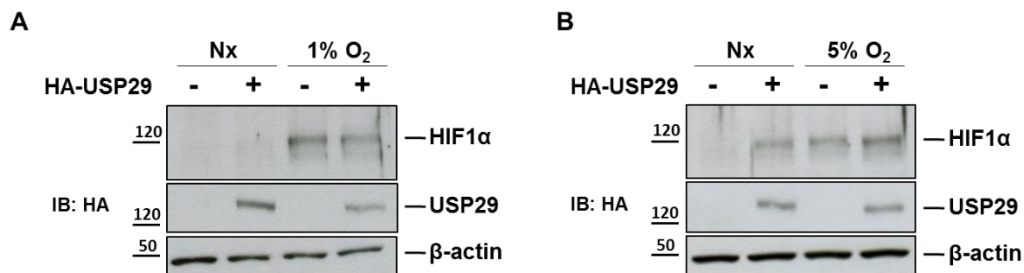


Figure 4.17: USP29 affects HIF-1 α in mild hypoxia. HEK293T cells were transfected with HA-USP29 or with empty vector and incubated in normoxia, 1% O₂ or 5% O₂ for 4h prior to lysis and western blotting. *Experiments were performed by EB lab members.*

4.13 Further FLIM-FRET experiments: USP29 - HIF- α interaction

Apart from the FLIM-based FRET measurements presented before we performed further experiments to explore how robust the FRET-measured interaction between USP29 and HIF- α was. For that purpose different fluorescent-fusion constructs that were available in the lab were used. As well as constructs with the fluorescent tag fused to the opposite end of the protein of interest, we were able to swap FRET donor and FRET acceptor in some conditions. Table 4.1 resumes the possible combinations and the performed FLIM-FRET measurements.

Table 4.1: Combinations of available FRET donor and FRET acceptor constructs and the measured fluorescence lifetimes of the donors in the absence and the presence of the acceptors. ND = not determined.

FRET donor \ FRET acceptor	mCherry-USP29	HIF-2 α -dsRedXP
HIF-1 α DM-Clover (2.86 \pm 0.017 ns)	✓ Figure 4.10A (2.70 \pm 0.093 ns)	ND
Clover- HIF-1 α DM (2.95 \pm 0.027 ns)	✓ Figure 4.18A (2.85 \pm 0.078 ns)	ND
HIF-2 α DM-GFP (2.39 \pm 0.011 ns)	✓ Figure 4.11A (2.28 \pm 0.057 ns)	ND
GFP-USP29 (2.39 \pm 0.016 ns)	✓ Figure 5.7 (2.36 \pm 0.028 ns)	✓ Figure 4.18B (2.34 \pm 0.040 ns)

When having Clover attached to the N-terminus instead of to the C-terminus of HIF-1 α DM, we were still able to measure FRET between HIF-1 α DM and USP29. Clover-HIF-1 α DM's lifetime decreased significantly from 2.95 \pm 0.027 ns to 2.85 \pm 0.078 ns in the presence of mCherry-USP29 ($p = 1.06 \cdot 10^{-5}$) and the lifetime recovered by photobleaching of the acceptor fluorophore mCherry (Figure 4.18A).

Unsurprisingly, we also found that USP29 interacted with wildtype HIF-2 α . GFP-USP29's lifetime decreased from 2.39 \pm 0.016 ns to 2.34 \pm 0.040 ns in the presence of HIF-2 α -dsRedXP ($p = 1.16 \cdot 10^{-5}$) and acceptor photobleaching reversed this effect (Figure 4.18B). Besides, we also saw a clear redistribution of GFP-USP29 as it was moved from a homogenous nuclear localisation into the typical HIF-2 α speckles (Taylor et al., 2016).

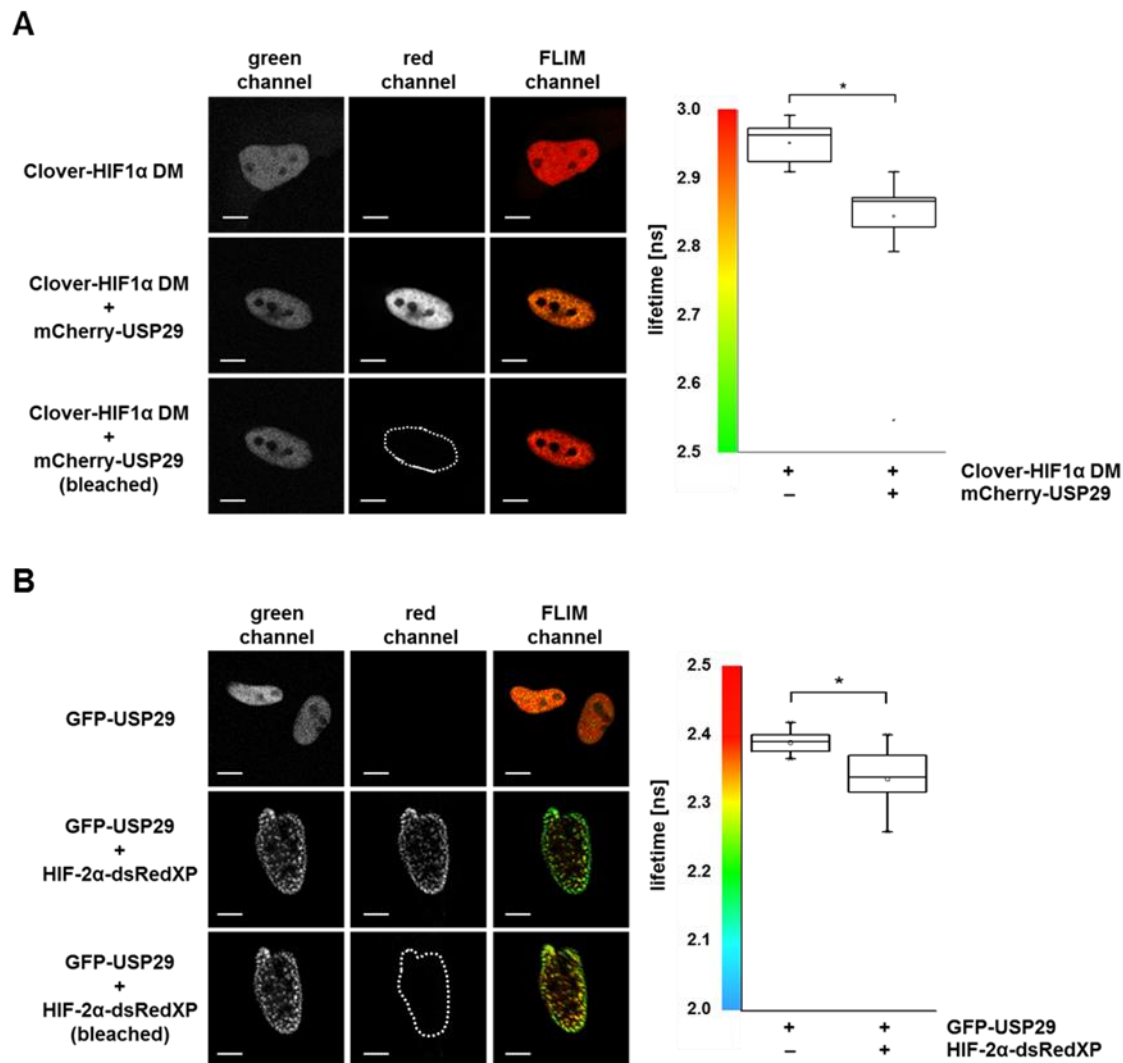


Figure 4.18: USP29 and HIF- α interact with each other. HeLa cells were transfected with a green fluorescent FRET donor alone or together with a red fluorescent FRET acceptor. Representative fluorescence and pseudo-coloured fluorescence lifetime (FLIM) images are shown in the first two and the last column, respectively. The white dotted line shows the region of interest that was photobleached. Average fluorescence lifetimes of the nuclear FRET donor were extracted from the images and represented in the box plot (right panel). (A) 14 cells expressing Clover-HIF1 α DM^(PP/AA) and 19 cells co-expressing Clover-HIF1 α DM^(PP/AA) and mCherry-USP29 from 2 different experiments were analysed. (B) 25 cells expressing GFP-USP29 and 20 cells co-expressing GFP-USP29 and HIF-2 α -dsRedXP from 3 different experiments were analysed. Scale bars are 10 μ m long. *Experiments were performed by me.*

4.14 Searching for HIF-1 α 's non-canonical ubiquitin E3 ligase

We have showed that USP29 stabilised HIF-1 α without affecting prolyl-hydroxylation by PHDs or poly-ubiquitination by pVHL. Furthermore, upon depletion of endogenous USP29 hypoxic induction of HIF-1 α accumulation was impaired and HIF-1 α DM^(PP/AA) poly-ubiquitination was increased (Figure 4.10). This pointed towards the existence of an ubiquitin E3-ligase that targets HIF-1 α for proteasomal degradation independently of cellular oxygen tension and whose function is opposed by USP29. Several non-canonical HIF-1 α ubiquitin E3 ligases have been

described previously (Table 4.2) and we checked whether they also down-regulated HIF-1 α DM^(PP/AA). We further tested whether an additional set of components of E3 ligase complexes that we found to interact with USP29 (see 0) affected HIF-1 α DM^(PP/AA) levels.

Table 4.2: Potential non-canonical ubiquitin E3 ligases for HIF-1 α . Ubiquitin E3 ligases and components of such complexes described as modulators of HIF-1 α or identified in USP29's interactome (chapter 0)

	HIF-1 α modulators	USP29's interactome
PARK2	(Sarraf et al., 2013)	No
STUB1/CHIP	(Luo et al., 2010)	yes (2/3)
MDM2	(Ravi et al., 2000)	No
TRIM28	(Li et al., 2003)	yes (3/3)
Fbw7	(Cassavaugh et al., 2011)	No
TRAF6	(Sun et al., 2013)	No
DDB1	No	yes (3/3)
SKP1	No	yes (3/3)
HUWE1	No	yes (2/3)
RLIM	No	yes (2/3)

Therefore, we monitored the protein level of HIF-1 α DM^(PP/AA) in HEK293T cells upon siRNA-mediated depletion of each individual ubiquitin E3 ligase complex component (Figure 4.19). Silencing of most of the tested E3 ligases resulted either in no change or in a drop of HIF-1 α DM^(PP/AA) levels. In particular, HIF-1 α DM^(PP/AA) levels were not increased in any condition, as it would be expected when silencing the negative regulator. This suggested that either a novel ubiquitin E3 ligase was responsible for targeting HIF-1 α DM^(PP/AA) for degradation or that, even though good silencing efficiencies were achieved (Figure 4.19), residual ubiquitination activity was sufficient to keep targeting HIF-1 α DM^(PP/AA) for degradation.

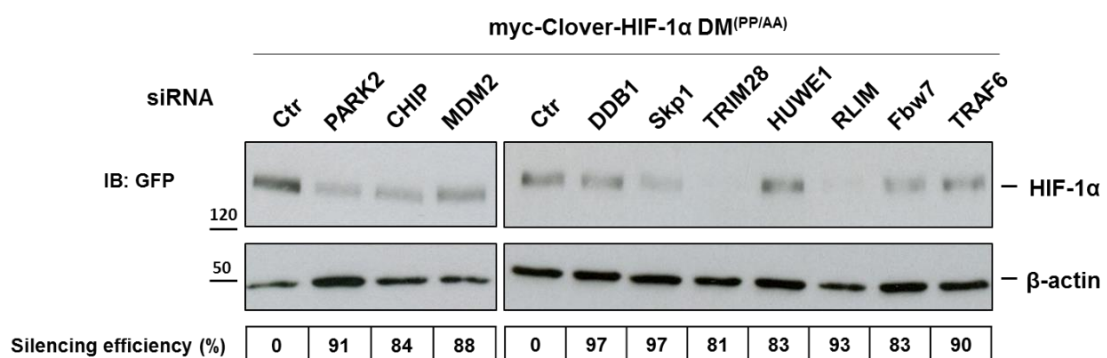


Figure 4.19: HIF-1 α DM^(PP/AA) is not down-regulated by the selected potential ubiquitin E3-ligases. E3 ligases were depleted from HEK293T cells with siRNAs and the silencing efficiency was determined using qPCR (bottom). HIF-1 α DM^(PP/AA) was overexpressed in the silenced cells and HIF-1 α DM^(PP/AA) protein levels were determined by immunoblotting. Experiment was performed by me.

4.15 Discussion

We sought to find new regulators of hypoxia signalling in the hope of improving the understanding of why HIF- α levels do not always correlate with oxygen levels present in the cells. This is particularly prevalent in cancer where HIF- α has even been described to be a negative prognostic factor (Trastour et al., 2007; Zhong et al., 1999). As HIF- α 's are tightly regulated through ubiquitination followed by proteasomal degradation, a protein that deconjugates ubiquitin – a deubiquitinase – would be a logical candidate for being a HIF- α stabiliser.

A DUB screen performed in Edurne Berra's lab revealed USP29 as a potential novel activator of the hypoxia signalling. The data presented in manuscript form in this chapter confirm USP29's role as a HIF- α stabiliser. USP29 binds to both, HIF-1 α and HIF-2 α , in a hydroxyproline (and pVHL-) independent manner and deubiquitinates them very efficiently *in cellulo*, thereby protecting them from proteasomal degradation even in normoxic conditions. The mechanism through which USP29 acts on HIF- α is therefore fundamentally different from how the DUB Cezanne/OTUD7B affects HIF-1 α . Cezanne has recently been shown to stabilise HIF-1 α through a mechanism that depends on pVHL and protects HIF- α from lysosomal degradation, presumably by deconjugating K11-linked poly-ubiquitin (Bremm et al., 2014).

Further, USP29 is the only deubiquitinase known today that exhibits catalytical activity towards HIF-2 α , and besides USP28 the second deubiquitinase that is known to rescue HIF-1 α from PHD/pVHL-independent targeting to the proteasome (Flugel et al., 2012). However, while it has been shown that Fbw7 is the ubiquitin E3 ligase that is counteracted by USP28, no ubiquitin E3 ligase has been reported to act on the very C-terminus of HIF- α , which we found to be targeted by USP29. In this region we identified a cluster of three conserved lysine residues and their mutation to arginines considerably reduced basal ubiquitination of HIF-1 α DM^(PP/AA) that translated into higher stability of the protein. No function has been previously ascribed to these lysines and accordingly, when we knocked down known ubiquitin E3 ligases for HIF- α , in none of the conditions was HIF- α DM^(PP/AA) stabilised. The same was true when we tested a panel of ubiquitin E3 ligase complexes that we found to be associated with USP29. Hence, the identity of HIF- α DM^(PP/AA)'s negative regulator remains unknown, however our data propose that it assembles proteasome-targeting K48-linked poly-ubiquitin on HIF- α .

Furthermore, the fact that the overexpression of USP29 protected both, endogenous wildtype HIF- α and oxygen-insensitive HIF- α DM^(PP/AA), very efficiently from normoxic proteasomal degradation suggested that this unidentified HIF- α -E3 ligase was continuously active and limiting HIF- α availability in a similar way as does pVHL. Moreover, we found evidence for endogenous USP29 to be continuously stabilising HIF-1 α , as siUSP29-mediated knock-down resulted in reduction of HIF-1 α levels. The fact that USP29 levels were below detection limit with commercially available antibodies suggested that although being scarce, USP29 was catalytically highly active. Therefore, we propose that USP29 and the opposed ubiquitin E3 ligase contribute to HIF- α steady-state levels in normoxia independently of oxygenation.

Their inactivation or hyperactivation either genetically or via post-translational regulations are therefore likely to have an important impact on HIF homeostasis and might be implicated in various diseases that are known to have deregulated hypoxia signalling. In particular, sustained HIF-1 α levels and consequential active HIF signalling could be caused either by the inactivation of the ubiquitin E3 ligase or by the hyperactivation of USP29, respectively. The development of HIF inhibitors has yielded some promising results recently (Chen et al., 2016; Cho et al., 2016), but targeting the responsible deregulated upstream regulator might be a more promising and more specific alternative. The presence of conserved cysteine or metalloprotease active sites in DUBs makes them potentially more easily druggable than the ubiquitin E3 ligases which lack a canonical active site.

Taken together, it is tempting to speculate about USP29's potential use as a drug target in conditions where overexpressed and/or overactive USP29 is responsible for inappropriate HIF signalling. In physiological conditions USP29 expression is thought to be very tightly controlled on a transcriptional level. The *USP29* gene is imprinted and hence we and others found endogenous USP29 mRNA and protein levels barely above background by qPCR and Western Blot, respectively, using commercially available antibodies for protein detection (Kim et al., 2000; Liu et al., 2011). The epigenetic mechanisms that control USP29 expression and how those mechanisms are disturbed in cancer remain to be determined. For instance, LOI (loss of imprinting)-mediated activation of the normally silent maternal allele might cause an USP29 upregulation. Furthermore, Liu and co-workers suggested that *USP29* expression was induced upon oxidative stress (Liu et al., 2011). In their experimental setup H₂O₂ treatment induced cooperative binding of FBP (FUSE binding protein) and AIMP2 (JTV1/p38) to *USP29*'s Far Upstream Sequence Element (FUSE), thereby triggering *USP29* transcription. Notably, AIMP2-DX2, an AIMP2 splice-variant, was particularly effective in inducing *USP29* expression (Liu et al., 2011) and high AIMP2-DX2 expression has been correlated with lung cancer progression (Choi et al., 2011). Independently of the molecular mechanism underlying the transcriptional USP29 upregulation, the inactivation of USP29 activity could have the potential to reverse pathological hypoxia signalling efficiently. In particular, this would not interfere with the physiological signalling pathway that allows for adaptation to hypoxia. A specific and adequately dosed drug that targets USP29, despite being delivered to all cells of the body, would only affect cells with high amounts of USP29 where it could normalise HIF- α levels.

Both, academic research, as well as pharmaceutical companies are currently trying to develop specific DUB inhibitors (Ndubaku and Tsui, 2015). However, to date no specific USP29 inhibitor is available yet. The catalytic cysteine protease domain might be a druggable domain, but USP29 has also other domains with unknown functions that might be worth investigating. However, before the exploration of potential drugs targeting USP29 it is also crucial to understand how USP29 itself is regulated and which other signalling pathways would be potentially affected upon USP29 inhibition in order to anticipate possible detrimental side effects of treatment.

Chapter 5: Biochemical characterisation of USP29

5.1 Introduction

In the previous chapter we established the ubiquitin specific protease 29 (USP29) as a new non-canonical positive regulator of HIF- α stability and hypoxia signalling. We further found a positive correlation between *USP29* mRNA levels and prostate cancer progression and severity. Therefore, USP29 might become a possible therapeutic target in the future. However, while the discovery of the paternally expressed *USP29* gene dates back to the year 2000, the USP29 protein has hardly received any scientific attention (Kim et al., 2000). To date, only two reports about USP29's function have been published (Liu et al., 2011; Martin et al., 2015). While they describe USP29's implication in p53 and caspase stabilisation, no information about the USP29 protein itself is available.

To close this gap in the literature, our objective was to biochemically characterise the USP29 protein. We wanted to find out whether apart from its strong transcriptional regulation by imprinting, USP29 was also regulated on a post-translational level. Furthermore, in order to better understand in which other biological processes USP29 might be implicated we performed pull-down experiments with ectopic USP29 to find proteins that were associated with USP29.

In this chapter we therefore present novel insights into the properties of the so far poorly characterised USP29. We have here investigated how USP29 auto-regulates its own stability as well as present an interactome of USP29.

5.2 USP29 autoregulation

5.2.1 USP29^{C294S} is degraded by the proteasome

In accordance with previously published data (Urbe et al., 2012), HA- and GFP-tagged USP29 are localised in the nucleus, as well as the catalytically inactive mutant GFP-USP29^{C294S} (Figure 5.1).

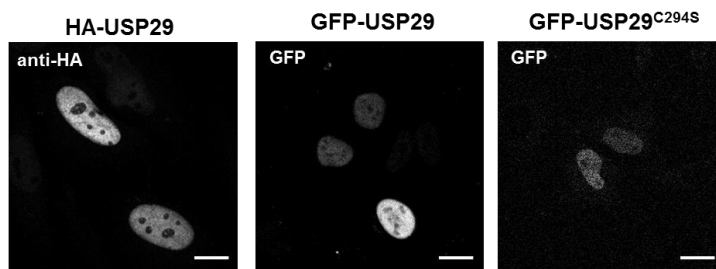


Figure 5.1: Localisation of USP29. HeLa cells were transfected with HA-USP29, fixed, and stained with anti-HA-antibody. GFP-USP29 and GFP-USP29^{C294S} transfected cells were imaged live. Scale bars are 20 μm .

In line with the weaker fluorescence of GFP-USP29^{C294S} (Figure 5.1), we found that its expression levels were greatly decreased compared to GFP-USP29 when transfecting the same amount of both plasmids (Figure 5.2A). To assess whether degradation of GFP-USP29^{C294S} by the proteasome was responsible for its low expression levels, we treated cells with the proteasome inhibitor MG132. Indeed, while GFP-USP29 levels remained unaffected by this inhibition, GFP-USP29^{C294S} levels were considerably increased (Figure 5.2B). To confirm that MG132 exerted its effect on USP29^{C294S} via the proteasome, we treated the cells with the more specific proteasome inhibitor epoxomicin. Epoxomicin also led to accumulation of GFP-USP29^{C294S}. In agreement with USP29^{C294S}'s proteasomal degradation, we found USP29^{C294S} to be less stable than USP29 in cycloheximide experiments. While catalytically active USP29 was stable throughout 6 hours, the half-life of USP29^{C294S} was heavily reduced to less than 1 hour (Figure 5.2C).

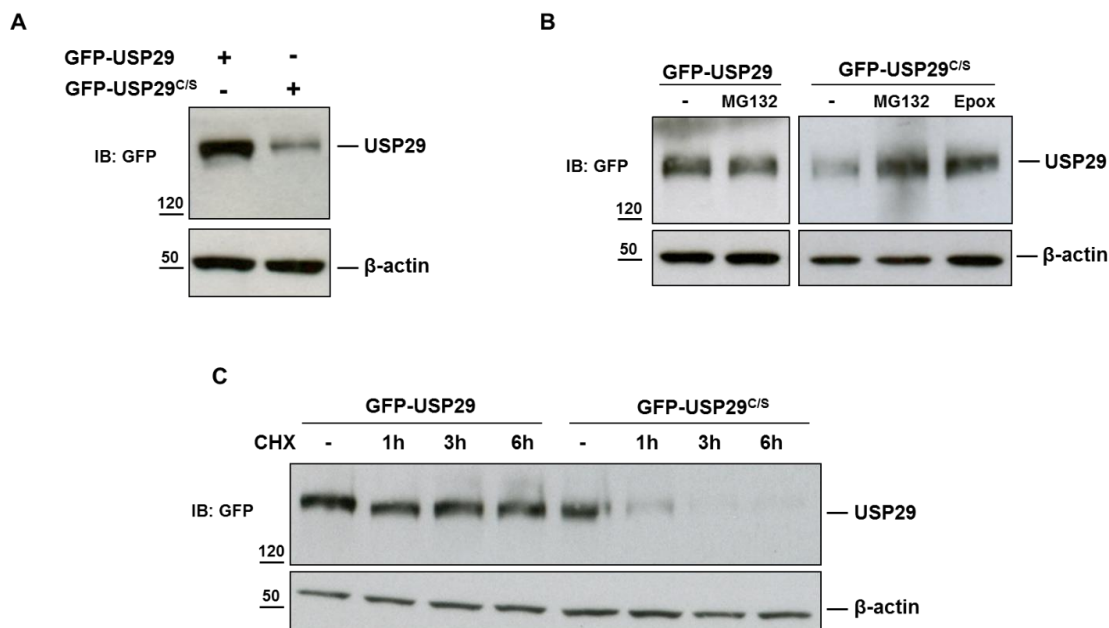


Figure 5.2: USP29^{C294S} is less stable than USP29. HEK293T cells were transfected with GFP-USP29 or GFP-USP29^{C294S}. A: same amounts of plasmids were transfected. B: cells were left untreated or treated for 4 h in the presence of 10 μ M MG132 or epoxomicin. C: 8-fold more GFP-USP29^{C294S} than GFP-USP29 was transfected, cells were treated with cycloheximide (0.05 mg/ml) and cell extracts were prepared at the indicated times after treatment.

5.2.2 USP29 auto-deubiquitinates itself

To investigate whether catalytic activity of USP29 was sufficient to avoid the proteasomal degradation of the inactive mutant, HA-USP29 was co-transfected together with GFP-USP29^{C294S}. In the presence of catalytically active HA-USP29, USP29^{C294S} protein levels were increased and reached similar levels to GFP-USP29 (Figure 5.3A).

Interestingly, USP29 catalytic activity did accumulate USP29^{C294S} more efficiently than the inhibition of the proteasome using MG132. Therefore, we tested whether USP29^{C294S} might also be degraded through the autophagic pathway, the second major protein destruction machinery. To this end, HEK293T cells transfected with GFP-USP29^{C294S} were treated either with the proteasome inhibitor MG132 or the autophagy inhibitor chloroquine or both together for 6h prior to lysis (Figure 5.3B). Autophagy was efficiently inhibited as seen by the appearance of the lower band of LC3, LC3-II. No significant accumulation of USP29^{C294S} upon inhibition of the autophagic pathway was seen, and inhibition of both pathways at the same time did not further increase USP29^{C294S} levels as compared to MG132-treatment alone. This suggested that the autophagic machinery was not implicated in USP29^{C294S} degradation and that the difference seen in USP29^{C294S} levels between MG132 treatment and overexpression of catalytically active USP29 might be due to incomplete inhibition of the proteasome.

On the basis of these previous data, we hypothesised that USP29's catalytic activity was required to auto-deubiquitinate itself, thereby preventing its degradation by the proteasome. To test this hypothesis, GFP-USP29 or GFP-USP29^{C294S} were co-transfected together with FLAG-ubiquitin in the absence or presence of HA-USP29. Prior to lysis, cells were treated for 2h with

MG132 and GFP-tagged proteins were pulled down with GFP-traps® under denaturing conditions. Ubiquitinated forms were not detectable for GFP-USP29 (Figure 5.3C). In the case of GFP-USP29^{C294S} however, we detected very little non-modified GFP-USP29^{C294S} and a great amount of poly-ubiquitinated GFP-USP29^{C294S}, which was visible as a high molecular weight smear. This poly-ubiquitination was completely removed in the presence of HA-USP29, showing that USP29 is able to intermolecularly deubiquitinate USP29.

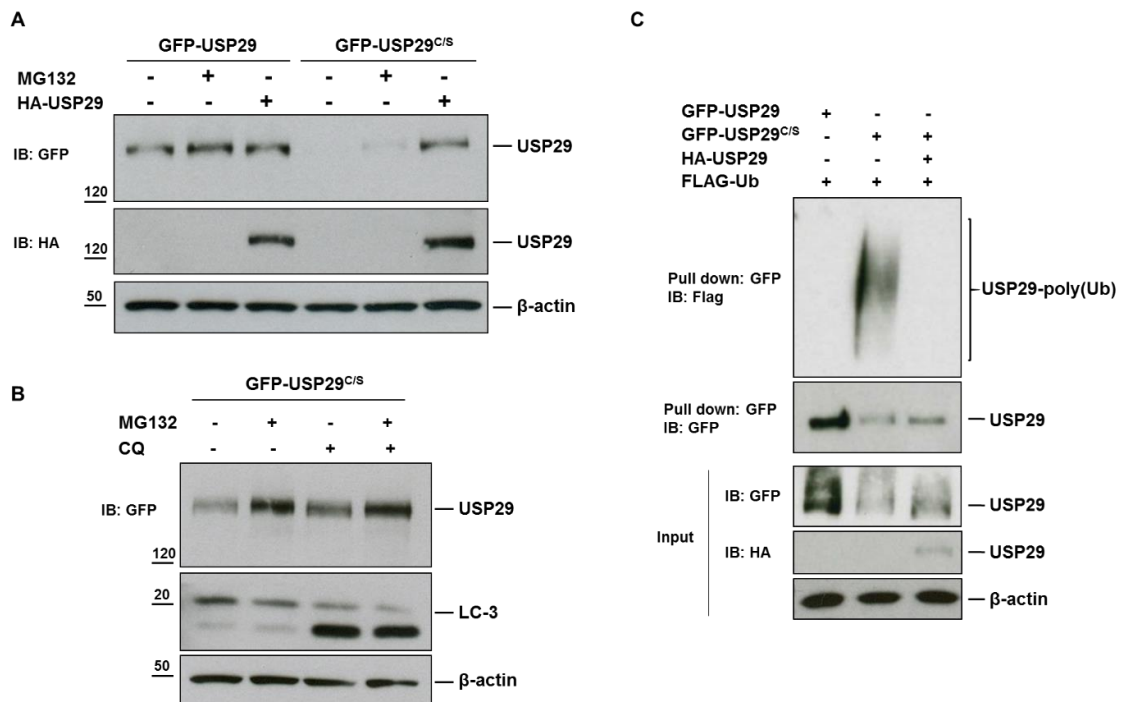


Figure 5.3: USP29 catalytic activity is sufficient to protect USP29^{C294S} from proteasomal degradation. A: HEK293T cells were transfected with same amounts of GFP-USP29 and GFP-USP29^{C294S} plasmids in the absence or presence of catalytic active HA-USP29. Cells were left untreated or treated with MG132 (10 μM) for 4h. B: HEK293T cells were transfected with GFP-USP29^{C294S} and treated with 10 μM MG132 and/or 30 μg/ml chloroquine for 6h. C: HEK293T cells were co-transfected with FLAG-ubiquitin and GFP-USP29, GFP-USP29^{C294S} or GFP-USP29^{C294S} and HA-USP29. Cells were treated with MG132 for 2h and GFP-tagged USP29 was pulled-down under denaturing conditions with GFP-traps®. Eluted proteins were run on gradient gels and non-modified and ubiquitinated forms detected by WB.

5.2.3 Identification of USP29's ubiquitination target residues

We sought to identify the lysine residue(s) subjected to ubiquitination that are thereby determining the stability of USP29. To this end, GFP-USP29^{C/S} eluted from GFP-trap® under denaturing conditions was migrated on a SDS gel and stained with SYPRO® (Figure 5.4A). A broad band covering high molecular weight and potentially ubiquitinated GFP-USP29^{C/S} was cut out, digested with trypsin and loaded on the mass spectrometer. The analysis achieved 51% of sequence coverage, and two lysine residues were identified to be modified by ubiquitination, K127 and K668 (Figure 5.4B). Furthermore, the canonical signal for proteasomal degradation - K48-linked polyubiquitin - was present in the sample. Additionally, in an experiment aimed at exploring proteins that interact with USP29 (see paragraph 5.3.1) we found USP29 to be modified by ubiquitination at K599. Interestingly, the same peptide was found to be

phosphorylated either at threonine 584 or serine 587 (Figure 5.4C), however ubiquitination and phosphorylation seemed to be mutually exclusive. With the exception of the rodent lineage, all three identified lysine residues were evolutionary conserved, which highlighted their potential functional importance (Figure 5.4D).

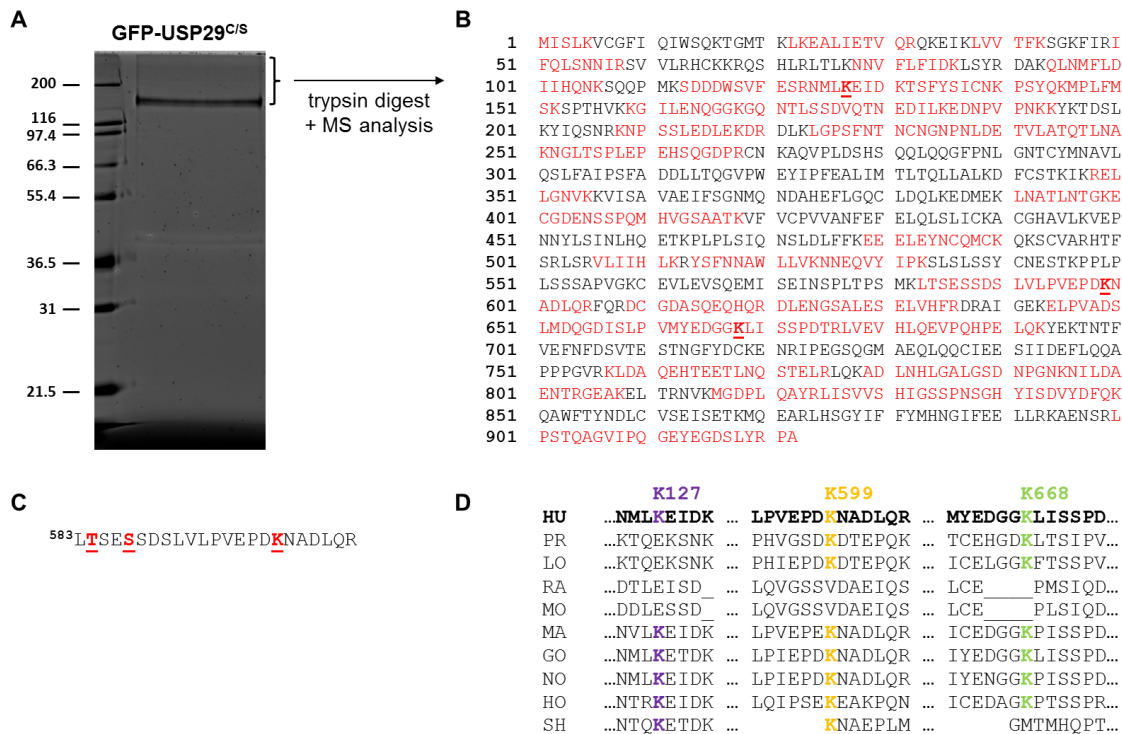


Figure 5.4: MassSpec analysis of GFP-USP29^{C/S}. GFP-USP29^{C/S} was co-transfected into HEK293T cells together with FLAG-ubiquitin, treated with MG132 for 4 h, lysed and incubated with GFP-traps®. Traps were washed with stringent buffers before GFP-USP29^{C/S} got eluted. Eluate was migrated on a SDS gel and bands stained with SYPRO® (A). Indicated gel slice was digested with trypsin and analysed by MS. (B) Red sequences were identified in the MS, underlined K residues were found to be ubiquitinated. (C) Peptide that was found to be either ubiquitinated (K599) or phosphorylated (T584 or S587), on the red residues. (D) Sequence alignment of the lysine residues that were identified to be ubiquitinated. HU: human, PR: hyrax, LO: elephant, RA: rat, MO: mouse, MA: rhesus macaque, GO: gorilla NO: gibbon monkey, HO: horse, SH: sheep.

Single mutation of lysine residues 127 and 668 to arginine (K127R and K668R) did not alter USP29^{C/S}'s expression levels and behaviour upon proteasome inhibition (Figure 5.5A). In order to exclude that there was some cooperative effect between the potential ubiquitination sites, USP29^{C/S} double mutants (K127/668R and K599/668R) as well as the triple mutant K127/599/668R were generated. None of these constructs displayed increased expression levels as compared to USP29^{C/S}. Accordingly, all constructs continued to be regulated by the proteasome, indicating that the tested lysines were not directly and uniquely responsible for USP29^{C/S}'s degradation (Figure 5.5B). It is however possible that their ubiquitination might have degradation-independent regulatory functions. This is supported by the fact that we identified phosphorylation of two residues (T and S) in the very close proximity of K599, but only when K599 was not ubiquitinated. It has yet to be determined whether and how these phosphorylations affect USP29 behaviour. It is tempting to speculate that K599-ubiquitination

antagonises the phosphorylation of the neighbouring residues by preventing or mediating the binding of the responsible kinase or phosphatase, respectively. Vice versa, the phosphorylation status of the T and S residues might dictate further ubiquitination.

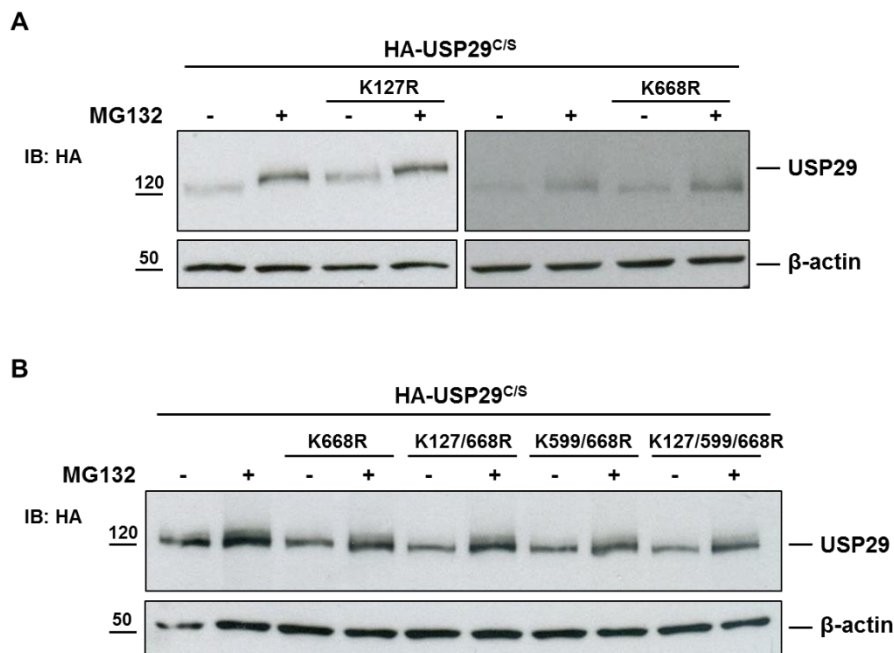


Figure 5.5: K127, K599 and K668 are not sufficient to regulate the proteasomal degradation of USP29^{C/S}. HEK293T cells were transfected with HA-USP29^{C/S} and the single K/R-mutants HA-USP29^{C/S} K127R or HA-USP29^{C/S} K668R (A) and the multiple K/R mutants HA-USP29^{C/S} K127/668R, K599/668R and K127/599/668R (B). Cells were left untreated or were treated with MG132 for 4h before lysis.

5.2.4 USP29 forms dimers

The fact that USP29 was able to remove poly-ubiquitin from USP29^{C294S}, suggested that USP29 interacted with USP29^{C294S}. USP29 does not only contain a split catalytic domain, but with its PH domain also a putative homodimerisation site (see Figure 1.5) and therefore, we investigated whether USP29 was able to form dimers. HEK293T cells were transiently transfected with HA-USP29 and lysed under native conditions. The lysate was separated by size exclusion chromatography and parts of the fractions were run on SDS-PAGE and probed for the presence of HA-USP29 (Figure 5.6A and B). USP29 was present not only in the peak corresponding to aggregates, but also in several other fractions (Figure 5.6B). These fractions were further run on a native gel in order to analyse whether USP29 ran as a monomer, a dimer or an oligomer. The WB of the native gel reveals one clear band corresponding to the approximately correct size of the monomeric HA-USP29 in the fractions B6-B1 (Figure 5.6C). Interestingly, in the higher molecular weight fractions B6 and B5 additional bands that could correspond to dimeric, trimeric and tetrameric HA-USP29 were also detected.

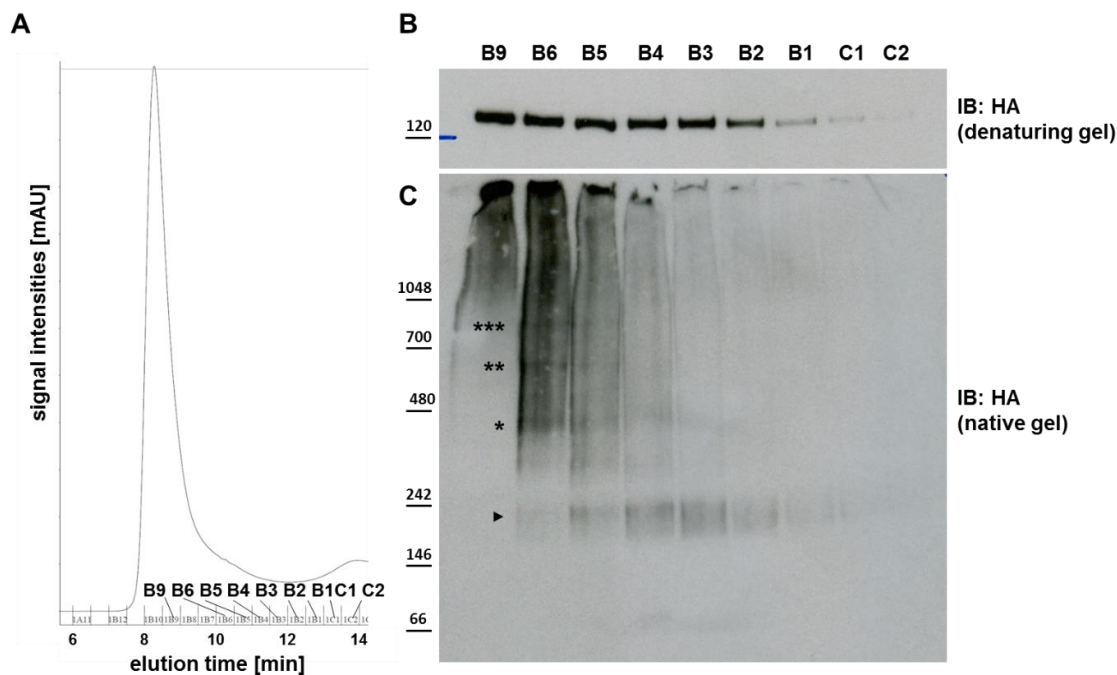


Figure 5.6: USP29 exists as monomer and oligomer. HEK293T cells were transfected with HA-USP29, lysed in native conditions and loaded onto a Superdex 200 10/300 GL column. Elution fractions (500 μ l) were collected (A) and 1/50th of these fractions were migrated in a denaturing (B) or a native (C) gel and immunoblotted for HA-USP29. The arrowhead and asterisks correspond to the monomeric and oligomeric forms of HA-USP29, respectively. As an internal control, we identified dimeric BSA of 134 kDa size eluted in fraction B2.

For a more direct proof of the interaction, we further used FLIM-based FRET measurements. The fluorescence excitation of a donor fluorophore can only be transferred to an appropriate acceptor fluorophore if both fluorophores are in very close proximity, typically within as little as 6 nm (Lam et al., 2012). Here, we used GFP-USP29 as the FRET donor and mCherry-USP29 or mCherry-USP29^{C/S} as the FRET acceptor. We found GFP-USP29's lifetime to be significantly decreased from 2.39 ± 0.013 ns to 2.36 ± 0.028 ns in the presence of mCherry-USP29 (Figure 5.7A). Importantly, the lifetime decrease was readily reversed when mCherry was photobleached, confirming that this decrease was indeed due to FRET (Figure 5.7A, bottom images). Furthermore, GFP-USP29 also bound to mCherry-USP29^{C/S} as reflected by a lifetime decrease from 2.40 ± 0.008 ns in the absence to 2.37 ± 0.022 ns in the presence of mCherry-USP29^{C/S} (Figure 5.7B). These results clearly demonstrated that USP29 homodimerisation did not require catalytic activity, and further support the deubiquitination of USP29^{C/S} by USP29.

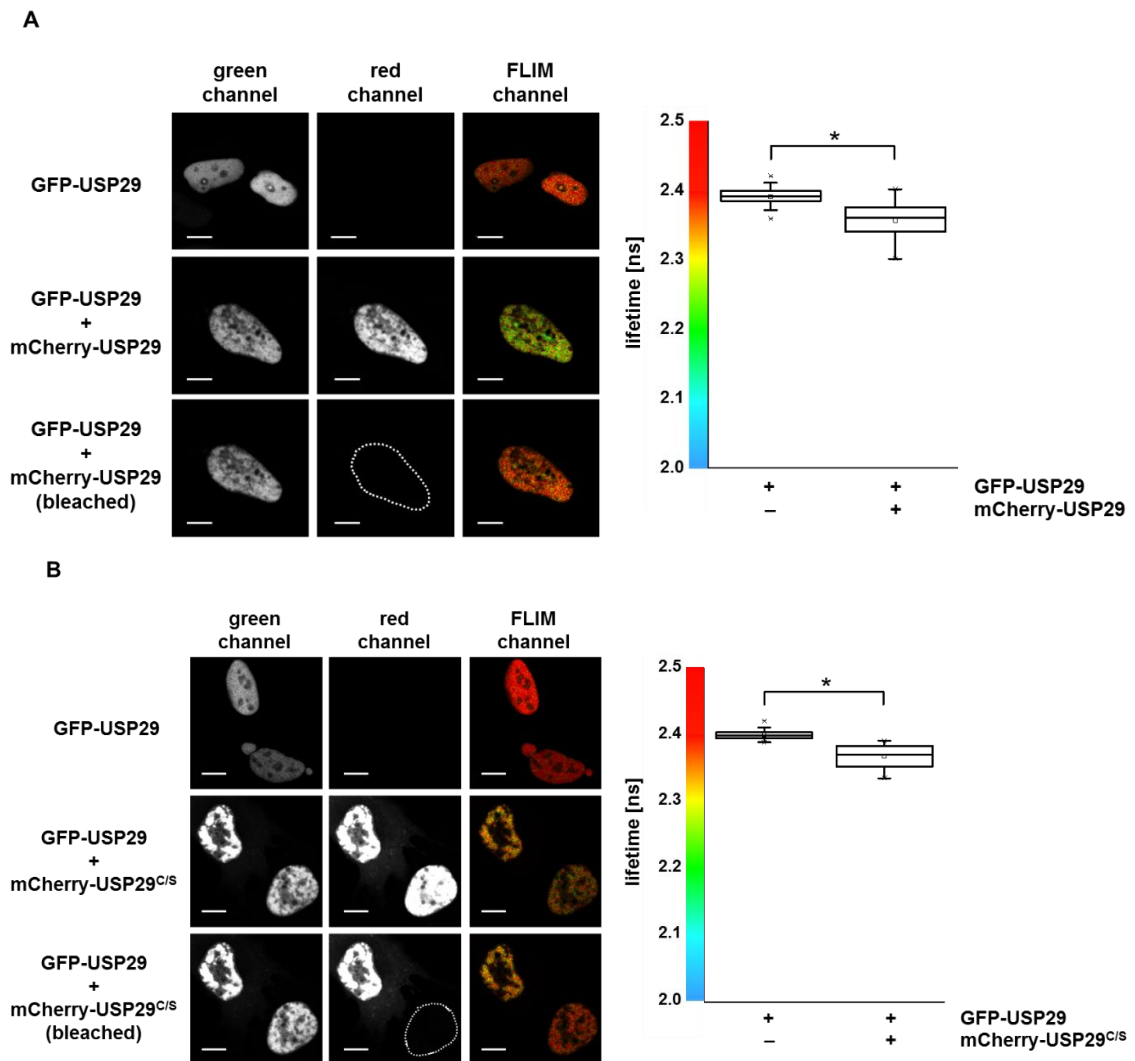


Figure 5.7: USP29 homodimerises. HeLa cells were transfected with GFP-USP29 alone or together with mCherry-USP29 (A) or mCherry-USP29^{C/S} (B) and 24 h post-transfection, cells were imaged. Representative fluorescence and pseudo-coloured fluorescence lifetime (FLIM) images are shown in the first two and the last column, respectively. The white dotted line shows the region of interest that was photobleached. Average fluorescence lifetimes of nuclear GFP-USP29 were extracted from the images and represented in the box plot (right panel). (A) 53 cells expressing GFP-USP29 and 38 cells co-expressing GFP-USP29 and mCherry-USP29 from 5 different experiments were analysed ($p = 5.4 \times 10^{-9}$). (B) 18 cells expressing GFP-USP29 and 9 cells co-expressing GFP-USP29 and mCherry-USP29^{C/S} from 2 different experiments were analysed ($p = 0.002$). Scale bars are 10 μm .

5.2.5 Ube3a is not USP29's E3-ligase

As USP29 is the first imprinted DUB described and there is only one known imprinted E3-ligase (Ube3a), we tested whether they might be counterplayers. However, HA-Ube3a was neither able to decrease basal GFP-USP29^{C/S} levels nor HA-USP29-dependent accumulation of GFP-USP29^{C/S} (Figure 5.8).

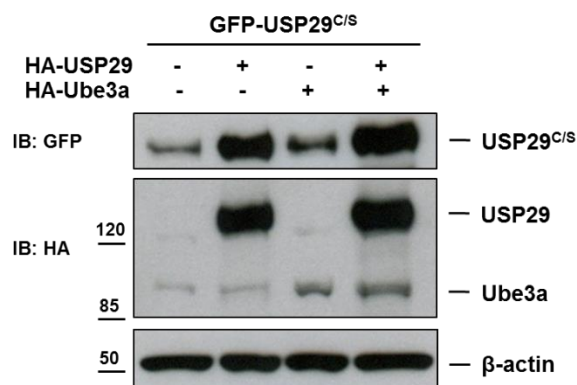


Figure 5.8: Ube3a does not regulate USP29^{C/S} protein levels. HEK293T cells were transfected with GFP-USP29^{C/S} alone or in combination with HA-USP29 and/or HA-Ube3a.

5.3 USP29's protein interaction landscape

5.3.1 USP29's interactome

In order to identify proteins that might be implicated in the regulation of USP29 protein stability and catalytic activity as well as the downstream pathway triggered by USP29, a proteomic approach was applied. GFP-tagged USP29 or GFP alone was pulled down in native conditions from HEK293T cells and co-immunoprecipitated proteins were migrated on a SDS gel (Figure 5.9A). The gel was cut in slices, subjected to trypsin digestion and analysed by MS. Only proteins that were at least 3-fold enriched in the GFP-USP29 catch as compared to the GFP-bait were considered. The experiment was performed three times and remarkably, there was a set of 69 USP29-interacting proteins that was present in all the three independent replicates and another 222 proteins were detected in at least 2 samples (Figure 5.9B). Of the 69 common proteins, 47 were interconnected and participate in a variety of biological processes (Figure 5.9C). USP29 interacted with mitochondrial and ribosomal proteins, proteins involved in the cytoskeletal organisation of the cell, and in concordance with its primarily nuclear localisation with proteins that bind to chromatin, DNA and mRNA. A complete list of these 291 proteins can be found in Appendix Table 12.

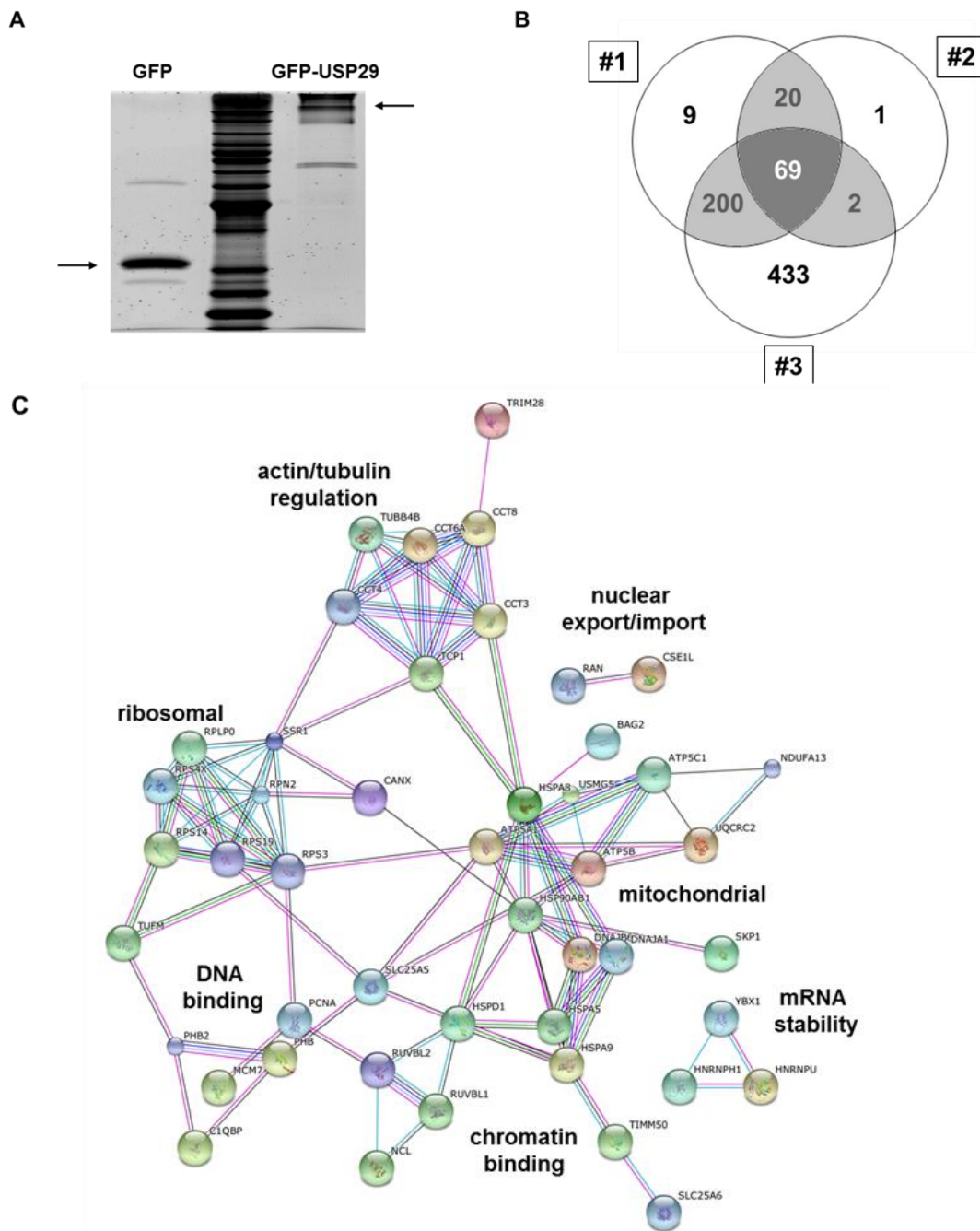


Figure 5.9: MassSpec analysis of the USP29 interactome. In three independent experiments GFP-tagged USP29 was pulled down with GFP-traps® from HEK293T cells and the co-immunoprecipitated proteins were migrated on a SDS gel (A: representative picture). The gel was cut in slices, subjected to trypsin digestion and analysed by mass spectrometry and compared with the catch of GFP alone. (B) Overlap of the USP29-specific proteins between the three replicates. (C) Functional clustering of the proteins that were identified in all three replicates (created with STRING).

In their work “Defining the Human Deubiquitinating Enzyme Interaction Landscape” Sowa and co-workers identified interacting proteins of 75 DUBs by co-IPs followed by MS analysis (Sowa et al., 2009). An overlap of 108 proteins stands out when comparing their catch using USP29 as a bait with our own approach (Figure 5.10A). Globally 60% of the 69 proteins that

we identified in all three replicates and in particular our top 10 proteins were confirmed (Figure 5.10B). Because of the high abundance of mitochondrial proteins among the interactors they postulated that USP29 was a mitochondrial protein.

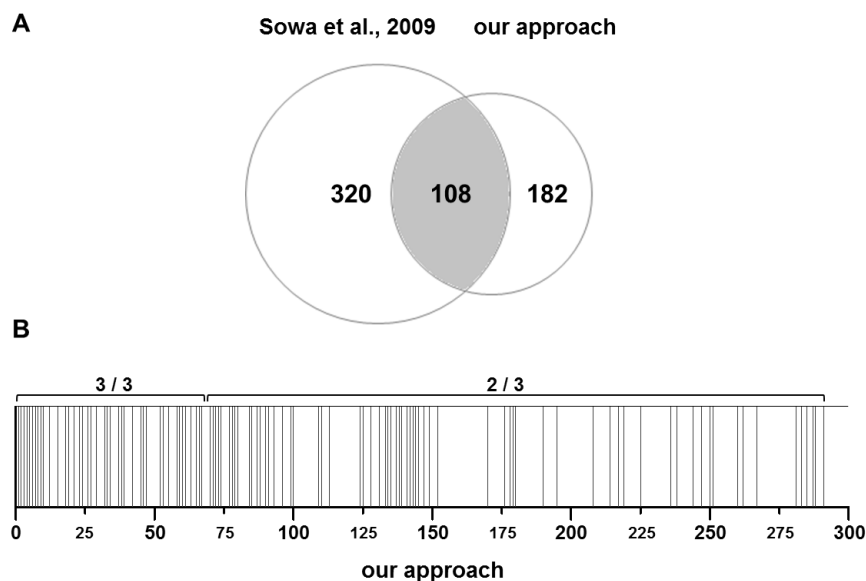


Figure 5.10: Comparison of our USP29 interactome with a previously published one. (A) Overlap of the USP29 interacting proteins that we identified in at least 2 out of 3 replicates (2/3) with the dataset from Sowa et al. (B) Each line represents a protein that is also present in Sowa's dataset.

However, based on a scoring system that incorporated for each detected protein the individual counts of its unique peptides in the MS analysis, as well as its natural abundance and the reproducibility in other replicates, Sowa et al. proposed that the only specific interactor was cathepsin B. As a consequence, they state that all other detected proteins were non-specifically interacting with the bait. In line with that, there is a very substantial overlap of our USP29 interactome with the CRAPome (www.crapome.org). The CRAPome is a collection of data from negative controls of affinity purification experiments that allows identifying common contaminants in such experiments (Mellacheruvu et al., 2013). Among the most abundant CRAPome proteins are heat-shock proteins, tubulins, actins, elongation factors, ribonucleoproteins and ribosomal proteins, and the authors explain their unspecific enrichment by their high abundance in the cell. Indeed, these are groups of proteins that we found enriched in our USP29 interactome (Figure 5.9C). Of the 290 identified proteins, 282 are represented in the CRAPome and 50 of them are such common contaminants that they are found in more than half of all the 441 control experiments included in the repository. Furthermore, neither Sowa's cathepsin B, nor the other previously described USP29 interactors, p53 (Liu et al., 2011) and claspin (Martin et al., 2015) or HIF-1 α were present in our MS data. This very clearly questioned the usefulness of our approach, but nevertheless we tried to show some validity of our data by a co-immunoprecipitation followed by conventional WB.

5.3.2 PCNA is interacting with USP29

Proliferating cell nuclear antigen (PCNA) was one of the top 20 interacting proteins of USP29 in the proteomic approach (see Figure 5.9), both in terms of reproducibility and abundance. CIC bioGUNE's Paco Blanco performed a bioinformatical analysis of the sequence of USP29 and found that USP29 contained the canonical PIP-box (PCNA interacting protein-box) sequence ⁴⁶⁹QxxLxxFF⁴⁷⁷, a motif commonly seen in proteins that bind to PCNA (Warbrick, 1998). Furthermore, Mosbech and co-workers mention in their paper from 2013 without displaying experimental evidence that “USP29 but not USP44 reversed ubiquitylation of several other factors, including proliferating cell nuclear antigen (PCNA)” (Mosbech et al., 2013). This encouraged us to test the potential interaction of the nuclear protein PCNA with USP29, despite the fact that PCNA is listed as a common contaminant according to the CRAPome (present in 23% of all listed control experiments). Hence, USP29 was immunoprecipitated from cells using GFP-traps® and the eluate was probed for PCNA (Figure 5.11). And indeed, PCNA co-immunoprecipitated with GFP-USP29, but not with GFP only, confirming their interaction seen by mass spectrometry. Furthermore, PCNA also co-immunoprecipitated with catalytically inactive GFP-USP29^{C/S}. This indicated that the interaction was not dependent on USP29's catalytic activity and supported the idea that USP29's PIP-box may be responsible for PCNA binding.

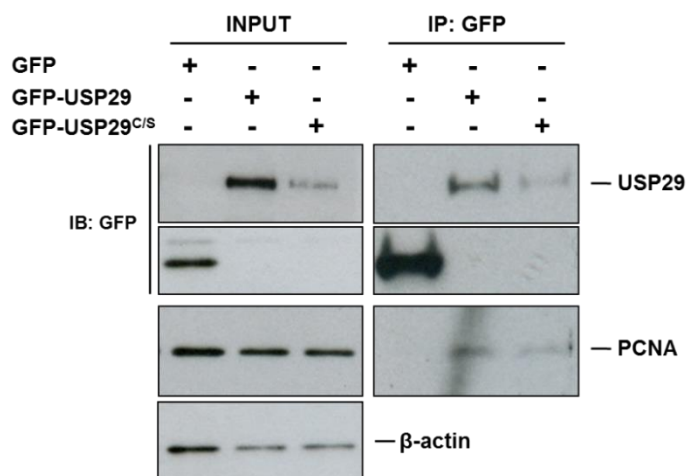


Figure 5.11: PCNA interacts with USP29 independently of its catalytic activity. HEK293T cells were transfected with GFP, GFP-USP29 or GFP-USP29^{C/S} and lysed 24h post-transcription. GFP and GFP-fusion proteins were pulled down in native conditions with GFP-traps® and eluates were subjected to SDS-PAGE followed by WB against endogenous PCNA protein.

5.3.3 Potential Ub E3 ligases for USP29

The fact that we had found a PIP-box in USP29's sequence and were able to co-immunoprecipitate endogenous PCNA together with USP29, encouraged us to test other proteins of our interactome approach. Hence, we analysed the list of interactors by focusing on potential upstream regulators of USP29. Among the proteins detected in at least 2 replicates there were several candidate ubiquitin E3 ligases or components of ubiquitin E3 ligase complexes that could be responsible for the regulation of USP29 stability (Table 5.1). In order to study their potential role as regulators of USP29, we silenced them individually using siRNAs. As USP29 deubiquitinates not only itself but also HIF-1 α , we hypothesised that both proteins might be targeted by the same Ub-E3 ligase and therefore included additional siRNAs targeting known HIF-1 α Ub-E3 ligases.

Table 5.1: Ub-E3 ligases or components of Ub-E3 ligase complexes that could be potential regulators of USP29^{C/S}.

	USP29 interactome	HIF1 α modulator
DDB1	yes (3/3)	No
SKP1	yes (3/3)	No
TRIM28	yes (3/3)	(Li et al., 2003)
HUWE1	yes (2/3)	No
STUB1/CHIP	yes (2/3)	(Luo et al., 2010)
RLIM	yes (2/3)	No
Fbw7	No	(Cassavaugh et al., 2011)
PARK2	No	(Sarraf et al., 2013)
TRAF6	No	(Sun et al., 2013)
MDM2	No	(Ravi et al., 2000)
pVHL	No	(Maxwell et al., 1999)

All siRNA sequences efficiently silenced their target mRNA as determined by quantitative real-time PCR (Figure 5.12 bottom). We analysed the effect of each silencing condition by monitoring the protein levels of the catalytic inactive USP29^{C/S}. USP29^{C/S} levels remained unchanged or were reduced in most samples, however in the absence of HUWE1, USP29^{C/S} protein levels increased substantially and to a comparable extent as upon proteasome inhibition (Figure 5.12). This suggested that HUWE1 might be responsible for the destabilisation of USP29^{C/S}.

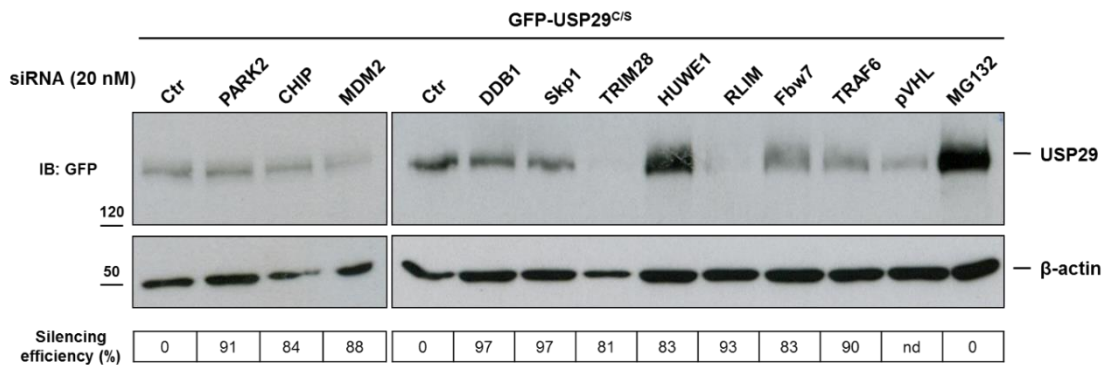


Figure 5.12: Potential Ub-E3 ligases for USP29. HEK293T cells were silenced with siRNAs against a panel of E3-ligases or components of E3-ligase complexes and transfected with GFP-USP29^{C/S}. As a positive control, control cells were treated with MG132 for 4h. The silencing efficiency was determined by TaqMan® qPCR of RNAs of cells simultaneously transfected and lysed.

In order to confirm and further characterise the effect HUWE1 showed to have on USP29^{C/S}, HUWE1-depleted cells were treated with the proteasome inhibitor MG132 and USP29^{C/S} protein levels monitored. The depletion of HUWE1 with siRNA resulted in increased basal USP29^{C/S} protein levels comparable to those in control cells upon inhibition of proteasomal degradation (Figure 5.13). Furthermore, USP29^{C/S} levels were further increased when inhibiting the proteasomal degradation pathway alongside with the depletion of HUWE1.

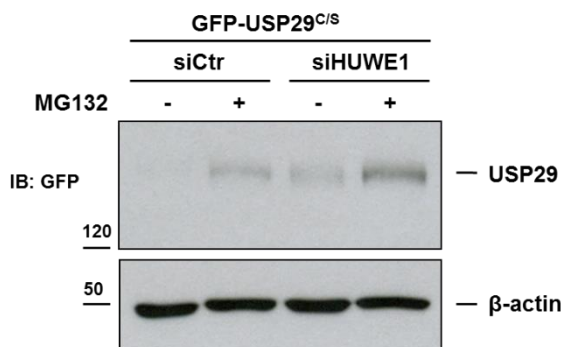


Figure 5.13: USP29^{C/S} accumulates upon knock-down of HUWE1. HEK293T cells were silenced with control and siRNA targeting HUWE1, transfected with GFP-USP29^{C/S} and left untreated or treated with MG132 for 4h. USP29^{C/S} levels in whole cell extracts were assessed by WB.

This suggested that HUWE1 downregulated USP29^{C/S} by targeting it for proteasomal degradation. In the light of HUWE1 being an ubiquitin E3 ligase, we hypothesised that HUWE1 poly-ubiquitinated USP29^{C/S}. To test this, GFP-tagged USP29^{C/S} was co-expressed together with FLAG-ubiquitin and after treatment with MG132, USP29^{C/S} was pulled down under denaturing conditions using GFP-traps®. Unexpectedly, upon knock-down of endogenous HUWE1 protein with siRNA, USP29^{C/S} polyubiquitination was clearly increased, while the presence of HA-USP29 diminished USP29^{C/S}'s ubiquitination (Figure 5.14A). Moreover, when we subjected the samples to MS analysis, only K48-linked poly-ubiquitin was detected in the control condition and upon silencing of HUWE1 the sample contained additionally K6-, K11- and K63-linked polyubiquitin (Figure 5.14B).

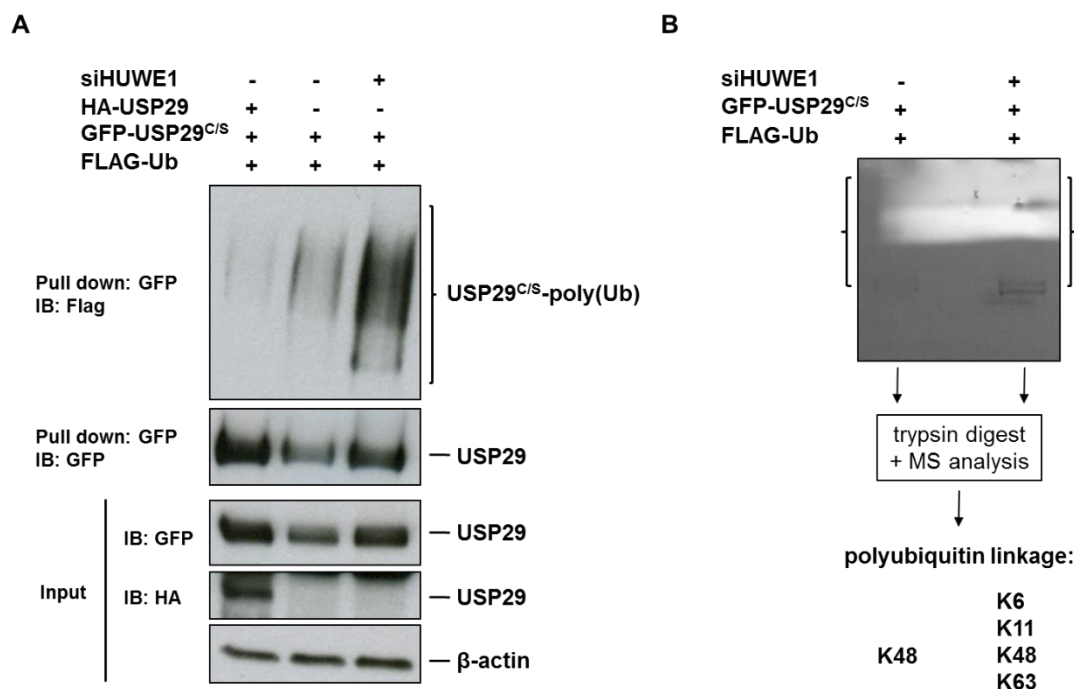


Figure 5.14: Silencing of HUWE1 increases the poly-ubiquitination of USP29^{C/S}. HEK293T silenced with either control siRNA or siHUWE1 were co-transfected with GFP-USP29^{C/S} and FLAG-ubiquitin and HA-USP29. Cells were treated with MG132 for 4h and GFP-tagged USP29^{C/S} was pulled-down under denaturing conditions with GFP-traps®. (A) Eluted proteins were run on gradient gels and non-modified and ubiquitinated forms detected by WB. (B) Eluted proteins were run on a SDS gel and stained with SYPRO®. The gel was cut above the main band of GFP-USP29^{C/S} to recover poly-ubiquitinated populations (brackets), subjected to trypsin digestion and analysed by MS.

While a confirmation of these results with a second independent siHUWE1 is required, we hypothesize that HUWE1 might be binding to USP29^{C/S} in a way that prevents the binding of other ubiquitin ligases that are responsible for stabilising ubiquitination to USP29^{C/S}. Another scenario is that HUWE1 might negatively regulate the stability of those ubiquitin E3 ligases which are therefore able to polyubiquitinate USP29^{C/S} only when HUWE1 is silenced. Strikingly, in their own approach Sowa and co-workers found HUWE1 to be associated with several other members of the USP family of DUBs, including USP7, USP49, USP50 and VCPIP1 (Sowa et al., 2009). However, according to the CRAPome repository also HUWE1 is a common contaminant (present in 18% of all control experiments on www.crapome.org).

5.3.4 USP29 and mitochondria

As we (Figure 5.9) and others (Sowa et al., 2009) found USP29 to be associated with many mitochondrial proteins, including some of the inner mitochondrial membrane, such as subunits of the mitochondrial ATP synthase (Figure 5.9C), we wondered whether we would be able to find colocalisation of USP29 with mitochondrial structures. We therefore performed some preliminary studies and stained the mitochondria of HeLa cells transfected with GFP-USP29 with MitoTracker (Figure 5.15). However, as shown previously, GFP-USP29 was only localised in the nucleus and no overlap of USP29 with mitochondrial signal was found. Moreover, there was no obvious change in mitochondria morphology in the presence of GFP-USP29 as compared to GFP alone.

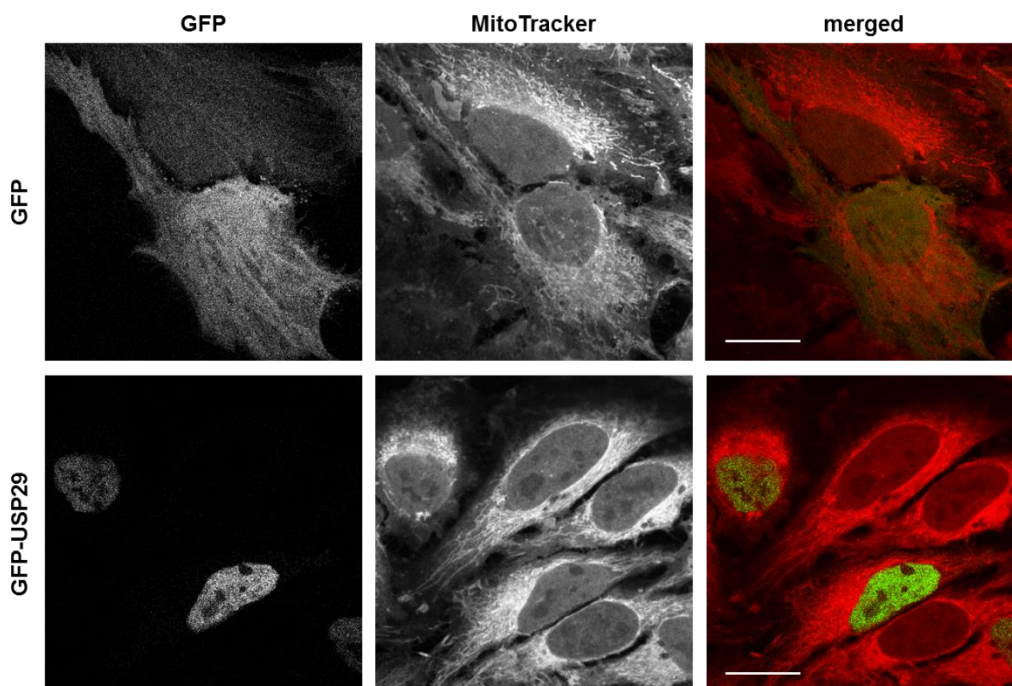


Figure 5.15: USP29 does not colocalise with mitochondria. HeLa cells were transfected with GFP (upper row) or GFP-USP29 (lower row), stained with MitoTracker CM-H₂XRos, fixed and imaged. Scale bars are 20 μ m.

Several scenarios could explain why we found interaction of USP29 with mitochondrial proteins. GFP-USP29 binding to mitochondrial proteins might be usually prevented by compartmentalisation but rendered possible after lysis during sample preparation and would therefore represent an artefact. We found USP29 to be bound to high amounts of heat shock proteins of the HSP70 family, that act as folding chaperones. While facilitating the folding of USP29 they might also independently be chaperoning the maturation of mitochondrial proteins as they emerge from the ribosome and before they get sorted to the mitochondria. However, we can't exclude the possibility that there might be a small population of USP29 that localises to mitochondria and specifically interacts with some proteins, however our techniques might not be sensitive enough to detect this subpopulation.

5.4 Discussion

In this chapter we present the first biochemical characterisation of the poorly studied deubiquitinase USP29 and its potential regulators and binding partners. We found evidence that additionally to its tight transcriptional regulation by imprinting (Kim et al., 2000), USP29 is regulated on a post-translational level. More precisely, USP29 is subjected to poly-ubiquitination which targets USP29 for proteasomal degradation. However, this constant degradation is only seen for catalytically inactive USP29^{C/S}. USP29's own catalytic activity is sufficient for auto-deubiquitination and hence USP29 escapes the proteasomal targeting.

This proposed mechanism of auto-deubiquitination is not a novel mechanism among DUBs. For instance, USP19 has been described to be subjected to ubiquitination by SIAH and to subsequent degradation by the proteasome (Velasco et al., 2013). In analogy to what we found for USP29, the catalytic active form of USP19 is able to prevent the degradation through deconjugation of the polyubiquitin chains (Mei et al., 2011). Similarly, also UCH-L1 and USP4 have been shown to reverse their own mono-ubiquitination, even though in both cases rather than affecting their stability, this did affect the DUB activity (Meray and Lansbury, 2007; Wijnhoven et al., 2015).

We used mass spectrometry to identify the lysine residues in USP29 that were subjected to ubiquitination. As would be expected for poly-ubiquitinated proteasome substrates, the sample contained K48-linked polyubiquitin. Furthermore, three ubiquitinated lysine residues were found, K127, K599 and K668, and they turned out to be reasonably conserved throughout evolution with the exception of the rodent lineage. The individual or combinatorial mutation of the identified lysines however did not affect the protein levels of USP29^{C/S}, suggesting that they were not exclusive determinant(s) for USP29 stability. They could however be modulating the catalytic activity and/or stability of USP29 by mediating or preventing further post-translational modifications or interactions with regulatory proteins. In this context it would be worth exploring the function of a specific peptide of USP29, which was consistently either phosphorylated or ubiquitinated. The phosphorylation might inhibit ubiquitination or vice versa. Such a mutually exclusive regulation has been reported for ubiquitinated or SUMOylated USP25, which results either in activation or inhibition of its catalytic activity, respectively (Denuc et al., 2009; Meulmeester et al., 2008). Furthermore, it has been suggested that DUBs containing ubiquitin binding domain (UBD) were regulated by mono-ubiquitination. The mono-ubiquitin associates intra-molecularly with the UBD and hence prevents the DUB from binding to its ubiquitinated target proteins (Di Fiore et al., 2003; Hoeller et al., 2006). Other reports have shown that the ubiquitination of DUBs stimulated their ubiquitin-specific protease activities (Denuc et al., 2009; Todi et al., 2009). Phosphorylation of DUBs has been described to impact on their ability to bind to and/or deubiquitinate their substrates (Edelmann et al., 2010; Fernandez-Montalvan et al., 2007; Hutti et al., 2007).

We next sought to find the ubiquitin E3 ligase that was responsible for the destabilisation of USP29^{C/S}, as well as potential downstream targets of USP29. To that end we set up an experiment that allowed us to identify by mass spectrometry proteins that associated with ectopic USP29 *in cellulo*. Even though the overlap with the CRAPome was substantial,

indicating that many proteins were rather contaminants than specific interactors, we were able to confirm the interaction of USP29 with PCNA, a protein that was identified in all replicates, by co-immunoprecipitation experiments. Interestingly, USP29 contains a canonical PCNA-interacting protein (PIP) box within the N-terminal catalytic domain. Among the other identified proteins we found the ubiquitin E3 ligase HUWE1. Among HUWE1's many substrates are p53, PCNA and n-myc, indicating HUWE1's wide implication in cellular fate (Chen et al., 2005; Choe et al., 2016; King et al., 2016). When we depleted HUWE1 with siRNA, catalytic inactive USP29^{C/S} accumulated significantly and in a similar extent as it did upon proteasome inhibition. To our surprise however, silencing of HUWE1 not only accumulated poly-ubiquitinated-USP29^{C/S} but also expanded the type of conjugated Ub-chains. This indicated that HUWE1 rather than being a conventional Ub E3 ligase, which directly controls USP29 stability, might play a more complex role that needs to be further explored. For instance, HUWE1 might recruit a destabilising ubiquitin E3 ligase or might prevent the binding of a stabilising ubiquitin E3 ligase to USP29.

Finally, we found that USP29 was able to form homo-dimers/oligomers in cells. This was not a surprise considering the fact that USP29 was able to remove poly-ubiquitin intermolecularly. Furthermore, USP29 contains a putative N-terminal homodimerisation domain, suggesting that the USP29 might be a functional dimer. In the case that the dimerisation of USP29 was crucial for its proteolytical activity towards its target proteins, the dimerisation interface could become a promising target, would USP29 inhibition become desirable in the future.

Chapter 6: Discussion

6.1 The (dis)advantages of fluorescence microscopy

The use of antibodies for the detection of endogenous cellular proteins is still the gold standard biochemical method for the analysis of localisation and behaviour of a protein of interest. The antibody needs to be able to bind specifically and efficiently to the protein of interest. However, sometimes such antibody is not available or endogenous protein levels in the model system are below the detection limit. Additionally, antibody staining requires fixation and permeabilisation of the sample. Apart from not being compatible with live cell applications, these procedures can also introduce major artefacts that can lead to the misinterpretation of the data (Schnell et al., 2012).

Fluorescence imaging in contrast, permits the investigation of protein localisation and dynamics in real time in living cells without the perturbations caused by harsh treatments. For this purpose, the protein(s) of interest need(s) to be tagged with (a) fluorescent protein tag(s). The green and red fluorescent protein were originally isolated from *Aequorea victoria* and *Discosoma*, respectively (Matz et al., 1999; Shimomura et al., 1962). Through mutations a broad palette of fluorescent proteins within the visible spectrum is available nowadays, which allows for multi-colour imaging (Day and Davidson, 2009). However, the tag needs to be fused to the protein of interest by molecular cloning methods and the expression plasmid needs to be transfected into cells. As a result, the fusion protein is likely to be expressed at levels that do not reflect their physiological abundance. This could be circumvented using the new CRISPR/Cas9 genome editing technology (Jinek et al., 2012). The technology allows to specifically insert the sequence of a fluorescence tag in-frame with the gene of interest, resulting in the expression of the fluorescence-labelled endogenous protein under its own promoter. Apart from that, it should be noted that tags can also interfere with the behaviour of the protein of interest. The wrong localisation and the enhanced aggregation, as well as functional impairment of the tagged protein described in this thesis, are examples of such label-induced perturbations.

Once the protein of interest has been successfully fused to a fluorescent label and the chimeric protein has been validated to be functional and it reproduces the cellular distribution of the endogenous protein, a variety of fluorescence imaging techniques can be used to explore properties that would be difficult to characterise using classical biochemical approaches. Rather than showing us simple one- or two-dimensional snap-shots of an inanimate biological system, modern fluorescence microscopy allows us to acquire four-dimensional data of living organisms. The third spatial dimension is added by z-sectioning or by using 3D imaging techniques such as light-sheet microscopes. Additionally, through the consecutive recording of the same frame, dynamic changes in the sample over time can be registered. Depending on the experimental setup such dynamics can range from a few milliseconds up to days and therefore permit us to image short and long processes, from intracellular protein diffusion and shuttling to

embryonic development. Furthermore, advanced fluorescence imaging techniques enable us to obtain highly quantitative data from the sample. FRAP, RICS and FCS can be used to measure the diffusion coefficients of proteins in the different compartments of the cell, for example (Kim et al., 2010). Apart from fluorescence live cell imaging techniques, there are currently no other biochemical means to obtain this information. In contrast, whether two proteins interact with each other, can be investigated with imaging techniques, such as FRET and FCCS as well as with classical biochemical methods, such as co-immunoprecipitations (co-IP) and proximity-ligation assays (PLA). While distance-dependent photophysics are prerequisite to obtain positive FRET between two proteins, co-IPs and PLA can also yield positive results when the two proteins are both associated via a third (bridging) protein (Figure 6.1). PLA for example still gives a positive signal when proteins are separated by as much as 40 nm (Zatloukal et al., 2014) and additionally the PLA signal has been shown to saturate early, resulting in only semi-quantitative results (Mocanu et al., 2011). Hence, here imaging techniques are superior to biochemical ones, as they do not only have a much higher spatial resolution, but can also be performed in living systems, therefore accounting for dynamic changes over time.

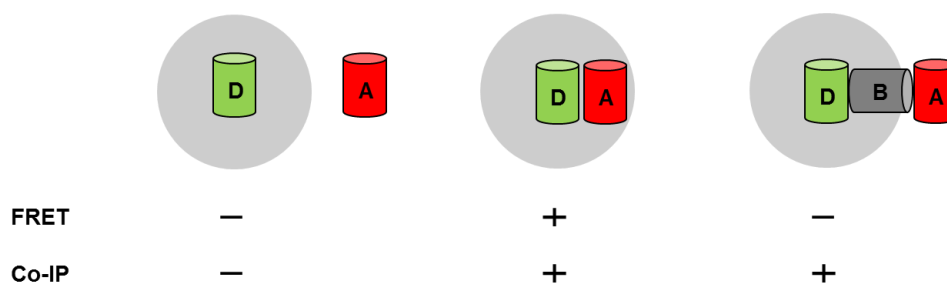


Figure 6.1: Comparison of FRET and Co-IPs to measure interaction. Whether two proteins (D and A) interact can be measured by FRET or Co-IP. FRET can only occur when the two proteins are within the Förster radius (grey circle), but not if they are physically connected, but spatially separated by a bridging protein (B).

6.2 UPS and non-canonical HIF signalling

Hypoxia signalling via HIF triggers important adaptive processes to limited oxygen availability that strongly impact the cell and its environment. But HIF homeostasis is not only regulated in an oxygen-dependent manner by the subsequent action of its canonical regulators PHD and pVHL and their counteracting deubiquitinases (Figure 6.2 left). Other ubiquitin E3 ligases have been described to poly-ubiquitinate HIF-1 α , leading to its non-canonical proteasomal degradation or sending HIF-1 α for chaperone-mediated autophagy (CMA) (Figure 6.2 right). As for the canonical pathway, deubiquitinases that reverse these processes have also been identified. Therefore, stimuli other than the oxygen tension can also modulate HIF signalling. And while there is growing knowledge of the identity of the responsible regulators, the conditions that trigger their action remain widely elusive.

As a matter of fact, the presence of HIF- α and consequently sustained HIF signalling is a recognised negative prognostic factor in most cancers (Semenza, 2012b). Likewise, the deubiquitinases UCHL1 and USP28 have been shown to be overexpressed and to act as biomarkers in multiple myeloma and bladder cancer, respectively (Goto et al., 2015; Guo et al.,

2014a). While no direct link with hypoxia signalling was established by the authors, in those cancers the overexpression of USP28 and UCHL1 might lead directly to HIF-1 α stabilisation. Similarly, changes in expression levels or activity and mutations of any other of the HIF- α regulators could tip HIF homeostasis to one side or the other and hence cause inappropriate signalling.

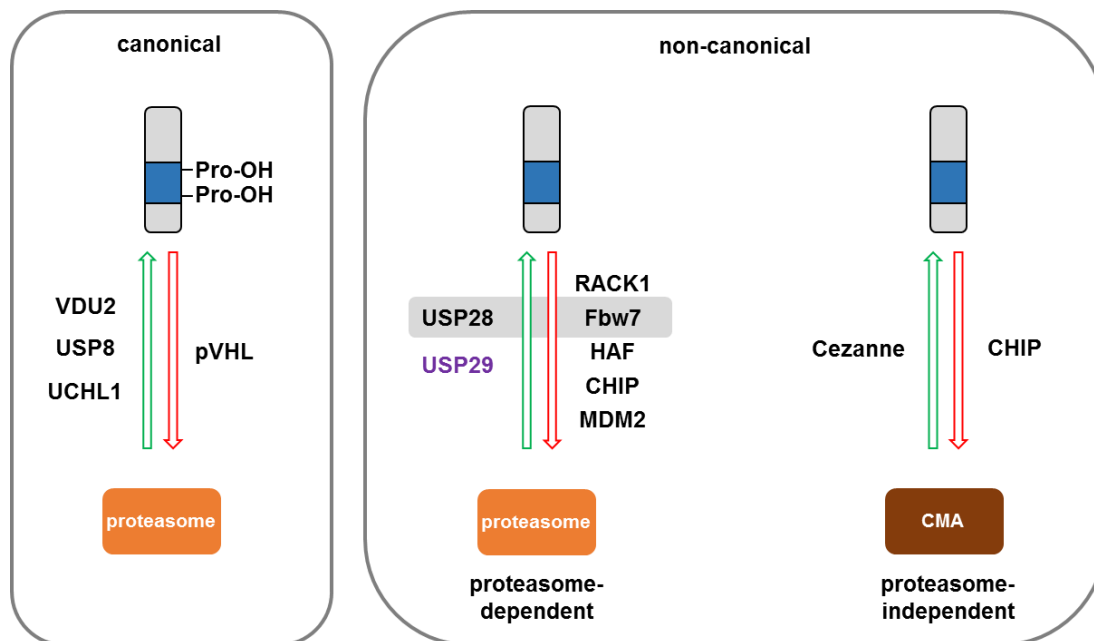


Figure 6.2: Ub E3 ligases and DUBs implicated in canonical and non-canonical HIF-1 α regulation. Ubiquitin E3 ligases target HIF-1 α for different degradation pathways by poly-ubiquitinating them (red arrow). Deubiquitinases de-conjugate the ubiquitin (green arrow) and therefore stabilise HIF-1 α . The grey box indicates that the two proteins antagonise each other. Included are only E3 ligases and DUBs whose molecular mechanism of action is sufficiently elucidated.

6.3 Targeting hypoxia signalling via DUBs

Sustained hypoxia signalling is found in many cancers and has been related to resistance to chemo- and radiotherapy, and hence many efforts have been made to pharmacologically inhibit the pathway by inhibiting HIF translation, stabilisation, dimerisation and activity (Figure 6.3) (Semenza, 2012b). In line with this, recent work by two groups demonstrated the specificity and efficacy of a small molecule that binds to HIF-2 α and inhibits the dimerisation with HIF-1 β in clear cell renal cell carcinomas in preclinical trials in mice (Chen et al., 2016; Cho et al., 2016).

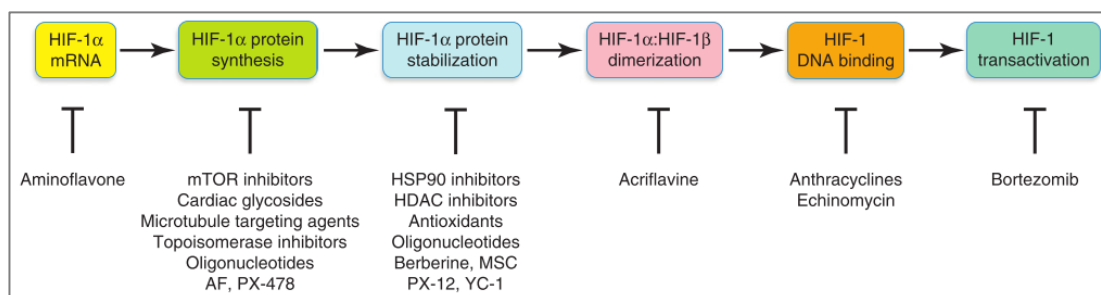


Figure 6.3: Drugs that inhibit HIF-1 signalling at different levels. From (Semenza, 2012b)

However, a systematic inhibition of HIF signalling might not always be beneficial as it would impair physiological hypoxic adaptation in other sites of the body. Therefore, targeting the de-regulated upstream regulator of HIF could be a more promising and more cancer-specific approach. The rise of personalised medicine aspires to thoroughly analyse and compare each individual patient's diseased and healthy tissue in the future and to be able to pin down the exact proteins and pathways that are deregulated in each particular case (Collins et al., 2016). Targeting those specifically would have a differential effect on the cancer tissue as compared to the healthy tissue.

If the upregulation of a DUB is responsible for the inappropriate activation of a protein or signalling pathway, as we found evidence for with USP29 in prostate cancer, then targeting this DUB could be beneficial. Hence, DUBs are currently being explored as drug targets, both in academia and in industry. As they contain a conserved active site, they are potentially more readily targeted than their counter-players, the ubiquitin E3 ligases (D'Arcy et al., 2015). Small molecule inhibitors that bind to and modify the catalytic site of DUBs are being identified and tested, and while some DUBs can already be inhibited specifically, many drugs display low specificity and act as pan-inhibitors (Table 6.1).

Table 6.1: Small molecule inhibitors for DUBs. From (D'Arcy et al., 2015)

Compound	Reported activity/ target
P022077	USP7
P5091	USP7
Cpd 14	USP7 and USP47
P22077	USP7/USP47
HBX 41,108	USP7
HBX-19,818	USP7
HBX-28,258	USP7
HBX 90,397	USP8
Ethyloxyimino-9H-indeno [1,2-b]pyrazine-2,3- dicarbonitrile	USP8
IU1	USP14
Isatin O-acyl oxime derivatives	UCHL1
LDN91946	UCHL1
LS1	UCHL3
NSC112200, NSC267309	TRABID/ZRANB1
PR-619	Broad spectrum DUB inhibition

Apart from high-throughput compound screenings, structure-based drug discovery strategies could help to improve the drug development progress where structural data of the DUB to be targeted is available (Lionta et al., 2014). In this context, a better understanding of the structure and biochemistry of the DUB might also help to find alternative druggable sites, which could

allow for more specific targeting. The interaction of two proteins with each other could be interrupted by targeting the protein-protein interaction (PPI) surface with drugs. This approach has been successful with Nutlin-3, which binds to MDM2 and therefore prevents MDM2 from binding to and poly-ubiquitinating p53 (Vassilev et al., 2004). While MDM2 is an ubiquitin E3 ligase, there is no reason why targeting a DUB's PPI surface would not also be possible. In the case of USP29 it is tempting to speculate that its dimerisation might offer the possibility for active site-independent targeting.

6.4 The potential role of USP29 dimerisation

We have shown in this thesis that USP29 deubiquitinates itself and that USP29 dimers exist *in cellulo*. However, whether the USP29 dimerisation is required for its catalytical activity has not been investigated. Several scenarios are possible. The C-terminus of a single USP29 molecule could fold in, in order to complete the catalytical triad intra-molecularly (Figure 6.4A). However, the dimerisation of two USP29 molecules via their putative N-terminal homo-dimerisation domains might be necessary for the conformational changes to occur. Upon dimerisation either one or both molecules could reconstitute their catalytical triad intra-molecularly, creating one or two active sites, respectively (Figure 6.4B, C). Alternatively, the C-terminal catalytical domain of one or both molecules within the USP29 dimer could fold in such a way that it builds up the catalytical triad together with the cysteine of the other molecule (Figure 6.4D, E). This way, the dimer would form one or two inter-molecular catalytic sites, respectively. All hypothetical dimers could retain proteolytic activity in one active site even if one of the molecules contains a mutation of one of the crucial residues. Dimers consisting of the USP29^{C/S} mutant, however, are unable to reconstitute the required catalytical triad.

Interestingly, the lysine residues that we found to be ubiquitinated without having a direct impact on USP29 stability, are located N-terminally of (K127) and just behind (K599 and K668) the first catalytic domain. While K127 could therefore affect USP29 dimerisation, the latter two are likely to be part of the hinge region that is formed when the C-terminus folds in. Their ubiquitination might either sterically hinder the curve formation or facilitate it by interacting with ubiquitin-binding domains intra- or inter-molecularly. Other post-translational modifications, such as phosphorylations, could similarly affect USP29 folding and/or dimerisation.

As previously mentioned, if USP29 dimerisation was crucial for USP29 catalytic activity, then preventing the dimerisation with small molecules could be a promising approach to specifically reduce USP29 downstream effects. Of note, this could be more specific to USP29 than drugs that target USP29's catalytic domain, as cysteine protease domains are very common. Such targeting of a homo-dimerisation interface with an engineered peptide has been recently successful in the case of estrogen receptor (Chakraborty et al., 2016).

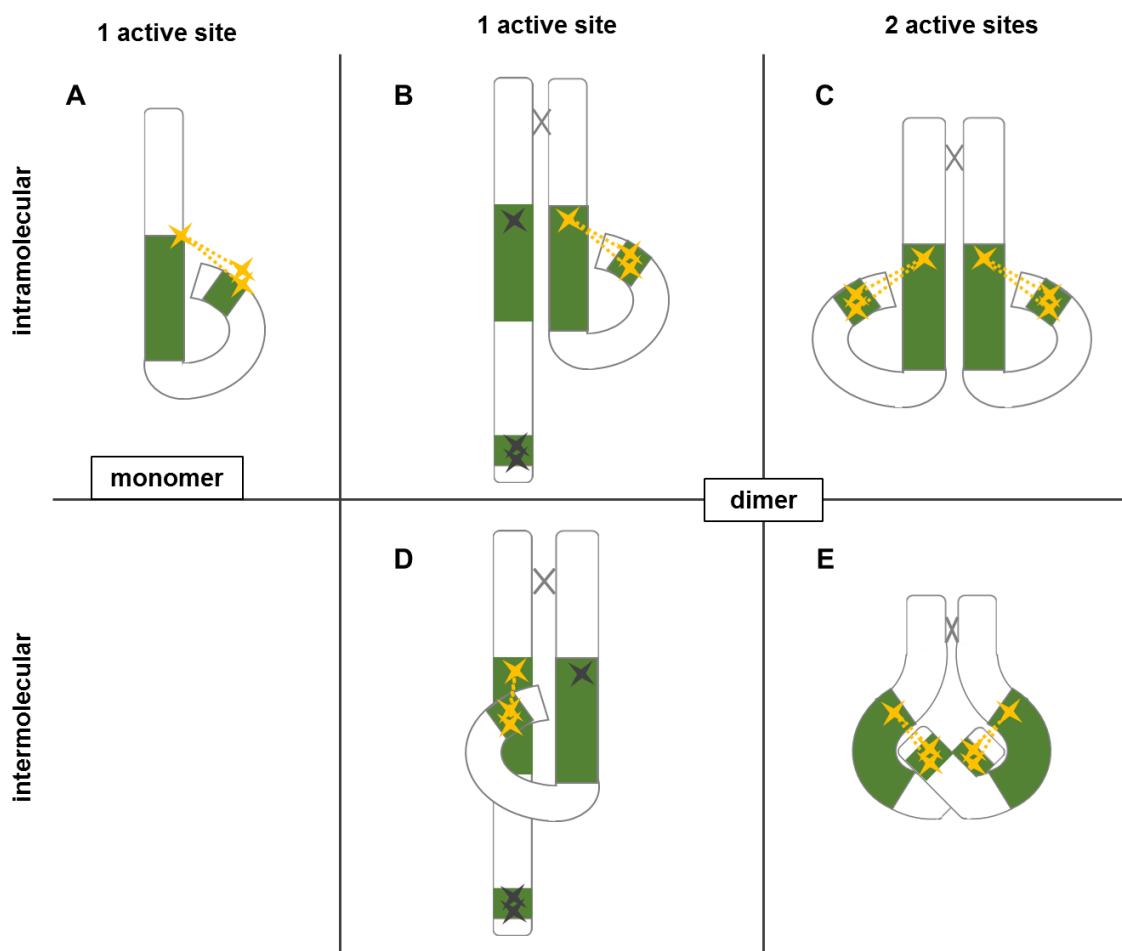


Figure 6.4: Possible formations of active sites in USP29 dimers. Two USP29 molecules dimerise via their putative homo-dimerisation domain (grey cross), their split catalytical domains are coloured in green. The catalytical triad residues (C294, H840 and N857) are displayed as yellow stars if they form part of a complete active site or as grey stars if they don't.

6.5 Expression of USP29

The expression of the *USP29* gene has been described to be very low because of its selective transcription from the paternal allele (Kim et al., 2000). In fact, in early Northern Blot studies murine *usp29* mRNA was detectable in brain and testis, and human *USP29* mRNA was only present in testis tissue extracts (Kim et al., 2000). However, other's and our data suggest that USP29 is also expressed in other cell types (Liu et al., 2011; Martin et al., 2015). While we were unable to detect endogenous USP29 protein with commercially available antibodies in HEK293T cells, RNAi-mediated depletion of *USP29* mRNA impacted on HIF- α . Together with the fact that we were able to rescue this effect by re-introducing a siRNA-resistant USP29, this indicated that even though below the detection limit, USP29 was present and exhibited considerable catalytic activity. In the light of USP29 regulating not only HIF- α , but also caspase and p53 stability, any upregulation of *USP29* expression might cause extensive perturbations of important cellular processes, including cell cycle progression, DNA integrity and HIF signalling. Accordingly, USP29 basal levels need to be limited in order for the cell to be able to function properly. Liu and co-workers suggest that AIMP2 induces USP29 transcription in

response to oxidative stress via FUSE binding protein 1 (FBP1). The alternative splice-variant AIMP2-DX2 was particularly successful in inducing *USP29* expression (Liu et al., 2011), and this splice variant has been associated with lung cancer (Choi et al., 2011). Similarly, the loss of imprinting of the maternal *USP29* allele could increase *USP29* expression levels. In this regard, chromatin-modifying drugs that are widely used in cancer treatment, such as HDAC inhibitors could weaken the transcriptional repression.

Bioinformatic analysis of an mRNA-based dataset of prostate tissue showed that *USP29* transcription was indeed upregulated in primary and metastatic tissue as compared to healthy prostate and that *USP29* mRNA levels correlated with disease progression and severity as determined with the Gleason Score. Whether the *USP29* up-regulation is a side effect of the oncogenic transformation in prostate cancer or whether it has a more decisive role in the transformation process remains to be investigated. In this context, it would also be important to confirm that the higher *USP29* mRNA levels translate into higher USP29 protein levels. The fact that there was a positive correlation between *USP29* and *Ca9* mRNA levels indicates that this may indeed be the case.

In order to study USP29's function in healthy cells as well as in oncogenic transformation and cancer progression, there is a need for appropriate models. Mouse models are currently not available and given that in early studies *USP29* showed different expression patterns in human and rodents, their usefulness needs to be scrutinised. In this regard, it is interesting to mention the case of bovine *USP29*, which shows 73% sequence identity with the human homologue (Kim et al., 2007). Bovine *USP29* mRNA was found to be exclusively expressed in brain, however it has lost protein coding function and does not contain any ORF (Kim et al., 2007). The function of the long non-coding RNA is not well understood, however mouse data suggest that it might be involved in the promoter methylation status of the neighbouring *zfp264* gene (He et al., 2016).

6.6 USP29 - an integrator of cell signals?

In response to oxidative stress, USP29 has been shown to stabilise p53, which subsequently induced apoptosis (Liu et al., 2011). Furthermore, USP29 has been reported to stabilise claspin, a protein that is required for replication and DNA damage repair and therefore USP29-depleted cells displayed delays in G1- to S-phase progression (Martin et al., 2015). In this thesis we established USP29 as an activator of hypoxia signalling (chapter 4). We and others also found USP29 to bind to PCNA, a protein crucial for DNA replication and involved in DNA damage response, however we did not investigate yet whether PCNA is a USP29 target protein. We further show that USP29 also auto-regulates its ubiquitination status and hence its stability (chapter 5).

Considering its low abundance, the question arises how USP29 chooses among its different targets (Figure 6.5). Does USP29 bind all its ubiquitinated targets with equal affinity and is therefore the sole presence of the ubiquitinated substrate sufficient for USP29 binding? Or does USP29 have preference for a specific target which is hence stabilised preferably even in the

presence of other substrates? Moreover, are there USP29 modifications that modulate the affinity towards its target proteins? How is this whole process of substrate selection influenced by USP29's own ubiquitination and/or dimerisation status? When USP29 itself is subjected to ubiquitination by its ubiquitin E3 ligase and hence has to auto-stabilise, is this reflected by a reduction of deubiquitination activity towards other targets?

Hence, it is possible that USP29 chooses between HIF- α , p53 and claspin depending on their relative availabilities in the cell and USP29's current deubiquitination potential. Furthermore, other regulators could interfere with the selection by modulating USP29's catalytic activity and its post-translational modifications or its nuclear distribution. For example, USP29 could be sequestered by PCNA via its PIP-box depending on the cell cycle stage and the integrity of the DNA.

By channelling the response via central transcriptional effectors such as HIF- α and p53, USP29 could represent an integrator of various cellular signals.

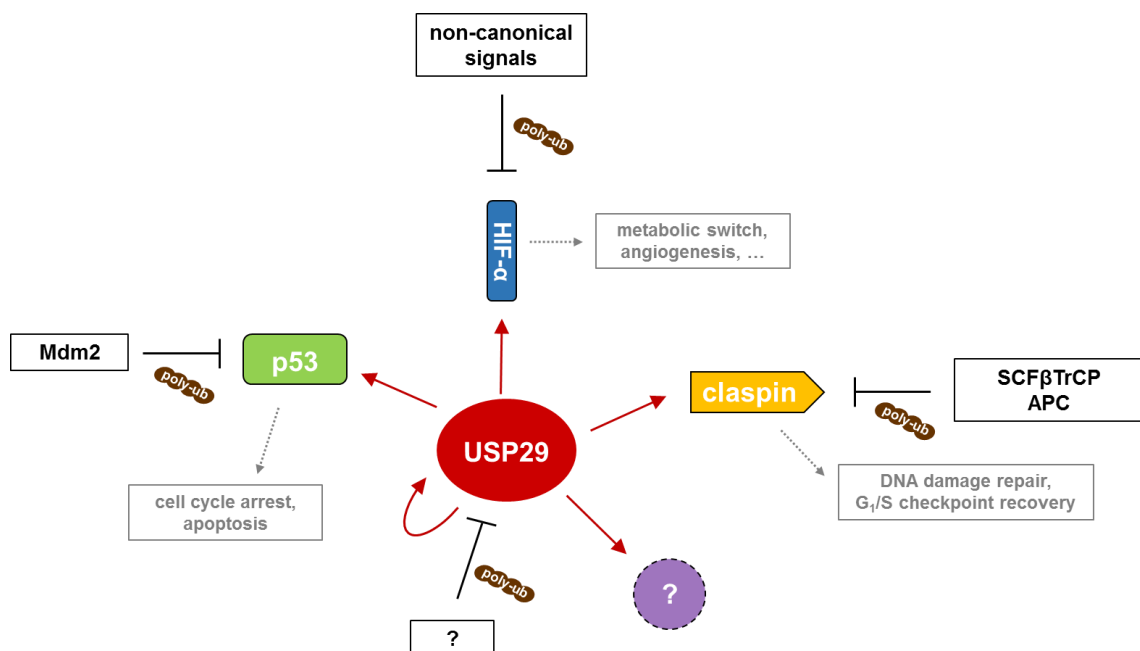


Figure 6.5: USP29 as an integrator of cell signals. USP29 itself and its target proteins are ubiquitinated (black lines) in response to various signals. USP29 removes the polyubiquitin (red arrows) and therefore protects them from proteasomal degradation, allowing them to execute their cellular functions (grey).

6.7 Outlook and perspective

While we have discovered many novel regulatory mechanisms during this project, more fundamental regulatory principles are still to be revealed. Which ubiquitin E3 ligase(s) are responsible for ubiquitination of HIF- α and USP29 and which residues in USP29 are targeted? How does HUWE1 interfere with USP29's ubiquitination? And do PTM's modulate USP29's ubiquitination status and/or its activity?

Further questions are whether *USP29* mRNA levels are altered or USP29 mutated in pathophysiological contexts other than prostate cancer and whether the alterations are implicated in the formation and progression of the disease or whether they occur as a concomitant of the cellular transformation. Depending on the answer, the next logical step would be the exploration of USP29 as a drug target. Is it feasible to target USP29 specifically and safely to manipulate HIF signalling in disease and what are the potential side effects?

Furthermore, a new PhD project in Edurne Berra's lab will be dedicated to investigate the basis and consequences of USP29's interaction with PCNA and how this is regulated by or regulating DNA integrity.

For many of these questions the use of the CRISPR/Cas9 system in model organisms could become a useful tool to manipulate USP29 expression levels, introduce specific mutations or add tags that facilitate USP29 detection.

BIBLIOGRAPHY

- Abdelmaksoud-Dammak, R., Saadallah-Kallel, A., Miladi-Abdennadher, I., Ayedi, L., Khabir, A., Sallemi-Boudawara, T., Frikha, M., Daoud, J., and Mokdad-Gargouri, R. (2015). CpG methylation of ubiquitin carboxyl-terminal hydrolase 1 (UCHL1) and P53 mutation pattern in sporadic colorectal cancer. *Tumour biology : the journal of the International Society for Oncodevelopmental Biology and Medicine*.
- Abdul Rehman, S.A., Kristariyanto, Y.A., Choi, S.Y., Nkosi, P.J., Weidlich, S., Labib, K., Hofmann, K., and Kulathu, Y. (2016). MINDY-1 Is a Member of an Evolutionarily Conserved and Structurally Distinct New Family of Deubiquitinating Enzymes. *Molecular cell* 63, 146-155.
- Altun, M., Zhao, B., Velasco, K., Liu, H., Hassink, G., Paschke, J., Pereira, T., and Lindsten, K. (2012). Ubiquitin-specific protease 19 (USP19) regulates hypoxia-inducible factor 1 α (HIF-1 α) during hypoxia. *The Journal of biological chemistry* 287, 1962-1969.
- Amelio, I., Inoue, S., Markert, E.K., Levine, A.J., Knight, R.A., Mak, T.W., and Melino, G. (2015). TAp73 opposes tumor angiogenesis by promoting hypoxia-inducible factor 1 α degradation. *Proceedings of the National Academy of Sciences of the United States of America* 112, 226-231.
- An, J., Mo, D., Liu, H., Veena, M.S., Srivatsan, E.S., Massoumi, R., and Rettig, M.B. (2008). Inactivation of the CYLD deubiquitinase by HPV E6 mediates hypoxia-induced NF-kappaB activation. *Cancer cell* 14, 394-407.
- Anderson, K., Nordquist, K.A., Gao, X., Hicks, K.C., Zhai, B., Gygi, S.P., and Patel, T.B. (2011). Regulation of cellular levels of Sprouty2 protein by prolyl hydroxylase domain and von Hippel-Lindau proteins. *The Journal of biological chemistry* 286, 42027-42036.
- Appelhoff, R.J., Tian, Y.M., Raval, R.R., Turley, H., Harris, A.L., Pugh, C.W., Ratcliffe, P.J., and Gleadow, J.M. (2004). Differential function of the prolyl hydroxylases PHD1, PHD2, and PHD3 in the regulation of hypoxia-inducible factor. *The Journal of biological chemistry* 279, 38458-38465.
- Aprelikova, O., Chandramouli, G.V., Wood, M., Vasselli, J.R., Riss, J., Maranchie, J.K., Linehan, W.M., and Barrett, J.C. (2004). Regulation of HIF prolyl hydroxylases by hypoxia-inducible factors. *Journal of cellular biochemistry* 92, 491-501.
- Arany, Z., Huang, L.E., Eckner, R., Bhattacharya, S., Jiang, C., Goldberg, M.A., Bunn, H.F., and Livingston, D.M. (1996). An essential role for p300/CBP in the cellular response to hypoxia. *Proceedings of the National Academy of Sciences of the United States of America* 93, 12969-12973.
- Bacia, K., Kim, S.A., and Schwille, P. (2006). Fluorescence cross-correlation spectroscopy in living cells. *Nature methods* 3, 83-89.
- Bae, S.H., Jeong, J.W., Park, J.A., Kim, S.H., Bae, M.K., Choi, S.J., and Kim, K.W. (2004). Sumoylation increases HIF-1 α stability and its transcriptional activity. *Biochemical and biophysical research communications* 324, 394-400.

- Baird, G.S., Zacharias, D.A., and Tsien, R.Y. (2000). Biochemistry, mutagenesis, and oligomerization of DsRed, a red fluorescent protein from coral. *Proceedings of the National Academy of Sciences of the United States of America* 97, 11984-11989.
- Becker, W. (2012). Fluorescence lifetime imaging--techniques and applications. *Journal of microscopy* 247, 119-136.
- Bento, C.F., Fernandes, R., Ramalho, J., Marques, C., Shang, F., Taylor, A., and Pereira, P. (2010). The chaperone-dependent ubiquitin ligase CHIP targets HIF-1 α for degradation in the presence of methylglyoxal. *PloS one* 5, e15062.
- Berra, E., Benizri, E., Ginouves, A., Volmat, V., Roux, D., and Pouyssegur, J. (2003). HIF prolyl-hydroxylase 2 is the key oxygen sensor setting low steady-state levels of HIF-1 α in normoxia. *The EMBO journal* 22, 4082-4090.
- Berta, M.A., Mazure, N., Hattab, M., Pouyssegur, J., and Brahimi-Horn, M.C. (2007). SUMOylation of hypoxia-inducible factor-1 α reduces its transcriptional activity. *Biochemical and biophysical research communications* 360, 646-652.
- Bett, J.S., Ibrahim, A.F., Garg, A.K., Kelly, V., Pedrioli, P., Rocha, S., and Hay, R.T. (2013). The P-body component USP52/PAN2 is a novel regulator of HIF1A mRNA stability. *The Biochemical journal* 451, 185-194.
- Bignell, G.R., Warren, W., Seal, S., Takahashi, M., Rapley, E., Barfoot, R., Green, H., Brown, C., Biggs, P.J., Lakhani, S.R., *et al.* (2000). Identification of the familial cylindromatosis tumour-suppressor gene. *Nature genetics* 25, 160-165.
- Bremm, A., Freund, S.M., and Komander, D. (2010). Lys11-linked ubiquitin chains adopt compact conformations and are preferentially hydrolyzed by the deubiquitinase Cezanne. *Nature structural & molecular biology* 17, 939-947.
- Bremm, A., Moniz, S., Mader, J., Rocha, S., and Komander, D. (2014). Cezanne (OTUD7B) regulates HIF-1 α homeostasis in a proteasome-independent manner. *EMBO reports* 15, 1268-1277.
- Bruick, R.K., and McKnight, S.L. (2001). A conserved family of prolyl-4-hydroxylases that modify HIF. *Science (New York, N.Y)* 294, 1337-1340.
- Bullen, J.W., Tchernyshyov, I., Holewinski, R.J., DeVine, L., Wu, F., Venkatraman, V., Kass, D.L., Cole, R.N., Van Eyk, J., and Semenza, G.L. (2016). Protein kinase A-dependent phosphorylation stimulates the transcriptional activity of hypoxia-inducible factor 1. *Science signaling* 9, ra56.
- Cai, Q., and Robertson, E.S. (2010). Ubiquitin/SUMO modification regulates VHL protein stability and nucleocytoplasmic localization. *PloS one* 5.
- Cai, Q., Verma, S.C., Kumar, P., Ma, M., and Robertson, E.S. (2010). Hypoxia inactivates the VHL tumor suppressor through PIASy-mediated SUMO modification. *PloS one* 5, e9720.
- Cassavaugh, J.M., Hale, S.A., Wellman, T.L., Howe, A.K., Wong, C., and Lounsbury, K.M. (2011). Negative regulation of HIF-1 α by an FBW7-mediated degradation pathway during hypoxia. *Journal of cellular biochemistry* 112, 3882-3890.
- Chakraborty, S., Asare, B.K., Biswas, P.K., and Rajnarayanan, R.V. (2016). Designer interface peptide grafts target estrogen receptor alpha dimerization. *Biochemical and biophysical research communications* 478, 116-122.

- Chan, C.H., Li, C.F., Yang, W.L., Gao, Y., Lee, S.W., Feng, Z., Huang, H.Y., Tsai, K.K., Flores, L.G., Shao, Y., *et al.* (2012). The Skp2-SCF E3 ligase regulates Akt ubiquitination, glycolysis, herceptin sensitivity, and tumorigenesis. *Cell* *149*, 1098-1111.
- Chau, V., Tobias, J.W., Bachmair, A., Marriott, D., Ecker, D.J., Gonda, D.K., and Varshavsky, A. (1989). A multiubiquitin chain is confined to specific lysine in a targeted short-lived protein. *Science (New York, N.Y)* *243*, 1576-1583.
- Chen, D., Kon, N., Li, M., Zhang, W., Qin, J., and Gu, W. (2005). ARF-BP1/Mule is a critical mediator of the ARF tumor suppressor. *Cell* *121*, 1071-1083.
- Chen, N., Chen, X., Huang, R., Zeng, H., Gong, J., Meng, W., Lu, Y., Zhao, F., Wang, L., and Zhou, Q. (2009). BCL-xL is a target gene regulated by hypoxia-inducible factor-1a. *The Journal of biological chemistry* *284*, 10004-10012.
- Chen, W., Hill, H., Christie, A., Kim, M.S., Holloman, E., Pavia-Jimenez, A., Homayoun, F., Ma, Y., Patel, N., Yell, P., *et al.* (2016). Targeting renal cell carcinoma with a HIF-2 antagonist. *Nature* *539*, 112-117.
- Cho, H., Du, X., Rizzi, J.P., Liberzon, E., Chakraborty, A.A., Gao, W., Carvo, I., Signoretti, S., Bruick, R.K., Josey, J.A., *et al.* (2016). On-target efficacy of a HIF-2alpha antagonist in preclinical kidney cancer models. *Nature* *539*, 107-111.
- Choe, K.N., Nicolae, C.M., Constantin, D., Imamura Kawasawa, Y., Delgado-Diaz, M.R., De, S., Freire, R., Smits, V.A., and Moldovan, G.L. (2016). HUWE1 interacts with PCNA to alleviate replication stress. *EMBO reports* *17*, 874-886.
- Choi, J.W., Kim, D.G., Lee, A.E., Kim, H.R., Lee, J.Y., Kwon, N.H., Shin, Y.K., Hwang, S.K., Chang, S.H., Cho, M.H., *et al.* (2011). Cancer-associated splicing variant of tumor suppressor AIMP2/p38: pathological implication in tumorigenesis. *PLoS genetics* *7*, e1001351.
- Clague, M.J., Barsukov, I., Coulson, J.M., Liu, H., Rigden, D.J., and Urbé, S. (2013). Deubiquitylases from genes to organism. *Physiol Rev* *93*, 1289-1315.
- Clague, M.J., Liu, H., and Urbe, S. (2012). Governance of endocytic trafficking and signaling by reversible ubiquitylation. *Developmental cell* *23*, 457-467.
- Collins, D.C., Sundar, R., Lim, J.S., and Yap, T.A. (2016). Towards Precision Medicine in the Clinic: From Biomarker Discovery to Novel Therapeutics. *Trends in pharmacological sciences*.
- Colombo, M., Vallese, S., Peretto, I., Jacq, X., Rain, J.C., Colland, F., and Guedat, P. (2010). Synthesis and biological evaluation of 9-oxo-9H-indeno[1,2-b]pyrazine-2,3-dicarbonitrile analogues as potential inhibitors of deubiquitinating enzymes. *ChemMedChem* *5*, 552-558.
- Coyne, E.S., and Wing, S.S. (2016). The business of deubiquitination - location, location, location. *F1000Research* *5*.
- D'Arcy, P., and Linder, S. (2014). Molecular pathways: translational potential of deubiquitinases as drug targets. *Clinical cancer research : an official journal of the American Association for Cancer Research* *20*, 3908-3914.
- D'Arcy, P., Wang, X., and Linder, S. (2015). Deubiquitinase inhibition as a cancer therapeutic strategy. *Pharmacology & therapeutics* *147*, 32-54.

- Day, R.N., and Davidson, M.W. (2009). The fluorescent protein palette: tools for cellular imaging. *Chemical Society reviews* 38, 2887-2921.
- Deng, L., Wang, C., Spencer, E., Yang, L., Braun, A., You, J., Slaughter, C., Pickart, C., and Chen, Z.J. (2000). Activation of the I κ B kinase complex by TRAF6 requires a dimeric ubiquitin-conjugating enzyme complex and a unique polyubiquitin chain. *Cell* 103, 351-361.
- Denuc, A., Bosch-Comas, A., Gonzalez-Duarte, R., and Marfany, G. (2009). The UBA-UIM domains of the USP25 regulate the enzyme ubiquitination state and modulate substrate recognition. *PloS one* 4, e5571.
- Di Fiore, P.P., Polo, S., and Hofmann, K. (2003). When ubiquitin meets ubiquitin receptors: a signalling connection. *Nature reviews. Molecular cell biology* 4, 491-497.
- Dimova, E.Y., Michiels, C., and Kietzmann, T. (2009). Kinases as upstream regulators of the HIF system: their emerging potential as anti-cancer drug targets. *Current pharmaceutical design* 15, 3867-3877.
- Duan, C. (2016). Hypoxia-inducible factor 3 biology: complexities and emerging themes. *American journal of physiology. Cell physiology* 310, C260-269.
- Edelmann, M.J., Kramer, H.B., Altun, M., and Kessler, B.M. (2010). Post-translational modification of the deubiquitinating enzyme otubain 1 modulates active RhoA levels and susceptibility to *Yersinia* invasion. *The FEBS journal* 277, 2515-2530.
- Ehrlich, E.S., Wang, T., Luo, K., Xiao, Z., Niewiadomska, A.M., Martinez, T., Xu, W., Neckers, L., and Yu, X.F. (2009). Regulation of Hsp90 client proteins by a Cullin5-RING E3 ubiquitin ligase. *Proceedings of the National Academy of Sciences of the United States of America* 106, 20330-20335.
- Ema, M., Taya, S., Yokotani, N., Sogawa, K., Matsuda, Y., and Fujii-Kuriyama, Y. (1997). A novel bHLH-PAS factor with close sequence similarity to hypoxia-inducible factor 1 α regulates the VEGF expression and is potentially involved in lung and vascular development. *Proceedings of the National Academy of Sciences of the United States of America* 94, 4273-4278.
- Epstein, A.C., Gleadle, J.M., McNeill, L.A., Hewitson, K.S., O'Rourke, J., Mole, D.R., Mukherji, M., Metzen, E., Wilson, M.I., Dhanda, A., *et al.* (2001). *C. elegans* EGL-9 and mammalian homologs define a family of dioxygenases that regulate HIF by prolyl hydroxylation. *Cell* 107, 43-54.
- Fernandez-Montalvan, A., Bouwmeester, T., Joberty, G., Mader, R., Mahnke, M., Pierrat, B., Schlaeppli, J.M., Worpenberg, S., and Gerhartz, B. (2007). Biochemical characterization of USP7 reveals post-translational modification sites and structural requirements for substrate processing and subcellular localization. *The FEBS journal* 274, 4256-4270.
- Ferreira, J.V., Fofu, H., Bejarano, E., Bento, C.F., Ramalho, J.S., Girao, H., and Pereira, P. (2013). STUB1/CHIP is required for HIF1A degradation by chaperone-mediated autophagy. *Autophagy* 9, 1349-1366.
- Flugel, D., Gorlach, A., and Kietzmann, T. (2012). GSK-3 β regulates cell growth, migration, and angiogenesis via Fbw7 and USP28-dependent degradation of HIF-1 α . *Blood* 119, 1292-1301.

- Flugel, D., Gorch, A., Michiels, C., and Kietzmann, T. (2007). Glycogen synthase kinase 3 phosphorylates hypoxia-inducible factor 1alpha and mediates its destabilization in a VHL-independent manner. *Molecular and cellular biology* 27, 3253-3265.
- Förster, T. (1948). Zwischenmolekulare Energiewanderung und Fluoreszenz. *Ann. Phys.* 437, 35-55.
- Fraile, J.M., Quesada, V., Rodriguez, D., Freije, J.M., and Lopez-Otin, C. (2012). Deubiquitinases in cancer: new functions and therapeutic options. *Oncogene* 31, 2373-2388.
- Fukuba, H., Yamashita, H., Nagano, Y., Jin, H.G., Hiji, M., Ohtsuki, T., Takahashi, T., Kohriyama, T., and Matsumoto, M. (2007). Siah-1 facilitates ubiquitination and degradation of factor inhibiting HIF-1alpha (FIH). *Biochemical and biophysical research communications* 353, 324-329.
- Gong, Y., Zack, T.I., Morris, L.G., Lin, K., Hukkelhoven, E., Raheja, R., Tan, I.L., Turcan, S., Veeriah, S., Meng, S., *et al.* (2014). Pan-cancer genetic analysis identifies PARK2 as a master regulator of G1/S cyclins. *Nature genetics* 46, 588-594.
- Goto, Y., Zeng, L., Yeom, C.J., Zhu, Y., Morinibu, A., Shinomiya, K., Kobayashi, M., Hirota, K., Itasaka, S., Yoshimura, M., *et al.* (2015). UCHL1 provides diagnostic and antimetastatic strategies due to its deubiquitinating effect on HIF-1alpha. *Nature communications* 6, 6153.
- Gu, Y.Y., Yang, M., Zhao, M., Luo, Q., Yang, L., Peng, H., Wang, J., Huang, S.K., Zheng, Z.X., Yuan, X.H., *et al.* (2015). The de-ubiquitinase UCHL1 promotes gastric cancer metastasis via the Akt and Erk1/2 pathways. *Tumour biology : the journal of the International Society for Oncodevelopmental Biology and Medicine*.
- Gu, Y.Z., Moran, S.M., Hogenesch, J.B., Wartman, L., and Bradfield, C.A. (1998). Molecular characterization and chromosomal localization of a third alpha-class hypoxia inducible factor subunit, HIF3alpha. *Gene expression* 7, 205-213.
- Guo, G., Xu, Y., Gong, M., Cao, Y., and An, R. (2014a). USP28 is a potential prognostic marker for bladder cancer. *Tumour biology : the journal of the International Society for Oncodevelopmental Biology and Medicine* 35, 4017-4022.
- Guo, J., Shinriki, S., Su, Y., Nakamura, T., Hayashi, M., Tsuda, Y., Murakami, Y., Tasaki, M., Hide, T., Takezaki, T., *et al.* (2014b). Hypoxia suppresses cylindromatosis (CYLD) expression to promote inflammation in glioblastoma: possible link to acquired resistance to anti-VEGF therapy. *Oncotarget* 5, 6353-6364.
- Haas, T.L., Emmerich, C.H., Gerlach, B., Schmukle, A.C., Cordier, S.M., Rieser, E., Feltham, R., Vince, J., Warnken, U., Wenger, T., *et al.* (2009). Recruitment of the linear ubiquitin chain assembly complex stabilizes the TNF-R1 signaling complex and is required for TNF-mediated gene induction. *Molecular cell* 36, 831-844.
- Hall, J.R., Kow, E., Nevis, K.R., Lu, C.K., Luce, K.S., Zhong, Q., and Cook, J.G. (2007). Cdc6 stability is regulated by the Huwe1 ubiquitin ligase after DNA damage. *Molecular biology of the cell* 18, 3340-3350.
- Han, B., Tiwari, A., and Kenworthy, A.K. (2015). Tagging strategies strongly affect the fate of overexpressed caveolin-1. *Traffic* 16, 417-438.

- Hanahan, D., and Weinberg, R.A. (2011). Hallmarks of cancer: the next generation. *Cell* *144*, 646-674.
- He, H., and Kim, J. (2014). Regulation and function of the *peg3* imprinted domain. *Genomics & informatics* *12*, 105-113.
- He, H., Ye, A., and Kim, J. (2016). Transcriptional Truncation of the Long Coding Imprinted Gene *Usp29*. *PloS one* *11*, e0158004.
- Her, Y.R., and Chung, I.K. (2009). Ubiquitin Ligase RLIM Modulates Telomere Length Homeostasis through a Proteolysis of TRF1. *The Journal of biological chemistry* *284*, 8557-8566.
- Hicks, K.C., and Patel, T.B. (2016). Sprouty2 Protein Regulates Hypoxia-inducible Factor-alpha (HIFalpha) Protein Levels and Transcription of HIFalpha-responsive Genes. *The Journal of biological chemistry* *291*, 16787-16801.
- Hochreiter, B., Garcia, A.P., and Schmid, J.A. (2015). Fluorescent proteins as genetically encoded FRET biosensors in life sciences. *Sensors (Basel)* *15*, 26281-26314.
- Hoeller, D., Crosetto, N., Blagoev, B., Raiborg, C., Tikkanen, R., Wagner, S., Kowanzetz, K., Breitling, R., Mann, M., Stenmark, H., *et al.* (2006). Regulation of ubiquitin-binding proteins by monoubiquitination. *Nature cell biology* *8*, 163-169.
- Hong, S., Wang, Y.N., Yamaguchi, H., Sreenivasappa, H., Chou, C.K., Tsou, P.H., Hung, M.C., and Kameoka, J. (2010). MEASUREMENT of Protein 53 Diffusion Coefficient in Live HeLa Cells Using Raster Image Correlation Spectroscopy (RICS). *Journal of biomaterials and nanobiotechnology* *1*, 31-36.
- Huang, C., Han, Y., Wang, Y., Sun, X., Yan, S., Yeh, E.T., Chen, Y., Cang, H., Li, H., Shi, G., *et al.* (2009). SENP3 is responsible for HIF-1 transactivation under mild oxidative stress via p300 de-SUMOylation. *The EMBO journal* *28*, 2748-2762.
- Huang, J., Zhao, Q., Mooney, S.M., and Lee, F.S. (2002). Sequence determinants in hypoxia-inducible factor-1alpha for hydroxylation by the prolyl hydroxylases PHD1, PHD2, and PHD3. *The Journal of biological chemistry* *277*, 39792-39800.
- Huang, J.M., and Kim, J. (2009). DNA methylation analysis of the mammalian PEG3 imprinted domain. *Gene* *442*, 18-25.
- Huang, L.E., Arany, Z., Livingston, D.M., and Bunn, H.F. (1996). Activation of hypoxia-inducible transcription factor depends primarily upon redox-sensitive stabilization of its alpha subunit. *The Journal of biological chemistry* *271*, 32253-32259.
- Huang, L.E., Gu, J., Schau, M., and Bunn, H.F. (1998). Regulation of hypoxia-inducible factor 1alpha is mediated by an O2-dependent degradation domain via the ubiquitin-proteasome pathway. *Proceedings of the National Academy of Sciences of the United States of America* *95*, 7987-7992.
- Hubbi, M.E., Hu, H., Kshitiz, Ahmed, I., Levchenko, A., and Semenza, G.L. (2013). Chaperone-mediated autophagy targets hypoxia-inducible factor-1alpha (HIF-1alpha) for lysosomal degradation. *The Journal of biological chemistry* *288*, 10703-10714.
- Hussain, S., Bedekovics, T., Chesi, M., Bergsagel, P.L., and Galarzy, P.J. (2015). UCHL1 is a biomarker of aggressive multiple myeloma required for disease progression. *Oncotarget*.

- Hutti, J.E., Turk, B.E., Asara, J.M., Ma, A., Cantley, L.C., and Abbott, D.W. (2007). IkkappaB kinase beta phosphorylates the K63 deubiquitinase A20 to cause feedback inhibition of the NF-kappaB pathway. *Molecular and cellular biology* 27, 7451-7461.
- Isaacs, J.S., Jung, Y.J., Mimnaugh, E.G., Martinez, A., Cuttitta, F., and Neckers, L.M. (2002). Hsp90 regulates a von Hippel Lindau-independent hypoxia-inducible factor-1 alpha-degradative pathway. *The Journal of biological chemistry* 277, 29936-29944.
- Ivan, M., Kondo, K., Yang, H., Kim, W., Valiando, J., Ohh, M., Salic, A., Asara, J.M., Lane, W.S., and Kaelin, W.G., Jr. (2001). HIFalpha targeted for VHL-mediated destruction by proline hydroxylation: implications for O2 sensing. *Science (New York, N.Y)* 292, 464-468.
- Iyer, N.V., Kotch, L.E., Agani, F., Leung, S.W., Laughner, E., Wenger, R.H., Gassmann, M., Gearhart, J.D., Lawler, A.M., Yu, A.Y., *et al.* (1998). Cellular and developmental control of O2 homeostasis by hypoxia-inducible factor 1 alpha. *Genes & development* 12, 149-162.
- Jaakkola, P., Mole, D.R., Tian, Y.M., Wilson, M.I., Gielbert, J., Gaskell, S.J., von Kriegsheim, A., Hebestreit, H.F., Mukherji, M., Schofield, C.J., *et al.* (2001). Targeting of HIF-alpha to the von Hippel-Lindau ubiquitylation complex by O2-regulated prolyl hydroxylation. *Science (New York, N.Y)* 292, 468-472.
- Jeong, C.H. (2015). Inhibition of Ubiquitin-specific Peptidase 8 Suppresses Growth of Gefitinib-resistant Non-small Cell Lung Cancer Cells by Inducing Apoptosis. *Journal of cancer prevention* 20, 57-63.
- Jiang, B.H., Rue, E., Wang, G.L., Roe, R., and Semenza, G.L. (1996). Dimerization, DNA binding, and transactivation properties of hypoxia-inducible factor 1. *The Journal of biological chemistry* 271, 17771-17778.
- Jinek, M., Chylinski, K., Fonfara, I., Hauer, M., Doudna, J.A., and Charpentier, E. (2012). A programmable dual-RNA-guided DNA endonuclease in adaptive bacterial immunity. *Science (New York, N.Y)* 337, 816-821.
- Joshi, S., Singh, A.R., and Durden, D.L. (2014). MDM2 regulates hypoxic hypoxia-inducible factor 1alpha stability in an E3 ligase, proteasome, and PTEN-phosphatidylinositol 3-kinase-AKT-dependent manner. *The Journal of biological chemistry* 289, 22785-22797.
- Kalousi, A., Mylonis, I., Politou, A.S., Chachami, G., Paraskeva, E., and Simos, G. (2010). Casein kinase 1 regulates human hypoxia-inducible factor HIF-1. *Journal of cell science* 123, 2976-2986.
- Kim, J., Ashworth, L., Branscomb, E., and Stubbs, L. (1997). The human homolog of a mouse-imprinted gene, Peg3, maps to a zinc finger gene-rich region of human chromosome 19q13.4. *Genome Res* 7, 532-540.
- Kim, J., Bergmann, A., Choo, J.H., and Stubbs, L. (2007). Genomic organization and imprinting of the Peg3 domain in bovine. *Genomics* 90, 85-92.
- Kim, J., Lu, X., and Stubbs, L. (1999). Zim1, a maternally expressed mouse Kruppel-type zinc-finger gene located in proximal chromosome 7. *Human molecular genetics* 8, 847-854.
- Kim, J., Noskov, V.N., Lu, X., Bergmann, A., Ren, X., Warth, T., Richardson, P., Kouprina, N., and Stubbs, L. (2000). Discovery of a novel, paternally expressed

ubiquitin-specific processing protease gene through comparative analysis of an imprinted region of mouse chromosome 7 and human chromosome 19q13.4. *Genome Res* 10, 1138-1147.

Kim, J.D., Kang, K., and Kim, J. (2009). YY1's role in DNA methylation of Peg3 and Xist. *Nucleic acids research* 37, 5656-5664.

Kim, J.O., Kim, S.R., Lim, K.H., Kim, J.H., Ajjappala, B., Lee, H.J., Choi, J.I., and Baek, K.H. (2015). Deubiquitinating enzyme USP37 regulating oncogenic function of 14-3-3gamma. *Oncotarget* 6, 36551-36576.

Kim, S.A., Sanabria, H., Digman, M.A., Gratton, E., Schwille, P., Zipfel, W.R., and Waxham, M.N. (2010). Quantifying translational mobility in neurons: comparison between current optical techniques. *The Journal of neuroscience : the official journal of the Society for Neuroscience* 30, 16409-16416.

King, B., Boccalatte, F., Moran-Crusio, K., Wolf, E., Wang, J., Kayembe, C., Lazaris, C., Yu, X., Aranda-Orgilles, B., Lasorella, A., *et al.* (2016). The ubiquitin ligase Huwe1 regulates the maintenance and lymphoid commitment of hematopoietic stem cells. *Nature immunology* 17, 1312-1321.

Kirisako, T., Kamei, K., Murata, S., Kato, M., Fukumoto, H., Kanie, M., Sano, S., Tokunaga, F., Tanaka, K., and Iwai, K. (2006). A ubiquitin ligase complex assembles linear polyubiquitin chains. *The EMBO journal* 25, 4877-4887.

Kluba, M., Engelborghs, Y., Hofkens, J., and Mizuno, H. (2015). Inhibition of Receptor Dimerization as a Novel Negative Feedback Mechanism of EGFR Signaling. *PloS one* 10, e0139971.

Koh, M.Y., Darnay, B.G., and Powis, G. (2008). Hypoxia-associated factor, a novel E3-ubiquitin ligase, binds and ubiquitinates hypoxia-inducible factor 1alpha, leading to its oxygen-independent degradation. *Molecular and cellular biology* 28, 7081-7095.

Koh, M.Y., Nguyen, V., Lemos, R., Jr., Darnay, B.G., Kiriakova, G., Abdelmelek, M., Ho, T.H., Karam, J., Monzon, F.A., Jonasch, E., *et al.* (2015). Hypoxia-induced SUMOylation of E3 ligase HAF determines specific activation of HIF2 in clear-cell renal cell carcinoma. *Cancer research* 75, 316-329.

Koivunen, P., Tiainen, P., Hyvarinen, J., Williams, K.E., Sormunen, R., Klaus, S.J., Kivirikko, K.I., and Myllyharju, J. (2007). An endoplasmic reticulum transmembrane prolyl 4-hydroxylase is induced by hypoxia and acts on hypoxia-inducible factor alpha. *The Journal of biological chemistry* 282, 30544-30552.

Komander, D., Clague, M.J., and Urbe, S. (2009). Breaking the chains: structure and function of the deubiquitinases. *Nature reviews. Molecular cell biology* 10, 550-563.

Kuroiwa, Y., Kaneko-Ishino, T., Kagitani, F., Kohda, T., Li, L.L., Tada, M., Suzuki, R., Yokoyama, M., Shiroishi, T., Wakana, S., *et al.* (1996). Peg3 imprinted gene on proximal chromosome 7 encodes for a zinc finger protein. *Nature genetics* 12, 186-190.

Lakowicz, J.R. (2006). *Principles of fluorescence spectroscopy*, 3rd edn (New York: Springer).

Lam, A.J., St-Pierre, F., Gong, Y., Marshall, J.D., Cranfill, P.J., Baird, M.A., McKeown, M.R., Wiedenmann, J., Davidson, M.W., Schnitzer, M.J., *et al.* (2012). Improving FRET dynamic range with bright green and red fluorescent proteins. *Nature methods* 9, 1005-1012.

- Landgraf, D., Okumus, B., Chien, P., Baker, T.A., and Paulsson, J. (2012). Segregation of molecules at cell division reveals native protein localization. *Nature methods* 9, 480-482.
- Lando, D., Peet, D.J., Whelan, D.A., Gorman, J.J., and Whitelaw, M.L. (2002). Asparagine hydroxylation of the HIF transactivation domain a hypoxic switch. *Science (New York, N.Y)* 295, 858-861.
- Lee, J.G., Baek, K., Soetandyo, N., and Ye, Y. (2013). Reversible inactivation of deubiquitinases by reactive oxygen species in vitro and in cells. *Nature communications* 4, 1568.
- Lee, S.Y., Ramirez, J., Franco, M., Lectez, B., Gonzalez, M., Barrio, R., and Mayor, U. (2014). Ube3a, the E3 ubiquitin ligase causing Angelman syndrome and linked to autism, regulates protein homeostasis through the proteasomal shuttle Rpn10. *Cellular and molecular life sciences : CMLS* 71, 2747-2758.
- Li, J., Wang, Q.E., Zhu, Q., El-Mahdy, M.A., Wani, G., Praetorius-Ibba, M., and Wani, A.A. (2006). DNA damage binding protein component DDB1 participates in nucleotide excision repair through DDB2 DNA-binding and cullin 4A ubiquitin ligase activity. *Cancer research* 66, 8590-8597.
- Li, L., Keverne, E.B., Aparicio, S.A., Ishino, F., Barton, S.C., and Surani, M.A. (1999). Regulation of maternal behavior and offspring growth by paternally expressed Peg3. *Science (New York, N.Y)* 284, 330-333.
- Li, X., Stevens, P.D., Yang, H., Gulhati, P., Wang, W., Evers, B.M., and Gao, T. (2013). The deubiquitination enzyme USP46 functions as a tumor suppressor by controlling PHLPP-dependent attenuation of Akt signaling in colon cancer. *Oncogene* 32, 471-478.
- Li, Z., Wang, D., Messing, E.M., and Wu, G. (2005). VHL protein-interacting deubiquitinating enzyme 2 deubiquitinates and stabilizes HIF-1alpha. *EMBO reports* 6, 373-378.
- Li, Z., Wang, D., Na, X., Schoen, S.R., Messing, E.M., and Wu, G. (2002). Identification of a deubiquitinating enzyme subfamily as substrates of the von Hippel-Lindau tumor suppressor. *Biochemical and biophysical research communications* 294, 700-709.
- Li, Z., Wang, D., Na, X., Schoen, S.R., Messing, E.M., and Wu, G. (2003). The VHL protein recruits a novel KRAB-A domain protein to repress HIF-1alpha transcriptional activity. *The EMBO journal* 22, 1857-1867.
- Lieb, M.E., Menzies, K., Moschella, M.C., Ni, R., and Taubman, M.B. (2002). Mammalian EGLN genes have distinct patterns of mRNA expression and regulation. *Biochemistry and cell biology = Biochimie et biologie cellulaire* 80, 421-426.
- Lionta, E., Spyrou, G., Vassilatis, D.K., and Cournia, Z. (2014). Structure-based virtual screening for drug discovery: principles, applications and recent advances. *Current topics in medicinal chemistry* 14, 1923-1938.
- Liu, J., Chung, H.-J., Vogt, M., Jin, Y., Malide, D., He, L., Dunder, M., and Levens, D. (2011). JTV1 co-activates FBP to induce USP29 transcription and stabilize p53 in response to oxidative stress. *The EMBO journal* 30, 846-858.

- Liu, Y.V., Baek, J.H., Zhang, H., Diez, R., Cole, R.N., and Semenza, G.L. (2007). RACK1 competes with HSP90 for binding to HIF-1alpha and is required for O(2)-independent and HSP90 inhibitor-induced degradation of HIF-1alpha. *Molecular cell* 25, 207-217.
- Lombard-Banek, C., Moody, S.A., and Nemes, P. (2016). Single-Cell Mass Spectrometry for Discovery Proteomics: Quantifying Translational Cell Heterogeneity in the 16-Cell Frog (*Xenopus*) Embryo. *Angew Chem Int Ed Engl* 55, 2454-2458.
- Lucifero, D., Mann, M.R., Bartolomei, M.S., and Trasler, J.M. (2004). Gene-specific timing and epigenetic memory in oocyte imprinting. *Human molecular genetics* 13, 839-849.
- Luo, W., Zhong, J., Chang, R., Hu, H., Pandey, A., and Semenza, G.L. (2010). Hsp70 and CHIP selectively mediate ubiquitination and degradation of hypoxia-inducible factor (HIF)-1alpha but Not HIF-2alpha. *The Journal of biological chemistry* 285, 3651-3663.
- Luong le, A., Fragiadaki, M., Smith, J., Boyle, J., Lutz, J., Dean, J.L., Harten, S., Ashcroft, M., Walmsley, S.R., Haskard, D.O., *et al.* (2013). Cezanne regulates inflammatory responses to hypoxia in endothelial cells by targeting TRAF6 for deubiquitination. *Circulation research* 112, 1583-1591.
- Mahon, P.C., Hirota, K., and Semenza, G.L. (2001). FIH-1: a novel protein that interacts with HIF-1alpha and VHL to mediate repression of HIF-1 transcriptional activity. *Genes & development* 15, 2675-2686.
- Martin, Y., Cabrera, E., Amoedo, H., Hernandez-Perez, S., Dominguez-Kelly, R., and Freire, R. (2015). USP29 controls the stability of checkpoint adaptor Claspin by deubiquitination. *Oncogene* 34, 1058-1063.
- Maruyama, T., Kadowaki, H., Okamoto, N., Nagai, A., Naguro, I., Matsuzawa, A., Shibuya, H., Tanaka, K., Murata, S., Takeda, K., *et al.* (2010). CHIP-dependent termination of MEKK2 regulates temporal ERK activation required for proper hyperosmotic response. *The EMBO journal* 29, 2501-2514.
- Marxsen, J.H., Stengel, P., Doege, K., Heikkinen, P., Jokilehto, T., Wagner, T., Jelkmann, W., Jaakkola, P., and Metzzen, E. (2004). Hypoxia-inducible factor-1 (HIF-1) promotes its degradation by induction of HIF-alpha-prolyl-4-hydroxylases. *The Biochemical journal* 381, 761-767.
- Massoumi, R. (2011). CYLD: a deubiquitination enzyme with multiple roles in cancer. *Future Oncol* 7, 285-297.
- Matsumoto, M.L., Wickliffe, K.E., Dong, K.C., Yu, C., Bosanac, I., Bustos, D., Phu, L., Kirkpatrick, D.S., Hymowitz, S.G., Rape, M., *et al.* (2010). K11-linked polyubiquitination in cell cycle control revealed by a K11 linkage-specific antibody. *Molecular cell* 39, 477-484.
- Matz, M.V., Fradkov, A.F., Labas, Y.A., Savitsky, A.P., Zaraisky, A.G., Markelov, M.L., and Lukyanov, S.A. (1999). Fluorescent proteins from nonbioluminescent Anthozoa species. *Nature biotechnology* 17, 969-973.
- Maxwell, P.H., Wiesener, M.S., Chang, G.W., Clifford, S.C., Vaux, E.C., Cockman, M.E., Wykoff, C.C., Pugh, C.W., Maher, E.R., and Ratcliffe, P.J. (1999). The tumour suppressor protein VHL targets hypoxia-inducible factors for oxygen-dependent proteolysis. *Nature* 399, 271-275.

- Mayer, A., Hockel, M., and Vaupel, P. (2008). Endogenous hypoxia markers: case not proven! *Advances in experimental medicine and biology* 614, 127-136.
- Mei, Y., Hahn, A.A., Hu, S., and Yang, X. (2011). The USP19 deubiquitinase regulates the stability of c-IAP1 and c-IAP2. *The Journal of biological chemistry* 286, 35380-35387.
- Mellacheruvu, D., Wright, Z., Couzens, A.L., Lambert, J.P., St-Denis, N.A., Li, T., Miteva, Y.V., Hauri, S., Sardi, M.E., Low, T.Y., *et al.* (2013). The CRAPome: a contaminant repository for affinity purification-mass spectrometry data. *Nature methods* 10, 730-736.
- Meray, R.K., and Lansbury, P.T., Jr. (2007). Reversible monoubiquitination regulates the Parkinson disease-associated ubiquitin hydrolase UCH-L1. *The Journal of biological chemistry* 282, 10567-10575.
- Metzen, E., Berchner-Pfannschmidt, U., Stengel, P., Marxsen, J.H., Stolze, I., Klinger, M., Huang, W.Q., Wotzlaw, C., Hellwig-Burgel, T., Jelkmann, W., *et al.* (2003). Intracellular localisation of human HIF-1 alpha hydroxylases: implications for oxygen sensing. *Journal of cell science* 116, 1319-1326.
- Meulmeester, E., Kunze, M., Hsiao, H.H., Urlaub, H., and Melchior, F. (2008). Mechanism and consequences for paralog-specific sumoylation of ubiquitin-specific protease 25. *Molecular cell* 30, 610-619.
- Mieruszynski, S., Digman, M.A., Gratton, E., and Jones, M.R. (2015). Characterization of exogenous DNA mobility in live cells through fluctuation correlation spectroscopy. *Scientific reports* 5, 13848.
- Minamishima, Y.A., Moslehi, J., Padera, R.F., Bronson, R.T., Liao, R., and Kaelin, W.G., Jr. (2009). A feedback loop involving the Phd3 prolyl hydroxylase tunes the mammalian hypoxic response in vivo. *Molecular and cellular biology* 29, 5729-5741.
- Mocanu, M.M., Varadi, T., Szollosi, J., and Nagy, P. (2011). Comparative analysis of fluorescence resonance energy transfer (FRET) and proximity ligation assay (PLA). *Proteomics* 11, 2063-2070.
- Moniz, S., Bandarra, D., Biddlestone, J., Campbell, K.J., Komander, D., Bremm, A., and Rocha, S. (2015). Cezanne regulates E2F1-dependent HIF2alpha expression. *Journal of cell science* 128, 3082-3093.
- Mosbech, A., Lukas, C., Bekker-Jensen, S., and Mailand, N. (2013). The deubiquitylating enzyme USP44 counteracts the DNA double-strand break response mediated by the RNF8 and RNF168 ubiquitin ligases. *The Journal of biological chemistry* 288, 16579-16587.
- Nakagawa, K., Kohara, T., Uehata, Y., Miyakawa, Y., Sato-Ueshima, M., Okubo, N., Asaka, M., Takeda, H., and Kobayashi, M. (2015). PIAS3 enhances the transcriptional activity of HIF-1alpha by increasing its protein stability. *Biochemical and biophysical research communications*.
- Nakayama, K., Frew, I.J., Hagensen, M., Skals, M., Habelhah, H., Bhoumik, A., Kadoya, T., Erdjument-Bromage, H., Tempst, P., Frappell, P.B., *et al.* (2004). Siah2 regulates stability of prolyl-hydroxylases, controls HIF1alpha abundance, and modulates physiological responses to hypoxia. *Cell* 117, 941-952.

- Nakayama, K., Gazdoui, S., Abraham, R., Pan, Z.Q., and Ronai, Z. (2007). Hypoxia-induced assembly of prolyl hydroxylase PHD3 into complexes: implications for its activity and susceptibility for degradation by the E3 ligase Siah2. *The Biochemical journal* *401*, 217-226.
- Ndubaku, C., and Tsui, V. (2015). Inhibiting the deubiquitinating enzymes (DUBs). *Journal of medicinal chemistry* *58*, 1581-1595.
- Nunez-O'Mara, A., Gerpe-Pita, A., Pozo, S., Carlevaris, O., Urzelai, B., Lopitz-Otsoa, F., Rodriguez, M.S., and Berra, E. (2015). PHD3-SUMO conjugation represses HIF1 transcriptional activity independently of PHD3 catalytic activity. *Journal of cell science* *128*, 40-49.
- Oehme, F., Ellinghaus, P., Kolkhof, P., Smith, T.J., Ramakrishnan, S., Hutter, J., Schramm, M., and Flamme, I. (2002). Overexpression of PH-4, a novel putative proline 4-hydroxylase, modulates activity of hypoxia-inducible transcription factors. *Biochemical and biophysical research communications* *296*, 343-349.
- Ohh, M., Park, C.W., Ivan, M., Hoffman, M.A., Kim, T.Y., Huang, L.E., Pavletich, N., Chau, V., and Kaelin, W.G. (2000). Ubiquitination of hypoxia-inducible factor requires direct binding to the beta-domain of the von Hippel-Lindau protein. *Nature cell biology* *2*, 423-427.
- Paatero, I., Jokilammi, A., Heikkinen, P.T., Iljin, K., Kallioniemi, O.P., Jones, F.E., Jaakkola, P.M., and Elenius, K. (2012). Interaction with ErbB4 promotes hypoxia-inducible factor-1alpha signaling. *The Journal of biological chemistry* *287*, 9659-9671.
- Palczewska, M., Casafont, I., Ghimire, K., Rojas, A.M., Valencia, A., Lafarga, M., Mellstrom, B., and Naranjo, J.R. (2011). Sumoylation regulates nuclear localization of repressor DREAM. *Biochimica et biophysica acta* *1813*, 1050-1058.
- Park, I.S., Han, Y., Chung, H.J., Jung, Y.W., Kim, Y., and Kim, H. (2016). SUMOylation regulates nuclear localization and stability of TRAIIP/RNF206. *Biochemical and biophysical research communications* *470*, 881-887.
- Pawson, T., and Nash, P. (2000). Protein-protein interactions define specificity in signal transduction. *Genes & development* *14*, 1027-1047.
- Pescador, N., Cuevas, Y., Naranjo, S., Alcaide, M., Villar, D., Landázuri, M.O., and Del Peso, L. (2005). Identification of a functional hypoxia-responsive element that regulates the expression of the egl nine homologue 3 (egln3/phd3) gene. *The Biochemical journal* *390*, 189-197.
- Pickart, C.M. (2001). Mechanisms underlying ubiquitination. *Annual review of biochemistry* *70*, 503-533.
- Popov, N., Wanzel, M., Madiredjo, M., Zhang, D., Beijersbergen, R., Bernards, R., Moll, R., Elledge, S.J., and Eilers, M. (2007). The ubiquitin-specific protease USP28 is required for MYC stability. *Nature cell biology* *9*, 765-774.
- Quesada, V., Diaz-Perales, A., Gutierrez-Fernandez, A., Garabaya, C., Cal, S., and Lopez-Otin, C. (2004). Cloning and enzymatic analysis of 22 novel human ubiquitin-specific proteases. *Biochemical and biophysical research communications* *314*, 54-62.
- Rankin, E.B., and Giaccia, A.J. (2008). The role of hypoxia-inducible factors in tumorigenesis. *Cell death and differentiation* *15*, 678-685.

- Rantanen, K., Pursiheimo, J., Hogel, H., Himanen, V., Metzen, E., and Jaakkola, P.M. (2008). Prolyl hydroxylase PHD3 activates oxygen-dependent protein aggregation. *Molecular biology of the cell* *19*, 2231-2240.
- Rantanen, K., Pursiheimo, J.P., Hogel, H., Miikkulainen, P., Sundstrom, J., and Jaakkola, P.M. (2013). p62/SQSTM1 regulates hypoxia response by attenuating PHD3 activity through aggregate sequestration and enhanced degradation. *Journal of cell science*.
- Ravi, R., Mookerjee, B., Bhujwala, Z.M., Sutter, C.H., Artemov, D., Zeng, Q., Dillehay, L.E., Madan, A., Semenza, G.L., and Bedi, A. (2000). Regulation of tumor angiogenesis by p53-induced degradation of hypoxia-inducible factor 1alpha. *Genes & development* *14*, 34-44.
- Redman, K.L., and Rechsteiner, M. (1989). Identification of the long ubiquitin extension as ribosomal protein S27a. *Nature* *338*, 438-440.
- Reincke, M., Sbiera, S., Hayakawa, A., Theodoropoulou, M., Osswald, A., Beuschlein, F., Meitinger, T., Mizuno-Yamasaki, E., Kawaguchi, K., Saeki, Y., *et al.* (2015). Mutations in the deubiquitinase gene USP8 cause Cushing's disease. *Nature genetics* *47*, 31-38.
- Ribet, D., and Cossart, P. (2010). Post-translational modifications in host cells during bacterial infection. *FEBS letters* *584*, 2748-2758.
- Richard, D.E., Berra, E., Gothie, E., Roux, D., and Pouyssegur, J. (1999). p42/p44 mitogen-activated protein kinases phosphorylate hypoxia-inducible factor 1alpha (HIF-1alpha) and enhance the transcriptional activity of HIF-1. *The Journal of biological chemistry* *274*, 32631-32637.
- Roy, A., Zhang, M., Saad, Y., and Kolattukudy, P.E. (2013). Antidicer RNase activity of monocyte chemotactic protein-induced protein-1 is critical for inducing angiogenesis. *American journal of physiology. Cell physiology* *305*, C1021-1032.
- Salceda, S., and Caro, J. (1997). Hypoxia-inducible factor 1alpha (HIF-1alpha) protein is rapidly degraded by the ubiquitin-proteasome system under normoxic conditions. Its stabilization by hypoxia depends on redox-induced changes. *The Journal of biological chemistry* *272*, 22642-22647.
- Sarraf, S.A., Raman, M., Guarani-Pereira, V., Sowa, M.E., Huttlin, E.L., Gygi, S.P., and Harper, J.W. (2013). Landscape of the PARKIN-dependent ubiquitylome in response to mitochondrial depolarization. *Nature* *496*, 372-376.
- Schnell, U., Dijk, F., Sjollem, K.A., and Giepmans, B.N. (2012). Immunolabeling artifacts and the need for live-cell imaging. *Nature methods* *9*, 152-158.
- Scholz, C.C., Rodriguez, J., Pickel, C., Burr, S., Fabrizio, J.A., Nolan, K.A., Spielmann, P., Cavadas, M.A., Crifo, B., Halligan, D.N., *et al.* (2016). FIH Regulates Cellular Metabolism through Hydroxylation of the Deubiquitinase OTUB1. *PLoS biology* *14*, e1002347.
- Scortegagna, M., Subtil, T., Qi, J., Kim, H., Zhao, W., Gu, W., Kluger, H., and Ronai, Z.A. (2011). USP13 enzyme regulates Siah2 ligase stability and activity via noncatalytic ubiquitin-binding domains. *The Journal of biological chemistry* *286*, 27333-27341.

- Seeler, J.S., and Dejean, A. (2003). Nuclear and unclear functions of SUMO. *Nature reviews. Molecular cell biology* 4, 690-699.
- Semenza, G.L. (2012a). Hypoxia-inducible factors in physiology and medicine. *Cell* 148, 399-408.
- Semenza, G.L. (2012b). Hypoxia-inducible factors: mediators of cancer progression and targets for cancer therapy. *Trends in pharmacological sciences* 33, 207-214.
- Semenza, G.L., Neufelt, M.K., Chi, S.M., and Antonarakis, S.E. (1991). Hypoxia-inducible nuclear factors bind to an enhancer element located 3' to the human erythropoietin gene. *Proceedings of the National Academy of Sciences of the United States of America* 88, 5680-5684.
- Semenza, G.L., and Wang, G.L. (1992). A nuclear factor induced by hypoxia via de novo protein synthesis binds to the human erythropoietin gene enhancer at a site required for transcriptional activation. *Molecular and cellular biology* 12, 5447-5454.
- Shimomura, O., Johnson, F.H., and Saiga, Y. (1962). Extraction, purification and properties of aequorin, a bioluminescent protein from the luminous hydromedusan, *Aequorea*. *Journal of cellular and comparative physiology* 59, 223-239.
- Sowa, M.E., Bennett, E.J., Gygi, S.P., and Harper, J.W. (2009). Defining the human deubiquitinating enzyme interaction landscape. *Cell* 138, 389-403.
- Spence, J., Sadis, S., Haas, A.L., and Finley, D. (1995). A ubiquitin mutant with specific defects in DNA repair and multiubiquitination. *Molecular and cellular biology* 15, 1265-1273.
- Sripathy, S.P., Stevens, J., and Schultz, D.C. (2006). The KAP1 corepressor functions to coordinate the assembly of de novo HP1-demarcated microenvironments of heterochromatin required for KRAB zinc finger protein-mediated transcriptional repression. *Molecular and cellular biology* 26, 8623-8638.
- Stokes, G.G. (1852). On the Change of Refrangibility of Light. *Phil. Trans. R. Soc. Lond.* 142, 463-562.
- Sun, H., Li, X.B., Meng, Y., Fan, L., Li, M., and Fang, J. (2013). TRAF6 upregulates expression of HIF-1alpha and promotes tumor angiogenesis. *Cancer research* 73, 4950-4959.
- Szabelski, M., Ilijev, D., Sarkar, P., Luchowski, R., Gryczynski, Z., Kapusta, P., Erdmann, R., and Gryczynski, I. (2009). Collisional quenching of erythrosine B as a potential reference dye for impulse response function evaluation. *Applied spectroscopy* 63, 363-368.
- Takahashi, M., Rapley, E., Biggs, P.J., Lakhani, S.R., Cooke, D., Hansen, J., Blair, E., Hofmann, B., Siebert, R., Turner, G., *et al.* (2000). Linkage and LOH studies in 19 cylindromatosis families show no evidence of genetic heterogeneity and refine the CYLD locus on chromosome 16q12-q13. *Human genetics* 106, 58-65.
- Talks, K.L., Turley, H., Gatter, K.C., Maxwell, P.H., Pugh, C.W., Ratcliffe, P.J., and Harris, A.L. (2000). The expression and distribution of the hypoxia-inducible factors HIF-1alpha and HIF-2alpha in normal human tissues, cancers, and tumor-associated macrophages. *The American journal of pathology* 157, 411-421.
- Tang, T.T.-L., and Lasky, L.A. (2003). The forkhead transcription factor FOXO4 induces the down-regulation of hypoxia-inducible factor 1 alpha by a von Hippel-

Lindau protein-independent mechanism. *The Journal of biological chemistry* 278, 30125-30135.

Taylor, S.E., Bagnall, J., Mason, D., Levy, R., Fernig, D.G., and See, V. (2016). Differential sub-nuclear distribution of hypoxia-inducible factors (HIF)-1 and -2 alpha impacts on their stability and mobility. *Open biology* 6.

Thiaville, M.M., Kim, H., Frey, W.D., and Kim, J. (2013). Identification of an evolutionarily conserved cis-regulatory element controlling the Peg3 imprinted domain. *PloS one* 8, e75417.

Todi, S.V., Winborn, B.J., Scaglione, K.M., Blount, J.R., Travis, S.M., and Paulson, H.L. (2009). Ubiquitination directly enhances activity of the deubiquitinating enzyme ataxin-3. *The EMBO journal* 28, 372-382.

Tojo, M., Matsuzaki, K., Minami, T., Honda, Y., Yasuda, H., Chiba, T., Saya, H., Fujii-Kuriyama, Y., and Nakao, M. (2002). The aryl hydrocarbon receptor nuclear transporter is modulated by the SUMO-1 conjugation system. *The Journal of biological chemistry* 277, 46576-46585.

Trastour, C., Benizri, E., Ettore, F., Ramaioli, A., Chamorey, E., Pouyssegur, J., and Berra, E. (2007). HIF-1alpha and CA IX staining in invasive breast carcinomas: prognosis and treatment outcome. *International journal of cancer. Journal international du cancer* 120, 1451-1458.

Troilo, A., Alexander, I., Muehl, S., Jaramillo, D., Knobloch, K.-P., and Krek, W. (2014). HIF1 α deubiquitination by USP8 is essential for ciliogenesis in normoxia. *EMBO reports* 15, 77-85.

Urbe, S., Liu, H., Hayes, S.D., Heride, C., Rigden, D.J., and Clague, M.J. (2012). Systematic survey of deubiquitinase localization identifies USP21 as a regulator of centrosome- and microtubule-associated functions. *Molecular biology of the cell* 23, 1095-1103.

van Hagen, M., Overmeer, R.M., Abolvardi, S.S., and Vertegaal, A.C. (2010). RNF4 and VHL regulate the proteasomal degradation of SUMO-conjugated Hypoxia-Inducible Factor-2alpha. *Nucleic acids research* 38, 1922-1931.

Vassilev, L.T., Vu, B.T., Graves, B., Carvajal, D., Podlaski, F., Filipovic, Z., Kong, N., Kammlott, U., Lukacs, C., Klein, C., *et al.* (2004). In vivo activation of the p53 pathway by small-molecule antagonists of MDM2. *Science (New York, N.Y)* 303, 844-848.

Velasco, K., Zhao, B., Callegari, S., Altun, M., Liu, H., Hassink, G., Masucci, M.G., and Lindsten, K. (2013). An N-terminal SIAH-interacting motif regulates the stability of the ubiquitin specific protease (USP)-19. *Biochemical and biophysical research communications* 433, 390-395.

Verma, R., Aravind, L., Oania, R., McDonald, W.H., Yates, J.R., 3rd, Koonin, E.V., and Deshaies, R.J. (2002). Role of Rpn11 metalloprotease in deubiquitination and degradation by the 26S proteasome. *Science (New York, N.Y)* 298, 611-615.

Wang, G.L., Jiang, B.H., Rue, E.A., and Semenza, G.L. (1995). Hypoxia-inducible factor 1 is a basic-helix-loop-helix-PAS heterodimer regulated by cellular O₂ tension. *Proceedings of the National Academy of Sciences of the United States of America* 92, 5510-5514.

- Wang, G.L., and Semenza, G.L. (1993). General involvement of hypoxia-inducible factor 1 in transcriptional response to hypoxia. *Proceedings of the National Academy of Sciences of the United States of America* *90*, 4304-4308.
- Wang, G.L., and Semenza, G.L. (1995). Purification and characterization of hypoxia-inducible factor 1. *The Journal of biological chemistry* *270*, 1230-1237.
- Wang, J.H., Wei, W., Guo, Z.X., Shi, M., and Guo, R.P. (2015a). Decreased Cezanne expression is associated with the progression and poor prognosis in hepatocellular carcinoma. *Journal of translational medicine* *13*, 41.
- Wang, Z., Song, Q., Xue, J., Zhao, Y., and Qin, S. (2015b). Ubiquitin-specific protease 28 is overexpressed in human glioblastomas and contributes to glioma tumorigenicity by regulating MYC expression. *Exp Biol Med (Maywood)*.
- Warbrick, E. (1998). PCNA binding through a conserved motif. *BioEssays : news and reviews in molecular, cellular and developmental biology* *20*, 195-199.
- Warburg, O. (1956). On the origin of cancer cells. *Science (New York, N.Y)* *123*, 309-314.
- Warburg, O., Wind, F., and Negelein, E. (1927). The Metabolism of Tumors in the Body. *The Journal of general physiology* *8*, 519-530.
- Warfel, N.A., Dolloff, N.G., Dicker, D.T., Malysz, J., and El-Deiry, W.S. (2013). CDK1 stabilizes HIF-1alpha via direct phosphorylation of Ser668 to promote tumor growth. *Cell Cycle* *12*, 3689-3701.
- Wax, S.D., Rosenfield, C.L., and Taubman, M.B. (1994). Identification of a novel growth factor-responsive gene in vascular smooth muscle cells. *The Journal of biological chemistry* *269*, 13041-13047.
- Wen, Y.A., Stevens, P.D., Gasser, M.L., Andrei, R., and Gao, T. (2013). Downregulation of PHLPP expression contributes to hypoxia-induced resistance to chemotherapy in colon cancer cells. *Molecular and cellular biology* *33*, 4594-4605.
- Wijnhoven, P., Konietzny, R., Blackford, A.N., Travers, J., Kessler, B.M., Nishi, R., and Jackson, S.P. (2015). USP4 Auto-Deubiquitylation Promotes Homologous Recombination. *Molecular cell* *60*, 362-373.
- Wolff, M., Jelkmann, W., Dunst, J., and Depping, R. (2013). The Aryl Hydrocarbon Receptor Nuclear Translocator (ARNT/HIF-1beta) is Influenced by Hypoxia and Hypoxia-Mimetics. *Cellular physiology and biochemistry : international journal of experimental cellular physiology, biochemistry, and pharmacology* *32*, 849-858.
- Wu, A.R., Neff, N.F., Kalisky, T., Dalerba, P., Treutlein, B., Rothenberg, M.E., Mburu, F.M., Mantalas, G.L., Sim, S., Clarke, M.F., *et al.* (2014). Quantitative assessment of single-cell RNA-sequencing methods. *Nature methods* *11*, 41-46.
- Wu, H., and Leng, R.P. (2015). MDM2 mediates p73 ubiquitination: a new molecular mechanism for suppression of p73 function. *Oncotarget* *6*, 21479-21492.
- Yau, R., and Rape, M. (2016). The increasing complexity of the ubiquitin code. *Nature cell biology* *18*, 579-586.
- Ye, Y., Scheel, H., Hofmann, K., and Komander, D. (2009). Dissection of USP catalytic domains reveals five common insertion points. *Molecular bioSystems* *5*, 1797-1808.

- Zatloukal, B., Kufferath, I., Thueringer, A., Landegren, U., Zatloukal, K., and Haybaeck, J. (2014). Sensitivity and specificity of in situ proximity ligation for protein interaction analysis in a model of steatohepatitis with Mallory-Denk bodies. *PloS one* 9, e96690.
- Zhao, D., Zheng, H.Q., Zhou, Z., and Chen, C. (2010). The Fbw7 tumor suppressor targets KLF5 for ubiquitin-mediated degradation and suppresses breast cell proliferation. *Cancer research* 70, 4728-4738.
- Zheng, X., Zhai, B., Koivunen, P., Shin, S.J., Lu, G., Liu, J., Geisen, C., Chakraborty, A.A., Moslehi, J.J., Smalley, D.M., *et al.* (2014). Prolyl hydroxylation by EglN2 destabilizes FOXO3a by blocking its interaction with the USP9x deubiquitinase. *Genes & development* 28, 1429-1444.
- Zhong, H., De Marzo, A.M., Laughner, E., Lim, M., Hilton, D.A., Zagzag, D., Buechler, P., Isaacs, W.B., Semenza, G.L., and Simons, J.W. (1999). Overexpression of hypoxia-inducible factor 1alpha in common human cancers and their metastases. *Cancer research* 59, 5830-5835.
- Zhong, J., and Kyriakis, J.M. (2004). Germinal center kinase is required for optimal Jun N-terminal kinase activation by Toll-like receptor agonists and is regulated by the ubiquitin proteasome system and agonist-induced, TRAF6-dependent stabilization. *Molecular and cellular biology* 24, 9165-9175.
- Zhou, J., Kohl, R., Herr, B., Frank, R., and Brune, B. (2006). Calpain mediates a von Hippel-Lindau protein-independent destruction of hypoxia-inducible factor-1alpha. *Molecular biology of the cell* 17, 1549-1558.

Appendix 1: REVIEW ARTICLE



DUBs, New Members in the Hypoxia Signaling cUb

Amelie S. Schober^{1,2} and Edurne Berra^{1*}

¹Centro de Investigación Cooperativa en Biociencias, CIC bioGUNE, Derio, Spain, ²Faculty of Health and Life Sciences, Center for Cell Imaging, Institute of Integrative Biology, University of Liverpool, Liverpool, UK

Cellular protein homeostasis is tightly regulated by ubiquitination. Responsible for target protein ubiquitination is a class of enzymes, the so-called ubiquitin E3 ligases. They are opposed to a second class of enzymes, called deubiquitinating enzymes (DUBs), which can remove polyubiquitin chains from their specific target proteins. The coaction of the two sets of enzymes allows the cell to adapt its overall protein content and the abundance of particular proteins to a variety of cellular and environmental stresses, including hypoxia. In recent years, DUBs have been highlighted to play major roles in many diseases, including cancer, both as tumor suppressors and oncogenes. Therefore, DUBs are emerging as promising targets for cancer-cell specific treatment. Here, we will review the current understanding of DUBs implicated in the control of hypoxia-inducible factor, the regulation of DUBs by hypoxia, and the use of DUB-specific drugs to target tumor hypoxia-signaling.

Keywords: DUBs, ubiquitination, HIF, protein homeostasis, cancer

OPEN ACCESS

Edited by:

Christian Gomez,
University of Mississippi Medical
Center, USA

Reviewed by:

Valerio Donato,
New York University Medical
Center, USA

Keith R. Laderoute,
SRI International, USA

***Correspondence:**

Edurne Berra
eberra@cicbiogune.es

Specialty section:

This article was submitted to
Molecular and Cellular Oncology,
a section of the journal
Frontiers in Oncology

Received: 04 December 2015

Accepted: 22 February 2016

Published: 09 March 2016

Citation:

Schober AS and Berra E (2016)
DUBs, New Members in the Hypoxia
Signaling cUb.
Front. Oncol. 6:53.
doi: 10.3389/fonc.2016.00053

INTRODUCTION

Like most other posttranslational modifications (PTMs), ubiquitin (Ub) conjugation is a reversible modification (1). Ub E3 ligases covalently attach monomers of Ub to lysine (and also cysteine) residues of their target proteins. Furthermore, ligases also convert monoubiquitination into polyubiquitin chains by attaching one by one further Ub monomers to one of the seven internal lysine residues (K6/K11/K27/K29/K33/K48/K63) of the preceding Ub molecule. In contrast, the family of DeUbiquitinating enzymes (DUBs) breaks down those mono- and polyubiquitin chains from the target protein. Besides counteracting the action of the Ub E3 ligases, DUBs are proteases that process Ub precursors.

Of the nearly 100 DUBs encoded by the human genome, 79 are predicted to be active and mostly cleave particular types of Ub chain linkages from their respective target proteins. DUBs can be grouped into six families based on sequence and structure similarity: ubiquitin-specific proteases (USPs) that comprise the largest and most diverse subfamily, ubiquitin carboxyl-terminal hydrolases (UCHs), ovarian tumor proteases (OTUs), Josephins, JAB1/MPN/MOV34 (JAMMs), and the more recently discovered monocyte chemotactic protein-induced proteins (MCPIP). With the exception of JAMMs, which belong to the Zn²⁺-dependent metalloproteases, all the rest use the classical cysteine protease triad in the catalytic side (2).

Classically, the reversal of the polyubiquitination protects the target protein from being degraded by the proteasome, but ubiquitination has also been shown to have a broad range of non-catabolic functions (3). Thus, it is not surprising that DUB activity or inappropriate expression impacts on the regulation of multiple biological processes and several signaling pathways that are frequently altered

in many disorders from cancer over neurodegenerative pathologies to inflammatory diseases [for more details, please refer to Ref. (4)]. Because of their direct or indirect implications in those diseases and because of their potential druggability, DUBs have become of increasing interest in recent years.

Hypoxia is a feature of most human cancers (5). The cancer cells and their environment adapt to and survive under low oxygen availability. The activation of the hypoxia-inducible factor (HIF) that orchestrates the hypoxia-signaling pathway is instrumental to this adaptation. HIF is a heterodimeric transcription factor that consists of a constitutively expressed β -subunit (HIF- β) and HIF- α , whose expression is tightly regulated through the ubiquitin-proteasome system (UPS) (6–8). HIF triggers the expression of hundreds of direct target genes, indirect transcription factors, and non-coding RNAs that enable cancer cell survival and tumor progression by promoting, among others, angiogenesis, metabolic rewiring, genomic instability, drug resistance, and the self-renewal capacity of cancer stem cells. HIFs are also activated by genetic alterations in human cancers, such as the von Hippel-Lindau protein (pVHL) loss of function in clear-cell renal carcinoma (9). Accordingly, sustained expression of HIF- α in tumors has been associated with higher aggressiveness, migratory, and metastasis-initiating potential and therefore worse prognosis (10, 11).

In this review, we will summarize the current knowledge about the action of DUBs on HIF- α and the regulation of those enzymes by hypoxia. We will also discuss the potential of exploiting DUBs to target tumor hypoxia signaling.

THE CANONICAL HIF SIGNALING PATHWAY

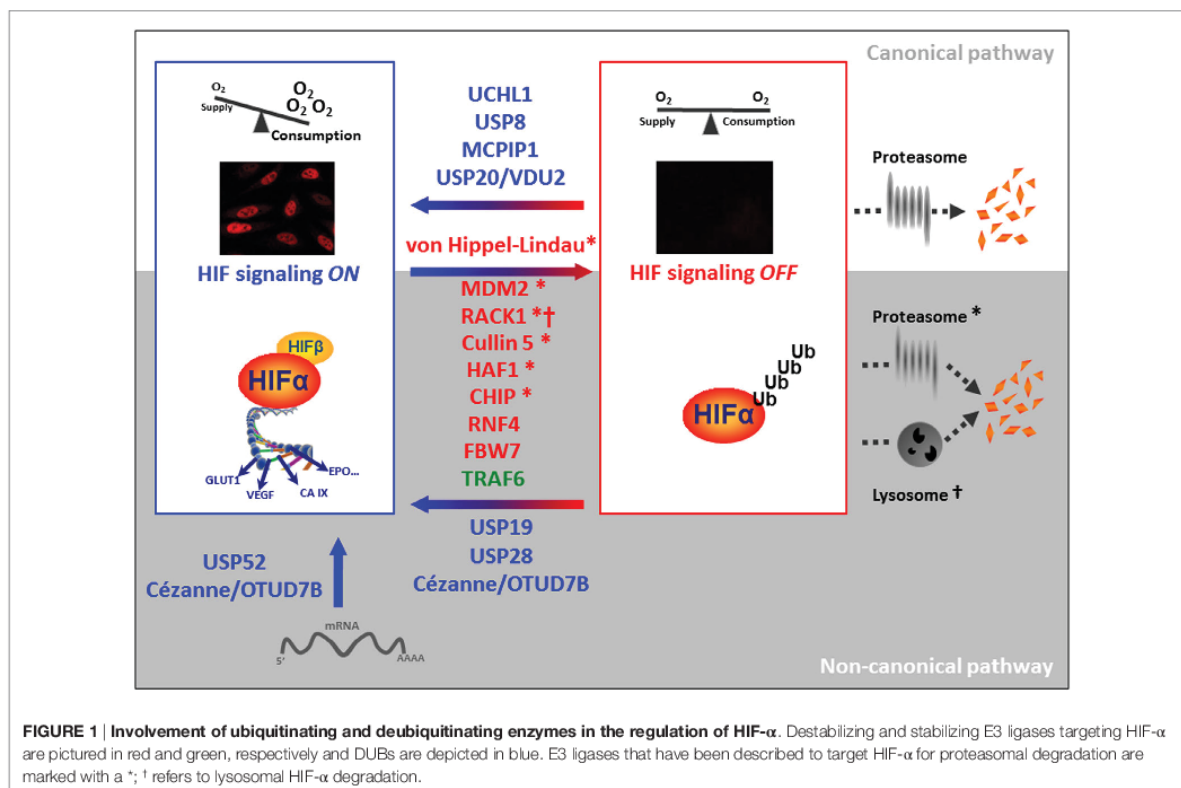
The adaptive cellular program in response to low oxygen availability is mainly triggered by two HIF- α subunits (HIF-1 α and HIF-2 α), which share several common targets but also exhibit non-redundant functions (12). Anyhow, the levels of both HIF- α subunits result from the dynamic interplay between their ubiquitination and deubiquitination. In well-oxygenated cells, HIF- α is very unstable, as it is degraded by the proteasome within approximately <5 min after translation, whereas HIF- α 's half-life is greatly increased in hypoxia (7, 8, 13). Proteasomal degradation is triggered by the continuous polyubiquitination of HIF- α by pVHL (9). pVHL is part of an E3 ligase complex and binds to HIF- α after the hydroxylation of two designated proline residues in HIF- α 's oxygen-dependent degradation domain (ODDD), the central regulatory domain that confers its oxygen sensibility (8). This binding can be stabilized by SSAT2, therefore enhancing HIF- α ubiquitination (14). The family of prolyl hydroxylase domain-containing proteins (PHDs), the oxygen sensors also referred to as EGLNs or HPHs, catalyze the hydroxylation of HIF- α (Pro⁴⁰² and Pro⁵⁶⁴, in the case of HIF-1 α) (15–19). HIF- α also harbors an N-terminal basic helix-loop-helix (bHLH) domain that mediates HIF-binding to the target DNA after heterodimerization with HIF- β /ARNT via the adjacent PAS domain. Of the two transactivation domains (TAD), the N-terminal TAD (N-TAD) lies within the ODDD, while the C-terminal TAD (C-TAD) is responsible for the recruitment of CBP/p300 needed to successfully induce

the transcription of the HIF target genes that are characterized by having one or more HREs (hypoxia response elements) (20, 21). This C-TAD contains an asparagine residue (Asn⁸⁰³, in the case of HIF-1 α) that upon oxygen-dependent hydroxylation by FIH (factor inhibiting HIF) hinders the successful interaction of HIF with CBP/p300 and therefore, HIF's transactivation activity is reduced (22). Interestingly, HIF induces the expression of two of its negative regulators, PHD2 and PHD3, in order to ensure its own rapid degradation upon reoxygenation (19, 23). However, in conditions of chronic hypoxia, once the transcriptional adaptive program has been triggered, HIF- α levels drop again to avoid sustained HIF signaling and assure cell survival (24).

In the context of the canonical HIF signaling pathway, so far there are relatively few DUBs reported in the literature, and reports are mostly focused on the impact on HIF-1 α (Figure 1 upper part). *USP20* (also called pVHL interacting DUB2, VDU2) was the first DUB to be described to reverse pVHL-mediated HIF-1 α ubiquitination (25). In turn, *USP20* is a pVHL target (26). *MCPIP1* also deubiquitinates HIF-1 α to promote angiogenesis (27). In the context of ciliogenesis, *USP8* has been found to bind to HIF-1 α 's PAS domain and to partially protect HIF-1 α from degradation (28). More recently, *UCHL1* has been shown to be a positive regulator of HIF-1 α protein stability acting on HIF-1 α 's ODDD (29).

THE NON-CANONICAL HIF SIGNALING

Not surprisingly because of HIF's crucial role in cell fate, many more proteins have been described to be involved in the control of its stability (Figure 1 lower part). The heat-shock protein 90 (HSP90) that interacts with the PAS domain of HIF- α regulates its degradation in an O₂/PHD/pVHL-independent manner (30). HSP90 competes with RACK1 for binding to HIF- α and prevents the recruitment of the elongin C/B Ub E3 ligase complex (31). A similar mechanism has been proposed for HIF- α activation by ErbB4 (32). As for other HSP90 client proteins, Cullin5 also regulates HIF- α degradation independently of elongin C/B function (33). The tumor suppressors p53, Tap73, and pTEN promote the Ub-mediated degradation of HIF-1 α via recruitment of the Ub E3 ligase Mdm2 (34–36). Furthermore, Fbw7 ubiquitinates and induces HIF-1 α degradation following phosphorylation by GSK3 β (37, 38). Interestingly, this degradation can be antagonized by the Ub-specific protease (*USP28*) (38). Until now, this is the only non-canonical Ub E3 ligase–DUB pair identified for proteasomal degradation of HIF- α . HAF, the hypoxia-associated factor, seems to play a dual role in the control of HIF- α stability and/or activity. While HAF acts as an Ub E3 ligase targeting HIF-1 α for degradation independently of oxygen availability, hypoxia-induced SUMOylated HAF promotes HIF-2 α transactivation without affecting its stability (39, 40). Furthermore, RNF4 controls the levels of SUMOylated HIF-2 α (41). *USP19* seems to be required for the hypoxic accumulation of HIF-1 α , though the effect is not dependent on its deubiquitinase activity (42). *USP19* is further substrate of Siah-1 and Siah-2 Ub E3 ligases, which also control the stability of PHD1, PHD3, and FIH (43–45). Thus, further studies are necessary to clarify the direct impact of *USP19* in HIF-1 α ubiquitination.



The chaperone-dependent Ub ligase CHIP targets HIF-1 α but not HIF-2 α for degradation either by the proteasome or by the autophagic machinery, the second big protein degradation and recycling pathway that has been implicated in the elimination of ubiquitinated HIF- α (46–49). In this regard, *Cezanne* (OTUD7B), a deubiquitinase targeting K11 Ub chains (50), has been reported to protect HIF-1 α from lysosomal degradation. While this process is independent of HIF-1 α prolyl hydroxylation, it depends on the presence of pVHL (51).

Calpain and the activation of the forkhead transcription factor FOXO4 destabilize HIF- α , although the underlying molecular mechanisms are unknown (52, 53). Further studies are also needed to characterize the role of Parkin in the regulation of HIF- α , based on its identification within the Parkin-dependent ubiquitinome by a proteomic approach (54). In contrast with all the previous reports, it is worth mentioning the role played by the Ub E3 ligase TRAF6. TRAF6 increases HIF-1 α but not HIF-2 α polyK-63 ubiquitination and protects the protein from proteasomal degradation (55).

In addition to HIF- α stability, mRNA expression and activity of the transcriptional complex fine-tune HIF regulation. In this regard, USP52 is required for the protection of HIF-1 α (but not HIF-2 α) mRNA from premature degradation and therefore, allows the normal hypoxic induction of HIF-1 α (56). The case of USP52 is somewhat special as this protein, although structurally related to the family of USPs, lacks the catalytic cysteine (57).

Besides protecting HIF-1 α protein from its degradation, *Cezanne*'s catalytic activity is also required for maintaining basal levels of the E2F1 transcription factor. Moniz et al. demonstrated that E2F1 controls the expression of HIF-2 α mRNA and therefore, established an indirect role of the DUB *Cezanne* in HIF-2 α expression (58).

Finally, a number of DUBs have been shown to regulate transcription factors and signaling pathways that cross talk with HIFs, likely contributing to the complexity and specificity of the cellular hypoxic response, even though they go beyond the scope of this review (59–61).

REGULATION OF DUBs BY HYPOXIA

As for other enzymes, there are several possible layers of regulation of DUB activity. Next to the transcriptional regulation, the stability and translation of the mRNA can be regulated by mRNA-processing enzymes. The turnover and therefore, the availability of the mature protein can be set by a variety of PTMs. PTMs can also interfere with the binding of the DUBs to their target proteins or other interactors, as well as modulate reversibly and irreversibly the (auto) catalytic activity of the DUB. Hypoxia, being an extreme cellular stress condition, should be able to regulate deubiquitinating activity on all the possible different layers in order to adapt DUB functions to the cell's needs. However, the literature about the regulation of specific DUBs by hypoxia (1% O₂, if not specified differently) is still scarce and

almost exclusively restricted to transcriptional regulation. For instance, the expression of *USP13* is reduced upon treatment with as little as 6 h of 2% O₂ in melanoma cell lines (59). The reduction of the mRNA also translates to the protein level and causes the loss of Siah-2 stabilization. Similarly, in colon cancer cells hypoxia reduces *USP46* mRNA and protein levels and, therefore, diminishes *USP46*'s stabilizing effect on the tumor suppressors *PHLPP1* and *PHLPP2*, conferring to the colon cancer cells an increased paclitaxel resistance (62, 63). Guo et al. provide more detailed information about the hypoxia-mediated transcriptional regulation of the UCH *CYLD*. They suggest that the decrease of *CYLD* mRNA and protein seen in glioblastoma cells is due to the hypoxia-induced increase of the transcriptional repressors Snail and Hes1 (64). In contrast, hypoxia has been shown to increase *Cezanne* via p38 MAPK (65).

An et al. claimed that *CYLD* is targeted for proteasomal degradation after interaction with the HPV E6 protein in hypoxia (66). This is to date the only report of a posttranslational regulation of DUB activity by hypoxia. However, Lee et al. present evidence that the activity of many, if not most, DUBs depends on the redox state of the cell. They show that the catalytically active cysteine residue can be oxidized, for instance, by intracellular hydrogen peroxide, leading to the abolishment of the deubiquitinating activity. The inactivating oxidation can be reversed in the presence of reducing agents, such as DTT, or prevented by antioxidants (67). As hypoxia and mitochondrial ROS production are intrinsically linked it might not be too far-fetched to propose that hypoxia directly modulates DUB activity via ROS.

DYSREGULATION OF HYPOXIA-RELATED DUBs IN CANCER

Given the importance of Ub-mediated changes in protein function and homeostasis, it is not by chance that the entire process is highly regulated. Disruption of the ubiquitination cycle by mutations or altered expression of specific components within the cascade has been associated with several disorders. In particular, more than 30 DUBs have been associated with cancer directly or indirectly. Both, the loss of a specific DUB activity or its hyperactivity are non-desired events if the targets are tumor suppressors or oncogenes, respectively. Recurrent mutations of DUBs are rare in cancer with only few exceptions. Gene fusions with *RUNX* are reported for *USP42* and *USP16* in hematologic diseases, such as chronic myelomonocytic leukemia and acute myeloid leukemia. However, dysregulated mRNA levels of DUBs are implicated in many malignancies. Here, we will focus only on a few examples of hypoxia-related DUBs, for a more extensive overview please refer to the very comprehensive review by D'Arcy et al. (68).

Germline mutations of the tumor-suppressor gene *CYLD* are prevalent in familial cylindromatosis, a genetic condition that leads to predisposition for developing multiple skin tumors (69, 70). In addition, *CYLD* deubiquitinating activity has been seen to be abolished in different cancers on the protein level by inactivating phosphorylations or destabilizing polyubiquitination

(71). More recently, it has been reported that *USP8* is frequently mutated in adenomas causing Cushing's disease (72).

USP28 is a DUB whose overexpression has been reported in breast and colon cancer and glioblastoma (73, 74). A recent publication has proposed *USP28* to be a potential predictive marker in bladder cancer, as they found correlation of *USP28* with tumor histological grade, clinical stage, recurrence, and survival (75). Similar to *USP28*, *UCHL1* has also been proposed to be a useful biomarker, being overexpressed in gastric cancer (76) and in myeloma (77), and epigenetically down-regulated in colorectal cancer (78). As mentioned above, downregulation of *USP46* may serve as a biomarker of resistance to chemotherapy in colon cancer (63). Finally, despite being inconsistent to its role in the regulation of HIF-1 α and HIF-2 α , decreased *Cezanne* expression is associated with the progression and poor prognosis in hepatocellular carcinoma (79).

DUBs AS DRUGGABLE TARGETS FOR THERAPY

Modulators of individual UPS components are emerging as a novel class of anticancer drugs. The initial research focus had been directed toward targeting the proteasome, with activity described for many compounds with proteasome inhibitory activity, including bortezomib. Because Ub E3 ligases provide substrate specificity, their direct targeting may avoid the deleterious side effects associated with the global inhibition of the proteasome, making them interesting candidates as drug targets. Nutlin-3 and JNJ-26854165 are classic examples directed against the Ub E3 ligase MDM2 and are currently undergoing clinical evaluation as anticancer therapy.

Newly arising, DUBs may serve as equally or more useful targets. Indeed, DUBs are highly specialized and evolutionary linked to proteases, a typified pharmaceutical target class for drug discovery, thanks to their well-characterized catalytic domain. Several partial and specific inhibitors against a small number of DUBs have been developed, have proved active in preclinical studies as reviewed recently by D'Arcy and Linder (80), and have provided feasibility for targeting these enzymes for anticancer purposes. Among them, HBX 41,108 is a partially selective USP inhibitor because it inhibits *USP5*, *USP7*, *USP8*, and *UCHL3* in addition to caspase 3 (81). This is to our knowledge the only DUB inhibitor so far described as targeting one of the DUBs linked to the HIF signaling pathway. Interestingly, the inhibition of *USP8* suppresses growth of gefitinib-resistant non-small cell lung cancer cells, though no link to the potential impact on HIF-1 α is reported (82). It is tempting to speculate about new drugs directed against hypoxia-related DUBs that succeed to fight intratumoral hypoxia-signaling in the coming years.

CONCLUSION

HIF- α protein homeostasis is tightly controlled in healthy cells in order to avoid inappropriate activation of HIF signaling. A variety of E3 ligases and DUBs are involved in this task by triggering and protecting HIF- α from its degradation, respectively. Permanent

activation of the HIF signaling pathway has been found in many tumors and seems to be beneficial for tumor growth and cancer progression. In most cases, the reason for sustained HIF- α protein levels in the tumor cells are still not revealed, but a possible mechanism is the pathological increase of HIF- α specific DUB activity. In recent years, the dysregulation of deubiquinating enzymes in cancer (and other diseases) has become of increasing interest, and alterations of their expression and activities have been shown to have diagnostic value. Whether cancer-related events that lead to the upregulation of DUB activity are the primary cause of uncontrolled HIF signaling, or whether initial hypoxia upregulates DUB expression as a positive feed-back-loop is not determined. But in the light of DUBs being druggable enzymes, it is important to understand their implications in HIF and tumor hypoxia-signaling.

REFERENCES

- Clague MJ, Heride C, Urbe S. The demographics of the ubiquitin system. *Trends Cell Biol* (2015) 25:417–26. doi:10.1016/j.tcb.2015.03.002
- Fraile JM, Quesada V, Rodriguez D, Freije JM, Lopez-Otin C. Deubiquitinases in cancer: new functions and therapeutic options. *Oncogene* (2012) 31:2373–88. doi:10.1038/onc.2011.443
- Komander D, Rape M. The ubiquitin code. *Annu Rev Biochem* (2012) 81:203–29. doi:10.1146/annurev-biochem-060310-170328
- Heideker J, Wertz IE. DUBs, the regulation of cell identity and disease. *Biochem J* (2015) 467:191. doi:10.1042/bj4670191
- Semenza GL. Hypoxia-inducible factors: mediators of cancer progression and targets for cancer therapy. *Trends Pharmacol Sci* (2012) 33:207–14. doi:10.1016/j.tips.2012.01.005
- Wang GL, Semenza GL. Purification and characterization of hypoxia-inducible factor 1. *J Biol Chem* (1995) 270:1230–7. doi:10.1074/jbc.270.3.1230
- Salceda S, Caro J. Hypoxia-inducible factor 1 α (HIF-1 α) protein is rapidly degraded by the ubiquitin-proteasome system under normoxic conditions. Its stabilization by hypoxia depends on redox-induced changes. *J Biol Chem* (1997) 272:22642–7. doi:10.1074/jbc.272.36.22642
- Huang LE, Gu J, Schau M, Bunn HF. Regulation of hypoxia-inducible factor 1 α is mediated by an O₂-dependent degradation domain via the ubiquitin-proteasome pathway. *Proc Natl Acad Sci U S A* (1998) 95:7987–92. doi:10.1073/pnas.95.14.7987
- Maxwell PH, Wiesener MS, Chang GW, Clifford SC, Vaux EC, Cockman ME, et al. The tumour suppressor protein VHL targets hypoxia-inducible factors for oxygen-dependent proteolysis. *Nature* (1999) 399:271–5. doi:10.1038/20459
- Zhong H, De Marzo AM, Laughner E, Lim M, Hilton DA, Zagzag D, et al. Overexpression of hypoxia-inducible factor 1 α in common human cancers and their metastases. *Cancer Res* (1999) 59:5830–5.
- Trastour C, Benizri E, Ettore F, Ramaoli A, Chamorey E, Pouyssegur J, et al. HIF-1 α and CA IX staining in invasive breast carcinomas: prognosis and treatment outcome. *Int J Cancer* (2007) 120:1451–8. doi:10.1002/ijc.22436
- Keith B, Johnson RS, Simon MC. HIF1 α and HIF2 α : sibling rivalry in hypoxic tumour growth and progression. *Nat Rev Cancer* (2012) 12:9–22. doi:10.1038/nrc3183
- Berra E, Roux D, Richard DE, Pouyssegur J. Hypoxia-inducible factor-1 α (HIF-1 α) escapes O₂-driven proteasomal degradation irrespective of its subcellular localization: nucleus or cytoplasm. *EMBO Rep* (2001) 2:615–20. doi:10.1093/embo-reports/kve130
- Baek JH, Liu YV, McDonald KR, Wesley JB, Hubbi ME, Byun H, et al. Spermidine/spermine-N1-acetyltransferase 2 is an essential component of the ubiquitin ligase complex that regulates hypoxia-inducible factor 1 α . *J Biol Chem* (2007) 282:23572–80. doi:10.1074/jbc.M703504200
- Bruick RK, McKnight SL. A conserved family of prolyl-4-hydroxylases that modify HIF. *Science* (2001) 294:1337–40. doi:10.1126/science.1066373
- Epstein AC, Gleadow JM, McNeill LA, Hewitson KS, O'Rourke J, Mole DR, et al. *C. elegans* EGL-9 and mammalian homologs define a family of dioxygenases

AUTHOR CONTRIBUTIONS

ASS and EB contributed with review writing, editing, and final approval of the manuscript.

ACKNOWLEDGMENTS

The authors would like to thank all the laboratory members for discussions and comments. We apologize to the many research groups whose work was not cited due to space constraints.

FUNDING

Our research is supported by the Plan Nacional of I+D BFU-2013-46647. ASS is a Liverpool-bioGUNE partnership fellow.

- that regulate HIF by prolyl hydroxylation. *Cell* (2001) 107:43–54. doi:10.1016/S0092-8674(01)00507-4
- Ivan M, Kondo K, Yang H, Kim W, Valiando J, Ohh M, et al. HIF1 α targeted for VHL-mediated destruction by proline hydroxylation: implications for O₂ sensing. *Science* (2001) 292:464–8. doi:10.1126/science.1059817
- Jaakkola P, Mole DR, Tian YM, Wilson MI, Gielbert J, Gaskell SJ, et al. Targeting of HIF-1 α to the von Hippel-Lindau ubiquitylation complex by O₂-regulated prolyl hydroxylation. *Science* (2001) 292:468–72. doi:10.1126/science.1059796
- Berra E, Benizri E, Ginouves A, Volmat V, Roux D, Pouyssegur J. HIF prolyl-hydroxylase 2 is the key oxygen sensor setting low steady-state levels of HIF-1 α in normoxia. *EMBO J* (2003) 22:4082–90. doi:10.1093/emboj/cdg392
- Wang GL, Semenza GL. General involvement of hypoxia-inducible factor 1 in transcriptional response to hypoxia. *Proc Natl Acad Sci U S A* (1993) 90:4304–8. doi:10.1073/pnas.90.9.4304
- Arany Z, Huang LE, Eckner R, Bhattacharya S, Jiang C, Goldberg MA, et al. An essential role for p300/CBP in the cellular response to hypoxia. *Proc Natl Acad Sci U S A* (1996) 93:12969–73. doi:10.1073/pnas.93.23.12969
- Lando D, Peet DJ, Whelan DA, Gorman JJ, Whitelaw ML. Asparagine hydroxylation of the HIF transactivation domain a hypoxic switch. *Science* (2002) 295:858–61. doi:10.1126/science.1068592
- Pescador N, Cuevas Y, Naranjo S, Alcaide M, Villar D, Landázuri MO, et al. Identification of a functional hypoxia-responsive element that regulates the expression of the egl nine homologue 3 (egln3/phd3) gene. *Biochem J* (2005) 390:189–97. doi:10.1042/bj20042121
- Ginouves A, Ilc K, Macias N, Pouyssegur J, Berra E. PHDs overactivation during chronic hypoxia "desensitizes" HIF1 α and protects cells from necrosis. *Proc Natl Acad Sci U S A* (2008) 105:4745–50. doi:10.1073/pnas.0705680105
- Li Z, Wang D, Messing EM, Wu G. VHL protein-interacting deubiquitinating enzyme 2 deubiquitinates and stabilizes HIF-1 α . *EMBO Rep* (2005) 6:373–8. doi:10.1038/sj.embo.7400377
- Li Z, Wang D, Na X, Schoen SR, Messing EM, Wu G. Identification of a deubiquitinating enzyme subfamily as substrates of the von Hippel-Lindau tumor suppressor. *Biochem Biophys Res Commun* (2002) 294:700–9. doi:10.1016/S0006-291X(02)00534-X
- Roy A, Zhang M, Saad Y, Kolattukudy PE. Antidicer RNase activity of monocyte chemotactic protein-induced protein-1 is critical for inducing angiogenesis. *Am J Physiol Cell Physiol* (2013) 305:C1021–32. doi:10.1152/ajpcell.00203.2013
- Troilo A, Alexander I, Muehl S, Jaramillo D, Knobloch K-P, Krek W. HIF1 α deubiquitination by USP8 is essential for ciliogenesis in normoxia. *EMBO Rep* (2014) 15:77–85. doi:10.1002/embr.201337688
- Goto Y, Zeng L, Yeom CJ, Zhu Y, Morinibu A, Shinomiya K, et al. UCHL1 provides diagnostic and antimetastatic strategies due to its deubiquitinating effect on HIF-1 α . *Nat Commun* (2015) 6:6153. doi:10.1038/ncomms7153
- Isaacs JS, Jung YJ, Mimnaugh EG, Martinez A, Cuttitta F, Neckers LM. Hsp90 regulates a von Hippel Lindau-independent hypoxia-inducible factor-1

- alpha-degradative pathway. *J Biol Chem* (2002) **277**:29936–44. doi:10.1074/jbc.M204733200
31. Liu YV, Baek JH, Zhang H, Diez R, Cole RN, Semenza GL. RACK1 competes with HSP90 for binding to HIF-1alpha and is required for O(2)-independent and HSP90 inhibitor-induced degradation of HIF-1alpha. *Mol Cell* (2007) **25**:207–17. doi:10.1016/j.molcel.2007.01.001
 32. Paatero I, Jokilampi A, Heikkinen PT, Iljin K, Kallioniemi OP, Jones FE, et al. Interaction with ErbB4 promotes hypoxia-inducible factor-1alpha signaling. *J Biol Chem* (2012) **287**:9659–71. doi:10.1074/jbc.M111.299537
 33. Ehrlich ES, Wang T, Luo K, Xiao Z, Niewiadomska AM, Martinez T, et al. Regulation of Hsp90 client proteins by a Cullin5-RING E3 ubiquitin ligase. *Proc Natl Acad Sci U S A* (2009) **106**:20330–5. doi:10.1073/pnas.0810571106
 34. Ravi R, Mookerjee B, Bhujwala ZM, Sutter CH, Artemov D, Zeng Q, et al. Regulation of tumor angiogenesis by p53-induced degradation of hypoxia-inducible factor 1alpha. *Genes Dev* (2000) **14**:34–44. doi:10.1101/gad.14.1.34
 35. Joshi S, Singh AR, Durden DL. MDM2 regulates hypoxic hypoxia-inducible factor 1alpha stability in an E3 ligase, proteasome, and PTEN-phosphatidylinositol 3-kinase-AKT-dependent manner. *J Biol Chem* (2014) **289**:22785–97. doi:10.1074/jbc.M114.587493
 36. Amelio I, Inoue S, Markert EK, Levine AJ, Knight RA, Mak TW, et al. TAp73 opposes tumor angiogenesis by promoting hypoxia-inducible factor 1alpha degradation. *Proc Natl Acad Sci U S A* (2015) **112**:226–31. doi:10.1073/pnas.1410609111
 37. Cassavaugh JM, Hale SA, Wellman TL, Howe AK, Wong C, Lounsbury KM. Negative regulation of HIF-1alpha by an FBW7-mediated degradation pathway during hypoxia. *J Cell Biochem* (2011) **112**:3882–90. doi:10.1002/jcb.23321
 38. Flugel D, Goralch A, Kietzmann T. GSK-3beta regulates cell growth, migration, and angiogenesis via Fbw7 and USP28-dependent degradation of HIF-1alpha. *Blood* (2012) **119**:1292–301. doi:10.1182/blood-2011-08-375014
 39. Koh MY, Darnay BG, Powis G. Hypoxia-associated factor, a novel E3-ubiquitin ligase, binds and ubiquitinates hypoxia-inducible factor 1alpha, leading to its oxygen-independent degradation. *Mol Cell Biol* (2008) **28**:7081–95. doi:10.1128/MCB.00773-08
 40. Koh MY, Nguyen V, Lemos R Jr, Damay BG, Kiriakova G, Abdelmelek M, et al. Hypoxia-induced SUMOylation of E3 ligase HAF determines specific activation of HIF2 in clear-cell renal cell carcinoma. *Cancer Res* (2015) **75**:316–29. doi:10.1158/0008-5472.CAN-13-2190
 41. van Hagen M, Overmeer RM, Abolvardi SS, Vertegaal AC. RNF4 and VHL regulate the proteasomal degradation of SUMO-conjugated hypoxia-inducible factor-2alpha. *Nucleic Acids Res* (2010) **38**:1922–31. doi:10.1093/nar/gkp1157
 42. Altun M, Zhao B, Velasco K, Liu H, Hassink G, Paschke J, et al. Ubiquitin-specific protease 19 (USP19) regulates hypoxia-inducible factor 1alpha (HIF-1alpha) during hypoxia. *J Biol Chem* (2012) **287**:1962–9. doi:10.1074/jbc.M111.305615
 43. Nakayama K, Frew IJ, Hagensen M, Skals M, Habelhah H, Bhoumik A, et al. Siah2 regulates stability of prolyl-hydroxylases, controls HIF1alpha abundance, and modulates physiological responses to hypoxia. *Cell* (2004) **117**:941–52. doi:10.1016/j.cell.2004.06.001
 44. Fukuba H, Yamashita H, Nagano Y, Jin HG, Hiji M, Ohtsuki T, et al. Siah-1 facilitates ubiquitination and degradation of factor inhibiting HIF-1alpha (FIH). *Biochem Biophys Res Commun* (2007) **353**:324–9. doi:10.1016/j.bbrc.2006.12.051
 45. Velasco K, Zhao B, Callegari S, Altun M, Liu H, Hassink G, et al. An N-terminal SIAH-interacting motif regulates the stability of the ubiquitin specific protease (USP)-19. *Biochem Biophys Res Commun* (2013) **433**:390–5. doi:10.1016/j.bbrc.2013.02.094
 46. Bento CF, Fernandes R, Ramalho J, Marques C, Shang F, Taylor A, et al. The chaperone-dependent ubiquitin ligase CHIP targets HIF-1alpha for degradation in the presence of methylglyoxal. *PLoS One* (2010) **5**:e15062. doi:10.1371/journal.pone.0015062
 47. Luo W, Zhong J, Chang R, Hu H, Pandey A, Semenza GL. Hsp70 and CHIP selectively mediate ubiquitination and degradation of hypoxia-inducible factor (HIF)-1alpha but not HIF-2alpha. *J Biol Chem* (2010) **285**:3651–63. doi:10.1074/jbc.M109.068577
 48. Ferreira JV, Fofu H, Bejarano E, Bento CF, Ramalho JS, Girao H, et al. STUB1/CHIP is required for HIF1A degradation by chaperone-mediated autophagy. *Autophagy* (2013) **9**:1349–66. doi:10.4161/aut.25190
 49. Hubbi ME, Hu H, Kshitz, Ahmed I, Levchenko A, Semenza GL. Chaperone-mediated autophagy targets hypoxia-inducible factor-1alpha (HIF-1alpha) for lysosomal degradation. *J Biol Chem* (2013) **288**:10703–14. doi:10.1074/jbc.M112.414771
 50. Bremm A, Freund SM, Komander D. Lys11-linked ubiquitin chains adopt compact conformations and are preferentially hydrolyzed by the deubiquitinase Cezanne. *Nat Struct Mol Biol* (2010) **17**:939–47. doi:10.1038/nsmb.1873
 51. Bremm A, Moniz S, Mader J, Rocha S, Komander D. Cezanne (OTUD7B) regulates HIF-1alpha homeostasis in a proteasome-independent manner. *EMBO Rep* (2014) **15**:1268–77. doi:10.15252/embr.201438850
 52. Tang TT-L, Lasky LA. The forkhead transcription factor FOXO4 induces the down-regulation of hypoxia-inducible factor 1 alpha by a von Hippel-Lindau protein-independent mechanism. *J Biol Chem* (2003) **278**:30125–35. doi:10.1074/jbc.M302042200
 53. Zhou J, Kohl R, Herr B, Frank R, Brune B. Calpain mediates a von Hippel-Lindau protein-independent destruction of hypoxia-inducible factor-1alpha. *Mol Biol Cell* (2006) **17**:1549–58. doi:10.1091/mbc.E05-08-0770
 54. Sarraf SA, Raman M, Guarani-Pereira V, Sowa ME, Huttlin EL, Gygi SP, et al. Landscape of the PARKIN-dependent ubiquitylome in response to mitochondrial depolarization. *Nature* (2013) **496**:372–6. doi:10.1038/nature12043
 55. Sun H, Li XB, Meng Y, Fan L, Li M, Fang J. TRAF6 upregulates expression of HIF-1alpha and promotes tumor angiogenesis. *Cancer Res* (2013) **73**:4950–9. doi:10.1158/0008-5472.CAN-13-0370
 56. Bett JS, Ibrahim AF, Garg AK, Kelly V, Pedrioli P, Rocha S, et al. The P-body component USP52/PAN2 is a novel regulator of HIF1A mRNA stability. *Biochem J* (2013) **451**:185–94. doi:10.1042/BJ20130026
 57. Quesada V, Diaz-Perales A, Gutierrez-Fernandez A, Garabaya C, Cal S, Lopez-Otin C. Cloning and enzymatic analysis of 22 novel human ubiquitin-specific proteases. *Biochem Biophys Res Commun* (2004) **314**:54–62. doi:10.1016/j.bbrc.2003.12.050
 58. Moniz S, Bandarra D, Biddlestone J, Campbell KJ, Komander D, Bremm A, et al. Cezanne regulates E2F1-dependent HIF2alpha expression. *J Cell Sci* (2015) **128**:3082–93. doi:10.1242/jcs.168864
 59. Scortegagna M, Subtil T, Qi J, Kim H, Zhao W, Gu W, et al. USP13 enzyme regulates Siah2 ligase stability and activity via noncatalytic ubiquitin-binding domains. *J Biol Chem* (2011) **286**:27333–41. doi:10.1074/jbc.M111.218214
 60. Zheng X, Zhai B, Koivunen P, Shin SJ, Lu G, Liu J, et al. Prolyl hydroxylation by EglN2 destabilizes FOXO3a by blocking its interaction with the USP9x deubiquitinase. *Genes Dev* (2014) **28**:1429–44. doi:10.1101/gad.242131.114
 61. Kim JO, Kim SR, Lim KH, Kim JH, Ajjappala B, Lee HJ, et al. Deubiquitinating enzyme USP37 regulating oncogenic function of 14-3-3gamma. *Oncotarget* (2015) **6**:36551–76. doi:10.18632/oncotarget.5336
 62. Li X, Stevens PD, Yang H, Gulhati P, Wang W, Evers BM, et al. The deubiquitination enzyme USP46 functions as a tumor suppressor by controlling PHLPP-dependent attenuation of Akt signaling in colon cancer. *Oncogene* (2013) **32**:471–8. doi:10.1038/onc.2012.66
 63. Wen YA, Stevens PD, Gasser ML, Andrei R, Gao T. Downregulation of PHLPP expression contributes to hypoxia-induced resistance to chemotherapy in colon cancer cells. *Mol Cell Biol* (2013) **33**:4594–605. doi:10.1128/MCB.00695-13
 64. Guo J, Shinriki S, Su Y, Nakamura T, Hayashi M, Tsuda Y, et al. Hypoxia suppresses cylindromatosis (CYLD) expression to promote inflammation in glioblastoma: possible link to acquired resistance to anti-VEGF therapy. *Oncotarget* (2014) **5**:6353–64. doi:10.18632/oncotarget.2216
 65. Luong le A, Fragiadaki M, Smith J, Boyle J, Lutz J, Dean JL, et al. Cezanne regulates inflammatory responses to hypoxia in endothelial cells by targeting TRAF6 for deubiquitination. *Circ Res* (2013) **112**:1583–91. doi:10.1161/CIRCRESAHA.111.300119
 66. An J, Mo D, Liu H, Veena MS, Srivatsan ES, Massoumi R, et al. Inactivation of the CYLD deubiquitinase by HPV E6 mediates hypoxia-induced NF-kappaB activation. *Cancer Cell* (2008) **14**:394–407. doi:10.1016/j.ccr.2008.10.007
 67. Lee JG, Baek K, Soetandyo N, Ye Y. Reversible inactivation of deubiquitinases by reactive oxygen species in vitro and in cells. *Nat Commun* (2013) **4**:1568. doi:10.1038/ncomms2532
 68. D'Arcy B, Wang X, Linder S. Deubiquitinase inhibition as a cancer therapeutic strategy. *Pharmacol Ther* (2015) **147**:32–54. doi:10.1016/j.pharmthera.2014.11.002
 69. Bignell GR, Warren W, Seal S, Takahashi M, Rapley E, Barfoot R, et al. Identification of the familial cylindromatosis tumour-suppressor gene. *Nat Genet* (2000) **25**:160–5. doi:10.1038/76006

70. Takahashi M, Rapley E, Biggs PJ, Lakhani SR, Cooke D, Hansen J, et al. Linkage and LOH studies in 19 cylindromatosis families show no evidence of genetic heterogeneity and refine the CYLD locus on chromosome 16q12-q13. *Hum Genet* (2000) **106**:58–65. doi:10.1007/s004399900227
71. Massoumi R. CYLD: a deubiquitination enzyme with multiple roles in cancer. *Future Oncol* (2011) **7**:285–97. doi:10.2217/fon.10.187
72. Reincke M, Sbera S, Hayakawa A, Theodoropoulou M, Osswald A, Beuschlein F, et al. Mutations in the deubiquitinase gene USP8 cause Cushing's disease. *Nat Genet* (2015) **47**:31–8. doi:10.1038/ng.3166
73. Popov N, Wanzel M, Madiredjo M, Zhang D, Beijersbergen R, Bernards R, et al. The ubiquitin-specific protease USP28 is required for MYC stability. *Nat Cell Biol* (2007) **9**:765–74. doi:10.1038/ncb1601
74. Wang Z, Song Q, Xue J, Zhao Y, Qin S. Ubiquitin-specific protease 28 is overexpressed in human glioblastomas and contributes to glioma tumorigenicity by regulating MYC expression. *Exp Biol Med (Maywood)* (2015) **241**(3):255–64. doi:10.1177/1535370215595468
75. Guo G, Xu Y, Gong M, Cao Y, An R. USP28 is a potential prognostic marker for bladder cancer. *Tumour Biol* (2014) **35**:4017–22. doi:10.1007/s13277-013-1525-1
76. Gu YY, Yang M, Zhao M, Luo Q, Yang L, Peng H, et al. The de-ubiquitinase UCHL1 promotes gastric cancer metastasis via the Akt and Erk1/2 pathways. *Tumour Biol* (2015) **36**(11):8379–87. doi:10.1007/s13277-015-3566-0
77. Hussain S, Bedekovics T, Chesi M, Bergsagel PL, Galaray PJ. UCHL1 is a biomarker of aggressive multiple myeloma required for disease progression. *Oncotarget* (2015) **6**(38):40704–18. doi:10.18632/oncotarget.5727
78. Abdelmaksoud-Dammak R, Saadallah-Kallel A, Miladi-Abdennadher I, Ayedi L, Khahir A, Sallemi-Boudawara T, et al. CpG methylation of ubiquitin carboxyl-terminal hydrolase 1 (UCHL1) and P53 mutation pattern in sporadic colorectal cancer. *Tumour Biol* (2015) 1–8. doi:10.1007/s13277-015-3902-4
79. Wang JH, Wei W, Guo ZX, Shi M, Guo RP. Decreased Cezanne expression is associated with the progression and poor prognosis in hepatocellular carcinoma. *J Transl Med* (2015) **13**:41. doi:10.1186/s12967-015-0396-1
80. D'Arcy P, Linder S. Molecular pathways: translational potential of deubiquitinases as drug targets. *Clin Cancer Res* (2014) **20**:3908–14. doi:10.1158/1078-0432.CCR-14-0568
81. Colombo M, Vallese S, Peretto I, Jacq X, Rain JC, Colland F, et al. Synthesis and biological evaluation of 9-oxo-9H-indeno[1,2-b]pyrazine-2,3-dicarbonitrile analogues as potential inhibitors of deubiquitinating enzymes. *ChemMedChem* (2010) **5**:552–8. doi:10.1002/cmdc.200900409
82. Jeong CH. Inhibition of ubiquitin-specific peptidase 8 suppresses growth of gefitinib-resistant non-small cell lung cancer cells by inducing apoptosis. *J Cancer Prev* (2015) **20**:57–63. doi:10.15430/JCP.2015.20.1.57

Conflict of Interest Statement: The authors declare that the research was conducted in the absence of any commercial or financial relationships that could be construed as a potential conflict of interest.

Copyright © 2016 Schober and Berra. This is an open-access article distributed under the terms of the Creative Commons Attribution License (CC BY). The use, distribution or reproduction in other forums is permitted, provided the original author(s) or licensor are credited and that the original publication in this journal is cited, in accordance with accepted academic practice. No use, distribution or reproduction is permitted which does not comply with these terms.

Appendix 2: USP29 INTERACTOME

Appendix Table 1: USP29 interacting proteins as determined by mass spectrometry. UniProt accession numbers and descriptions of the proteins that interacted with GFP-USP29 and were at least 3-fold more enriched when compared with the GFP bait. Proteins that were detected in all 3 independent replicates are in grey, proteins that were detected in 2 out of the three replication white.

Accession	Description
P33993	DNA replication licensing factor MCM7 OS=Homo sapiens GN=MCM7 PE=1 SV=4 - [MCM7_HUMAN]
P25705	ATP synthase subunit alpha, mitochondrial OS=Homo sapiens GN=ATP5A1 PE=1 SV=1 - [ATPA_HUMAN]
P08107	Heat shock 70 kDa protein 1A/1B OS=Homo sapiens GN=HSPA1A PE=1 SV=5 - [HSP71_HUMAN]
Q9HBJ7	Ubiquitin carboxyl-terminal hydrolase 29 OS=Homo sapiens GN=USP29 PE=2 SV=1 - [UBP29_HUMAN]
P68371	Tubulin beta-4B chain OS=Homo sapiens GN=TUBB4B PE=1 SV=1 - [TBB4B_HUMAN]
P11142	Heat shock cognate 71 kDa protein OS=Homo sapiens GN=HSPA8 PE=1 SV=1 - [HSP7C_HUMAN]
P08238	Heat shock protein HSP 90-beta OS=Homo sapiens GN=HSP90AB1 PE=1 SV=4 - [HS90B_HUMAN]
P07437	Tubulin beta chain OS=Homo sapiens GN=TUBB PE=1 SV=2 - [TBB5_HUMAN]
P12004	Proliferating cell nuclear antigen OS=Homo sapiens GN=PCNA PE=1 SV=1 - [PCNA_HUMAN]
Q9Y230	RuvB-like 2 OS=Homo sapiens GN=RUVBL2 PE=1 SV=3 - [RUVB2_HUMAN]
O43175	D-3-phosphoglycerate dehydrogenase OS=Homo sapiens GN=PHGDH PE=1 SV=4 - [SERA_HUMAN]
Q14257	Reticulocalbin-2 OS=Homo sapiens GN=RCN2 PE=1 SV=1 - [RCN2_HUMAN]
Q7L5D6	Golgi to ER traffic protein 4 homolog OS=Homo sapiens GN=GET4 PE=1 SV=1 - [GET4_HUMAN]
Q9UL15	BAG family molecular chaperone regulator 5 OS=Homo sapiens GN=BAG5 PE=1 SV=1 - [BAG5_HUMAN]
P67809	Nuclease-sensitive element-binding protein 1 OS=Homo sapiens GN=YBX1 PE=1 SV=3 - [YBOX1_HUMAN]

O15355	Protein phosphatase 1G OS=Homo sapiens GN=PPM1G PE=1 SV=1 - [PPM1G_HUMAN]
P07197	Neurofilament medium polypeptide OS=Homo sapiens GN=NEFM PE=1 SV=3 - [NFM_HUMAN]
Q9Y285	Phenylalanine--tRNA ligase alpha subunit OS=Homo sapiens GN=FARSA PE=1 SV=3 - [SYFA_HUMAN]
Q07021	Complement component 1 Q subcomponent-binding protein, mitochondrial OS=Homo sapiens GN=C1QBP PE=1 SV=1 - [C1QBP_HUMAN]
P50990	T-complex protein 1 subunit theta OS=Homo sapiens GN=CCT8 PE=1 SV=4 - [TCPQ_HUMAN]
P17987	T-complex protein 1 subunit alpha OS=Homo sapiens GN=TCP1 PE=1 SV=1 - [TCPA_HUMAN]
P22695	Cytochrome b-c1 complex subunit 2, mitochondrial OS=Homo sapiens GN=UQCRC2 PE=1 SV=3 - [QCR2_HUMAN]
P31943	Heterogeneous nuclear ribonucleoprotein H OS=Homo sapiens GN=HNRNPH1 PE=1 SV=4 - [HNRH1_HUMAN]
P05141	ADP/ATP translocase 2 OS=Homo sapiens GN=SLC25A5 PE=1 SV=7 - [ADT2_HUMAN]
P62826	GTP-binding nuclear protein Ran OS=Homo sapiens GN=RAN PE=1 SV=3 - [RAN_HUMAN]
P23396	40S ribosomal protein S3 OS=Homo sapiens GN=RPS3 PE=1 SV=2 - [RS3_HUMAN]
P49411	Elongation factor Tu, mitochondrial OS=Homo sapiens GN=TUFM PE=1 SV=2 - [EFTU_HUMAN]
P50402	Emerin OS=Homo sapiens GN=EMD PE=1 SV=1 - [EMD_HUMAN]
Q9Y265	RuvB-like 1 OS=Homo sapiens GN=RUVBL1 PE=1 SV=1 - [RUVB1_HUMAN]
P36542	ATP synthase subunit gamma, mitochondrial OS=Homo sapiens GN=ATP5C1 PE=1 SV=1 - [ATPG_HUMAN]
O75190	DnaJ homolog subfamily B member 6 OS=Homo sapiens GN=DNAJB6 PE=1 SV=2 - [DNJB6_HUMAN]
P49368	T-complex protein 1 subunit gamma OS=Homo sapiens GN=CCT3 PE=1 SV=4 - [TCPG_HUMAN]
O95816	BAG family molecular chaperone regulator 2 OS=Homo sapiens GN=BAG2 PE=1 SV=1 - [BAG2_HUMAN]
Q16531	DNA damage-binding protein 1 OS=Homo sapiens GN=DDB1 PE=1 SV=1 -

	[DDB1_HUMAN]
O00767	Acyl-CoA desaturase OS=Homo sapiens GN=SCD PE=1 SV=2 - [ACOD_HUMAN]
P46379	Large proline-rich protein BAG6 OS=Homo sapiens GN=BAG6 PE=1 SV=2 - [BAG6_HUMAN]
Q13263	Transcription intermediary factor 1-beta OS=Homo sapiens GN=TRIM28 PE=1 SV=5 - [TIF1B_HUMAN]
P62263	40S ribosomal protein S14 OS=Homo sapiens GN=RPS14 PE=1 SV=3 - [RS14_HUMAN]
P63208	S-phase kinase-associated protein 1 OS=Homo sapiens GN=SKP1 PE=1 SV=2 - [SKP1_HUMAN]
Q96IX5	Up-regulated during skeletal muscle growth protein 5 OS=Homo sapiens GN=USMG5 PE=1 SV=1 - [USMG5_HUMAN]
P43307	Translocon-associated protein subunit alpha OS=Homo sapiens GN=SSR1 PE=1 SV=3 - [SSRA_HUMAN]
P19338	Nucleolin OS=Homo sapiens GN=NCL PE=1 SV=3 - [NUCL_HUMAN]
P50991	T-complex protein 1 subunit delta OS=Homo sapiens GN=CCT4 PE=1 SV=4 - [TCPD_HUMAN]
P06733	Alpha-enolase OS=Homo sapiens GN=ENO1 PE=1 SV=2 - [ENOA_HUMAN]
P11021	78 kDa glucose-regulated protein OS=Homo sapiens GN=HSPA5 PE=1 SV=2 - [GRP78_HUMAN]
P31689	DnaJ homolog subfamily A member 1 OS=Homo sapiens GN=DNAJA1 PE=1 SV=2 - [DNJA1_HUMAN]
Q3ZCQ8	Mitochondrial import inner membrane translocase subunit TIM50 OS=Homo sapiens GN=TIMM50 PE=1 SV=2 - [TIM50_HUMAN]
P06576	ATP synthase subunit beta, mitochondrial OS=Homo sapiens GN=ATP5B PE=1 SV=3 - [ATPB_HUMAN]
P18085	ADP-ribosylation factor 4 OS=Homo sapiens GN=ARF4 PE=1 SV=3 - [ARF4_HUMAN]
P35232	Prohibitin OS=Homo sapiens GN=PHB PE=1 SV=1 - [PHB_HUMAN]
P04181	Ornithine aminotransferase, mitochondrial OS=Homo sapiens GN=OAT PE=1 SV=1 - [OAT_HUMAN]
Q15293	Reticulocalbin-1 OS=Homo sapiens GN=RCN1 PE=1 SV=1 - [RCN1_HUMAN]
P10809	60 kDa heat shock protein, mitochondrial OS=Homo sapiens GN=HSPD1 PE=1 SV=2 - [CH60_HUMAN]

P04844	Dolichyl-diphosphooligosaccharide--protein glycosyltransferase subunit 2 OS=Homo sapiens GN=RPN2 PE=1 SV=3 - [RPN2_HUMAN]
P39019	40S ribosomal protein S19 OS=Homo sapiens GN=RPS19 PE=1 SV=2 - [RS19_HUMAN]
Q04695	Keratin, type I cytoskeletal 17 OS=Homo sapiens GN=KRT17 PE=1 SV=2 - [K1C17_HUMAN]
P61204	ADP-ribosylation factor 3 OS=Homo sapiens GN=ARF3 PE=1 SV=2 - [ARF3_HUMAN]
P55209	Nucleosome assembly protein 1-like 1 OS=Homo sapiens GN=NAP1L1 PE=1 SV=1 - [NP1L1_HUMAN]
P38646	Stress-70 protein, mitochondrial OS=Homo sapiens GN=HSPA9 PE=1 SV=2 - [GRP75_HUMAN]
P08670	Vimentin OS=Homo sapiens GN=VIM PE=1 SV=4 - [VIME_HUMAN]
P12236	ADP/ATP translocase 3 OS=Homo sapiens GN=SLC25A6 PE=1 SV=4 - [ADT3_HUMAN]
Q99623	Prohibitin-2 OS=Homo sapiens GN=PHB2 PE=1 SV=2 - [PHB2_HUMAN]
P05388	60S acidic ribosomal protein P0 OS=Homo sapiens GN=RPLP0 PE=1 SV=1 - [RLA0_HUMAN]
Q9P0J0	NADH dehydrogenase [ubiquinone] 1 alpha subcomplex subunit 13 OS=Homo sapiens GN=NDUFA13 PE=1 SV=3 - [NDUAD_HUMAN]
Q00839	Heterogeneous nuclear ribonucleoprotein U OS=Homo sapiens GN=HNRNPU PE=1 SV=6 - [HNRPU_HUMAN]
P62701	40S ribosomal protein S4, X isoform OS=Homo sapiens GN=RPS4X PE=1 SV=2 - [RS4X_HUMAN]
P27824	Calnexin OS=Homo sapiens GN=CANX PE=1 SV=2 - [CALX_HUMAN]
P55060	Exportin-2 OS=Homo sapiens GN=CSE1L PE=1 SV=3 - [XPO2_HUMAN]
P40227	T-complex protein 1 subunit zeta OS=Homo sapiens GN=CCT6A PE=1 SV=3 - [TCPZ_HUMAN]
P62913	60S ribosomal protein L11 OS=Homo sapiens GN=RPL11 PE=1 SV=2 - [RL11_HUMAN]
P07900	Heat shock protein HSP 90-alpha OS=Homo sapiens GN=HSP90AA1 PE=1 SV=5 - [HS90A_HUMAN]
P35998	26S protease regulatory subunit 7 OS=Homo sapiens GN=PSMC2 PE=1 SV=3 - [PRS7_HUMAN]

P62269	40S ribosomal protein S18 OS=Homo sapiens GN=RPS18 PE=1 SV=3 - [RS18_HUMAN]
P11177	Pyruvate dehydrogenase E1 component subunit beta, mitochondrial OS=Homo sapiens GN=PDHB PE=1 SV=3 - [ODPB_HUMAN]
Q9Y5M8	Signal recognition particle receptor subunit beta OS=Homo sapiens GN=SRPRB PE=1 SV=3 - [SRPRB_HUMAN]
P42677	40S ribosomal protein S27 OS=Homo sapiens GN=RPS27 PE=1 SV=3 - [RS27_HUMAN]
P62244	40S ribosomal protein S15a OS=Homo sapiens GN=RPS15A PE=1 SV=2 - [RS15A_HUMAN]
P62249	40S ribosomal protein S16 OS=Homo sapiens GN=RPS16 PE=1 SV=2 - [RS16_HUMAN]
O60884	DnaJ homolog subfamily A member 2 OS=Homo sapiens GN=DNAJA2 PE=1 SV=1 - [DNJA2_HUMAN]
P27348	14-3-3 protein theta OS=Homo sapiens GN=YWHAQ PE=1 SV=1 - [1433T_HUMAN]
P11441	Ubiquitin-like protein 4A OS=Homo sapiens GN=UBL4A PE=1 SV=1 - [UBL4A_HUMAN]
Q9P035	Very-long-chain (3R)-3-hydroxyacyl-CoA dehydratase 3 OS=Homo sapiens GN=PTPLAD1 PE=1 SV=2 - [HACD3_HUMAN]
P12956	X-ray repair cross-complementing protein 6 OS=Homo sapiens GN=XRCC6 PE=1 SV=2 - [XRCC6_HUMAN]
Q9UBS4	DnaJ homolog subfamily B member 11 OS=Homo sapiens GN=DNAJB11 PE=1 SV=1 - [DJB11_HUMAN]
P02545	Prelamin-A/C OS=Homo sapiens GN=LMNA PE=1 SV=1 - [LMNA_HUMAN]
Q9BSD7	Cancer-related nucleoside-triphosphatase OS=Homo sapiens GN=NTPCR PE=1 SV=1 - [NTPCR_HUMAN]
P17812	CTP synthase 1 OS=Homo sapiens GN=CTPS1 PE=1 SV=2 - [PYRG1_HUMAN]
P05387	60S acidic ribosomal protein P2 OS=Homo sapiens GN=RPLP2 PE=1 SV=1 - [RLA2_HUMAN]
P61221	ATP-binding cassette sub-family E member 1 OS=Homo sapiens GN=ABCE1 PE=1 SV=1 - [ABCE1_HUMAN]
Q9BQE3	Tubulin alpha-1C chain OS=Homo sapiens GN=TUBA1C PE=1 SV=1 - [TBA1C_HUMAN]

P60709	Actin, cytoplasmic 1 OS=Homo sapiens GN=ACTB PE=1 SV=1 - [ACTB_HUMAN]
P46782	40S ribosomal protein S5 OS=Homo sapiens GN=RPS5 PE=1 SV=4 - [RS5_HUMAN]
P05023	Sodium/potassium-transporting ATPase subunit alpha-1 OS=Homo sapiens GN=ATP1A1 PE=1 SV=1 - [AT1A1_HUMAN]
P51149	Ras-related protein Rab-7a OS=Homo sapiens GN=RAB7A PE=1 SV=1 - [RAB7A_HUMAN]
P62857	40S ribosomal protein S28 OS=Homo sapiens GN=RPS28 PE=1 SV=1 - [RS28_HUMAN]
Q9BUF5	Tubulin beta-6 chain OS=Homo sapiens GN=TUBB6 PE=1 SV=1 - [TBB6_HUMAN]
Q9NS69	Mitochondrial import receptor subunit TOM22 homolog OS=Homo sapiens GN=TOMM22 PE=1 SV=3 - [TOM22_HUMAN]
P51571	Translocon-associated protein subunit delta OS=Homo sapiens GN=SSR4 PE=1 SV=1 - [SSRD_HUMAN]
Q13200	26S proteasome non-ATPase regulatory subunit 2 OS=Homo sapiens GN=PSMD2 PE=1 SV=3 - [PSMD2_HUMAN]
P20700	Lamin-B1 OS=Homo sapiens GN=LMNB1 PE=1 SV=2 - [LMNB1_HUMAN]
O75489	NADH dehydrogenase [ubiquinone] iron-sulfur protein 3, mitochondrial OS=Homo sapiens GN=NDUFS3 PE=1 SV=1 - [NDUS3_HUMAN]
P08134	Rho-related GTP-binding protein RhoC OS=Homo sapiens GN=RHOC PE=1 SV=1 - [RHOC_HUMAN]
Q9Y5V3	Melanoma-associated antigen D1 OS=Homo sapiens GN=MAGED1 PE=1 SV=3 - [MAGD1_HUMAN]
P11310	Medium-chain specific acyl-CoA dehydrogenase, mitochondrial OS=Homo sapiens GN=ACADM PE=1 SV=1 - [ACADM_HUMAN]
P53007	Tricarboxylate transport protein, mitochondrial OS=Homo sapiens GN=SLC25A1 PE=1 SV=2 - [TXTP_HUMAN]
P07195	L-lactate dehydrogenase B chain OS=Homo sapiens GN=LDHB PE=1 SV=2 - [LDHB_HUMAN]
Q96EY1	DnaJ homolog subfamily A member 3, mitochondrial OS=Homo sapiens GN=DNAJA3 PE=1 SV=2 - [DNJA3_HUMAN]
P00403	Cytochrome c oxidase subunit 2 OS=Homo sapiens GN=MT-CO2 PE=1 SV=1 - [COX2_HUMAN]
Q00325	Phosphate carrier protein, mitochondrial OS=Homo sapiens GN=SLC25A3 PE=1 SV=2 - [MPCP_HUMAN]

O43242	26S proteasome non-ATPase regulatory subunit 3 OS=Homo sapiens GN=PSMD3 PE=1 SV=2 - [PSMD3_HUMAN]
P00338	L-lactate dehydrogenase A chain OS=Homo sapiens GN=LDHA PE=1 SV=2 - [LDHA_HUMAN]
Q96A26	Protein FAM162A OS=Homo sapiens GN=FAM162A PE=1 SV=2 - [F162A_HUMAN]
P0CW22	40S ribosomal protein S17-like OS=Homo sapiens GN=RPS17L PE=1 SV=1 - [RS17L_HUMAN]
Q9H3N1	Thioredoxin-related transmembrane protein 1 OS=Homo sapiens GN=TMX1 PE=1 SV=1 - [TMX1_HUMAN]
Q9UG63	ATP-binding cassette sub-family F member 2 OS=Homo sapiens GN=ABCF2 PE=1 SV=2 - [ABCF2_HUMAN]
Q9UJS0	Calcium-binding mitochondrial carrier protein Aralar2 OS=Homo sapiens GN=SLC25A13 PE=1 SV=2 - [CMC2_HUMAN]
O43852	Calumenin OS=Homo sapiens GN=CALU PE=1 SV=2 - [CALU_HUMAN]
O00148	ATP-dependent RNA helicase DDX39A OS=Homo sapiens GN=DDX39A PE=1 SV=2 - [DX39A_HUMAN]
Q9Y2R0	Cytochrome c oxidase assembly factor 3 homolog, mitochondrial OS=Homo sapiens GN=COA3 PE=1 SV=1 - [COA3_HUMAN]
P60468	Protein transport protein Sec61 subunit beta OS=Homo sapiens GN=SEC61B PE=1 SV=2 - [SC61B_HUMAN]
P0CG48	Polyubiquitin-C OS=Homo sapiens GN=UBC PE=1 SV=3 - [UBC_HUMAN]
O60762	Dolichol-phosphate mannosyltransferase subunit 1 OS=Homo sapiens GN=DPM1 PE=1 SV=1 - [DPM1_HUMAN]
Q06210	Glutamine--fructose-6-phosphate aminotransferase [isomerizing] 1 OS=Homo sapiens GN=GFPT1 PE=1 SV=3 - [GFPT1_HUMAN]
P32119	Peroxiredoxin-2 OS=Homo sapiens GN=PRDX2 PE=1 SV=5 - [PRDX2_HUMAN]
P82650	28S ribosomal protein S22, mitochondrial OS=Homo sapiens GN=MRPS22 PE=1 SV=1 - [RT22_HUMAN]
P63244	Guanine nucleotide-binding protein subunit beta-2-like 1 OS=Homo sapiens GN=GNB2L1 PE=1 SV=3 - [GBLP_HUMAN]
Q9NX63	MICOS complex subunit MIC19 OS=Homo sapiens GN=CHCHD3 PE=1 SV=1 - [MIC19_HUMAN]
Q9UNE7	E3 ubiquitin-protein ligase CHIP OS=Homo sapiens GN=STUB1 PE=1 SV=2 -

	[CHIP_HUMAN]
P61619	Protein transport protein Sec61 subunit alpha isoform 1 OS=Homo sapiens GN=SEC61A1 PE=1 SV=2 - [S61A1_HUMAN]
Q13185	Chromobox protein homolog 3 OS=Homo sapiens GN=CBX3 PE=1 SV=4 - [CBX3_HUMAN]
P60866	40S ribosomal protein S20 OS=Homo sapiens GN=RPS20 PE=1 SV=1 - [RS20_HUMAN]
Q7Z6Z7	E3 ubiquitin-protein ligase HUWE1 OS=Homo sapiens GN=HUWE1 PE=1 SV=3 - [HUWE1_HUMAN]
P62906	60S ribosomal protein L10a OS=Homo sapiens GN=RPL10A PE=1 SV=2 - [RL10A_HUMAN]
P62750	60S ribosomal protein L23a OS=Homo sapiens GN=RPL23A PE=1 SV=1 - [RL23A_HUMAN]
P62241	40S ribosomal protein S8 OS=Homo sapiens GN=RPS8 PE=1 SV=2 - [RS8_HUMAN]
O94905	Erlin-2 OS=Homo sapiens GN=ERLIN2 PE=1 SV=1 - [ERLN2_HUMAN]
P04350	Tubulin beta-4A chain OS=Homo sapiens GN=TUBB4A PE=1 SV=2 - [TBB4A_HUMAN]
P62753	40S ribosomal protein S6 OS=Homo sapiens GN=RPS6 PE=1 SV=1 - [RS6_HUMAN]
P18621	60S ribosomal protein L17 OS=Homo sapiens GN=RPL17 PE=1 SV=3 - [RL17_HUMAN]
Q99832	T-complex protein 1 subunit eta OS=Homo sapiens GN=CCT7 PE=1 SV=2 - [TCPH_HUMAN]
Q9NZ01	Very-long-chain enoyl-CoA reductase OS=Homo sapiens GN=TECR PE=1 SV=1 - [TECR_HUMAN]
O43143	Putative pre-mRNA-splicing factor ATP-dependent RNA helicase DHX15 OS=Homo sapiens GN=DHX15 PE=1 SV=2 - [DHX15_HUMAN]
P78527	DNA-dependent protein kinase catalytic subunit OS=Homo sapiens GN=PRKDC PE=1 SV=3 - [PRKDC_HUMAN]
P52597	Heterogeneous nuclear ribonucleoprotein F OS=Homo sapiens GN=HNRNPF PE=1 SV=3 - [HNRPF_HUMAN]
Q92598	Heat shock protein 105 kDa OS=Homo sapiens GN=HSPH1 PE=1 SV=1 - [HS105_HUMAN]
Q15738	Sterol-4-alpha-carboxylate 3-dehydrogenase, decarboxylating OS=Homo sapiens GN=NSDHL PE=1 SV=2 - [NSDHL_HUMAN]

P26373	60S ribosomal protein L13 OS=Homo sapiens GN=RPL13 PE=1 SV=4 - [RL13_HUMAN]
P19013	Keratin, type II cytoskeletal 4 OS=Homo sapiens GN=KRT4 PE=1 SV=4 - [K2C4_HUMAN]
Q13885	Tubulin beta-2A chain OS=Homo sapiens GN=TUBB2A PE=1 SV=1 - [TBB2A_HUMAN]
P62820	Ras-related protein Rab-1A OS=Homo sapiens GN=RAB1A PE=1 SV=3 - [RAB1A_HUMAN]
P21796	Voltage-dependent anion-selective channel protein 1 OS=Homo sapiens GN=VDAC1 PE=1 SV=2 - [VDAC1_HUMAN]
P17980	26S protease regulatory subunit 6A OS=Homo sapiens GN=PSMC3 PE=1 SV=3 - [PRS6A_HUMAN]
P45880	Voltage-dependent anion-selective channel protein 2 OS=Homo sapiens GN=VDAC2 PE=1 SV=2 - [VDAC2_HUMAN]
O75396	Vesicle-trafficking protein SEC22b OS=Homo sapiens GN=SEC22B PE=1 SV=4 - [SC22B_HUMAN]
O00231	26S proteasome non-ATPase regulatory subunit 11 OS=Homo sapiens GN=PSMD11 PE=1 SV=3 - [PSD11_HUMAN]
P61026	Ras-related protein Rab-10 OS=Homo sapiens GN=RAB10 PE=1 SV=1 - [RAB10_HUMAN]
Q16891	MICOS complex subunit MIC60 OS=Homo sapiens GN=IMMT PE=1 SV=1 - [MIC60_HUMAN]
P63104	14-3-3 protein zeta/delta OS=Homo sapiens GN=YWHAZ PE=1 SV=1 - [1433Z_HUMAN]
P61106	Ras-related protein Rab-14 OS=Homo sapiens GN=RAB14 PE=1 SV=4 - [RAB14_HUMAN]
P35613	Basigin OS=Homo sapiens GN=BSG PE=1 SV=2 - [BASI_HUMAN]
Q9H9B4	Sideroflexin-1 OS=Homo sapiens GN=SFXN1 PE=1 SV=4 - [SFXN1_HUMAN]
P51148	Ras-related protein Rab-5C OS=Homo sapiens GN=RAB5C PE=1 SV=2 - [RAB5C_HUMAN]
P39656	Dolichyl-diphosphooligosaccharide--protein glycosyltransferase 48 kDa subunit OS=Homo sapiens GN=DDOST PE=1 SV=4 - [OST48_HUMAN]
P62195	26S protease regulatory subunit 8 OS=Homo sapiens GN=PSMC5 PE=1 SV=1 - [PRS8_HUMAN]

P61289	Proteasome activator complex subunit 3 OS=Homo sapiens GN=PSME3 PE=1 SV=1 - [PSME3_HUMAN]
O14828	Secretory carrier-associated membrane protein 3 OS=Homo sapiens GN=SCAMP3 PE=1 SV=3 - [SCAM3_HUMAN]
P24539	ATP synthase F(0) complex subunit B1, mitochondrial OS=Homo sapiens GN=ATP5F1 PE=1 SV=2 - [AT5F1_HUMAN]
P49720	Proteasome subunit beta type-3 OS=Homo sapiens GN=PSMB3 PE=1 SV=2 - [PSB3_HUMAN]
P61019	Ras-related protein Rab-2A OS=Homo sapiens GN=RAB2A PE=1 SV=1 - [RAB2A_HUMAN]
P14625	Endoplasmin OS=Homo sapiens GN=HSP90B1 PE=1 SV=1 - [ENPL_HUMAN]
Q15008	26S proteasome non-ATPase regulatory subunit 6 OS=Homo sapiens GN=PSMD6 PE=1 SV=1 - [PSMD6_HUMAN]
P40937	Replication factor C subunit 5 OS=Homo sapiens GN=RFC5 PE=1 SV=1 - [RFC5_HUMAN]
Q9Y277	Voltage-dependent anion-selective channel protein 3 OS=Homo sapiens GN=VDAC3 PE=1 SV=1 - [VDAC3_HUMAN]
Q9NWU2	Glucose-induced degradation protein 8 homolog OS=Homo sapiens GN=GID8 PE=1 SV=1 - [GID8_HUMAN]
O15173	Membrane-associated progesterone receptor component 2 OS=Homo sapiens GN=PGRMC2 PE=1 SV=1 - [PGRC2_HUMAN]
P30050	60S ribosomal protein L12 OS=Homo sapiens GN=RPL12 PE=1 SV=1 - [RL12_HUMAN]
P09661	U2 small nuclear ribonucleoprotein A' OS=Homo sapiens GN=SNRPA1 PE=1 SV=2 - [RU2A_HUMAN]
Q9Y3B4	Splicing factor 3B subunit 6 OS=Homo sapiens GN=SF3B6 PE=1 SV=1 - [SF3B6_HUMAN]
Q14974	Importin subunit beta-1 OS=Homo sapiens GN=KPNB1 PE=1 SV=2 - [IMB1_HUMAN]
P60842	Eukaryotic initiation factor 4A-I OS=Homo sapiens GN=EIF4A1 PE=1 SV=1 - [IF4A1_HUMAN]
Q9UNM6	26S proteasome non-ATPase regulatory subunit 13 OS=Homo sapiens GN=PSMD13 PE=1 SV=2 - [PSD13_HUMAN]
P08574	Cytochrome c1, heme protein, mitochondrial OS=Homo sapiens GN=CYC1 PE=1 SV=3 - [CY1_HUMAN]

Q02978	Mitochondrial 2-oxoglutarate/malate carrier protein OS=Homo sapiens GN=SLC25A11 PE=1 SV=3 - [M2OM_HUMAN]
O75251	NADH dehydrogenase [ubiquinone] iron-sulfur protein 7, mitochondrial OS=Homo sapiens GN=NDUFS7 PE=1 SV=3 - [NDUS7_HUMAN]
Q9NP72	Ras-related protein Rab-18 OS=Homo sapiens GN=RAB18 PE=1 SV=1 - [RAB18_HUMAN]
Q13616	Cullin-1 OS=Homo sapiens GN=CUL1 PE=1 SV=2 - [CUL1_HUMAN]
Q8WVX9	Fatty acyl-CoA reductase 1 OS=Homo sapiens GN=FAR1 PE=1 SV=1 - [FACR1_HUMAN]
Q15773	Myeloid leukemia factor 2 OS=Homo sapiens GN=MLF2 PE=1 SV=1 - [MLF2_HUMAN]
P62333	26S protease regulatory subunit 10B OS=Homo sapiens GN=PSMC6 PE=1 SV=1 - [PRS10_HUMAN]
P62258	14-3-3 protein epsilon OS=Homo sapiens GN=YWHAE PE=1 SV=1 - [1433E_HUMAN]
P61981	14-3-3 protein gamma OS=Homo sapiens GN=YWHAG PE=1 SV=2 - [1433G_HUMAN]
P60660	Myosin light polypeptide 6 OS=Homo sapiens GN=MYL6 PE=1 SV=2 - [MYL6_HUMAN]
P28066	Proteasome subunit alpha type-5 OS=Homo sapiens GN=PSMA5 PE=1 SV=3 - [PSA5_HUMAN]
O14818	Proteasome subunit alpha type-7 OS=Homo sapiens GN=PSMA7 PE=1 SV=1 - [PSA7_HUMAN]
P62304	Small nuclear ribonucleoprotein E OS=Homo sapiens GN=SNRPE PE=1 SV=1 - [RUXE_HUMAN]
O14925	Mitochondrial import inner membrane translocase subunit Tim23 OS=Homo sapiens GN=TIMM23 PE=1 SV=1 - [TIM23_HUMAN]
P49755	Transmembrane emp24 domain-containing protein 10 OS=Homo sapiens GN=TMED10 PE=1 SV=2 - [TMEDA_HUMAN]
O95292	Vesicle-associated membrane protein-associated protein B/C OS=Homo sapiens GN=VAPB PE=1 SV=3 - [VAPB_HUMAN]
P33991	DNA replication licensing factor MCM4 OS=Homo sapiens GN=MCM4 PE=1 SV=5 - [MCM4_HUMAN]
Q9NXW2	DnaJ homolog subfamily B member 12 OS=Homo sapiens GN=DNAJB12 PE=1 SV=4 - [DJB12_HUMAN]

Q14318	Peptidyl-prolyl cis-trans isomerase FKBP8 OS=Homo sapiens GN=FKBP8 PE=1 SV=2 - [FKBP8_HUMAN]
Q9BQA1	Methylosome protein 50 OS=Homo sapiens GN=WDR77 PE=1 SV=1 - [MEP50_HUMAN]
P31153	S-adenosylmethionine synthase isoform type-2 OS=Homo sapiens GN=MAT2A PE=1 SV=1 - [METK2_HUMAN]
O00487	26S proteasome non-ATPase regulatory subunit 14 OS=Homo sapiens GN=PSMD14 PE=1 SV=1 - [PSDE_HUMAN]
Q32P51	Heterogeneous nuclear ribonucleoprotein A1-like 2 OS=Homo sapiens GN=HNRNPA1L2 PE=2 SV=2 - [RA1L2_HUMAN]
P55735	Protein SEC13 homolog OS=Homo sapiens GN=SEC13 PE=1 SV=3 - [SEC13_HUMAN]
Q04917	14-3-3 protein eta OS=Homo sapiens GN=YWHAH PE=1 SV=4 - [1433F_HUMAN]
P13639	Elongation factor 2 OS=Homo sapiens GN=EEF2 PE=1 SV=4 - [EF2_HUMAN]
Q15369	Transcription elongation factor B polypeptide 1 OS=Homo sapiens GN=TCEB1 PE=1 SV=1 - [ELOC_HUMAN]
O95168	NADH dehydrogenase [ubiquinone] 1 beta subcomplex subunit 4 OS=Homo sapiens GN=NDUFB4 PE=1 SV=3 - [NDUB4_HUMAN]
P25788	Proteasome subunit alpha type-3 OS=Homo sapiens GN=PSMA3 PE=1 SV=2 - [PSA3_HUMAN]
P28074	Proteasome subunit beta type-5 OS=Homo sapiens GN=PSMB5 PE=1 SV=3 - [PSB5_HUMAN]
P19388	DNA-directed RNA polymerases I, II, and III subunit RPABC1 OS=Homo sapiens GN=POLR2E PE=1 SV=4 - [RPAB1_HUMAN]
P46783	40S ribosomal protein S10 OS=Homo sapiens GN=RPS10 PE=1 SV=1 - [RS10_HUMAN]
Q9BYN8	28S ribosomal protein S26, mitochondrial OS=Homo sapiens GN=MRPS26 PE=1 SV=1 - [RT26_HUMAN]
P57088	Transmembrane protein 33 OS=Homo sapiens GN=TMEM33 PE=1 SV=2 - [TMM33_HUMAN]
Q92499	ATP-dependent RNA helicase DDX1 OS=Homo sapiens GN=DDX1 PE=1 SV=2 - [DDX1_HUMAN]
A0FGR8	Extended synaptotagmin-2 OS=Homo sapiens GN=ESYT2 PE=1 SV=1 - [ESYT2_HUMAN]

Q12906	Interleukin enhancer-binding factor 3 OS=Homo sapiens GN=ILF3 PE=1 SV=3 - [ILF3_HUMAN]
P30837	Aldehyde dehydrogenase X, mitochondrial OS=Homo sapiens GN=ALDH1B1 PE=1 SV=3 - [AL1B1_HUMAN]
P51648	Fatty aldehyde dehydrogenase OS=Homo sapiens GN=ALDH3A2 PE=1 SV=1 - [AL3A2_HUMAN]
Q96AG4	Leucine-rich repeat-containing protein 59 OS=Homo sapiens GN=LRRC59 PE=1 SV=1 - [LRC59_HUMAN]
Q15645	Pachytene checkpoint protein 2 homolog OS=Homo sapiens GN=TRIP13 PE=1 SV=2 - [PCH2_HUMAN]
Q16342	Programmed cell death protein 2 OS=Homo sapiens GN=PDCD2 PE=1 SV=2 - [PDCD2_HUMAN]
P43686	26S protease regulatory subunit 6B OS=Homo sapiens GN=PSMC4 PE=1 SV=2 - [PRS6B_HUMAN]
O00232	26S proteasome non-ATPase regulatory subunit 12 OS=Homo sapiens GN=PSMD12 PE=1 SV=3 - [PSD12_HUMAN]
P19387	DNA-directed RNA polymerase II subunit RPB3 OS=Homo sapiens GN=POLR2C PE=1 SV=2 - [RPB3_HUMAN]
Q9BSV6	tRNA-splicing endonuclease subunit Sen34 OS=Homo sapiens GN=TSEN34 PE=1 SV=1 - [SEN34_HUMAN]
Q13148	TAR DNA-binding protein 43 OS=Homo sapiens GN=TARDBP PE=1 SV=1 - [TADBP_HUMAN]
Q9Y4P3	Transducin beta-like protein 2 OS=Homo sapiens GN=TBL2 PE=1 SV=1 - [TBL2_HUMAN]
P07741	Adenine phosphoribosyltransferase OS=Homo sapiens GN=APRT PE=1 SV=2 - [APT_HUMAN]
P62330	ADP-ribosylation factor 6 OS=Homo sapiens GN=ARF6 PE=1 SV=2 - [ARF6_HUMAN]
P40616	ADP-ribosylation factor-like protein 1 OS=Homo sapiens GN=ARL1 PE=1 SV=1 - [ARL1_HUMAN]
Q8WWC4	Uncharacterized protein C2orf47, mitochondrial OS=Homo sapiens GN=C2orf47 PE=1 SV=1 - [CB047_HUMAN]
O14735	CDP-diacylglycerol--inositol 3-phosphatidyltransferase OS=Homo sapiens GN=CDIPT PE=1 SV=1 - [CDIPT_HUMAN]
P24534	Elongation factor 1-beta OS=Homo sapiens GN=EEF1B2 PE=1 SV=3 -

	[EF1B_HUMAN]
O96000	NADH dehydrogenase [ubiquinone] 1 beta subcomplex subunit 10 OS=Homo sapiens GN=NDUFB10 PE=1 SV=3 - [NDUBA_HUMAN]
P62937	Peptidyl-prolyl cis-trans isomerase A OS=Homo sapiens GN=PPIA PE=1 SV=2 - [PPIA_HUMAN]
O00743	Serine/threonine-protein phosphatase 6 catalytic subunit OS=Homo sapiens GN=PPP6C PE=1 SV=1 - [PPP6_HUMAN]
P30041	Peroxiredoxin-6 OS=Homo sapiens GN=PRDX6 PE=1 SV=3 - [PRDX6_HUMAN]
P28072	Proteasome subunit beta type-6 OS=Homo sapiens GN=PSMB6 PE=1 SV=4 - [PSB6_HUMAN]
P51153	Ras-related protein Rab-13 OS=Homo sapiens GN=RAB13 PE=1 SV=1 - [RAB13_HUMAN]
P01111	GTPase NRas OS=Homo sapiens GN=NRAS PE=1 SV=1 - [RASN_HUMAN]
P61353	60S ribosomal protein L27 OS=Homo sapiens GN=RPL27 PE=1 SV=2 - [RL27_HUMAN]
P52815	39S ribosomal protein L12, mitochondrial OS=Homo sapiens GN=MRPL12 PE=1 SV=2 - [RM12_HUMAN]
Q96GC5	39S ribosomal protein L48, mitochondrial OS=Homo sapiens GN=MRPL48 PE=1 SV=2 - [RM48_HUMAN]
Q13405	39S ribosomal protein L49, mitochondrial OS=Homo sapiens GN=MRPL49 PE=1 SV=1 - [RM49_HUMAN]
P52434	DNA-directed RNA polymerases I, II, and III subunit RPABC3 OS=Homo sapiens GN=POLR2H PE=1 SV=4 - [RPAB3_HUMAN]
P62070	Ras-related protein R-Ras2 OS=Homo sapiens GN=RRAS2 PE=1 SV=1 - [RRAS2_HUMAN]
P62081	40S ribosomal protein S7 OS=Homo sapiens GN=RPS7 PE=1 SV=1 - [RS7_HUMAN]
P14678	Small nuclear ribonucleoprotein-associated proteins B and B' OS=Homo sapiens GN=SNRPB PE=1 SV=2 - [RSMB_HUMAN]
Q9Y3D9	28S ribosomal protein S23, mitochondrial OS=Homo sapiens GN=MRPS23 PE=1 SV=2 - [RT23_HUMAN]
Q9Y2Q9	28S ribosomal protein S28, mitochondrial OS=Homo sapiens GN=MRPS28 PE=1 SV=1 - [RT28_HUMAN]
O75934	Pre-mRNA-splicing factor SPF27 OS=Homo sapiens GN=BCAS2 PE=1 SV=1 - [SPF27_HUMAN]

P37108	Signal recognition particle 14 kDa protein OS=Homo sapiens GN=SRP14 PE=1 SV=2 - [SRP14_HUMAN]
Q9Y3D7	Mitochondrial import inner membrane translocase subunit TIM16 OS=Homo sapiens GN=PAM16 PE=1 SV=2 - [TIM16_HUMAN]
Q9BVC6	Transmembrane protein 109 OS=Homo sapiens GN=TMEM109 PE=1 SV=1 - [TM109_HUMAN]
Q9Y3A6	Transmembrane emp24 domain-containing protein 5 OS=Homo sapiens GN=TMED5 PE=1 SV=1 - [TMED5_HUMAN]
Q8NGC6	Olfactory receptor 4K17 OS=Homo sapiens GN=OR4K17 PE=2 SV=3 - [OR4KH_HUMAN]
P56192	Methionine--tRNA ligase, cytoplasmic OS=Homo sapiens GN=MARS PE=1 SV=2 - [SYMC_HUMAN]
Q8N7H5	RNA polymerase II-associated factor 1 homolog OS=Homo sapiens GN=PAF1 PE=1 SV=2 - [PAF1_HUMAN]
O95831	Apoptosis-inducing factor 1, mitochondrial OS=Homo sapiens GN=AIFM1 PE=1 SV=1 - [AIFM1_HUMAN]
P16615	Sarcoplasmic/endoplasmic reticulum calcium ATPase 2 OS=Homo sapiens GN=ATP2A2 PE=1 SV=1 - [AT2A2_HUMAN]
Q8IXI2	Mitochondrial Rho GTPase 1 OS=Homo sapiens GN=RHOT1 PE=1 SV=2 - [MIRO1_HUMAN]
P47897	Glutamine--tRNA ligase OS=Homo sapiens GN=QARS PE=1 SV=1 - [SYQ_HUMAN]
P13010	X-ray repair cross-complementing protein 5 OS=Homo sapiens GN=XRCC5 PE=1 SV=3 - [XRCC5_HUMAN]
P68104	Elongation factor 1-alpha 1 OS=Homo sapiens GN=EEF1A1 PE=1 SV=1 - [EF1A1_HUMAN]
P13647	Keratin, type II cytoskeletal 5 OS=Homo sapiens GN=KRT5 PE=1 SV=3 - [K2C5_HUMAN]
P02533	Keratin, type I cytoskeletal 14 OS=Homo sapiens GN=KRT14 PE=1 SV=4 - [K1C14_HUMAN]
P02538	Keratin, type II cytoskeletal 6A OS=Homo sapiens GN=KRT6A PE=1 SV=3 - [K2C6A_HUMAN]
P08779	Keratin, type I cytoskeletal 16 OS=Homo sapiens GN=KRT16 PE=1 SV=4 - [K1C16_HUMAN]
Q92928	Putative Ras-related protein Rab-1C OS=Homo sapiens GN=RAB1C PE=5 SV=2 -

	[RAB1C_HUMAN]
P27635	60S ribosomal protein L10 OS=Homo sapiens GN=RPL10 PE=1 SV=4 - [RL10_HUMAN]
P04843	Dolichyl-diphosphooligosaccharide--protein glycosyltransferase subunit 1 OS=Homo sapiens GN=RPN1 PE=1 SV=1 - [RPN1_HUMAN]
Q9BVK6	Transmembrane emp24 domain-containing protein 9 OS=Homo sapiens GN=TMED9 PE=1 SV=2 - [TMED9_HUMAN]
Q9UJZ1	Stomatin-like protein 2, mitochondrial OS=Homo sapiens GN=STOML2 PE=1 SV=1 - [STML2_HUMAN]
Q9UK99	F-box only protein 3 OS=Homo sapiens GN=FBXO3 PE=1 SV=3 - [FBX3_HUMAN]
Q9NVW2	E3 ubiquitin-protein ligase RLIM OS=Homo sapiens GN=RLIM PE=1 SV=3 - [RNF12_HUMAN]
P07196	Neurofilament light polypeptide OS=Homo sapiens GN=NEFL PE=1 SV=3 - [NFL_HUMAN]
Q5W0B1	RING finger protein 219 OS=Homo sapiens GN=RNF219 PE=1 SV=1 - [RN219_HUMAN]
Q9Y3Z3	Deoxynucleoside triphosphate triphosphohydrolase SAMHD1 OS=Homo sapiens GN=SAMHD1 PE=1 SV=2 - [SAMH1_HUMAN]
Q9ULX6	A-kinase anchor protein 8-like OS=Homo sapiens GN=AKAP8L PE=1 SV=3 - [AKP8L_HUMAN]
P48643	T-complex protein 1 subunit epsilon OS=Homo sapiens GN=CCT5 PE=1 SV=1 - [TCPE_HUMAN]
O95373	Importin-7 OS=Homo sapiens GN=IPO7 PE=1 SV=1 - [IPO7_HUMAN]
P15924	Desmoplakin OS=Homo sapiens GN=DSP PE=1 SV=3 - [DESP_HUMAN]
P04259	Keratin, type II cytoskeletal 6B OS=Homo sapiens GN=KRT6B PE=1 SV=5 - [K2C6B_HUMAN]
P06748	Nucleophosmin OS=Homo sapiens GN=NPM1 PE=1 SV=2 - [NPM_HUMAN]
P07910	Heterogeneous nuclear ribonucleoproteins C1/C2 OS=Homo sapiens GN=HNRNPC PE=1 SV=4 - [HNRPC_HUMAN]
P26641	Elongation factor 1-gamma OS=Homo sapiens GN=EEF1G PE=1 SV=3 - [EF1G_HUMAN]
Q96TA2	ATP-dependent zinc metalloprotease YME1L1 OS=Homo sapiens GN=YME1L1 PE=1 SV=2 - [YMEL1_HUMAN]
P10599	Thioredoxin OS=Homo sapiens GN=TXN PE=1 SV=3 - [THIO_HUMAN]

Appendix 3: POSTERS PRESENTED DURING THE THESIS

Poster presented at the University's Poster Day Online (April 2014):

Watching proteins move and interact within living cells

Amelie Schober*, Marco Marcello, Edurne Berra, Violaine Sée

* schobera@liv.ac.uk

Center for Cell Imaging, Institute of Integrative Biology, University of Liverpool in cooperation with CIC bioGUNE, Bilbao



Abstract

Signalling pathways in the cell rely on the interaction of two or more proteins with each other. Deregulation of those interactions can have deleterious effects on cells and can be the cause of diseases such as cancer. Understanding which proteins interact, how they interact and what kind of modifications are implicated is therefore of great interest. Classical approaches to address these questions are based on bulk cell analysis and do not account for cell-to-cell variability and dynamic changes. Here we applied two modern single live cell imaging techniques in order to understand how the SUMOylation of a protein involved in oxygen sensing affects its interaction with HIF-1 α , an important regulator of gene expression that has also been shown to be over-activated in many tumour tissues.

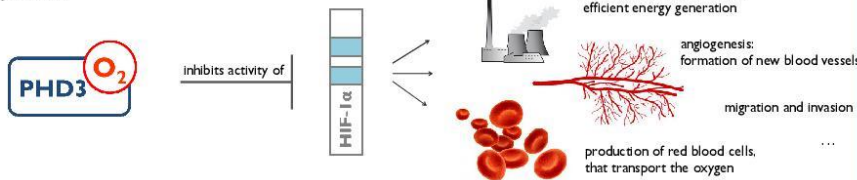
The proteins of the focus of interest

PHD3

(prolyl-hydroxylase domain containing protein 3): Oxygen sensor of the cell; in the presence of sufficient oxygen PHD3 targets HIF-1 α for degradation

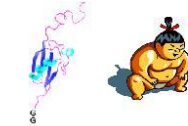
HIF-1 α (hypoxia inducible factor 1 α):

In the absence of sufficient oxygen HIF-1 α switches on a variety of processes that allow the cell and organism to survive



SUMO

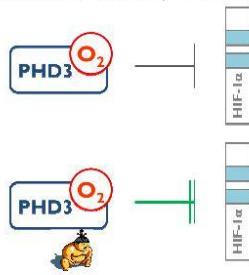
small ubiquitin like modifier



SUMO is a small protein that can be attached to another protein thereby affecting its localisation, stability, activity or interaction with other proteins

SUMO's effect on PHD3

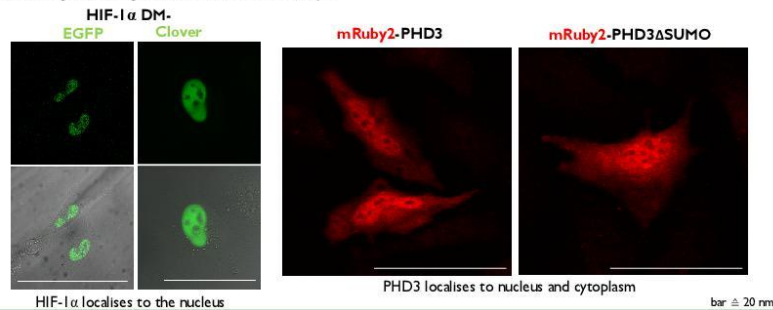
SUMOylation of PHD3 leads to a greater inhibition of HIF-1 α 's activity \rightarrow HOW?



CIC bioGUNE Núñez O'Mara et al., submitted

Making the proteins visible

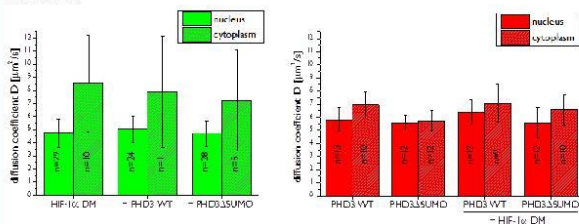
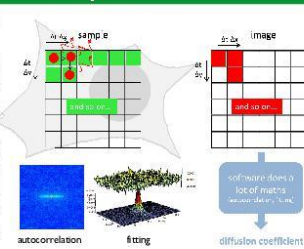
The attachment of a fluorescent protein to the proteins of interest allows the visualisation of the proteins within a living cell using a fluorescence microscope.



Measuring the movement of the proteins

Raster Image Correlation Spectroscopy (RICS)

With a fluorescence laser scanning microscope we can measure the velocity of a labelled protein within a living cell. While the laser scans the sample pixel by pixel, a moving fluorophore creates a trace on the image. With the temporal and spatial information inherent to the image, a diffusion coefficient can be calculated.

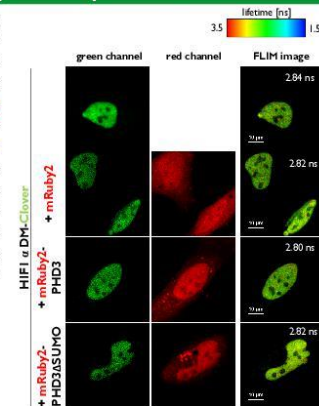


Neither PHD3 nor PHD3 Δ SUMO change HIF-1 α DM's diffusion coefficient and vice versa, suggesting that they might be part of the same complex regardless of PHD3's SUMOylation state.

Measuring the proximity of the proteins

Förster Resonance Energy Transfer (FRET)

FRET allows the measurement of distances of two labelled proteins like a molecular ruler. Only if the acceptor fluorophore is in very close proximity ($< 10^{-8}$ m) to the donor fluorophore, the excitation of the donor is transferred onto the acceptor. This results in a decrease of the fluorescence lifetime of the donor, that we can measure using a time-correlated single photon counting system.



We could not measure a clear decrease of HIF-1 α DM-Clover's lifetime in the presence of either mRuby2-PHD3 nor -PHD3 Δ SUMO. As it is known that PHD3 does bind to HIF-1 α DM, the system established so far requires optimisation.

Poster presented at the **1st Proteostasis Meeting** in Valencia (5. – 7.11.2014):

Effects of PHD-SUMOylation on the hypoxia signalling pathway – a live cell imaging approach



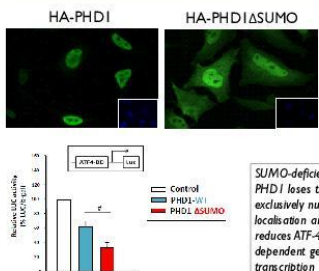
Amelie Schober*, Analía Núñez-O'Mara, Almudena Gerpe, Violaine Sée†, Edurne Berra
CIC bioGUNE, Bilbao in cooperation with †Center for Cell Imaging, University of Liverpool
*aschober.uol@icbiogune.es



Abstract

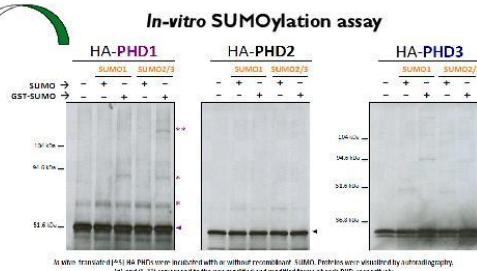
In response to low oxygen levels the dimeric transcription factor HIF activates the expression of hundreds of genes allowing for adaptation. In normoxic conditions the α -subunit of HIF is hydroxylated on conserved prolines by the prolyl hydroxylases (PHDs), that act as oxygen sensors. Hydroxyprolines serve as recognition signal for the E3-Ligase pVHL, which polyubiquitinates and therefore targets HIF- α for proteasomal degradation. But not only HIF- α but also PHDs underlie regulating post-transcriptional modifications. Here we show how SUMOylation impacts on PHD1 and PHD3 localisation and HIF-1 transcriptional activity, respectively. In particular we apply advanced fluorescent live cell imaging techniques such as FRAP, RICS and FLIM-FRET in order to characterise the dynamics of the SUMO-mediated altered protein properties on a single live cell level.

Biochemical studies

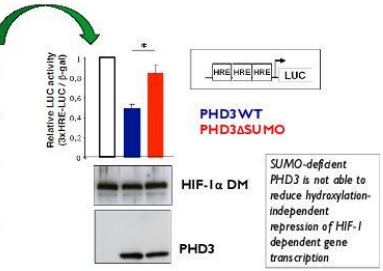


SUMO-deficient PHD1 loses the exclusively nuclear localisation and reduces ATF-4 dependent gene transcription

In-vitro SUMOylation assay

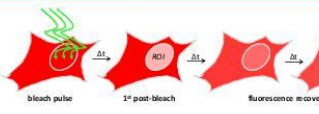


In vitro transcribed (±5) HA-PHDs were incubated with or without monomeric SUMO. Proteins were visualised by autoradiography. (*) and (**) correspond to the non modified and modified forms of each PHD, respectively.



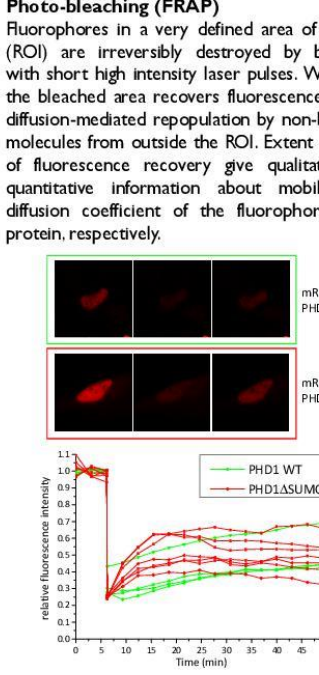
SUMO-deficient PHD3 is not able to reduce hydroxylation-independent repression of HIF-1 dependent gene transcription

PHD – nuclear-cytoplasmic diffusion



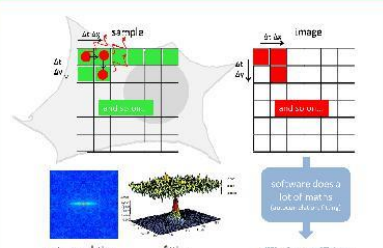
Fluorescence Recovery After Photo-bleaching (FRAP)

Fluorophores in a very defined area of the cell (ROI) are irreversibly destroyed by bleaching with short high intensity laser pulses. With time the bleached area recovers fluorescence due to diffusion-mediated repopulation by non-bleached molecules from outside the ROI. Extent and rate of fluorescence recovery give qualitative and quantitative information about mobility and diffusion coefficient of the fluorophore-tagged protein, respectively.



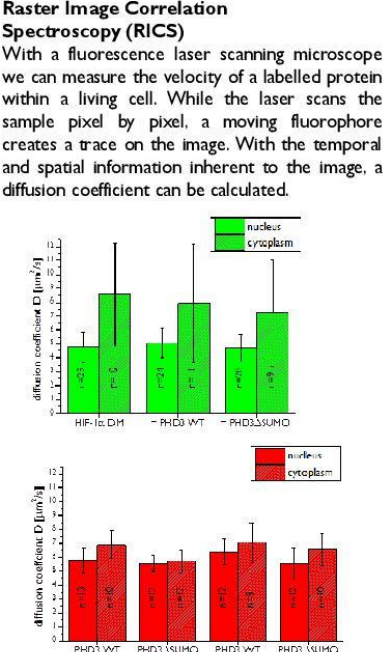
Both, PHD1 WT and PHD1ΔSUMO repopulate the bleached nucleus. PHD1ΔSUMO does so much quicker than PHD1 WT, presumably due to a bigger cytoplasmic pool of intact fluorophore-tagged protein. These results suggest that SUMOylation is not affecting nuclear import of PHD1, but might be required for nuclear retention.

PHD3 – diffusion




Raster Image Correlation Spectroscopy (RICS)

With a fluorescence laser scanning microscope we can measure the velocity of a labelled protein within a living cell. While the laser scans the sample pixel by pixel, a moving fluorophore creates a trace on the image. With the temporal and spatial information inherent to the image, a diffusion coefficient can be calculated.

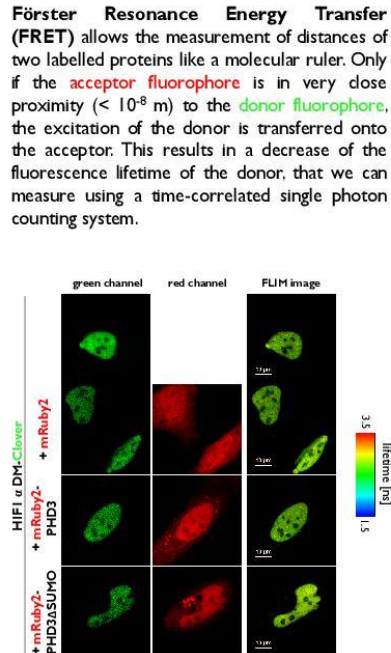


Neither PHD3 nor PHD3ΔSUMO change HIF-1 α DM's diffusion coefficient and vice versa, suggesting that they might be part of the same complex regardless of PHD3's SUMOylation state.

PHD3 – interaction with HIF-1 α




Förster Resonance Energy Transfer (FRET) allows the measurement of distances of two labelled proteins like a molecular ruler. Only if the **acceptor fluorophore** is in very close proximity ($< 10^{-8}$ m) to the **donor fluorophore**, the excitation of the donor is transferred onto the acceptor. This results in a decrease of the fluorescence lifetime of the donor, that we can measure using a time-correlated single photon counting system.




We could not measure a clear decrease of HIF-1 α DM-Clover's lifetime in the presence of neither mRuby2-PHD3 nor -PHD3ΔSUMO. As it is known that PHD3 does bind to HIF-1 α DM, the system established so far requires optimisation.

Poster presented at the **British Biophysical Society 2016 Biennial Meeting** in Liverpool (6. – 8.07.2016):



UNIVERSITY OF LIVERPOOL




CCI
CENTRE FOR CELL IMAGING

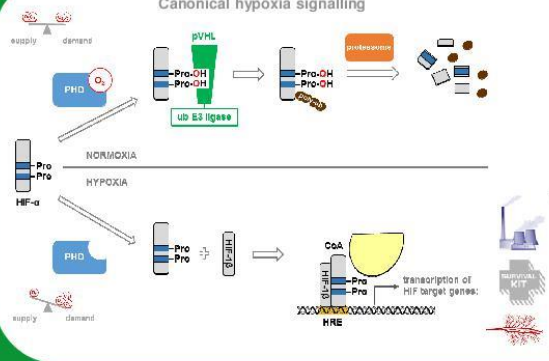
USP29 is a new regulator of Hypoxia Inducible Factor α (HIF- α)

Amelie Schober^{*1,2}, Onintza Carlevaris¹, Almudena Gerpe-Pita¹, Encarnación Pérez-Andrés¹, Sara Pozo¹, Edurne Berra¹ & Violaine Sée²

¹CIC bioGUNE, Bilbao ²Center for Cell Imaging, University of Liverpool ^{*}schobera@liv.ac.uk



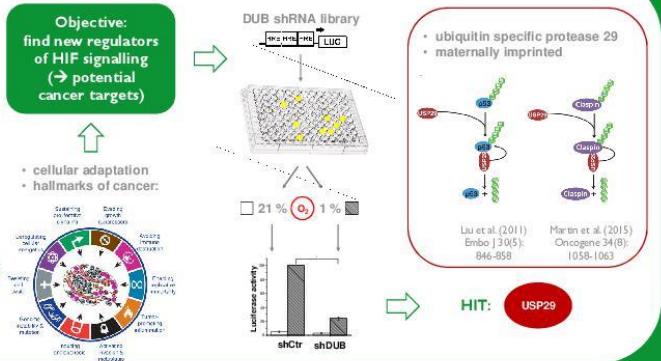
Introduction



Canonical hypoxia signalling

Objective: find new regulators of HIF signalling (\rightarrow potential cancer targets)

- cellular adaptation
- hallmarks of cancer:



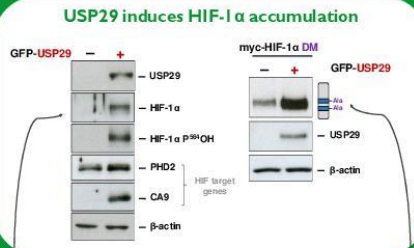
DUB shRNA library

- ubiquitin specific protease 29
- maternally imprinted

HIT: USP29

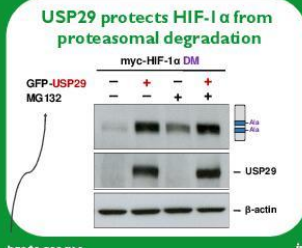
Results

USP29 induces HIF-1 α accumulation



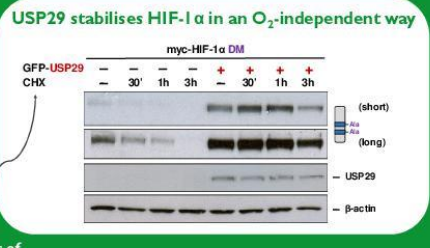
endogenous HIF-1 α **O₂-insensitive HIF-1 α**

USP29 protects HIF-1 α from proteasomal degradation



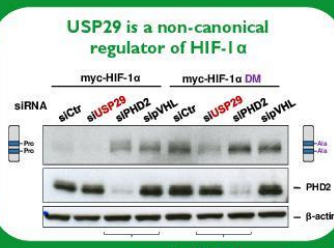
proteasome inhibitor

USP29 stabilises HIF-1 α in an O₂-independent way



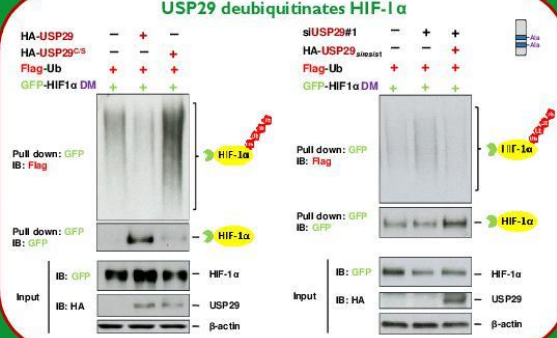
inhibitor of protein translation

USP29 is a non-canonical regulator of HIF-1 α

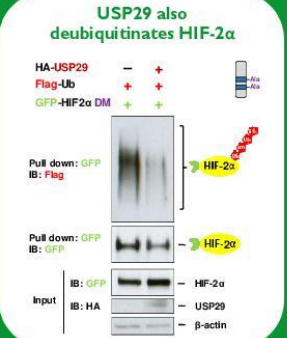


canonical HIF-1 α regulator

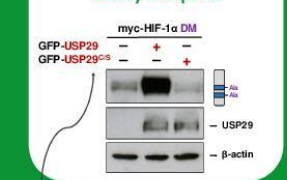
USP29 deubiquitinates HIF-1 α



USP29 also deubiquitinates HIF-2 α

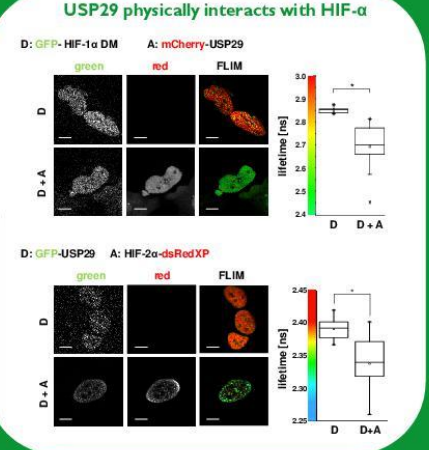


USP29's catalytic activity is required



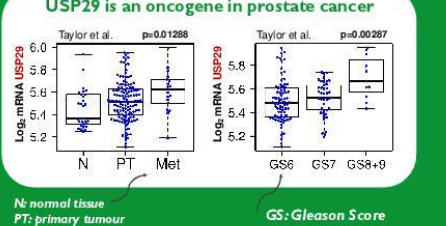
catalytic cysteine C294 replaced by serine

USP29 physically interacts with HIF- α



Tech-Box: FLIM-FRET
Foerster Resonance Energy Transfer (FRET)
Fluorescence Lifetime

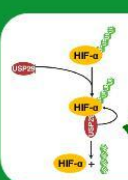
USP29 is an oncogene in prostate cancer



N: normal tissue
PT: primary tumour
Met: metastasis

GS: Gleason Score

Conclusions



- USP29 deubiquitinates HIF- α
- ... in an O₂-independent manner,
- ... thereby protecting it from proteasomal degradation
- ... and increasing its stability